UNIVERSITÀ DEGLI STUDI DI TRIESTE

E

UNIVERSITÀ CA'FOSCARI VENEZIA

XXXV CICLO DEL DOTTORATO DI RICERCA IN

CHIMICA

Istituto Italiano di Tecnologia – Center for Cultural Heritage Technology (CCHT@Ca'Foscari)

Advancing approaches in glass conservation: characterisation of altered archaeological glass and artificially aged glass replicas to shed light into the mechanisms of glass corrosion.

Settore scientifico-disciplinare: **CHIM/12**

DOTTORANDO / A
ROBERTA ZANINI

COORDINATORE
PROF. ENZO ALESSIO
PROF ELISA MORETTI

SUPERVISORE DI TESI
PROF. ELTI CATTARUZZA

CO-SUPERVISORE DI TESI
DOTT.SSA ARIANNA TRAVIGLIA

ANNO ACCADEMICO 2021/2022

"Today, glass is ordinary, on-the-kitchen-shelf stuff. But early in its history, glass was bling for kings."
by Carolyn Wilke

ABSTRACT

Glass finds application in multiple domains, from the technological to the artistic and archaeological one, and the study of its durability is crucial to determine its potential to replace several dangerous and polluting materials such as plastics, particularly now in the era of the circular economy. Because of the thermodynamic properties of glass and its high variety of compositions, the evaluation of glass durability and alteration mechanisms remains a challenge.

For this reason, the study of glass corrosion is considered a complex research topic that requires the ability to take into consideration a big number of factors, some of which are hardly represented in laboratory experiments. The most influential of these is with no doubt the time given to the transformation, which is directly responsible of both the kinetics and the dynamics of the processes involved.

The present PhD project aims to study the complex phenomenon of glass corrosion from the perspective of ancient glass samples, which represent unique evidence of the effect of long-lasting environmental ageing on such material. The goal is to highlight how the study of ancient and archaeological glass offers an outstanding opportunity to fill the gaps in the various theories about glass corrosion, which, in fact, have been formulated on the basis of research carried out under laboratory conditions and only partially reproducing the circumstances of environmental degradation.

The ultimate purpose is twofold. On one hand, this work wants to highlight how far research on glass corrosion has come by studying model systems created in laboratory to simulate different alteration conditions and glass compositions. On the other, it wants to point out what the critical aspects that still need to be investigated are and how the study of archaeological glass may complement the results obtained over the years in research carried out on laboratory models. Archaeological glass gives indeed the unique opportunity to observe the effect of long-term natural ageing on a real material, and the results obtained from its study are key to fill the gaps that are still present in the theory of glass corrosion.

This PhD thesis starts with the gathering of the results obtained about glass corrosion and its interaction with the environment, considering studies performed both on experimental and archaeological samples. The aim is to understand where the scientific today, what are the critical points that still need to be investigated and what may be the future perspective for glass preservation and applications (for instance for the development of sustainable protective treatments), to help the scientific community in the design of future, more complete, research.

An innovative strategy to approach the problem of glass corrosion and its stabilisation is proposed in this work: the development of an ideal conservation treatment able to slow down the alteration process of ancient glass requires the in-depth investigation of ancient glass and of

the artificially aged glass mock-ups in order to obtain a comprehensive evaluation of the modification of glass structure, its kinetic over time, and its final visible results. The information obtained from this course of the research of glass corrosion represent the basis and inspiration for a modern way of thinking about glass conservation that overcomes the limits imposed by traditional principles, such as reversibility, by exploiting the properties of cutting-edge technology such as nanotechnology.

This PhD project has been founded by Italian Institute of Technology (IIT) and has been performed in the Center for Cultural Heritage Technologies (CCHT-IIT) within Ca'Foscari University of Venice.

PUBLICATIONS AND PRESENTATIONS

First author publications

Zanini R., Franceschin G., Cattaruzza E., Traviglia A., *A review of glass corrosion: the unique contribution of studying ancient glass to validate glass alteration models*. Accepted by npj Material Degradation.

Zanini R., Moro G., Orsega E.F., Panighello S., Šelih V.S., Jaćimović R., van Elteren J.T., Mandruzzato L., Moretto L.M., Traviglia A., *Insight into the secondary glass production in Roman Aquileia: a preliminary study*. Under revision by Journal of Archaeological Science Reports.

Zanini R., Roman M., Cattaruzza E., Traviglia A., High-speed and high-resolution 2D and 3D elemental imaging of corroded ancient glass by Laser Ablation-ICP-MS. Accepted by Journal of Analytical Atomic Spectrometry.

Other publications

Franceschin G., Zanini R., Centenaro S. (2022). *Ancient glass alteration and advancement in active conservation strategies.* In ANTIFRAGILE GLASS edited by Maria Antonia Barucco, Elti Cattaruzza, Rosa Chiesa. (pp. 86-87), Anteferma ISBN 979-12-5953-096-7.

Oral Presentations

“Studying ancient glass to bring to light new insights into the mechanism of glass corrosion” at INART 2022: 5th international conference on innovation in art research and technology, 28 jun-1 jul 2022 Paris (France).

“Laser ablation ICP-MS elemental imaging to investigate corroded surfaces of ancient glass” at XXVII CONGRESSO NAZIONALE DELLA SOCIETÀ CHIMICA ITALIANA, 14 – 23 Sept. 2021, Online.

Poster Presentations

“Ancient glass alteration and advancement in active conservation strategies” at ANTIFRAGILE GLASS conference, Venezia 2022- 17-19 November 2022.

Franceschin G., Centenaro S., Zanini R., Cattaruzza E., Traviglia A. “A novel silica-based nanostructured system to consolidate and protect ancient glass” at InArt 2022: 5th International Conference on Innovation in Art Research and Technology, 28 jun-1 jul 2022 Paris (France).

CONTENT

LIST OF ABBREVIATIONS AND ACRONYMS

BSE	Back-Scattered Electrons
CID	Classic Inter-Diffusion
CMG	Corning Museum of Glass
CPS	Counts Per Second
EDX	Energy Dispersive X-Ray Analyses
FT-IR	Fourier Transform Infrared Spectroscopy
IDP	Interfacial Dissolution Precipitation
LA-ICP-MS	Laser Ablation Inductively Coupled Plasma Mass Spectrometry
Micro-CT	Micro Computed Tomography
NIST	National Institute for Standards and Tables
OM	Optical Microscopy
PCA	Principal Component Analyses
SE	Secondary Electrons
SEM	Scanning Electron Microscopy
SGT	Society of Glass Technology
SIMS	Secondary Ion Mass Spectrometry
SR micro-CT	Synchrotron Radiation Micro-Computed Tomography
SSL	Silica-Soda-Lime
TEM	Transmission Electron Microscopy
XPS	X-Ray Photoelectron Spectroscopy

INTRODUCTION OF THE RESEARCH

The properties of glass have been extensively studied within the most diverse sectors, from the technological field to the artistic and archaeological ones. However, its lack of long-range atomic order has hindered the formulation of a universally recognised theory about how it interacts with the environment. The understanding of such interaction and of the consequent degradation mechanisms it triggers have sparked, nonetheless, considerable interest in the scientific community, giving rise to abundant literature.

Due to its complex structure lacking long-range atomic order, despite the broad time span during which glass has been used and the considerable body of literature on this material, no theory about the mechanism responsible for its degradation has been universally accepted yet.

Standard approaches to the study of glass corrosion are limited in that they are valid in some specific experimental conditions but not in others Most of the studies are based on artificial ageing experiments that are designed to monitor step by step the process of glass alteration and the physicochemical evolution of the glass structure [1–4]. However, because of the great variability of the experimental conditions set in these studies, the results and conclusions retrieved are not comprehensive and the glass transformation process is only partially described. On this last aspect, studying corrosion on ancient glass through advanced analytical techniques offers an outstanding opportunity to observe the products of the alteration process as the result of the long-term transformation of glass structure in general. A better understanding of the glass corrosion mechanism, its processes and the nature of its final products is, as a matter of fact, key for identifying the most appropriate ways to preserve and protect in the long-term glass artefacts, both in the field of heritage science and in industrial and technical productions.

The first studies of glass in the domain of heritage science date back to the 1960s [5,6]. The chemistry community has recently paid new attention to this topic, giving rise to results that help shed light on the deep connection between compositions, structure, and surrounding environment in extremely complex materials. As an example, a recent review [7] reported about the possibility of employing mechanistic models to study aqueous glass alteration. Thanks to the development of such novel technique, glass alteration mechanisms and kinetics can be hypothesised by using non-conventional experimental methods (simulations) and without direct experimental validations. In parallel, the long-term perspective given by studying ancient vitreous objects can provide a proof or a refutation to the predictions obtained through simulation and laboratory methods, thus overcoming the lack of a future vision and the rigour of a historical time perspective typical of these approaches.

The kinetic of the glass corrosion process, the sequence of the events, and the prevalence of one over another of the interconnected mechanisms involved in the glass alteration depend both on the nature of the glassy material, i.e., its chemical composition and structure, and on the environmental conditions such as the amount of water that reacts, the nature of the solution (its chemistry and pH), and the reaction exposure time. In the case of ancient glass, water can be involved in different forms: rain on stained windows, seawater, aqueous solutions in the burial soil or vapour as humidity in the atmosphere or in museum surrounding. All these factors make the alteration of ancient (silicate) glass a complex phenomenon to explain. However, by the characterisation of altered ancient glass it is possible to obtain concrete evidence of the transformation of the vitreous structure, of the nature of the dissolution products, and of how a specific glass composition reacts to certain environment. The historical evolution of glass manufacturing gives us back today different typologies of glass such as Roman SSL, Medieval stained, or Venetian crystal glass (*Cristallo*). All these glass types constitute natural samples available to the scientific community to study and better understand the process involved in glass corrosion, because they have typical chemical stability due to own chemical composition and they aged in burial condition, underwater, or in confined space whit a specific microclimate for centuries.

In this framework, a comprehensive and multi-analytical study of ancient SSL glass -such as Roman glass- may provide decisive data to verify long-term prediction of SSL glass behaviour, having naturally aged in underground or underwater deposits for several centuries. This archaeological evidence offers an unprecedented opportunity to develop a comprehensive theory about glass degradation, starting from the advanced analyses of materials that naturally aged for several centuries. In the field of heritage science as well as in industrial and technical productions, improving the knowledge on the mechanism of glass corrosion, its processes and its products is essential to develop the most appropriate way of preservation and protection for glass artefacts.

To address this topic, this thesis is organised in three interconnected macro parts: the first will deal with the characterisation of Roman glass fragments in order to learn about their composition and the context in which they were buried for centuries; the second part will illustrate new analytical approaches to characterise degradation phenomena present on archaeological glass and the information that can be obtained from them in order to study the mechanism of glass corrosion; finally, the third part will describe an artificial aging test conducted in the laboratory and how to investigate the compositional changes that occur in the first layers of the glass surface during the alteration process.

CHAPTER 1 –
THE HISTORY AND SCIENCE OF GLASS: A LOOK INSIDE

1.1. BRIEF HISTORY OF GLASS AND ITS EVOLUTION

Natural glass has existed since the beginnings of time formed when rocks melt because of high-temperature phenomena such as volcanic eruptions (obsidian), lightning strikes (fulgurite) or the impact of meteorites (tektites), then cool, and solidify rapidly enough so that a liquid-like structure can be frozen in glassy state. Most well-known natural glass is obsidian, which is believed to be one of the first glass that appeared on earth at least 40 million years ago [8]. It was worked into tools by percussive flaking well before the first glass was made.

In this regard, it is still unknown the time and place of the origin of vitreous materials and its production. In *Naturalis Historia* Pliny the Elder wrote how glass has been discovered by chance. He describes how Phoenician merchants, who were shipping blocks of *natron* (a sodium carbonate used in the process of mummification), were cooking on a sandy beach using the natron as support for their pots. Whit the intense heat, the blocks would have eventually melted and mixed with the sand and wood used as fuel for the fire, resulting in the formation of glass.

Once glass fabrication was discovered, probably around the 3rd millennium BC in Mesopotamia and Egypt [9], the first glass-makers started to produce decorative objects, like vessels, and jewelleries simulating gems and semi-precious stones using silica with appropriate colorants such as copper, manganese, and iron salts. The pharaohs of ancient Egypt surrounded themselves with the stuff, even in death, leaving stunning specimens for archaeologists to uncover. His funerary mask sports blue glass inlays that alternate with gold to frame the king's face.

The most important developments in the early history of glass production include (i) the creation of Egyptian faience (4th millennium BC), (ii) the use of glass as independent material in Egypt and Mesopotamia (from 2500 BC), and (iii) the introduction of glass as a major industry in Egypt and Mesopotamia (from 1500 BC) [10,11]. Subsequently, the most relevant advance in glass fabrication was the invention of glassblowing by the Romans in modern day Syria around 100 BC, which increase the glass production centres throughout the Roman Empire and facilitate very much the shaping of objects as glass turned into an affordable commodity (*first golden age of glass*) [12–14].

During the Hellenistic and Roman time, glass was produced using natron as a flux, but its use progressively ended with the end of Western Roman Empire (5th AD) and replaced during the Middle Age with the use of wood ash as the main alkali that lead to the production of lower quality glass [9]. Early glass in the western world were almost all soda-lime-silica composition but varied with the availability of raw materials. During the roman period, but also during the Middle Ages, little attention was paid to the addition of alkaline earth elements, although they are known to be of utmost importance to prevent water diffusion and corrosion of glass. These elements were unintentionally added thank to the use of beach sands as ingredient for glass fabrication,

which contained enough lime and magnesia to yield chemical durability. The scares attention paid for the raw materials selection is also inferable from the fact that much glass objects of the Middle Ages appear dark green or dark brown as a result of the impurities that was present in the raw materials [15].

The glassmaking technologies declined until the 10th century AD when glass production was reintroduced and improved in Venice defining the period of the *second golden age of glass* [12]. The Venetian monopoly in the trade with Levant during the 12th and 13th century facilitated their exclusive access to high-quality plant ash sources, leading to the foundation of the famous Venetian glass industry and the production of the renowned *cristallo,* a very clear glass [10,16].

In the sixteenth century the glass making procedure involved the intentional addition of CaO with the invention of Bohême crystal, a type of glass similar to the *cristallo* one but that does not contain lead, but it is the combination of potash with chalk that is able to create a clear colourless glass, which was more stable than glass from Italy.

Many important evolutions characterised the period from the 17th and 18th century to the beginning of the 19th century. A real glass industry was developed all over the European continent leading to an important advancement of scientific knowledge by the introduction of scientific equipment such as microscopes, thermometers, chemical glassware, mirrors, lenses and so on. The use of glass in the modern society is so pivotal that is unimaginable thinking the human life without it, both as material used in everyday life and in scientific field, as well as in works of art.

1.1.1. Ancient glass raw materials for glassmaking.

The type of raw material selected have a crucial effect on the fusion and working properties of the glass made from it. Major, minor and trace components may be introduced in the glass batch by using primary raw materials (sand, and flux), or deliberately added colorants, opacifiers, and decolourants.The source of alkali that has been used to make the earliest glass was the ashes of halophytic plants.

The crucial characteristic that makes this typology of plant suitable for glassmaking is the presence of high quantity of sodium carbonate that interacts with silica reducing its melting temperature from c. 1720°C to a more manageable temperature of c. 1100°C for the production of soda-lime glass [17]. The halophytic plants was the dominant alkali source used in glass production in from c. 800 AD until the seventeenth century in the Middle East [9].

The chemical composition of glass can be determined by a variety of factors:

- Ash compositions differ according to the specific plant species used, and according to variations in ashing procedures because plant ash composition change with increasing temperature;

- The soil geo-chemistries in which the plants grow affect the chemical and mineralogical composition of the plants and their ashes;
- Purification of the ashes by dissolution, distillation and recrystallisation can reduce the levels of some insoluble components such as calcium and magnesium carbonate making the chemical composition of glass less durable;
- The melting conditions during glass production.

The specific concentration of alkaline and alkaline earth elements in the glass composition can provide provenance information about the glass made in particular location and period of time and can be used to know how the chemical composition of ashes were transfer directly into the glass determining its chemical and physical properties.

In particular, the practice of ashes purification, results in the reduction or removal of some insoluble salts of calcium and magnesium oxides, which play an important role in ancient glass as network stabiliser. Indeed, the crizzling of seventeenth-century Venetian glass can be easily attributed to the purification of ashes and to excess of alkali levels [18].

The use of *natron* as minerals flux for the manufacture of glass was introduced around the tenth century BC. This sodium-rich mineral, which occur at Wadi el Natrum on the edge of the Egyptian Western Desert, provided a purer source of alkali compared with plant ash [19].

Silica is a primary glass former used in ancient glass, which is present in soda-lime glass at levels of c. 65% to 70%. The source of silica for glassmaking could be quartz pebbles, riverine and coastal sand deposits or inland geological deposits. The purity of sand is greatly influenced by the type of rock from which it is derived and the distance over which the material has been transported before deposition. The presence of impurities, such as heavy minerals rare earth elements (REE), can be used to determine the geological provenance of sand use as raw material, as for example the relative levels of zirconium and titanium have been used to characterize the sand used in glass production [9]. Other impurities that occur in sand include shell fragments, which introduce the calcium-baring biogenic form of mineral aragonite ($Ca\,CO_3$) to the glass melt. In addition, feldspar often contain high alumina levels, and aluminium levels in ancient glass have been considered as having derived from feldspar in the silica used. Moreover, the so-called naturally coloured glass is a pale green colour caused by iron-rich impurities in the glass raw materials.

The third essential ingredient for glassmaking is a network stabiliser, such as calcium in most of the ancient glass, which provide glass durability. Although little attention was paid to the introduction of alkaline earth, beach sand and crude sources were rich in lime. In particular, the source of calcium in most natron glass is thought to be shell fragments, instead, in most plant ash glass is generally considered to be the plant used. The addition of such alkaline earth metals into the glass composition provide an increase of the chemical durability of glass itself, preventing water diffusion and network dissolution during corrosion processes [20].

Finally, metal ions such as Mn^{2+}, Mn^{3+}, Fe^{2+}, Fe^{3+}, Co^{2+}, and Cu^{2+} were added into the glass melt providing deep colours in translucent ancient glass. The huge of that colour depends not

only on the concentration of a specific transition element, and from its oxidation state (valence) that determines the number of electrons in the 3d orbitals, but also on the type of vitrifies (SiO_2, B_2O_3, etc.) and fluxes (Na_2O, K_2O, etc.) and on the procedure of manufacture (furnace atmosphere with oxidizing or reducing conditions). A series of factors can affect the colouring of the glass: i) types of raw materials, their processing and furnace temperature; ii) the use of transition metals ions; iii) the presence of opacifiers crystals; iv) the chemical environment and therefore the interaction between colouring elements and other elements in glass; and v) the atmosphere of the furnace (oxidizing atmosphere or reducing atmosphere) [21]. Iron, for example, gives a green colour to the glass as it is usually present as a mixture of ferrous ions Fe (II) (light blue) and ferric ions Fe (III) (yellow or brown). In Table 1.1 the main chromophores and the related colours are reported.

Table 1.1. Principal chromophores used in glass manufacturing and their coloring effects.

Colour	***Element/compound + chromophores ions***
Blue	cobalt oxide (Co^{2+})
Aquamarine	copper oxide (Cu^{2+})
Light blue	iron oxide (Fe^{2+})
Amethyst	manganese oxide Mn_2O_3 (Mn^{3+})
Violet	manganese oxide with trace of cobalt oxide
Transparent yellow	iron oxide (Fe^{3+}) – uranium oxide (fluorescent)
Opaque yellow	lead antimonate – lead stannate – cadmium sulfide – colloidal solution of silver
Amber yellow	sulphur-iron (in reducing conditions) $Fe^{2+}(O^{2-})3S^{2-}$
Green	chrome oxide (Cr^{3+}), iron oxide+copper oxide – cobalt oxide + lead antimonate or stannate
Orange	selenium – cadmium sulfide and cadmium sulpho-selenide
Red	colloidal solution of: Sulphur – cadium slenide –copper oxide or metal copper – gold
Opaque white	lead antimonate –tin oxide – lead arsenate – calcium or sodium fluoride
Black	mixture of iron, manganese, cobalt, and copper – carbon and sulfur – manganese oxide (high concentration).

In the western world, composition of ancient glass was mostly based on SSL combination, varying with the availability of raw materials in each production area. Also today, the 90% of the global manufactured glass is based on silica-soda-lime, composition that has been maintained quite similar over the centuries, except few changes introduced at the beginning of 1900 to improve the chemical durability and the resistance to devitrification. As well as SSL composition, many other types of historical glass exist, such as potash lime glass (K_2O – CaO – SiO_2), lead silicate glass (PbO – SiO_2), or potash lead silica glass (K_2O – PbO – SiO_2).

The historical evolution in the use of different raw materials in the production of glass means that today there are a wide variety of glass objects with different chemical composition that we can study to understand how the presence or absence of a particular element affects the

mechanism of alteration of the glassy material. This could be of fundamental importance to be able to attribute a more important influence in the mechanism of glass alteration to the chemical composition of the glass itself or to the environmental parameters (temperature, pH, humidity level) that interact with the material over time.

1.2. GLASS STRUCTURE AND ITS MODIFICATION

Glass, as ceramic materials, is produced from inorganic raw material at high temperatures. However, it stands out from other ceramics compounds since glass components are fused and subsequently cooled very slowly to rich solidification without crystallisation. Thus, a general definition of glass could be: "an inorganic product from the fusion cooled to a rigid condition without crystallisation. ASTM (C-162-92)". It can be deduced that glass has a non-crystalline, or amorphous, structure, where atoms are not regularly arranged, and there is no repetition and regularity at a wide range as is the case in a crystal lattice. From the thermodynamic point of view, glass solidifies in an unstable state and therefore has a higher internal energy compared to that of the corresponding crystalline phase with the same composition.

In nature, only few compounds have the intrinsic property to form glassy materials and crystallize slowly, for example silicon dioxide (SiO_2), boric anhydride (B_2O_3), germanium dioxide (GeO_2), etc. [22] For historical as well as for modern glass, silicon dioxide, called silica, is the main *network former* for inorganic glass. The elemental unit of the silica glass is the SiO_4^{4-} tetrahedron in which a silicon atom (ion) is bonded, whit an ionic-covalent bond, to four oxygen atoms (ions) (Figure 1.1) [23]. The SiO_4^{4-} tetrahedron shares only one corner with one neighbour but allocating all the available corners of each element.

The oxides that break the silica network are called *network modifiers*, and they are added to the silica glass in order to decrease the viscosity and improve its workability [8]. The oxygen of alkaline oxides, such as Na_2O and K_2O, or alkali-hearts oxides, such as CaO and MgO, fit inside the silica network breaking the SiO_4 tetrahedron resulting in the formation of oxygen ion with a non-shared electron, called non-bridging oxygen (NBO). Among modifier ions, the alkali (Na^+, K^+) are small, and their high mobility into the glass network decreases the chemical stability of the glass itself, favouring the aqueous corrosion. On the other hand, the alkaline-earth ions (Ca^{2+}, Pb^{2+}), with their two positive charges and the requirement of two non-bridged oxygen ions to compensate for their charge, are much less mobile and hinder the spread of alkaline ions. For this reason, the most common glass marketed contains both alkaline and alkaline-earth ions in order to reach easier manufacturing and higher chemical resistance [24] (Figure 1.2). The cations coming from the modifier oxides (Na^+, K^+, Ca^{2+}…) stay in the glass network as metallic ions ionically bound in the lattice interstices. Other oxides, known as *intermediary oxides*, are not able

to form a glassy network by themselves, but they can be added to an existing network, for example, Al_2O_3.

The bulk glass structure cannot be uniquely described, because it depends on modifiers concentration and type of network formers. When we consider, during the alteration process, complex glass composition whit different types of modifiers, the presence of non-bridging oxygen (NBO) causes the opening of the glass network while mobile ions (alkaline ions) diffuse [8]. The deleterious role of alkali can be limited by introducing alumina (Al_2O_3) and/or boron trioxide (B_2O_3) in the glass melt. The elevated resistance of natural glass over millions of years is to be attributed to their alluminosilicate-rich compositions, while borosilicate glass is commonly used for the construction of reagent bottles and laboratory flasks (in particular in pharmaceutical packaging) thank to its resistance to chemical agents [8].

The relative concentration of bridging and non-bridging oxygen atoms has an important influence on the properties of glass. The availability of modern and advanced techniques (such as X-Ray Phoelectron Spectroscopy, XPS, or Nuclear Magnetic Resonance, NMR) allows to describe glass and silica-based material in terms of local environment. In particular, XPS is one of the promising investigation technique in order to achieve better understanding of the complex phenomena of glass alteration mainly thanks to its ability to give information about the chemical bonds of the investigated atoms [25].

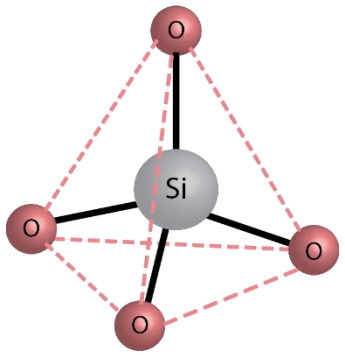

Figure 1.2-1.1. Schematic representation of a tetrahedral silica unit (not to scale).

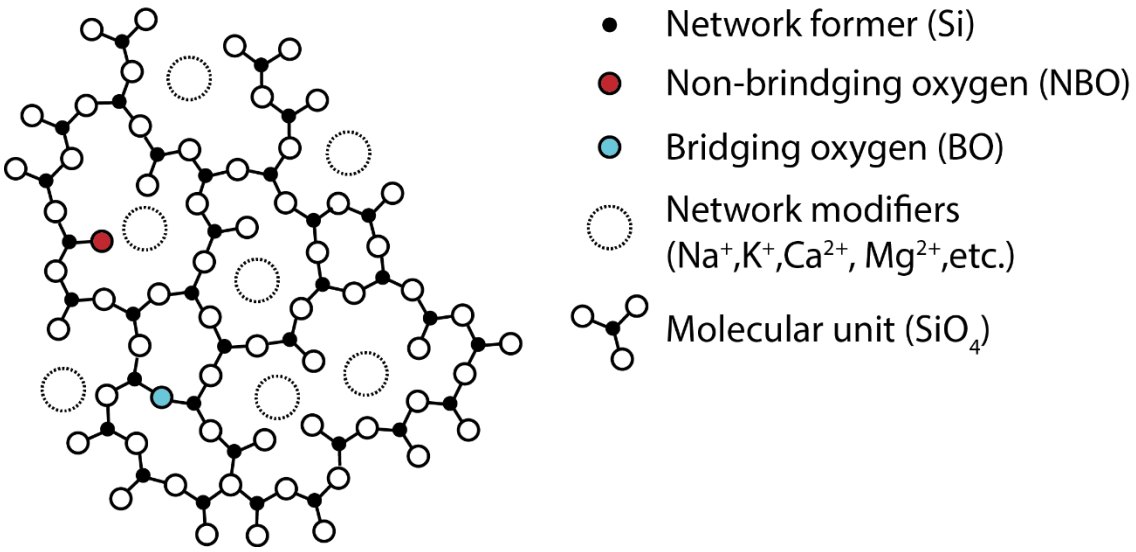

Figure 1.2. A planar scheme of the SSL network based on Zachariasen representation. For clarity's sake, only a few BOs and NBOs are highlighted.

Glass structure is out of thermodynamic equilibrium. The durability of glass can be considered as a function of both kinetic and thermodynamic stability of its oxide components. In thermodynamic equilibrium state, the chemical potential of the species on the glass surface and of the ones in solution are equal and thus no net mass transfer will take place. On the other hand, when one or more components are transported across the system's boundary, this system is defined open.

An essential factor to take into consideration for predicting the glass dissolution is knowing the relative concentration of bridging oxygen and non-bridging oxygen atoms [26]. The latter are bonded with only one silicon atom and their quantity within the glass network is proportional to modifier ions concentration. Addition of alkali cations breaks the Si-O-Si bond implicating a gradual loss of the silica network rigidity and a consequent depolymerisation of the vitreous material. Monovalent cations, Na^+ and K^+, connect to one NBO, while divalent cations, Ca^{2+}, connect to two NBO.

Considering the two possible configurations for an oxygen atom (BO and NBO), the silicon atom may be found in five forms of tetrahedral arrangement: Q_0, Q_1, Q_2, Q_3, and Q_4 where the subscript indicates the number of bridging oxygens (Figure 1.3) [27]. The structure of the glass network is the result of the rings and voids distribution regulated by the interconnection between these different silicate tetrahedra. The size of the voids in the network controls the rate of water diffusion, which is kinetically favored when the voids dimension is comparable with the diameter of water molecule (0.28 nm). In complex glass (mixed alkali glass), modifier cations can totally or partially fill voids, but, when the material is exposed to high relative humidity conditions, these alkali ions are leached from the surface of glass and replaced with hydrogen ions as part of the molecular water. Ion-exchange reaction drives the hydrolysis of glass network with kinetics depending both on the distribution of local structural units (Q_n) and on the modifier content. In

addition, the exchange of high-radius cations as K^+ from the bulk leaves a bigger void in the glass network than the exchange of smaller cation as Na^+, thus facilitating the entrance of water molecules in the deeper areas. In general, it can be said that the higher the concentration of NBO, the more ion exchange sites are available and the higher the rate of ion-exchange and network hydrolysis, following the reaction trend: $Q_1>Q_2>Q_3>Q_4$ [26]. For this reason, in the discussion about the kinetic of the processes of ionic exchange and hydrolysis reactions is essential to take into consideration the chemical composition of glass.

Taking into consideration what has been said above, knowing the chemical composition of complex glass and its Q_n concentration and distribution is fundamental to appreciate its chemical stability and its leaching resistance in order to adopt an adequate preventive conservation strategy.

Nevertheless, the glass reactivity does not depend on Q_n species only. Understanding the correlation between local structural features of the glass and the activation energies of individual bonds is also crucial to predict the dissolution mechanism of the glass network. Potential Mean Force (PMF) calculations estimated the activation barrier for Si dissolution in presence of aluminium (Al). They revealed that Al is easily dissociated from glass network, but Si dissociation is hindered when Al is present as a second neighbour [28]. As a result, Al causes opposing effects on glass durability if added at low and high concentrations: the addition of Al in small concentration increases the durability by reinforcing the strength of Si and increasing the polymerisation of the glass network, while at high Al concentration, the preferential release of Al results in the weakening of the silicate network. This predicting method can be extended to understand the role of Na, Mg, or B in more complex glass compositions.

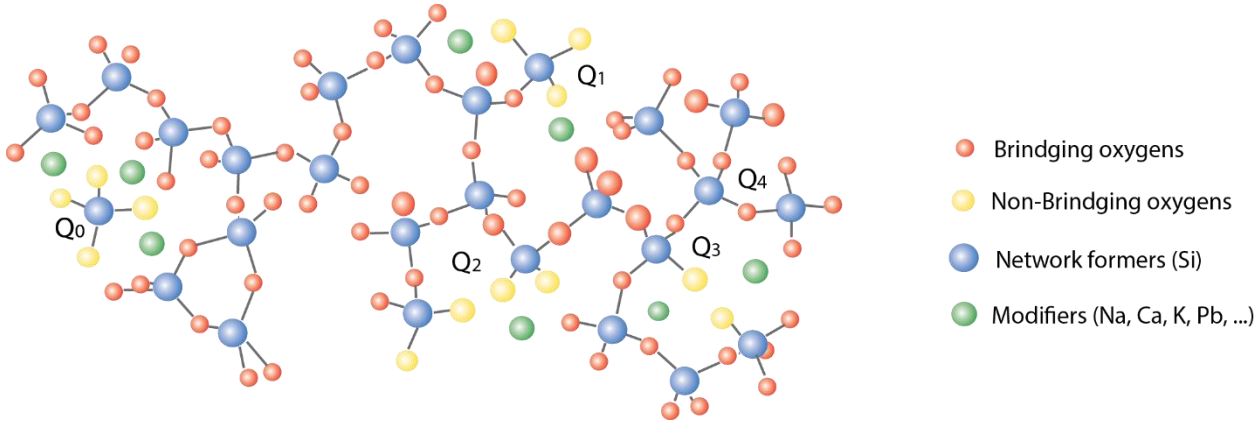

Figure 1.3. Q_n configuration in silica network.

Since the prediction of dissolution of glass network is a complicated topic of research, many recent works [29–31] reported the use of machine learning based approaches to account for the percentage of bridging oxygen species, network connectivity, average ring size, as well as the

composition modification due to the preferential release of modifier cations during the incongruent dissolution.

Several glass studies demonstrated the use of Raman spectroscopy as an analytical technique to discriminate the characteristic vibrational modes of each Q_n configuration [32–35]. Through the deconvolution of the Raman bands typically associated to the glass network, it is possible to determine the single Q_n distribution and to relate the variation of the area of relative Q_n band with the chemical composition of the sample analysed [36,37]. Using this analytical approach, Raman spectroscopy can be adopted as a technique to distinguish a stable glass from an unstable one, by the rigorous deconvolution of vibrational bands of glass network [27,36,38].

Nowadays, an analytical protocol that combines the potentialities of Raman spectroscopy described above with the advantages to use portable instrumentation is not available to evaluate the chemical stability of glass or to predict the glass network dissolution for preventive conservation purposes, or even to establish the suitability of glass as storage material for nuclear waste. Moreover, the in-depth space resolution of Raman spectroscopy is lacking if we want to determine the layered structures on an altered surface, which sometimes varies its features on the nanometric scale thickness. The association of other complementary analytical techniques would be ideal to optimize the reliability of Raman spectroscopy's results.

X-ray absorption near edge structure (XANES) spectroscopy is another interesting technique that has been used to study the polymerisation degree of SiO_4 tetrahedra silica glass. In XANES spectra, the position of the absorption peak is largely determined by charge of the absorber atom, which depends on the coordination of the nearest-neighbor atoms, the degree of polymerisation, and the presence of network modifiers and network substitutes [39]. A study conducted on silicate glass reported that the Si k-edge shifts towards higher energy with the increase of the polymerisation degree of the silica tetrahedra, while it shifts towards lower energy when Si is substituted by another network former (Al) [40].

The chemical changes occurring at the surface of a corroded glass often cause an alteration of the local environment of metal atoms, in particular of the metal-oxygen pair distribution, characteristics that have been measured using conventional and glancing angle geometry extended X-ray absorption fine structures (EXAFS) techniques. Examining modifiers distribution in the vicinity of the surface gives important hints on how the surface is modified as the corrosion advances [41].

As transition metal cations are generally of interest to apply X-ray absorption techniques, their study can be easily exploited to monitor the decay of historic glass. The modifications of the chemical environment of chromophore species (i.e., transition metal cations) can be recorded using both XANES and EXAFS techniques of a selected metal species in one altered glass sample. By this method, it was possible to determine the relationship between the oxidation state of Fe and Cu cations as the glass decay proceeds. On the contrary, Mn oxidation state was not directly correlated with the glass decay of the studied samples [42].

1.3. GLASS CORROSON

1.3.1. Introduction

Why do certain types of glass corrode?

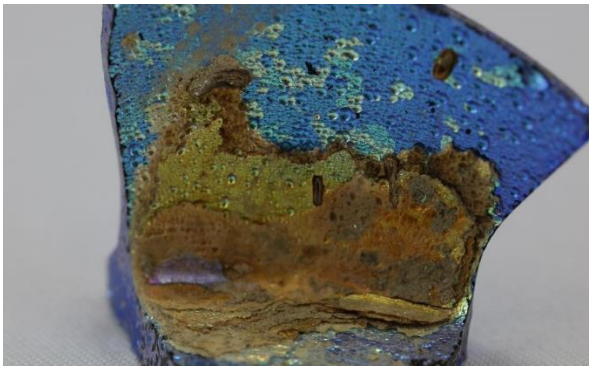

Figure 1.4. Severely corroded Roman glass

This is still a mystery and, despite numerous studies that have focused on the interaction between glass and the environment, the mechanism of glass corrosion is not fully understood yet. Different theories and hypothesis have been formulated about the process of glass degradation and published in scientific literature over the years. A universal and coherent model mechanism explaining the kinetic and dynamic of corrosion, and considering the different physicochemical conditions and glass composition, is still under debate.

The terminology used in the different published works is quite loose. The terms *corrosion*, *alteration*, *degradation*, and *dissolution* are often found interchangeably as synonyms, despite the different shades of meaning. For the sake of clarity, this dissertation will also use all this terms (i.e. *corrosion*, *alteration*, *degradation,* and *deterioration*) as synonyms when talking about all the phenomena inducing change of the materials' physicochemical properties, regardless the intrinsic or environmental factors that have determined it. On the other hands, the term *dissolution* will be used to refer only to the rupture of the Si-O covalent bonds and the breakup of the structural silica network, instead *leaching* will be used to identify the initial step of degradation, consisting in the loss of alkali and alkaline earths species ionically bonded to the silica network, and anticipating the network dissolution [43].

From an extrinsic point of view, during the 20th century glass alteration has been quite unanimously attributed to the reaction between the surface and the presence of water in contact with it. The phenomenon deriving from this interaction has been called *weathering*, and it takes

into consideration environments where water is present in both a liquid and a vapour state with relative humidity (RH) both > and < 100%. When water is in a vapour state (RH<100%) *weathering* is called *atmospheric alteration*.

1.3.2. Summary of mechanisms of glass alteration

According to Charles (1958) [44] three main chemical reactions occur: **(a)** penetration of water protons (H^+) into the glass network replacing the alkali ions (M^+); **(b)** rupture of the siloxane bonds by hydroxyl ion in solution; **(c)** production of hydroxyl ions from the non-bridging oxygen formed in reaction (1.b), which can react with H_2O forming OH^-species that are made available to repeat reaction (1.b), thus contributing to accelerate the process.

(1.a) $\equiv Si\text{-} OM + H_2O \rightarrow Si\text{--} OH + M^+ OH^-$

(1.b) $-Si - O - Si- + OH^- \rightarrow --Si -- OH + -Si -- O^-$

(1.c) $---Si -- O- + H_2O \rightarrow -Si -- OH + OH^-$

The interaction between water and glass can activate two different degradation phenomena, leaching and network brakeage, also depending on the pH of the solution in contact with the surface. During leaching, the aqueous solution in contact has typically pH<9 [45,46]. Initially, ion exchange occurs between alkali (Na, K) and alkaline earths (Ca, Mg) metals, forming ionic bonds with the oxygen of the glass network, and H^+ ion from the aqueous solution [24]. This is a diffusive phenomenon and the thickness of the glass region interested from the reaction (indicatively few microns) depends on the glass composition and on the time and temperature of the exposition. Altered layers formed on the surface can act as a diffusion barrier to further extraction, even if hazardous cracks allowing the penetration of water molecules into the pristine glass may form. The leaching type of alteration does not affect the Si atoms: the network distribution does not change, only Si-O-M bonds do, as we can see in reaction 1.a.
On the other hand, the ion exchange during leaching leads to a pH raise (above 9) due to the increase of alkaline metals' concentration in the water medium and the consequent depletion of H^+ concentration. An alkaline environment results in more aggressive attacks to glass network, since it promotes the dissolution of the Si–O bonds [47]. The reaction with hydroxyl ion (OH^-) breaks the Si-O–Si bonds (reaction 1.b) and silanol groups Si–OH are formed (reaction 1.c). Figure 1.5 reports a schematic representation of the reactions involved in the glass alteration process

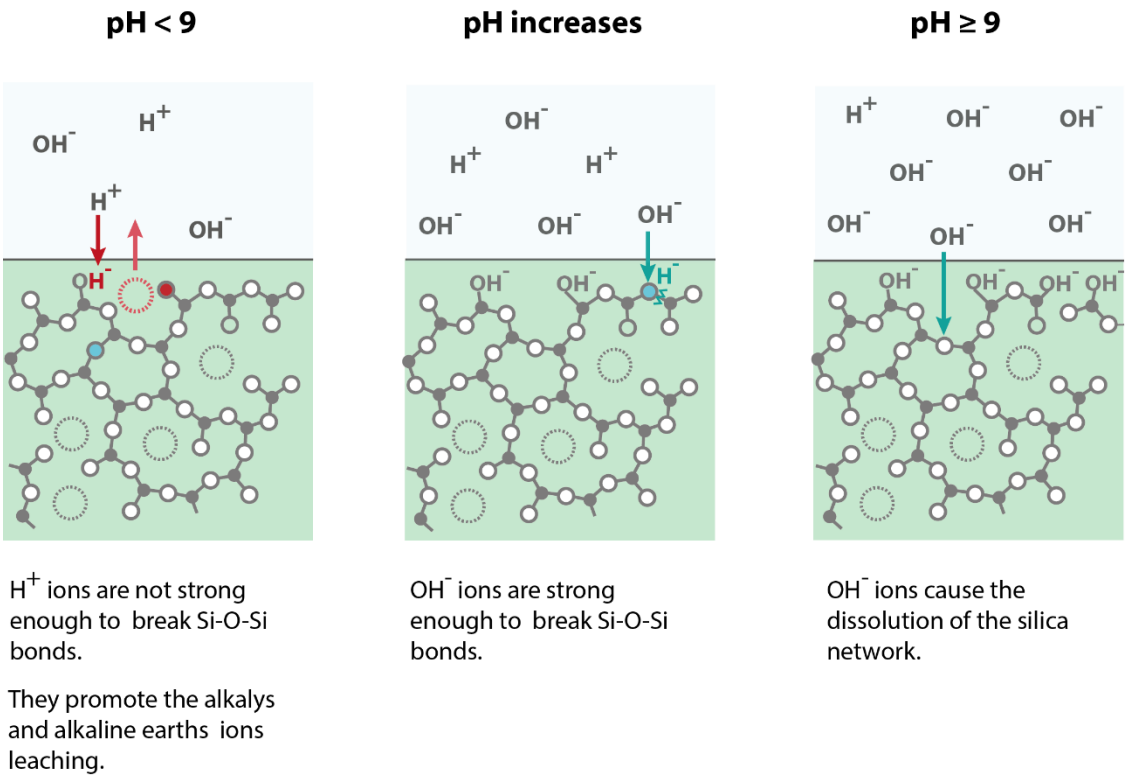

Figure 1.5. Schematic representation of the glass network's evolution in relation to the pH conditions of the environment and interaction with OH^- ions.

The sites left free by the leaching of cations from glass surface can be easily filled by hydrogen ions (having small ionic radius). The hydrolysis process induces the introduction of H_2O molecules and OH^- ions into the opened silica structure, increasing the rate of the hydration process and the ion exchange.

This model of glass corrosion is based on diffusion-controlled hydrolysis and ion exchange reactions, which lead to the formation of structurally and chemically distinct zones: an inner diffusion zone between the pristine glass and a depleted highly porous layer (gel layer) and an altered outer zone. The latter consists of a hydrated, cation-depleted layer resulting from a selective cation release. Depending on the alteration intrinsic and extrinsic conditions, secondary crystalline phases (i.e phyllosilicates) could be precipitated on the surface.

Besides water and alkaline solution, acidic agents, like fluorine and hydrofluoric acid solutions, determine more severe conditions for silica network's attack [48,49]. The breaking of the polar siloxane bonds Si-O-Si is susceptible to electrophilic attack, but the hydrogen ions alone are not strong enough to break the Si-O-Si bonds and to induce network depolymerisation [45]. Nevertheless, the presence of nucleophilic agents such as F^- and OH^- is responsible to increase the positive charge on the silicon atoms of the network, which can be attacked and dissolved.

However, the electrophilic attack of the oxygen atoms occurs only if the nucleophilic attack of the silicon atoms proceeds simultaneously. This situation takes place in the presence of hydrofluoric acid: the fluorine ion is a nucleophilic agent and, in the presence of H^+ ions, nucleophilic and electrophilic attack on the network can occur. Hydrochloric and hydroiodic acid can trigger simultaneous nucleophilic and electrophilic attack to the glass network too, but their degradation effect on silica is negligible [45].

The interactions and reactions that occur between aqueous solution and glass have been the object of extensive research over the years, both focusing on the pristine glass' surface and on the interface between pristine glass and altered layers, that is the area where the corrosion reactions take place. Studies were performed by using optical or scanning electron microscopy to see the changes in glass surface morphology due to the corrosion process [50], molecular spectroscopy such as Raman or Fourier-transform infrared (FTIR) spectroscopies to characterize the corrosion products [51] and to monitor the corrosion process observing the formation of Si-OH groups [52], respectively, and X-ray fluorescence (XRF) techniques for investigating the elemental composition [53]. In addition, surface techniques, such as Secondary Ion Mass Spectrometry (SIMS) and X-ray Photoelectron Spectroscopy (XPS), or ion beams analytical techniques (IBA) may provide information about the chemical composition of the first nanometres layers of altered ancient glass surface [54–56]. These analytical techniques give all together chemical and morphological information at different scales of observation, which have been key to support the formulation of the Classic theory of alteration and the Interfacial Dissolution Precipitation model for dissolution of vitreous materials.

1.3.3. The Classic Inter-diffusion model

The Classic Inter-Diffusion (CID) model of glass corrosion is based on diffusion-controlled hydrolysis and ion exchange reactions [57], which lead to the formation of structurally and chemically distinct zones: an inner diffusion zone between the pristine glass and a depleted highly porous layer (gel layer) and an altered outer zone. The latter consists of a hydrated, cation-depleted layer resulting from a selective cation release. Depending on the alteration intrinsic and extrinsic conditions, secondary crystalline phases (i.e phyllosilicates) could precipitate on the surface [58] (Figure 1.6). The concentration profile of highly soluble cations depends on their valence [59].

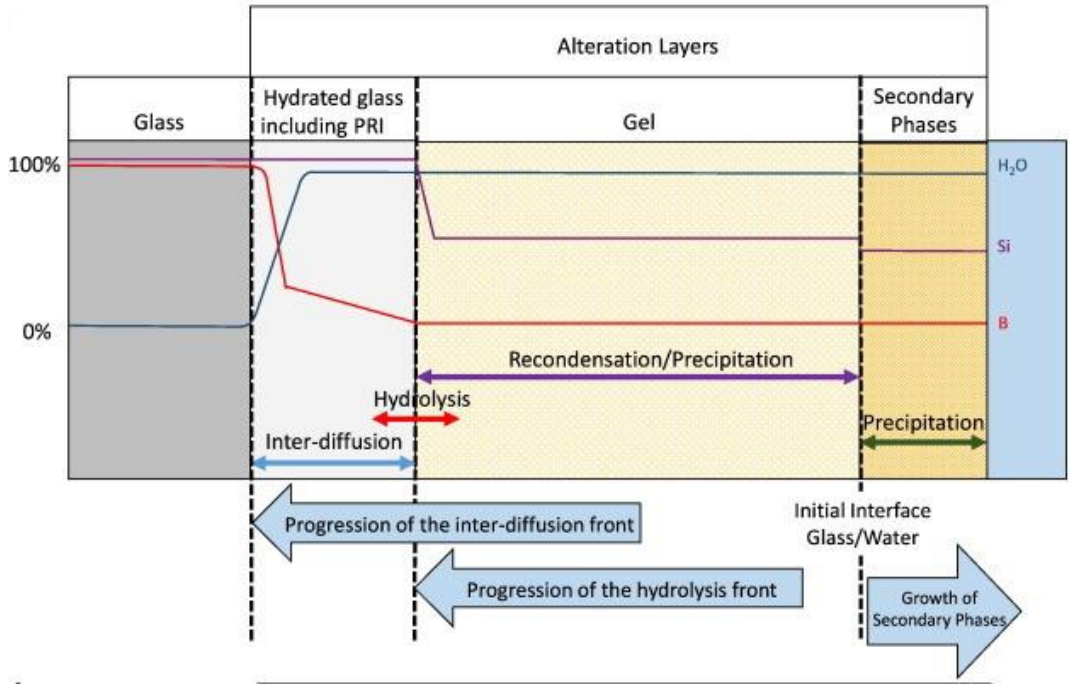

Figure 1.6. Schematic representation of the formation of the hydrated surface resulting from the inter-diffusion controlled glass corrosion mechanism (CID), Courtesy of Gin et al (2016).

The classic theory of glass corrosion is supported by different formulated models of ion-exchange that take into consideration the effects of the preferential dissolution of more soluble cations during the initial part of the leaching process [60,61].

Many experimental and theoretical results published in the last century reported that the leaching mechanism involves the preferential release of alkali and alkali-earth ions instead of network formers, such as Si or Al ions, with a consequent formation of alumina/silicate-rich layer on the surface of glass [45,61].

In general, the concept of preferential leaching is based on the thermodynamic and kinetic stability of the different glass modifiers. At lower temperature and for ions with the same charge, the diffusion of larger ions (for example Ba^{2+} or Ca^{2+}) becomes energetically unfavoured, while the smaller ions (for example Mg^{2+}) can move more easily through the glass network. In any case, double-charged ions show usually less diffusivity in SSL glass than single-charged ones, mainly for the marked effect of the very intense local electric fields acting on them. If the leaching mechanism proceeds, the solution becomes richer and richer in OH^- and its pH increases favouring the dissolution of silica and an opposite effect for the removal of alkali from the glass through the break of O-Si-O network. Preferential leaching supports the selective removal of specific cations (non-stoichiometric release) and designs a theory about incongruent dissolution of glass that explains the formation of altered surface layer.

In 1975, Doremus described the leaching process as an inter-diffusion of cations through the top layers of the glass network [57]. In mixed alkali glass, different modifier cations with different

diffusion coefficient are present and their mobility depends on multiple factors, such as their size and charge, the composition of pristine glass, and temperature [45]. When the temperature increases, the amount of extracted alkali increases in time, but it decreases as the alkali content in glass decreases. As a result, some glass compositions are more prone to leaching phenomena than others. For instance, silica rich glass –such as Roman glass- is more durable than poor silica glass, like medieval glass [62]. In addition, K^+, which is contained in medieval glass as monovalent cation stabilizer, is more susceptible to leach out from the deeper region of the glass network during atmospheric alteration than bivalent cations such as Ca^{2+}, present in Roman glass [63]. This behaviour is due to the bivalent cations forming stronger bonds with non-bridging oxygens, as previously mentioned. The preferential leaching of K^+ over Ca^{2+} during the weathering process has been confirmed also by an experimental study that investigated the weathering phenomena on naturally weathered potash-lime-silica-glass [64]. They observed this behaviour for K^+ cations even during leaching experiments in aqueous acidic solution.

In 1958 Gastev [65] calculated that the higher the Ca content is in glass composition, the deepest is the area interested by its leaching, but it remains less important than the depth interested by of leaching of Na and Si. In addition, the preferential leaching of Ca is enhanced when silica glass is acid-treated whit HF. In parallel, the presence of Ca contributes to controlling the Si extraction: higher Si extraction rates occur with low Ca concentration.

1.3.4. The Interfacial Dissolution Precipitation model

The technological development of the last decades allowed revealing increasingly more detailed evidence on the process controlling glass corrosion [66]. The chemical reactions proposed in the classic theory of glass corrosion (hydration, hydrolysis, and ion-exchange) are still considered as valid today in the most recent studies, but in the last years the attention of the scientific community has been focusing more on understanding how these reactions evolve kinetically and thermodynamically during alteration process, and how they influence the structural and microstructural properties of the alteration layer at the atomic scale [7,67].

In 2015, a nanometre-scale study [68] of glass corrosion performed using a combination of high mass and spatial resolution techniques supports a revised theory of glass corrosion, called *interfacial dissolution-reprecipitation* (IDP) model. The IDP model is based on the congruent dissolution of silicate glass coupled in space and time to the reprecipitation of amorphous spherical silica aggregates of variable size. In opposition with the traditional glass alteration model (Section 1.4.3), this recent theory asserts the stoichiometric dissolution of glass without interdiffusion-controlled ion-exchange mechanisms at the glass reaction front [68].

Hellmann et al. validated this model through the study of artificially aged borosilicate glass altered at 50°C in deionized water using a unique combination of techniques with high spatial and mass resolution [68]. By following the mobility of the major constituent elements of complex

borosilicate glass, an identical release behaviour has been noticed for modifier and former ions, independently to their charge. These results support two processes at the basis of this novel corrosion mechanism: the stoichiometric release of all the glass elements and the precipitation of amorphous silica with the formation of an altered surface layer. Furthermore, the interface between pristine glass and altered zone has been demonstrated to be chemically and structurally well sharp, with elemental gradients in the nano- to sub-nano-metric range.

A schematic representation of the IDP model is presented in Figure 1.7 according to the results of oxygen and silicon isotope tracer experiments in ternary borosilicate glass [69]. It can be outlined as follows:

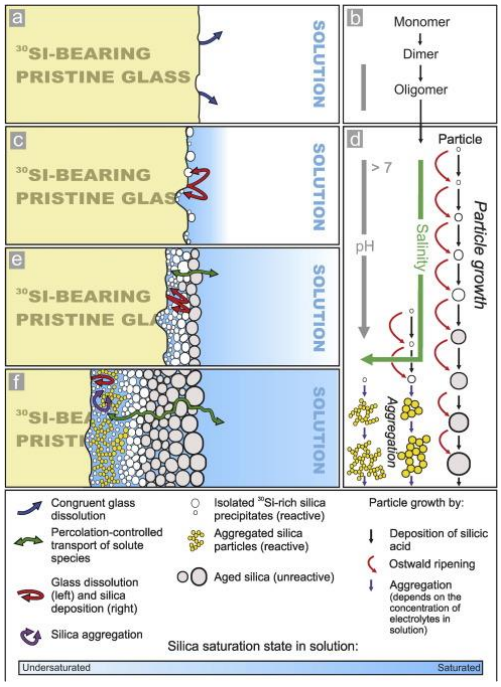

Figure 1.7. Schematic outline of the phases that describe the interfacial dissolution-reprecipitation model of glass corrosion. Courtesy of Geisler et al.

a. *Initial congruent dissolution of glass* is the first step occurring at the glass-water interface, when a silica-undersaturated solution is present. This stage continues until the amorphous silica solution is supersaturated and etching pits are formed on the surface. This stage includes microscopic reactions such as hydrolysis.

b. *Si-rich interfacial solution layer* is formed depending on the ratio of silica in solution to silica released during glass dissolution. Under this condition, the localised saturation of silica in solution promotes condensation and nucleation reactions that lead to the polymerisation of monomeric silica to form dimers and oligomers [66].

c. *Precipitation of silica* in the form of spheres on the dissolving glass surface occurs after silica supersaturation and nucleation in the solution.

d. *Formation of SAL* (Surface Alteration Layer) composed of altered amorphous silica proceeds along with congruent glass dissolution and further diffusion of dissolved species through the developing SAL. The local physicochemical state of the SAL determines the size of the precipitating silica particles, their arrangement, the number of chemical impurities that may be allocated in the silica layer formed, the distribution of glass, and the solution components across the SAL.

e. *Diffusive transport of water and dissolved species* through the corrosion rim continues depending on the porosity of the SAL, i.e., higher porosity values correspond to higher diffusion rates.

f. *Precipitation of secondary minerals* like zeolites and clays sometimes occurs within and at the silica surface. The nature of such minerals and their formation mechanism have not been well clarified yet, however they depend on the chemical properties of the alteration environment and the exogenous compounds present [70]. In the case of burial or undersea ageing conditions, when the glass is non-stop in contact with water, phyllosilicate is mainly formed through the intense hydrolysis and ion-reprecipitation processes. In addition, the alkaline and alkaline-earth ions released can react with the phosphates, carbonates and oxides present in the surrounding environment. Differently, in the case of discontinuous contact with water, which is typical of atmospheric alteration, the secondary crystalline phases are the result of the reaction between the leached glass ions and the gases of the atmosphere which forms a precipitation of sulphates and carbonates on the glass surface.

The reactions described above continue until the concentration equilibrium between glass composition and species in solution is reached, forming multilayer structures with alternating chemical composition, depending on the supersaturation-precipitation-supersaturation cycles that can eventually limit the transport of water and ions from the surface to the solution and vice-versa [69].

As described the IDP model entails the formation of alteration layer through the precipitation of hydrated species from the thin film of water to the hydrolysis front, with high degree of freedom to reorganize (Figure 1.8).This lead to a sharp concentration profile of highly soluble cations and an interstitial water layer that would allow an easy separation of the altered layer from the pristine glass [59].

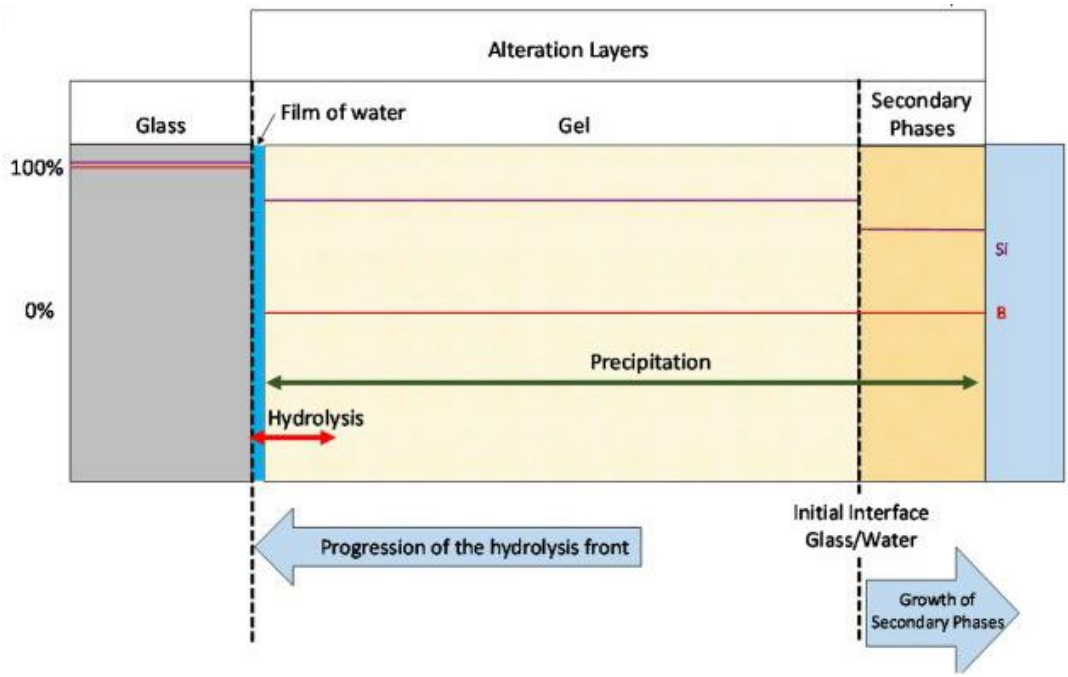

Figure 1.8. Schematic representation of the formation of the alteration layer resulting from the interfacial dissolution-precipitation model (IDP) of glass corrosion, Courtesy of Gin et al (2016).

1.3.5. Convergences between the two models and recent developments

The complexity of parameters influencing the glass alteration makes its prediction difficult by using simple descriptors arising from accelerated ageing tests. Three main kinetic regimes have been identified by the scientific community to describe the mechanisms controlling the alteration process [67].

- *Stage I,* the initial dissolution regime that takes place in diluted renewed solutions with high rate of glass hydration and fast glass transformation. This stage involves ion-exchange and matrix dissolution without condensation and precipitation reactions that impact the solution chemistry and the reactivity of the glass surface.
- *Stage II,* the residual alteration rate regime is established when the concentration of dissolved silica in solution is high enough to reduce the matrix dissolution, allowing the formation of a passivating alteration layer (low residual rate). This stage is associated with Si-saturated solution, the formation of passivated gel, and potential presence of secondary phases.
- *Stage III,* the potential alteration renewal which can trigger an acceleration of alteration for some glass types and boundary conditions. This acceleration is due to the partial or total loss of cohesion and barrier effect of the hydrated gel.

The rate of the reactions involve in the glass corrosion (ion-exchange, hydration, and dissolution) depends on factors such as glass composition, temperature, and pH. All of them may occur simultaneously during the process of alteration and can be rate-limiting as a function of the experimental conditions. For this reason, both the two models presented in literature (CID and IDP) are not able to describe universally the distribution of mobile ions and hydrous species inside the alteration layer.

A work published in 2017 [71] reported the in-depth characterisation using Atom Probe Tomography, TEM, and ToF-SIMS of the alteration layer formed under close-to-saturation conditions. The results revealed an alteration layer with a more complex structure in glass samples made of three different sub-layers (Figure 1.9): (i) close to the pristine glass, a thin hydrated layer containing all the glass components, (ii) moving towards the surface, a passivating layer with constant concentration of glass formers (Si, Al) and decreasing concentration of modifiers (Na, Ca) which is delimitated by a rough interface where alkali and alkaline earths are preferentially leached out, and (iii) an external nanometric layer where Si undergoes hydrolysis and condensation reactions [71]. These results are contradictory with the IDP model of glass corrosion recently designed, which highlights that many gaps are still present in the explanation of the mechanism of glass alteration.

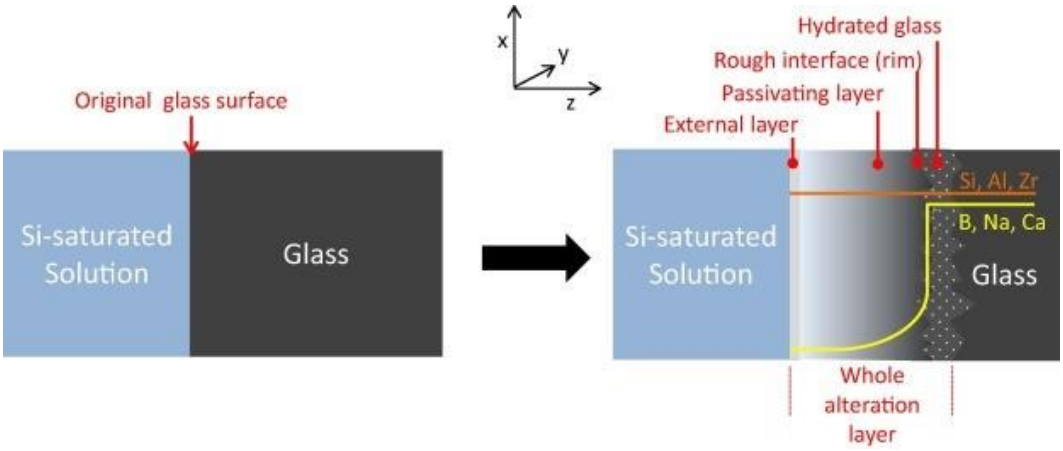

Figure 1.9. Schematic representation of the formation of the alteration layer resulting from the in-depth characterisation of borosilicate glass altered in silica saturated conditions, Courtesy of Gin et al. (2017).

A further recent study of a ternary borosilicate glass altered at pH 9, 90°C, and in condition close and far to saturation of amorphous silica validated an intermediate model for glass alteration [72]. This model describes glass corrosion as a result of competitive reactions of hydrolysis and in situ condensation. The predominance of one over the other strongly depends on the glass composition and environmental conditions.

On this point, it is important to underline that the universal application of the IDP model and others intermediate models to all silicate glass types remains an open question, since most of the latest research works have focused on artificial alteration of borosilicate glass only. The *trait d'union* between all silicate glass may be found by performing a multi analytical and high spatial and mass resolution investigation of different synthetic and geological glass compositions altered over long time periods. In this approach, the information retrieved from the observation of altered layers formed on ancient glass can be key to understand the complex interconnection between mechanisms responsible of the long-term transformation of glass network. The knowledge of the long-term behavior of glass structure is also of prime importance to predict the network dissolution in burial conditions in nuclear waste management studies [73,74].

1.3.6. Measuring glass deterioration on ancient samples

As emerged from the previous sections of this dissertation, the relationship between the processes of hydration, hydrolysis and ion-exchange during the glass alteration phenomenon is still a topic under discussion, since many and multiple factors play a role in the glass corrosion mechanism, making its explanation an almost unattainable scientific goal. This has represented an obstacle to the formulation of a universal theory capable of explaining the corrosion of glass up to the present day.

By observing how the knowledge of glass corrosion has developed over the decades, the key role of the study of the glass surface for a better understanding of its evolution clearly emerges. The most effective scientific approach available involves the analyses of glass from bulk to surface, which is intended as the interface with the atmosphere where the chemical and physical variations occur.

High-resolution surface techniques, such as XPS and ToF and/or dynamic SIMS, make it possible to investigate the chemical composition of the first nanometres of the glass surface and monitor its modification during the alteration process [75,76]. In particular, SIMS is one of the most appropriate techniques for the study of corroded glass [77], thanks to its capability to detect hydrogen. Another technique used to study the weathered surface of ancient glass that is often reported in literature is Laser Ablation Inductively Coupled Plasma Mass Spectrometry (LA-ICP-MS), which enable to obtain 2D and 3D elemental distribution with a spatial resolution as high as the spot size used for the analyses [78].

Critically speaking, the extensive study of glass surface composition using these advanced analytical techniques is still seldom considered when investigating the corrosion mechanism of glass both on ancient samples and through an artificial ageing approach in the laboratory [37,79,80]. It is essential to highlight that each surface technique has its own peculiar applications and limitations [81], but a combination of different techniques allows a complementary and more comprehensive characterisation of corroded glass.

To gain new understanding, well-designed experiments are crucial since the different mechanisms involved in glass corrosion, i.e., dissolution, molecular diffusion, ion exchange reaction, interdiffusion, formation of altered material, reactive transport, diffusive transport through altered layers, secondary phase formation, and environmental interaction, co-operate and influence each other. For this reason, it is fundamental to adopt a multi-scale analytical approach to investigate the process first from a macroscopic observation, then through a microscopic analysis, to achieve the chemical composition of the altered glass, and finally on a nanometre scale, to monitor the changes in the atomic configuration of the silica network occurring within the first surface layers. Only through the collection of all this morphological, structural and chemical information it is possible to have a complete picture of the evolution and the kinetics of the glass alteration process, including the modification of glass composition, and the knowledge of how and when to intervene for the conservation and preservation of glass objects, whether of industrial or historical interest.

Another key study for understanding ancient glass degradation is that of investigating the influence of intrinsic and extrinsic factors in the processes of alteration. This study is particularly apt to find the best conditions for preventive conservation of glass in museum collections or other sites of cultural interest. At the Victoria and Albert Museum, out of 6,500 glass vessels optically investigated more than 400 showed clear signs of glass deterioration [82]. More

recently, the glass storage conditions of the Royal Palace of Madrid and the Technological Museum of Glass (Segovia) were evaluated, detecting a high concentration of formic acid in the display cabinets and wardrobes, mainly due to the presence of wood, which results in a higher glass surface hygroscopicity (pH 8) [83]. Other similar surveys were performed in many different museums in Europe [84–86], demonstrating that a large number of glass objects in museum environments are in critical conditions due to extensive degradation. For this reason, the evaluation of storage parameters (relative humidity, temperature, and light) and glass conditions are an essential preventive action.

In addition, several methods have been used to categorise unstable glass in museum collections based on its appearance [87] or by analytical techniques, such as XRF [88], ion beam techniques (Particle -induced X-ray emission, PIXE, and Particle-induced gamma ray emission, PIGE) [89] or spectroscopic techniques (Raman and FTIR) [90,91], in order to determine glass composition. The application of these techniques in the analyses of cultural heritage objects encounters many operative limitations, as for instance the need to carry out micro-sampling or move the objects to specialised laboratories. The ideal analytical technique should allow the discrimination between stable or unstable glass even if its surface does not appear visibly signed. In addition, it should provide the chemical composition of the sample, be highly sensitive, and have a very fast time of analyses in order to characterise as many samples as possible in a short period of time. Consequently, it can be safely stated that no scientific and straightforward approach for understanding the chemical nature and composition of unstable glass in a non-invasive way and for large museum collections of glass objects has been developed yet.

1.3.7. Evolution of the surface alteration mechanism: composition and formation

The concept of glass surface alteration and its formation mechanism has evolved over time, together with the glass corrosion theory. This evolution was favoured by the possibility of using more and more technologically advanced techniques to observe the surface structure at a nanoscale, instead of limiting the observation to the macro- and microscopic scales of the early investigation approach.

In literature there is some confusion about the terminology used to refer to altered glass surface. Examples of the terms used include leached layer [92], gel layer [93], crust [94], silica rich layer, silica-rich film, alkali deficient layer, and hydrated layer [95]. The lack of an unambiguous term to indicate altered glass volume makes difficult to find a universal and acceptable description of the mechanism of formation of corroded glass surface and its composition. To avoid confusion, in a study which was carried out to explain the development of altered lamellae, Schalm used the term “transformed glass” to refer to the degraded glass surface [96].

One of the first characterisations of altered glass surface was conducted by Hench in 1975 [97], using a combination of analytical techniques that enables to obtain physicochemical information from different depths of the trasformed glass surface. He systematically studied the glass surface, using techniques like Auger electron spectroscopy (AES), infrared reflection spectroscopy (IRRS), and electron microprobe (EMP), and distinguished 6 main types of surfaces with increasing inclination to deterioration (Table 1.2.). Of these, only Type I is stable and shows no main differences with bulk glass. The other types are considered unstable and prone to deterioration over time. Type II and type IV are of interest for historical deterioration. Type II is formed when the glass contains a high level of network formers, and it involves the formation of a silica-rich layer on the surface that acts as a protective film, preventing the leaching of alkali ions and the rupture of the glass network (Si-O-Si). On the other hand, no protective film is formed for Type IV and so the leaching of alkali can proceed. This latter situation is typical of unstable glass.

According to Hench's classification, ancient glass has a surface that corresponds to Type II and Type IV surfaces, which are characterised respectively by the presence of silica-rich surface protective layers (when the concentration of network formers is high enough) and the presence of non-protective surface layers that allow the alkali leaching to proceed (when the soda to silica ratio is high enough) [97].

Table 1.2. The six types of glass surface described by Hench and Clark (1978).

Type I	Formation of a thin hydrated surface layer, without significant difference between the hydrated layer and the bulk glass. Stable glass.
Type II	Formation of a silica rich protective film due to ion-exchange of selective alkali ion, without further damage to the silica network.
Type III a	Formation of two layers of protective surface film of aluminium silica or calcium phosphate on top of a silica rich layer.
Type III b	Formation of multiple layers of hydroxides or oxides on the surface of the glass when exposed to water, especially on alkali borosilicate glass.
Type IV	Formation of silica rich non-protective film when the silica concentration in the glass composition is not high enough to prevent loss of alkali or destruction of the silica network. Unstable glass.
Type V	Formation of soluble glass with congruent dissolution and equal loss of alkali and silicate.

White described the structure of an altered glass surface in 1992 [60]. He reported the development of two distinct zones: a surface hydrated silica layer, also called silica gel, due to the precipitation of network former ions from the glass, and an interface zone between altered surface and the unaltered bulk glass called leached layer and formed because of the alkali extraction process. He also described the morphology of the surface hydrated layer as a non-planar surface that has a complex internal structure with metastable nature that can ultimately recrystallize [60].

Often, the surface of ancient glass found in poor conservation state is characterised by a multi-layer structure. Through the observation of ancient glass surface by transmission electron microscopy (TEM), a sequence of bands of different thickness has been recently distinguished [70], i.e., thinner bands called lamellae (20-50 nm) and thicker ones called laminations (0.1-4 μm), which consist in groups of laminae with the same orientation. The amorphous laminae, which are depleted of alkaline ions, are formed from the local rearrangement of glass elements resulting from the repetition of several cycles of interdiffusion and glass dissolution processes. Moreover, cracks are developed both perpendicularly and parallelly to the laminae and laminations. Based on this study, two main processes take place within the cracks, i.e., the migration of atmospheric solutions deeper into the bulk glass, thus moving the alteration front further, and the precipitation of secondary mineral phases which favours the mechanic separation and the loss of glass fragments.

Due to the ion exchange, which promotes the depletion of alkali, the alteration layers of ancient glass are normally high in silica and water content, but low in alkalis [98]. Many published research studies mention that also for glass samples altered in buried in soil the most common pathology observed is the formation of dealkalinisation layers [99–101]. One of these papers reports a stratigraphical analyses obtained by using a non-invasive technique (Laser Induced Breakdown Spectroscopy, LIBS) to observe the progressive dealkalinisation of glass bulk composition, reporting an increase in the calcium and sodium intensity signals on the glass surface [102].

In 2016, a study of the altered layers observed in ancient glass proposed a model to explain the formation process of this laminated degradation [103]. Thanks to optical microscope, FE-SEM and EDX analyses, it was possible to describe surface lamellae as an alternation of random amorphous silica nanoparticles with different packing densities and with thickness between 0.1 and 10 μm. Moreover, the growth of nanosized silica particles on the surface of the altered glass was observed to be one of the by-products of the leaching process of glass components that occurs under alkaline conditions. Even the novel theory of glass corrosion explained in Section 3.2 is underpinned by models that describe the formation of an alteration layer on the surface of corroded glass. Precisely, the ultimate stage of glass dissolution theory includes the formation of SAL [69]. Analytical observations of altered glass performed using high resolution techniques (such as atom probe tomography, APT, or energy-filtered transmission electron microscopy, EF-TEM) made it possible to assert that the SAL is chemically and physically well distinct from the pristine glass. The mechanism of its formation, however, is still being debated by the scientific community. The two main hypotheses are linked to the disputed models of glass corrosion and assume that the SAL results from the re-polymerisation reactions within the hydrated layer (after diffusion-controlled ion exchange reaction of mobile glass modifiers and condensation of silanol groups) in the first hypothesis, and from the precipitation of amorphous silica directly from solution in the second. Besides the novelty of the last research, further studies

are needed to validate the proposed model of lamellae formation using 3D and 3D higher-resolution imaging techniques, for example X-ray computed microtomography (XCT) both lab-based and synchrotron radiation-based, that enable the observation of nanostructured compounds deposited on the altered glass surface.

Another promising technique to investigate the altered surface of ancient glass is the above-mentioned LA-ICP-MS. Only one work, published in 2013 [78], presents the procedure to obtain elemental maps to investigate surface layer phenomena on pitted ancient glass. The results of this application showed that dealkalinisation is the main trigger mechanism for the formation of pits and of the so-called Liesegang rings on the surface of the sample. Despite the novelty of this research, the spot size of the laser beam used in the work (diameter of 80 µm) is higher than the average size of the corrosion marks present on ancient samples. The spatial resolution on the reconstructed maps can be improved by using smaller spot size of the laser beam (down to 10 µm) making it possible to obtain a resolution suitable for appreciating the chemical variability of extremely heterogeneous samples. This can potentially increase the understanding of the mechanisms of formation of these altered phases.

1.3.8. Intrinsic and extrinsic agents promoting glass deterioration

Many archaeological finds of SSL glass today are preserved intact, despite the alteration of the original physicochemical features caused by the burial environment they aged in over the centuries. Today, 90% of the glass manufactured globally is based on silica-soda-lime in a composition that has been maintained quite similar over the centuries, except for a few changes introduced at the beginning of 1900 to improve the chemical durability and the resistance to devitrification [104]. Besides SSL glass, many other types of ancient glass exist, such as potash lime glass ($K_2O – CaO – SiO_2$), lead silicate glass ($PbO – SiO_2$), or potash lead silica glass ($K_2O – PbO – SiO_2$) [17]. The optimal preservation of certain ancient samples and the complete collapse of others is the result of a complex interplay between their intrinsic material properties and the extrinsic factors acting on them.

Intrinsically, glass physicochemical properties play a significant role in determining its degradation behaviour. Such properties typically correspond to the chemical composition of glass, the nature of its surface, the presence of impurities, inclusions, inhomogeneity, and phase separations. In particular, the concentration of silica, alkali (soda, potash), stabiliser (lime, lead), as well as the inclusions of trace elements and additives like metal oxides, added into glass as chromophores, opacifiers and decoulorants all strongly affect material durability [105]. Small variations in the concentration of these components determine strong variations in glass durability. It has been reported that the durability of glass increases with the decrease of the ionic radius of the oxide species (M^+) present in the glass network as modifiers, in accordance with the thermodynamic stability of different types of binary alkaline earth silicate glass in water

[45]. Diffusion through the leached layer is more likely to occur for smaller ions, such as Na, Mg, Li, rather than for larger ones, i.e., Ca or Ba. Although all types of alkaline silicate glass are susceptible to weathering degradation, from a thermodynamic point of view stability increases as in the following: $K_2SiO_3 < Na_2SiO_3 < Li_2SiO_3$ [45].

The study of the varieties of composition of ancient glass and their resistance have made it possible to identify the presence of compositions that are more chemically stable than others and to define general conditions to discriminate between stable and unstable glass [106]. As mentioned in the previous section, in 1975, Hench studied the surface of glass and distinguished between 6 main types of surfaces with increasing inclination to deterioration in relation to their composition: the surface layers of the different glass types may have protective or non-protective properties for the glass substrate, depending on the capacity of reducing ion leaching and glass dissolution. This distinction leads to a definition of stable and unstable glass based on the different compositions of the alteration products that form the first surface layers.

A further way to discriminate a stable glass from an unstable one could be to use the ternary diagram of Figure 1.10, which was formulated in 1975 by Newton et al. [107] with a view to help predict the weathering behaviour of different types of glass. Plotting the concentration (mol. %) of network stabilisers (RO), network modifiers (R_2O), and silica (SiO_2) determines the chemical stability of a given glass composition, i.e., highly durable glasses are placed near the centre. This diagnostic model may work well when binary or ternary glass is considered, however complications may occur when classifying ancient glass, which has a more complex composition.

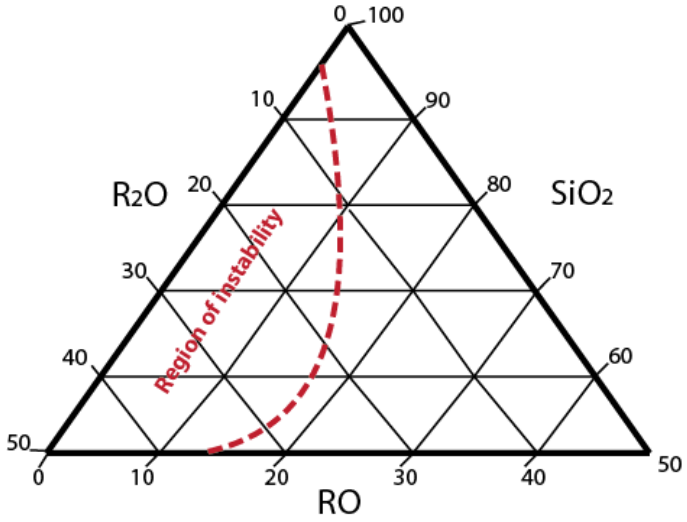

Figure 1.10. Triangular representation of the stability of glass composition. RO represent the content of network stabilizer, R_2O the content of network modifier, and SiO_2 the content of silica.

By using electron microprobe analyses (EMPA) and hydration-dehydration experiments on ancient glass Brill observed that a deficit of stabiliser (CaO content less than 4 wt%) combined with an excess of alkali (over 20 wt%) in SSL glass easily lead to an extensive surface deterioration

known as crizzling [95]. He defined as unstable glass the one with total alkali oxide concentration over 20%; this composition range determines silica network configurations that are open enough to facilitate the migration of monovalent cations. In line with these findings, other studies reported that an increase in the CaO to SiO_2 ratio increases glass stability, while a concentration of calcium oxide over 15 wt% entails rapid glass instability [45]. Recently, a comparison in terms of glass chemical stability was made using artificial mock-ups with different glass compositions which were exposed to high humidity environment and different levels of formic acid [104]. The results showed that glass with a higher content of stabilisers exhibits greater stability, especially glass with calcium.

The presence of potash as modifier and a low silica content in the composition make glass particularly fragile and susceptible to chemical alteration. Several works reported the considerable damage that affects medieval glass windows with Si-K-Ca-based composition, which is considered one of the most unstable [108–110]. Typical alteration marks are mainly pitting [111] or the formation of a corrosion crust [112] on the surface due to the combined attack of water and increased pollution in the air. The weathering crust is often very heterogeneous and fractured because of the wetting-drying cycle conditions and generally consists of calcite, gypsum and/or syngenite formed by the reaction between the alkaline elements released during ion-exchange and sulphur dioxide in the atmosphere [113].

In addition to the major elements discussed above, other minor elements may be present in the composition of ancient glass as decolorising, colorising or impurities of the raw materials used for their production. These minor elements can in turn contribute to the alteration process of the glass itself by giving rise to distinctive corrosion marks.

Using SIMS and nuclear reaction analyses (NRA) on the medieval glass paintings, exposed to ambient air for centuries, the weathering mechanism governed by ion exchange was observed to contribute to the alteration process resulting in the formation of an altered layer where K, Ca, Mg and Pb are depleted, and hydrogen is incorporated into the silicate structure. SEM-EDS chemical mapping confirmed the depletion of these alkaline and alkaline-earth elements in the altered layer and highlighted the presence of Mn where brown staining appears [114]. It has been well known that glass technologists used to add Mn, as well as Sb, to the glass melt as a decolorising agent, but it is also known that in this type of glass the appearance of brownish areas on the altered surface is due to an oxidation process of Mn(II) to higher oxidation states. It is generally observed that in the dark areas Mn is present in +IV oxidation state [115,116]. Nevertheless, a recent work performed using synchrotron radiation X-ray absorption (XAS) analyses on historical stained-glass windows, showed that the more extended brown altered areas contain Mn mainly in (+III) oxidation state [117]. Although brown/black staining has mostly been attributed to manganese compounds, iron (and titanium) compounds were often reported in association with the manganese [105].

Other elements which are often present in historical glass network as impurities can improve the chemical stability of glass. For example, low amounts of ZrO_2 (2 %wt) increase the acid and alkaline durability of glass [118], and a hydrated ZrO_2 surface can act as a barrier to further dissolution of other ionic species. More recently, it was demonstrated that substituting an insoluble oxide like zirconia to a fraction of silica slows the glass dissolution kinetics, but prevents the alteration gel reorganisation inhibiting the pore closure mechanisms and leading to greater degree of corrosion [119].

These results show that it is essential to know the exact composition of an ancient object to determine a range of the aging behaviour that it is prone to. To do that, it is important to consider also the presence of elements in lower or trace concentrations to fully describe the corrosion phenomenon and formulate models that are closer to real cases of ancient glass alteration.

Equally, studying the effect of extrinsic factors is essential to complete the prediction of the alteration, as they define the thermodynamic and kinetic of the ongoing process. Different environmental parameters have been indicated to have a role in activating and even enhancing the alteration reaction occurring in glass corrosion.

Water was observed to be the primary environmental ageing factor that causes glass deterioration by Lavoisier since the early 1770s [120]. Lavoisier also indicated two different mechanisms of water penetration into the glass network, i.e., through network voids between oxygen atoms in molecular form, and by hydrolysis and condensation reactions with the metal-oxygen bonds [26].

Besides water, other atmospheric conditions such as temperature, the pH of the environment, salts and ions concentration, relative pressure under burial or marine conditions, and the presence of water in liquid form (RH≥100%) or vapour (RH<100%), strongly influence the kinetic of the glass surface alteration and its chemical transformation. In particular, the alteration of silicate glass differs when it occurs in liquid-phase or in vapour-phase regime. In contact with water the glass surface undergoes chemical attack through ion-exchange and hydrolysis of metal-oxygen bonds. In vapour conditions (RH<100%) the hydration process does not release elements into the fluid, but it involves a redistribution of elements in the alteration layer [121]. The formed hydrated layer has chemical composition and porosity that are different from those obtained in liquid conditions, thus resulting in the glass durability properties specific for liquid or vapour-phase regimes. Even if the molecular process is the same, the interplay between the intrinsic and extrinsic variable changes affecting the macroscopic transformation of the material.

Many published papers of archaeological interest use the term weathering to refer to the typical degradation process that affects archaeological glass that has been exposed to particularly unfavourable environmental conditions (especially in burial and underwater contexts) [122], whereas the term atmospheric deterioration is used to describe glass that aged under the effect of water in the form of moisture (especially in protected environments like museum display

cases). From a scientific point of view, this distinction is confusing and partly incorrect since the phenomenon of weathering can also apply to degradation under atmospheric conditions. The only difference when dealing with atmospheric alteration is the state in which water is found in the environment, which is always in the form of vapour. On the other hand, weathering is a degradation process occurring through contact with water in the environment, both in the vapour and in the liquid state.

Palomar devoted many studies to weathering and to the comprehension of the environmental effect on the stages of glass alteration [123–125]. In particular, she reported the effect of coastal atmosphere on glass degradation [126], which is a scarcely investigated subject. The alteration of glass surface exposed to coastal environment is mainly caused by the high presence of liquid water that covers the glass surface, thus inducing a hydrolytic attack and the dealkalisation process, and by the high wind speed, which favours the transportation and deposition of sodium and chlorine ions on the glass surface. Marine aerosol in elevated concentrations represents a hazardous agent for the chemical stability of glass, since its action could increase the hygroscopicity of the glass surface and open the glass structure, allowing the alteration to proceed deeper into the glass.

Air pollution was identified as a particularly dangerous agent that enables to speed up and enhance alteration processes. In the museum context, the presence of carbonyl pollutants is generally the main cause of glass corrosion and of the formation on the glass surface of efflorescence salts as deterioration products [127]. With regards to historical stained glass, an experimental work carried out over a six-year period to quantify the influence of various air pollutants from different local environments (Europe and North America) on the degradation of potash-lime-silica glass, which has a similar composition to that of medieval stained glass, showed the formation, after exposure to rain and solar radiation, of crystalline carbon-rich products unlike those of samples aged under sheltered conditions [63].

The exposition to direct solar radiation is a further dangerous environmental factor for medieval stained glass since it could increase the surface temperature up to 40 °C on the hottest summer days. In particular, some coloured areas of glass windows seem to be more prone to an increase in surface temperature due to the presence of iron and copper ions as chromophores, which absorb the near IR radiation more easily [128].

A pivotal factor in determining the rate of glass corrosion is the pH of the attacking solution both in case of vapour and liquid conditions [4]. Under conditions of low pH (acidic solution), the deterioration mechanism predominantly involves the ion-exchange process due to the abundance of hydronium ions in solution and the formation of silanol groups [Si-OH], generating a hydrated gel on the surface which slows down degradation [129]. Differently, at high pH, the interaction between the glass surface and the alkaline solution leads to the dissolution of the silica network through the rupture of the Si-O-Si bonds, which implicates a

more aggressive condition. In the case of burial condition, the pH of the soil can determine both the kinetics and the outcome of the glass degradation phenomenon [129,130].

1.3.9. Evidence of degradation of ancient glass

Archaeological and ancient glass aged under different conditions (i.e., burial, in water, extreme environmental conditions) for several centuries shows multiple and clearly visible symptoms of deterioration that can help identify well distinguished classes of glass alteration. Specimen affected by dulling, pitting, discoloration and crizzling are common examples that can be observed. The formation of one rather than another of these visual effects depends on both the physicochemical properties of the glass and on the environmental factors they have been exposed to. More than one manifestation of alteration can be found in a single object, thus making sometimes difficult to individuate the most appropriate strategy of conservation and/or consolidation to apply.

1.3.9.1. Dulling and laminated surface layers

The term *dulling* is used for the loss of clarity and transparency typically observed in ancient glass and caused by the formation of layers of alteration products on the glass surface. As seen before in the general mechanism of glass corrosion (Section 1.4.1.), in presence of neutral or less acidic conditions, elements like alkali are typically leached out from the first glass layers onto the surface. These leached species, reacting with humidity and moisture of the environment, tend to form corrosion products (like salts) that build up on the object's surface and determine at first the loss of the original clarity [105]. In addition, at advanced stage of alteration, also hydrated silica (silica-gel) particles can also reprecipitate on the glass surface, leading to the formation of thicker alteration layers and causing an additional loss of glass transparency and the appearance of translucency [82]. This phenomenon is due to a combination of effects occurring between the local presence of water and the composition of glass, which determines the diffusion of ionic species from the first atomic layers under the surface to the environment and the consequent reprecipitation of hydrated silica and other alkali-derived compounds. The extent of the visual effect is much more considerable as the ion exchange proceeds and the thickness of the deposited layers on surface increases [92].

In more advanced stages, dulling can lead to the formation of thick iridescent multilayer patinas that may eventually detach in the form of crusts from the original glass substrate. These densely overlapping layers gradually penetrate deeper into the glass and they eventually change in colour towards darker hues [97]. The cationic species leached from the glass are often prone to reacting with the atmospheric anions, thus forming salts with hygroscopic properties on the surface. This generates a phenomenon called weeping, which was first described by Organ in

1956. Weeping can lead to the formation of crystals or solutions of salts, depending on their deliquescence relative humidity [131].

Figure 1.11 shows an example of the effect of an advanced stage of dulling on archaeological Roman glass. The optical microscope image shows a multi layered patina with peculiar iridescent metallic appearance, which was formed due to the interaction with burial elements during its ageing in contact with soil. Iridescence appears as a rainbow-like effect on the glass surface characterised by vivid colours like gold, pink and blue. It is a visible symptom caused by the change in the composition of weathered glass and it is often accompanied by the disintegration and flaking of the surface of early glass. In 1863 Brewster [132] demonstrated that this iridescent effect is due to the diffraction of incident light from layers of weathering products containing metal oxides formed after ion leaching. The rays of light are reflected from thin alternating layers of air and weathered glass crusts.

Another visible mark of the dissolution and precipitation reaction at the water-glass interface is the formation of peculiar chemical patterns that have been explained according to the theory of Liesegang rings (Figure 1.12). Diffusion, reaction, nucleation and crystal growth are all phenomena that have been used to formulate models that explain the Liesegang rings formation [133,134].

Dal Bianco et al. observed these weathering rings present on glass fragments from the Roman ship Iulia Felix found on the Grado lagoon, in North-East Italy, and dated back to the 2nd century AD [135,136]. This characterisation study showed a maximum diameter of the rings of about 1 mm and the interconnection of interface lines during the simultaneous growth of adjacent rings. This study did not report an exhaustive theory about the formation process of rings, but the authors observed that the structure was similar to the descriptions of Liesegang kinetic evolution of precipitates in gel found in other research works [137,138]. This assumption is acceptable since hardly corroded glass structure can be assumed as a gel where weakly soluble salts periodically precipitate due to the reaction between two soluble substances, one of which is dissolved in the gel medium. The final appearance of the precipitates depends on their solubility and on the initial concentration ratio of the reagents, but generally their aspect is concentric around the centre in which precipitation starts [139].

Nowadays, the formation of this type of rings on archaeological glass has been observed on the surface of samples recovered in submarine environment [92,140]: it is suggested that this specific environment play a role in the formation of the rings. The soluble substances present in marine water may react with soluble substances from the aged glass forming salt precipitates on the surface of glass that act as centre of nucleation for the growth of the concentric structure.

The mechanisms generating the formation of rings on altered glass surface has not been analytically confirmed and the study of the evolution of the kinetics that controls the ring growth on archaeological glass has not fully explained notwithstanding the availability of modern techniques.

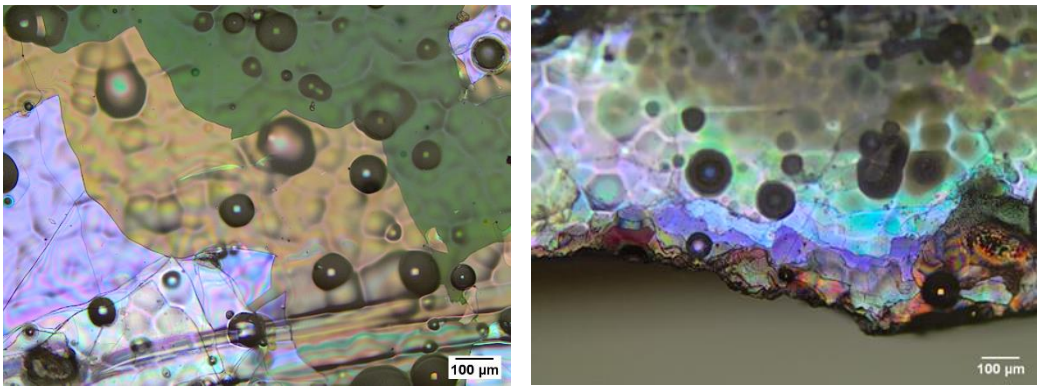

Figure 1.11. Bright Field Optical Microscopy images of an iridescent multilayer patina on a SSL archaeological glass sample, collected with Olympus BX43F optical microscope, x10 magnification. A detail of the indented rim where the overlapping of thin layers of altered patina is clearly visible (right panel).

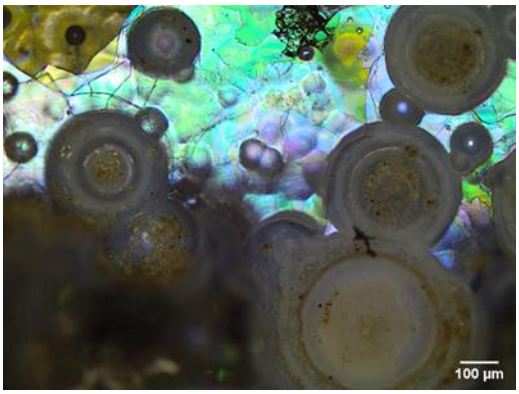

Figure 1.12. Bright Field Optical Microscopy image of alteration rings on the surface of a SSL archaeological glass sample, collected with an Olympus BX43F optical microscope, x10 magnification. It is possible to appreciate the interconnection between adjacent rings.

1.3.9.2. Pitting

The alteration phenomenon called pitting is described as micro, small or large based on pit size, and it can occur simultaneously at different individual sites that later merge into interconnected complex structures producing an altered top layer, which causes the loss of glass transparency [122].

Contrary to dulling, pitting is a visible mark of the weathering process, which occurs in alkaline solution [141]. As described in Section 1.4.1., during the alteration process in alkaline solution, the prevailing deterioration mechanism is the dissolution of the silica network through the breaking of Si-O-Si bonds. Subsequently, the prolonged exposition of glass surface to the

moist atmosphere causes an increase in the pH of the attacking solution, and ultimately pits are formed as a result of local dissolution of the silica network.

A model that explains the formation of altered pits was recently developed by observing the decay process of different silicate glasses in river and marine aquatic environments [123]. The experimental results showed that the alteration of SSL glass is characterised by a two-step mechanism. The first step, called “hydration period”, is short and causes the formation of isolate fissures, while the second step, called “pit development period”, involves the creation of basic species (OH-) during the dealkalinisation process that progressively break the silica network, thus widening the fissures to form pits. According to the results of this work [123], the formation of pits is correlated to a dynamic loss of mass, i.e., the slow rate of the first step of hydration allows the diffusion of solution and the consequent basic attack inside the fissures, causing local network dissolution. Figure 1.13 shows the surface of a Roman archaeological sample affected by pitting.

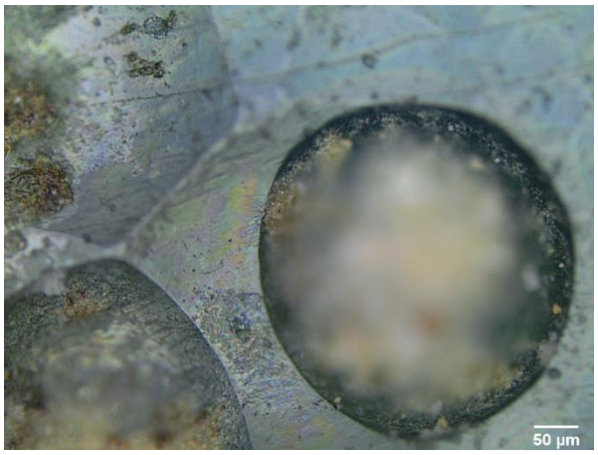

Figure 1. 13. Bright Field Optical Microscopy image of one pit on the surface of a SSL archaeological glass sample, collected with Olympus BX43F optical microscope, x10 magnification.

1.3.9.3. Discoloration

Discoloration effect can be often found on archaeological glass surface in combination with other types of weathering phenomena described above. It is caused by the migration of metal ions from the bulk to the surface of the glass. It is closely related to darkening, which occurs when the oxidation of certain leached ions, such as iron, manganese, and copper, changes the colour of weathering crusts, or due to the production of hydrogen sulphide by sulphur reducing bacteria in anaerobic environment and the formation of lead sulphide. The latter case occurs only when the glass contains high concentration of Pb oxide, and it is buried in anaerobic condition. In other cases, the presence of manganese and iron triggers the darkening of glass with the formation of brownish pits (Figure 1.14). Ancient glass contains these elements as impurity present in raw

materials (sand and wood ash) or thought their deliberate addition as chromophores or/and decolourant agent in form of minerals (i.e. pyrolusite)[9].

Many dark deposits are detected inside the dealkalinisation layer on the glass surface of Roman glass samples [102]. Secondary electron images showed that they are formed by the interconnection of spherical particles about 2 µm in size and the chemical analyses reported the iron and manganese oxides as main components of these deposits. During the leaching process, Fe (II) and Mn (II) ions are hydrated and oxidized giving rise to the formation of dark amorphous products which precipitate into pores of the leached silica film.

Several authors report that manganese inclusions may come from the burial environment accumulating among altered layers [142,143]. In particular, Schalm et al. [142]through the analyses of 14^{th}–17^{th} century window glass, concluded that the formation of Mn-rich inclusion takes place simultaneously with the growing of leached layers settling along interface among them and its concentration is caused by a strong contribution of the environment (soil) where the glass was buried for several centuries. Chemical studies on the composition of soil, where archaeological glass aged for centuries, may validate the hypothesis of ionic exchange between the elements of the soil and the elements of the glass network, presenting the opportunity to understand how the interaction with the external environment can drive the process of alteration in different types of glass.

The phenomena of discoloration and darkening seem to interest the behaviour of metal oxides, added to the glass composition as chromophores or decolourants in ancient glass. Their contribution in glass stability has not been considered yet in the study of glass alteration mechanism, but the analyses of the visible alteration features on archaeological glass can be considered a good approach in order to verify how the presence of colorant agents into the glass composition influences the properties of glass and its resistance to deterioration. Considering this aspect, further research may be conducted for a more complete design of the glass corrosion process.

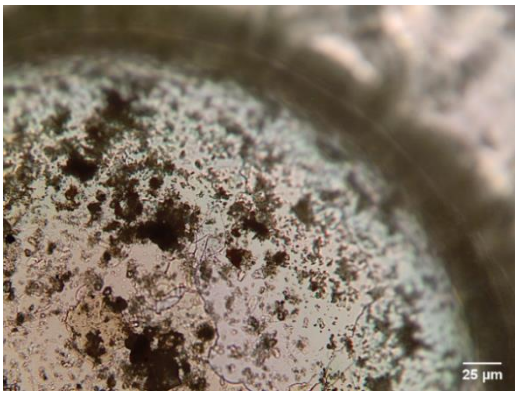

Figure 1.14 Bright Field Optical Microscopy image of brownish deposition formed on the surface of a colourless SSL archaeological glass sample, collected with Olympus BX43F optical microscope, x10 magnification.

1.3.9.4. Crizzling

Crizzling, also known as glass sickness or glass disease, has been identified as the appearance of minute cracks on the glass surface (Figure 1.15a), which develops over time and penetrates deeper in the body of the object, eventually leading to its physical collapse. Crizzling was found to be a major conservation problem for glasses stored in museums and in private collections, due to two main factors: the unstable composition and the storage in fluctuating humidity environments [144]. Better storage conditions can slow down, but not stop the deterioration, because the role of glass composition remains a key factor in the evolution of the crizzling alteration.

Early publications reported the chemical effects causing crizzling through experiments that reproduced the condition of glass alteration in the laboratory. The results showed that crizzling is mostly associated with glass compositions characterised by high alkali and low CaO contents, and/or a high K/Ca ratio [145].

In 1975 Brill [95] first used the term crizzled to describe glass with a decrease in its transparency due to the formation of fine cracks on the surface. He noted that certain glasses that were in contact with water for centuries do not exhibit a high degree of degradation, however, once they are exposed to museum storage conditions (light, low RH and temperature), the beginning of crizzling can be seen. This alteration mechanism is due to the dehydration of the glass surface, i.e., the low RH in museum display cases (15-20 %) causes a loss (up to twenty percent in weight) of the water that penetrated the gel layer of altered glass, bringing on a significant loss of volume in the gel layer itself which ultimately results in the cracking of the glass surface [95,144]. In general, the cracking of the hydrated gel layer that is formed on the surface of unstable glass can be attributed to several factors, including the dehydration of the gel layer itself, as mentioned above, the leaching process, which can lead to network contraction after the replacement of larger alkali ions (Na^+) by smaller hydrogen ions (H^+), and the different coefficient of expansion of the bulk glass and the gel layer [24].

The guidelines of Corning Museum of Glass [122] describes the process of crizzling in five stages. In the first stage (Initial stage) the glass has a blurred appearance due to the presence of leached alkali on the surface. During this phase, it is still possible to wash the surface and the glass can return to its original appearance. Conversely, in the second stage (Incipient crizzling) the haziness remains also after washing and the glass surface exhibits fine cracks similar to tiny silvery lines. Cracking progresses in stages three (Full blow crizzling) and four (Advanced crizzling) until it gets to the deepest regions, leading to the loss of small fragments. Eventually, crizzling is so deep that the glass loses its structural integrity, even without any external contribution (Fragmentation stage).

Often crizzled glass has a pinkish hue. When alkaline leaching occurs and the glass structure is open, the manganese ions present in the surface cracks oxidise, yielding a pink colour [144]. This phenomenon is more evident in ancient glass which contains manganese as a decolourant.

To limit the evolution of the crizzling process, preventive conservation is an essential strategy for the safety of museum glass objects. The Corning guidelines set the optimal RH range for glass conservation between 35 to 65 %, however crizzled glass or glass with a particularly fragile composition require specific individually controlled cases with a lower RH inside.

In the case of archaeological glass that was buried for centuries, cracks comparable to crizzling alteration are found on the surface of the glass fragments. These peculiar cracks (Figure 1.15b) are filled with mineralised material probably coming from the soil, and their formation mechanism is under study.

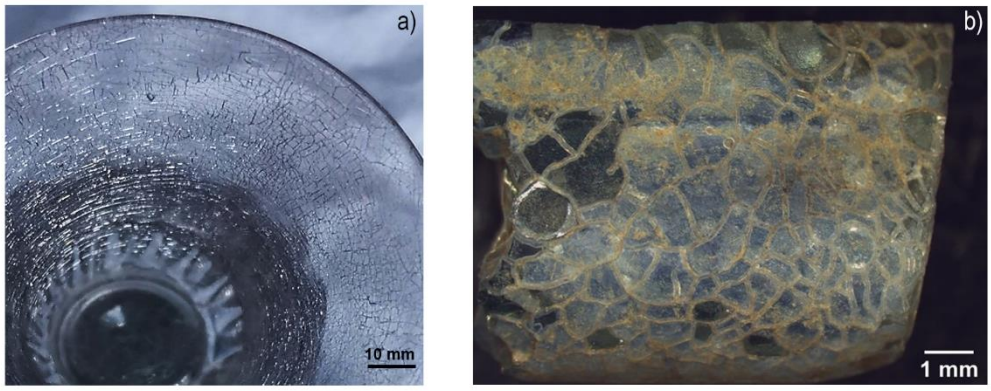

Figure 1.15 a) Macroscopical evidence of crizzling in historical Venetian glass object; b) Cracks filled with mineralised soil that covers the whole surface of a SSL archaeological glass sample collected with a NIKON SMZ 745T stereomicroscope, x2 magnification.

1.3.10. Reproducing glass alteration under experimental conditions

As mentioned in the previous sections, the characterisation of the physicochemical properties of ancient glass is pivotal for understanding the effects of intrinsic factors acting in the corrosion process. The same approach cannot apply to the study of extrinsic factors, as these are closely linked to the environmental conditions acting during the alteration process over centuries. For this reason, detailed knowledge of the effect of these extrinsic factors requires the development of appropriate artificial ageing protocols, which allow the modelling of the phenomenon as a function of these parameters.

Real cases of glass degradation are the result of the combined actions of the intrinsic and extrinsic factors reported above, which generate entangled mechanisms of ionic interdiffusion from the glass network to the environment and vice versa. From an experimental point of view,

studying this interconnected process of ionic interdiffusion and the formation and growth of novel phases implies the need of relying on simplified model systems to investigate the effect of specific variables to the detriment of others, which are kept constant.

The study of the effect of the various factors on glass degradation has attracted the curiosity of researchers since the beginning of the XX century. Already in 1925, G. W. Morey [146] stated that the subject was still in an empirical state, despite the considerable number of works carried out. At that time, to understand the effect of water on the alteration process many experiments were conducted by varying temperature, the pH of the environment and glass composition. While glass alteration in contact with water in a liquid state was widely studied during the 1900s, testing approaches in unsaturated atmosphere have been seldom explored until more recently [147]. In 2020, Majerus et al. [1] published an overview of the experimental protocols for glass alteration tests in unsaturated atmosphere. All the tests reported were conducted under RH<100% condition and, when a saline solution was present, their configuration ensured that the samples were never in contact with it.

Four types of set-ups can be distinguished in relation to the device used to control the experimental atmosphere: (i) a desiccator with or without saline solution; (ii) a climatic chamber; (iii) a hermetic box containing saline solution in a dedicated compartment; (iv) a Teflon-lined autoclave inside an aluminium container (to ensure homogenous temperature) containing saline solution and placed in an oven. These results obtained under RH<100% suggested that the glass alteration mechanism was different from the ones obtained in contact with liquid water (RH>100%). In the first alteration steps, the glass dissolution rate under unsaturated conditions increased with the RH value of the atmosphere, but it was always lower than the rate observed under liquid conditions [4,148], except for a few cases, where glass compositions classified as stable under liquid conditions became the least durable under vapour conditions (for instance Mg and Fe-rich compositions, or unstable mixed-alkali lime compositions of historical glass).

With unsaturated humidity, the dissolution rate of alumino-boro-silicate [4] glass and soda-magnesia-lime silicate glass were found to decrease as the alteration proceeded with time, sometimes following a square root time dependency, thus suggesting a diffusion-controlled hydration process for both these compositions. Instead, historical glass with mixed-alkali lime compositions showed an increment in the hydration rate with time, thus confirming that glass composition is a critical factor that influences the rate-controlling processes in the initial stages under unsaturated conditions.

Besides glass composition, even the chemical nature of the alteration layer is tightly controlled by the conditions under which it degrades. The only corrosion product that is always observed in all types of altered glass is a surface altered layer of variable thickness. The deposition of secondary phases, the formation of pitting, laminated layers and iridescence, and eventually the occurrence of crizzling are all phenomena that are preferentially encountered under specific

conditions, such as unsaturated humidity [4], burial [149], or alternating levels of high and low RH [95]. Under experimental conditions, these former corrosion types are hard to reproduce, since they are the result of complex synergetic effects of extrinsic and intrinsic alteration factors acting for long time-ranges that are not allowed by normal experimental set-ups.

In the last two decades, several works have been done to explore the effect of ageing in burial or marine environments on the alteration mechanisms of glass and on the formation of new alteration phenomena. A considerable number of works focused on the prediction of the durability of high-level nuclear waste glass and the migration of radioactive and non-radioactive elements into the burial soil [3,150,151].

In the field of cultural heritage glass, experimental studies simulating ageing in soil are less common [149,152,153]. In a recent work, Palomar et al. tried to replicate ageing in soil in a natural burial environment to understand the corrosion mechanisms acting on different ancient glass types (Roman, medieval, lead crystal glass, common window glass) [129]. The burial tests were set up to last 300 days and were carried out at 60°C, so as to accelerate the alteration processes. The pH of the burial soil and the glass composition showed to have a key role in controlling the reactions between the constituent glass elements and those from the environment.

Especially considering burial artificial alteration of mixed alkali glass compositions with low silica concentration, acidic or neutral conditions (pH 6.5 – 7.5) lead to the formation of micro pits and cracks, whereas an iridescent and translucent layer is formed on the surface of glass under alkaline soil condition (8.0 – 9.0) [130]. Instead, silica-soda-lime glass shows a different behaviour. In fact, in acidic soil the formation of both isolated and interconnected fissures may be observed. Whereas under neutral and alkaline soil conditions an increase in the number and depth of pits, whose rate of accretion depends on the content of alkaline oxides in the glass, can be detected, with a considerable increase in the diffusion of surface degradation under the alkaline condition [129]. This experimental evidence is a clear example of the necessity to consider glass composition and environmental factors simultaneously when approaching the understanding of the glass corrosion mechanism.

Other studies dedicated to the alteration of historical glass in museums environment have shown that no direct correlations between chemical stability and any parameters of the chemical compositions exist [1]. Many laboratory tests have been carried out to simulate the effect of the museum environment (room temperature and different RH values) on the degree and on the kinetic of the degradation [125,154]. They all highlight that the chemical stability is always influenced by both the overall glass composition and the characteristic parameters of the external environment.

Alloteau et al. recently demonstrated that the formation of the hydrated silica layer on surface is not correlated with the loss of alkali and alkaline-earth cations from the glass matrix [3]. To state that, they performed ageing test in static conditions (no T and RH cycling) at

controlled temperature and humidity (RH 85%) on three different types of unstable historical glass (soda-lime silicate from antiquity, mixed alkali silicate from middle-age/renaissance and potassium silicate from XVI-XVIII century). The conditions were set to avoid any liquid water flow on the samples during tests. A combination of analytical tools was used to characterise the aged samples from the structural and chemical point of view. Surface state analyses and hydration rate measurements suggested that, in water vapor conditions, the process of glass hydration is independent from dealkalinisation: at higher temperature (80°C) hydrolysis predominates over diffusion processes and solvation, whilst at lower temperature the two processes proceed together in parallel.

To conclude, as well as the content of alkalis and stabilisers in the glass composition, the parameters of temperature and humidity severely impact the chemical durability of a glass, because they strongly affect the concentration of alkalis and hydroxyl or non-bridging oxygens in the hydrated layer. It is not possible to determine generally which factor is more influent in the process of glass alteration, because the final degradation symptoms are always the result of a mutual effect between all the above-mentioned parameters. In addition, all the existing studies on the alteration of glass in museum considers static conditions of temperature and humidity, which is far from the real environmental conditions found in museum. Further investigations at cycling conditions would be significant to help assessing the risks of alteration and failure in most of the museums displaying unstable and fragile glass object.

The studies involving ancient glass compositions are still not numerous if compared to the studies carried out on glass alteration in other research fields [81,155,156]. The same compositions found for the altered layer of nuclear glass are often not confirmed by the few experimental studies involving typical ancient glass compositions [1]. Despite the broad spectrum of glass compositions reported in atmospheric alteration studies, a unified conclusion cannot be drawn because of the different experimental approaches (type of set-up, %RH, T, time duration, characterisation techniques) adopted in each glass application field. This lack of coherence is not surprising, since alteration phenomena are described differently in each applicative field. Ageing tests are generally performed at different time scales and operative temperatures, while characterisation techniques investigate different scales of observation. As an example, the cultural heritage community often describes the initial alteration stage with the formation of salts on the glass surface. In the cultural heritage field, where optical microscopy is routinely employed for detection purposes, the hydrated layer is generically called alteration layer, since it is not possible to characterise its chemical properties. Instead, nuclear glasses are characterised using more advanced methods with higher spatial resolutions (as scanning electron microscopy, SEM) and the chemical properties of the hydrated surface layer are revealed and always reported in literature. Moreover, the use of higher testing temperatures and RH values make the

comparison of results even more confusing, because of the influence of temperature on the reaction kinetics and the nature of product formations.

As it appears from this dissertation, over the years many experiments aimed at understanding the phenomenon have been reported in literature and almost as many methods have been proposed. Only few of them have led to comparable results without having to make several generalisations, as the reactions occurring are particularly affected by the experimental conditions and great care must be dedicated in defining these conditions when reporting the results. Nevertheless, this abundance of results represents an outstanding opportunity for future research studies in this field, which will be able to rely on advanced analytical approaches and more accessible high-resolution techniques even for the domain of cultural heritage science. For instance, FIB coupled with TEM and STEM-EDS can be used to observe the internal multi-layered structure of altered surface and the interface between the glass and the corrosion products, with the aim of following the mechanism involved in the formation of hydrated gel and other forms of glass alteration [72,74]. Another example, is the use of multi-elemental 2D and 3D laser ablation-ICP-mass spectrometry mapping procedure to obtain chemical images to retrieve in-depth chemical information and investigate surface layer phenomena [78].

1.4. AIM OF THIS THESIS

1.4.1. The troubled conservation of ancient glass

Ancient glass, when exposed to critical and adverse conditions, goes to meets its partial or total transformation due to the corrosion process, even when more chemically stable. Being glass a non-porous material, the interactions between a vitreous object and environmental agents (humidity, temperature, light) firstly interest the visible alteration of its surface, which may appear iridescent or opaque due to the formation of corrosion products or the exfoliation of altered layers. Often, salt depositions, mainly of a carbonate nature, are formed inside such alteration layers contributing to induce, apparently, cohesion among them [157]. For this reason, removing these salts during the glass cleaning treatment could represent a complication for the restorer because of the risk of complete disintegration of altered layers.

Another cause of glass degradation lies in the natural instability of the matrix of ancient glass that, based on its chemical composition, over a long time, tends to “reorganize” its amorphous structure towards the crystalline one as that of silica, the principal component of glass. This phenomenon, known as devitrification, brings on the formation of cracks that facilitate the aggression of environmental agents allowing the glass corrosion to proceed forwards until the complete pulverisation of the vitreous object.

In the light of these considerations, it can be stated that glass restoration is a complicated practice since rarely glass admits mistakes. For this reason, there are only few laboratories and

restorers specialised in the fine-tuning of a glass conservation strategy and its application to ancient glass*.

To resolve the conservative problems related to archaeological glass, two are the main actions needed: the identification of alterations and the attempt to contrast them delaying their effects by employing focused restoration work. The extensive study of the chemical, physical and structural properties of glassy materials is fundamental to identifying alteration phases developed on the ancient glass objects, implicating the need to perform laboratory analyses before acting any conservative treatment. In addition, this recommendable procedure finds further explanations considering that the intrinsic composition of glass strongly affects the formation of alteration phenomena, often independently from the surrounding conditions of conservation [158].

In the following chapters, we will see that a low concentration of alkaline-earth ions (such as Ca^{2+}) coupled with a high concentration of alkaline ions (such as Na^{+} or K^{+}) into the glass network favours the leaching out of latter that accumulate on the surface developing iridescent patina and alteration crusts. Nevertheless, even an excess of calcium content is dangerous for the chemical stability of glass, which induces a faster loss of alkaline ions with a consequent glass devitrification [24]. In addition, other metal ions added into the glass matrix as chromophores or opacifiers can influence the glass degradation process. For example, some recent research has demonstrated that the brownish depositions detected inside the dealkalinisation layers on the archaeological glass surface are composed of iron and manganese oxides [142].

Recently, at the Metropolitan Museum of Art in New York, hundreds of glass vessels have been subjected to new restoration work because of the degradation effects of inadequate storage and the inadequate consolidation strategies and materials used in previous treatments [157]. As mentioned above, erroneous cleaning operations are often the cause of irreversible effects of glass alteration.

The main evidence concerning glass conservation is the lack of a clear and shared technical-scientific planning among all the parts involved in this field, as instead is the case in other areas of restoration. The restorers should work in synergy with the chemists in choosing the best way of glass preservation and in researching and experimenting with novel materials developed for this purpose, considering that a glass artifact, depending on its composition and on the environmental conditions, to which had been exposed, undergoes to different physical and chemical processes. For this reason, the consolidation or preservation treatment must be responsive to the particular nature of the glass in question and its degradation, making it difficult to have a single solution that works for all situations.

** The most relevant: The Corning Museum of Glass (New York-USA), Centro di Conservazione e Restauro La Veneria Reale (Torino-Italy), Royal Institute for Cultural Heritage (Brussels-Belgium).*

1.4.2. Current conservation strategies

The practices adopted for ancient glass conservation can be generally divided into two categories [105]:

1. Passive conservation, which entails actions aimed at minimising and preventing the decay of the artefact. These measures consist of controlling the parameters of the surrounding environments where the glass artefacts are storage or displayed, without any direct conservation intervention on the artefact. This procedure deals with aspects such as humidity and temperature management, air movement, shock and vibrations damping, lighting systems and various pollutants control.
2. Active conservation, which entails actions directly applied to a glass object aimed at stopping damaging processes or reinforcing its structure. According to Koob, the three principal conservation interventions are [159]:
    - adhesion, also called assembly or repair, is one of the most common purposes of conservation treatments, consisting of the reconstruction of existing fragments that may not be presentable or intelligible;
    - loss compensation, also called gap filling, is a restoration technique that involves the partial or full replacement of missing parts for providing additional structural support or for aesthetic appreciation for museum display;
    - consolidation includes stabilisation, prevention of additional deterioration, or strengthening of the material surface for stabilisation purposes.

In the framework of active conservation, the cleaning treatment is the basis activity for each restoration intervention, and it can be carried out both mechanically and chemically. In more recent years, this procedure establishes to soften the scale (understood as corrosion products formed on the glass surface) to be removed, limiting the use of water, but preferring the application of organic solvents such as acetone, ethanol, or ammonium carbonate in different concentrations.

For the other purposes of glass restoration, such as the before mentioned replacement or reconstruction of missing parts, each restoration centre has an own protocol using different products based on the internal experimentation. This mainly because, to this day does not exist a specifically design product for the restoration of glass artefacts does not exist synthetic resins used for this scope are those used in other areas of restoration.

The most common resins used in the different phases of restoration (consolidation, adhesion and loss compensation) are: Paraloid B-72 (acrylic resin), Araldite 2020 and Epo 150 (epoxy resins). Since the 70s, Paraloid B-72 has been particularly used, as consolidant, in solvents as acetone or toluene, which allow the penetration of resin [159]. The consolidant solution should be prepared to achieve the desired result. In some cases, weathered layers are so thin and fragile that touching the surface causes loss. In this case, the better choice is to use a very low concentration (<3% w/v) that may impart little or no strength, while a high concentration (>15%) may not penetrate at all.

Even though Paraloid B-72 is much appreciated in the conservators' community, it is important to highlight that it shares, together with other organic materials used in this field, some issues related to vapour permeability and photochemical stability [160–162]. In the former case, depending to some extent from concentration and solvent type, vapours penetration can lead, over time, to salt or pollutants being trapped beneath the consolidant, attacking the glass surface. In the latter case, upon light aging, Paraloid B-72 is subjected to yellowing phenomena, tends to become brittle and to develop an acidic pH. The degree to which Paraloid B-72 is susceptible to these phenomena depends strongly on the environmental conditions. An indoor application, with a low UV exposure and controlled humidity and temperature conditions is far better than an outdoor application where weathering agents can give cause of concern over time.

Epoxy resins thermosetting resin systems made up of two parts: one incorporates the epoxide group, and the other is the hardener that reacts with the epoxide and cross-links the molecules. They have been successfully used to stabilize the cracks, in particular for glass objects affected by crizzling. One of their main drawbacks is related to the fact that these polymers are thermosetting, which means that they crosslink during the curing process, forming irreversible chemical bonds. Consequently, it is difficult to remove them if needed, because, when exposed to solvents epoxy resins will tend to swell. Moreover, even if there are formulations, like aliphatic epoxies, that are more resistant to UV light, yellowing phenomena are still a problem that occurs with time [163,164].

The latest research in the field of glass conservation, highlighted the possibility to use hybrid organic-inorganic treatments as glass consolidants. Tetraethoxysilane (TEOS) is one of the most diffused alkoxysilanes precursor used to obtain inorganic sol-gel materials used for prepared water-repellent sol-gel coating [165]. Different inorganic treatments through the sol-gel route have been studied to obtain silica thin films for the protection of soda-lime glass, lead glass and potash-lime-silica glass. In many case, these silica film are functionalised with various alkyl groups or metal ions to obtain specific properties such as hydrophobicity, or mechanical resistance [166].

Sol-gel proved to be a promising research area thanks to its versatility that allows formulations ranging from inorganic systems to hybrid ones. Nevertheless, improvements in the efficacy of these treatments are still necessary, in particular heat treatments should be limited as much as possible and tests on pre-aged samples should be carried out in order to verify the quality of the deposition even when the sample is not flat and smooth.

1.4.3. Diagnosis and conservation: how to conserve ancient and precious glass objects that present heavily degree of degradation?

Nowadays the glass degradation phenomenon is mainly studied using artificially aged mock-ups. This approach, as described above, has certainly helped the scientific community to design models of glass corrosion, but with the inherent limitation of not being able to extend the tests over a long period of time comparable to what glass as a material is thought to cover (i.e., nuclear waste applications).

For this reason, the research activities reported here should divulge, among the scientific community of glass, the importance of studying ancient glass as unique real proof of the interaction between different environments and specific glass composition during extremely prolonged periods of natural ageing process. This approach improves the knowledge of glass alteration, which will turn fundamental especially in the coming years, when the use of glass will further expand, thanks to its sustainable and recyclable properties. A deeper understanding of its physicochemical and mechanical properties will be the key to study new ways to improve material's performance and its corrosion resistance, to finally develop novel technological and industrial applications in the most different fields of application.

With this purpose, this thesis intends to shed light on how the comprehensive characterisation of ancient samples and the use of laboratory-based ageing methods can be used together as an instrument to get information from long-lasting real-case alterations from one side, and to monitor step-by-step the alteration process on the other. Indeed, the information obtained by this combined approach represents a unique opportunity to complement and unify the actual theories of glass corrosion, which cannot be reached exclusively from laboratory-based studies only, because of the clear experimental limitation of time.

Finally, a novel and complete strategy to approach the problem of ancient glass corrosion and stabilisation is here proposed. Combining the results of the multi-analytical characterisation of archaeological glass samples and artificially aged mock-ups, it represents a means to shed light and master the connection between composition, structure and properties of glass, in order to proceed towards the design – in the next future - of an innovative and advanced solution for glass consolidation and preservation.

1.5. REFERENCES

[1] O. Majérus, L. Patrice, I. Biron, F. Alloteau, S. Narayanasamy, D. Caurant, Glass alteration in atmospheric conditions: crossing perspectives from cultural heritage, glass industry, and nuclear waste management, Npj Mater. Degrad. 4 (2020) 27. https://doi.org/10.1038/s41529-020-00130-9.

[2] F. Alloteau, O. Majérus, I. Biron, P. Lehuédé, D. Caurant, T. Charpentier, A. Seyeux, Temperature-dependent mechanisms of the atmospheric alteration of a mixed-alkali lime silicate glass, Corros. Sci. 159 (2019) 108129. https://doi.org/10.1016/j.corsci.2019.108129.

[3] F. Alloteau, P. Lehuédé, O. Majérus, I. Biron, A. Dervanian, T. Charpentier, D. Caurant, New insight into atmospheric alteration of alkali-lime silicate glasses, Corros. Sci. 122 (2017) 12–25. https://doi.org/10.1016/j.corsci.2017.03.025.

[4] T.A. Abrajano, J.K. Bates, C.D. Byers, Aqueous corrosion of natural and nuclear waste glasses I. Comparative rates of hydration in liquid and vapor environments at elevated temperatures, J. Non-Cryst. Solids. 84 (1986) 251–257. https://doi.org/10.1016/0022-3093(86)90783-0.

[5] R.H. Brill, H.P. Hood, A New Method for Dating Ancient Glass, Nature. 189 (1961) 12–14. https://doi.org/10.1038/189012a0.

[6] K. Yamasaki, Y. Saito, Investigation of Corroded Ancient Glasses by X-ray Diffraction, Proc. Jpn. Acad. 36 (1960) 503–505. https://doi.org/10.2183/pjab1945.36.503.

[7] L. Deng, K. Miyatani, M. Suehara, S. Amma, M. Ono, S. Urata, J. Du, Ion-exchange mechanisms and interfacial reaction kinetics during aqueous corrosion of sodium silicate glasses, Npj Mater. Degrad. 5 (2021) 1–13. https://doi.org/10.1038/s41529-021-00159-4.

[8] E. Le Bourhis, Glass: Mechanics and Technology, 1st ed., Wiley, 2007. https://doi.org/10.1002/9783527617029.

[9] J. Henderson, Ancient Glass: An Interdisciplinary Exploration, Reprint edition, Cambridge University Press, Cambridge, United Kingdom New York, NY, USA Port Melbourne, VIC, Australia, 2016.

[10] S.C. Rasmussen, How Glass Changed the World, Springer, Berlin, Heidelberg, 2012. https://doi.org/10.1007/978-3-642-28183-9.

[11] M. Tite, A. Shortland, S. Paynter, The beginnings of vitreous materials in the Near East and Egypt, Acc. Chem. Res. 35 (2002) 585–593. https://doi.org/10.1021/ar000204k.

[12] E. Axinte, Glasses as engineering materials: A review, Mater. Des. 32 (2011) 1717–1732. https://doi.org/10.1016/j.matdes.2010.11.057.

[13] D. Foy, Technologie, géographie, économie : les ateliers de verriers primaires et secondaires en Occident. Esquisse d'une évolution de l'Antiquité au Moyen Âge, MOM Éditions. 33 (2000) 147–170.

[14] D. Foy, M. Picon, M. Vichy, V. Thirion-Merle, Caractérisation des verres de la fin de l'Antiquité en Méditerranée occidentale : l'émergence de nouveaux courants commerciaux, in Exchanges and trade in glass in the ancient world, international colloquium of AFAV, Aix-en -Provence and Marseille, June (2001) 41-86.

[15] J. Henderson, The raw materials of early glass production, Oxf. J. Archaeol. 4 (1985) 267–291. https://doi.org/10.1111/j.1468-0092.1985.tb00248.x.
[16] H. Tait, 5000 years of glass, London, British Museum, 2012.
[17] Th. Rehren, I.C. Freestone, Ancient glass: from kaleidoscope to crystal ball, J. Archaeol. Sci. 56 (2015) 233–241. https://doi.org/10.1016/j.jas.2015.02.021.
[18] D. Dungworth, C. Brain, Late 17th-Century Crystal Glass: An Analytical Investigation, J. Glass Stud. 51 (2009) 111–137.
[19] I. Freestone, Primary glass sources in the mid-first millennium A.D., Free. C 2003 Prim. Glass Sources -First Millenn. AD Ann. 15e Congr. L'Association Int. Pour L'Histoire Verre 111-115. (2003).
[20] G.S. Frankel, J.D. Vienna, J. Lian, J.R. Scully, S. Gin, J.V. Ryan, J. Wang, S.H. Kim, W. Windl, J. Du, A comparative review of the aqueous corrosion of glasses, crystalline ceramics, and metals, Npj Mater. Degrad. 2 (2018) 15. https://doi.org/10.1038/s41529-018-0037-2.
[21] E. Ferrara, J. Henderson, The Science and Archaeology of Materials: An Investigation of Inorganic Materials, Am. J. Archaeol. 106 (2002) 472. https://doi.org/10.2307/4126285.
[22] W.H. Zachariasen, The atomic arrangement in glass, J. Am. Chem. Soc. 54 (1932) 3841–3851. https://doi.org/10.1021/ja01349a006.
[23] G. Henderson, The structure of silicate melts: A glass perspective, Can. Mineral. 43 (1921) 1921–1958. https://doi.org/10.2113/gscanmin.43.6.1921.
[24] J.J. Kunicki-Goldfinger, Unstable historic glass: symptoms, causes, mechanisms and conservation, Stud. Conserv. 53 (2008) 47–60. https://doi.org/10.1179/sic.2008.53.Supplement-2.47.
[25] G. Pintori, E. Cattaruzza, XPS/ESCA on glass surfaces: A useful tool for ancient and modern materials, Opt. Mater. X. 13 (2022) 100108. https://doi.org/10.1016/j.omx.2021.100108.
[26] B.C. Bunker, Molecular mechanisms for corrosion of silica and silicate glasses, J. Non-Cryst. Solids. 179 (1994) 300–308. https://doi.org/10.1016/0022-3093(94)90708-0.
[27] P. Colomban, Polymerisation degree and Raman identification of ancient glasses used for jewelry, ceramic enamels and mosaics, J. Non-Cryst. Solids. 323 (2003) 180–187. https://doi.org/10.1016/S0022-3093(03)00303-X.
[28] K. Damodaran, J.-M. Delaye, A.G. Kalinichev, S. Gin, Deciphering the non-linear impact of Al on chemical durability of silicate glass, Acta Mater. 225 (2022) 117478. https://doi.org/10.1016/j.actamat.2021.117478.
[29] J. Du, X. Lu, S. Gin, J.-M. Delaye, L. Deng, M. Taron, N. Bisbrouck, M. Bauchy, J.D. Vienna, Predicting the dissolution rate of borosilicate glasses using QSPR analyses based on molecular dynamics simulations, J. Am. Ceram. Soc. 104 (2021) 4445–4458. https://doi.org/10.1111/jace.17857.
[30] J.N.P. Lillington, T.L. Goût, M.T. Harrison, I. Farnan, Assessing static glass leaching predictions from large datasets using machine learning, J. Non-Cryst. Solids. 546 (2020) 120276. https://doi.org/10.1016/j.jnoncrysol.2020.120276.
[31] N.M. Anoop Krishnan, S. Mangalathu, M.M. Smedskjaer, A. Tandia, H. Burton, M. Bauchy, Predicting the dissolution kinetics of silicate glasses using machine learning, J. Non-Cryst. Solids. 487 (2018) 37–45. https://doi.org/10.1016/j.jnoncrysol.2018.02.023.

[32] A. Cesaratto, P. Sichel, D. Bersani, P.P. Lottici, A. Montenero, E. Salvioli-Mariani, M. Catarsi, Characterisation of archeological glasses by micro-Raman spectroscopy, J. Raman Spectrosc. 41 (2010) 1682–1687. https://doi.org/10.1002/jrs.2613.
[33] P. Colomban, On-site Raman identification and dating of ancient glasses: A review of procedures and tools, J. Cult. Herit. 9 (2008) 55–60. https://doi.org/10.1016/j.culher.2008.06.005.
[34] B. Hruška, A. Nowicka, M. Chromčíková, E. Greiner-Wrona, J. Smolík, V. Soltézs, M. Liška, Raman spectroscopic study of corroded historical glass, Int. J. Appl. Glass Sci. 12 (2021) 613–620. https://doi.org/10.1111/ijag.16010.
[35] A. Quaranta, A. Rahman, G. Mariotto, C. Maurizio, E. Trave, F. Gonella, E. Cattaruzza, E. Gibaudo, J.E. Broquin, Spectroscopic Investigation of Structural Rearrangements in Silver Ion-Exchanged Silicate Glasses, J. Phys. Chem. C. 116 (2012) 3757.
[36] P. Colomban, M.-P. Etcheverry, M. Asquier, M. Bounichou, A. Tournié, Raman identification of ancient stained glasses and their degree of deterioration, J. Raman Spectrosc. 37 (2006) 614–626. https://doi.org/10.1002/jrs.1495.
[37] L. Robinet, C. Hall, K. Eremin, S. Fearn, J. Tate, Alteration of soda silicate glasses by organic pollutants in museums: Mechanisms and kinetics, J. Non-Cryst. Solids. 355 (2009) 1479.
[38] L. Robinet, C. Coupry, K. Eremin, C. Hall, The use of Raman spectrometry to predict the stability of historic glasses, J. Raman Spectrosc. 37 (2006) 789–797. https://doi.org/10.1002/jrs.1540.
[39] D. Li, G.M. Bancroft, M.E. Fleet, X.H. Feng, Silicon K-edge XANES spectra of silicate minerals, Phys. Chem. Miner. 22 (1995) 115–122. https://doi.org/10.1007/BF00202471.
[40] D. Li, G.M. Bancroft, M.E. Fleet, Coordination and local structure of Si and Al in silicate glasses: Si and Al K-edge XANES spectroscopy, Miner. Spectros. 5 (1996) 153–163.
[41] G.N. Greaves, Corrosion studies of glass using conventional and glancing angle EXAFS, J. Phys. Colloq. 47 (1986) C8-824. https://doi.org/10.1051/jphyscol:19868157.
[42] M. Abuín, A. Serrano, J. Chaboy, M.A. García, N. Carmona, XAS study of Mn, Fe and Cu as indicators of historical glass decay, J. Anal. At. Spectrom. 28 (2013) 1118–1124. https://doi.org/10.1039/C3JA30374H.
[43] A. Chabas, Modern Silica-Soda-Lime Glass in Polluted Atmosphere, in: Materials of Cultural Heritage in Their Environment, Edipuglia, R.-A. Lefèvre, 2004.
[44] R.J. Charles, Static Fatigue of Glass. I, J. Appl. Phys. 29 (1958) 1549–1553. https://doi.org/10.1063/1.1722991.
[45] A. Paul, Chemical durability of glasses; a thermodynamic approach, J. Mater. Sci. 12 (1977) 2246–2268. https://doi.org/10.1007/BF00552247.
[46] T.M. El-Shamy, J. Lewins, R.W. Douglas, The dependence on the pH of the decomposition of glasses by aqueous solutions, Glass Technol. 13 (1972) 81–87.
[47] R.H. Do Remus, Y. Mehrotra, W.A. Lanford, C. Burman, Reaction of water with glass: influence of a transformed surface layer, J. Mater. Sci. 18 (1983) 612–622. https://doi.org/10.1007/BF00560651.

[48] D.J. Backhouse, A.J. Fisher, J.J. Neeway, C.L. Corkhill, N.C. Hyatt, R.J. Hand, Corrosion of the International Simple Glass under acidic to hyperalkaline conditions, Npj Mater. Degrad. 2 (2018) 1–10. https://doi.org/10.1038/s41529-018-0050-5.
[49] I.C. Popovici, N. Lupascu, Chemical durability of soda-lime glass in aqueous acid solutions, Ovidius Univ. Ann. Chem. 23 (2012) 128–132. https://doi.org/10.2478/v10310-012-0021-6.
[50] E. Greiner-Wronowa, L. Stoch, Influence of environment on surface of the ancient glasses, J. Non-Cryst. Solids. 196 (1996) 118–127. https://doi.org/10.1016/0022-3093(95)00563-3.
[51] A. Winterstein-Beckmann, D. Möncke, D. Palles, E.I. Kamitsos, L. Wondraczek, A Raman-spectroscopic study of indentation-induced structural changes in technical alkali-borosilicate glasses with varying silicate network connectivity, J. Non-Cryst. Solids. 405 (2014) 196–206. https://doi.org/10.1016/j.jnoncrysol.2014.09.020.
[52] M.E. Lynch, D.C. Folz, D.E. Clark, Use of FTIR reflectance spectroscopy to monitor corrosion mechanisms on glass surfaces, J. Non-Cryst. Solids. 353 (2007) 2667–2674. https://doi.org/10.1016/j.jnoncrysol.2007.05.012.
[53] K. Janssens, G. Vittiglio, I. Deraedt, A. Aerts, B. Vekemans, L. Vincze, F. Wei, I. De Ryck, O. Schalm, F. Adams, A. Rindby, A. Knöchel, A. Simionovici, A. Snigirev, Use of microscopic XRF for non-destructive analyses in art and archaeometry, X-Ray Spectrom. 29 (2000) 73–91. https://doi.org/10.1002/(SICI)1097-4539(200001/02)29:1<73::AID-XRS416>3.0.CO;2-M.
[54] K. Cummings, W.A. Lanford, Nuclear Reaction Analyses of Corroded Glass Surfaces, in: P. Misaelides (Ed.), Appl. Part. Laser Beams Mater. Technol., Springer Netherlands, Dordrecht, (1995) 437–442. https://doi.org/10.1007/978-94-015-8459-3_29.
[55] M. Collin, S. Gin, P. Jollivet, L. Dupuy, V. Dauvois, L. Duffours, ToF-SIMS depth profiling of altered glass, Npj Mater. Degrad. 3 (2019) 1–10. https://doi.org/10.1038/s41529-019-0076-3.
[56] M. Mäder, D. Grambole, F. Herrmann, C. Neelmeijer, M. Schreiner, G. Woisetschläger, Non-destructive evaluation of glass corrosion states, Nucl. Instrum. Methods Phys. Res. Sect. B Beam Interact. Mater. At. 136–138 (1998) 863–868. https://doi.org/10.1016/S0168-583X(97)00749-0.
[57] R.H. Doremus, Interdiffusion of hydrogen and alkali ions in a glass surface, J. Non-Cryst. Solids. 19 (1975) 137–144. https://doi.org/10.1016/0022-3093(75)90079-4.
[58] S. Ribet, S. Gin, Role of neoformed phases on the mechanisms controlling the resumption of SON68 glass alteration in alkaline media, J. Nucl. Mater. 324 (2004) 152–164. https://doi.org/10.1016/j.jnucmat.2003.09.010.
[59] S. Gin, L. Neill, M. Fournier, P. Frugier, T. Ducasse, M. Tribet, A. Abdelouas, B. Parruzot, J. Neeway, N. Wall, The controversial role of inter-diffusion in glass alteration, Chem. Geol. 440 (2016) 115–123. https://doi.org/10.1016/j.chemgeo.2016.07.014.
[60] B. White, Theory of Corrosion of Glass and Ceramics, in: Corros. Glass Ceram. Ceram. Supercond., Noyes Publications, Park Ridge, (1992).
[61] J.C. Tait, D.L. Mandolesi, The chemical durability of alkali aluminosilicate glasses, Atomic Energy of Canada Limited, (1983).

[62] R.B. Heimann, Weathering of ancient and medieval glasses—potential proxy for nuclear fuel waste glasses. A perennial challenge revisited, Int. J. Appl. Glass Sci. 9 (2018) 29–41. https://doi.org/10.1111/ijag.12277.
[63] M. Melcher, M. Schreiner, Evaluation procedure for leaching studies on naturally weathered potash-lime-silica glasses with medieval composition by scanning electron microscopy, J. Non-Cryst. Solids. 351 (2005) 1210.
[64] G. Woisetschläger, M. Dutz, S. Paul, M. Schreiner, Weathering Phenomena on Naturally Weathered Potash-Lime-Silica-Glass with Medieval Composition Studied by Secondary Electron Microscopy and Energy Dispersive Microanalyses, Microchim. Acta. 135 (2000) 121–130. https://doi.org/10.1007/s006040070001.
[65] Y. Gastev, The structure of glass, Consultants Bureau translation, New York, (1958).
[66] T. Geisler, T. Nagel, M.R. Kilburn, A. Janssen, J.P. Icenhower, R.O.C. Fonseca, M. Grange, A.A. Nemchin, The mechanism of borosilicate glass corrosion revisited, Geochim. Cosmochim. Acta. 158 (2015) 112–129. https://doi.org/10.1016/j.gca.2015.02.039.
[67] S. Gin, J.-M. Delaye, F. Angeli, S. Schuller, Aqueous alteration of silicate glass: state of knowledge and perspectives, Npj Mater. Degrad. 5 (2021) 42. https://doi.org/10.1038/s41529-021-00190-5.
[68] R. Hellmann, S. Cotte, E. Cadel, S. Malladi, L.S. Karlsson, S. Lozano-Perez, M. Cabié, A. Seyeux, Nanometre-scale evidence for interfacial dissolution–reprecipitation control of silicate glass corrosion, Nat. Mater. 14 (2015) 307–311. https://doi.org/10.1038/nmat4172.
[69] C. Lenting, O. Plümper, M. Kilburn, P. Guagliardo, M. Klinkenberg, T. Geisler, Towards a unifying mechanistic model for silicate glass corrosion, Npj Mater. Degrad. 2 (2018) 28. https://doi.org/10.1038/s41529-018-0048-z.
[70] T. Lombardo, L. Gentaz, A. Verney-Carron, A. Chabas, C. Loisel, D. Neff, E. Leroy, Characterisation of complex alteration layers in medieval glasses, Corros. Sci. 72 (2013) 10–19. https://doi.org/10.1016/j.corsci.2013.02.004.
[71] S. Gin, P. Jollivet, G. Barba Rossa, M. Tribet, S. Mougnaud, M. Collin, M. Fournier, E. Cadel, M. Cabie, L. Dupuy, Atom-Probe Tomography, TEM and ToF-SIMS study of borosilicate glass alteration rim: A multiscale approach to investigating rate-limiting mechanisms, Geochim. Cosmochim. Acta. 202 (2017) 57–76. https://doi.org/10.1016/j.gca.2016.12.029.
[72] S. Gin, A.H. Mir, A. Jan, J.M. Delaye, E. Chauvet, Y. De Puydt, A. Gourgiotis, S. Kerisit, A General Mechanism for Gel Layer Formation on Borosilicate Glass under Aqueous Corrosion, J. Phys. Chem. C. 124 (2020) 5132–5144. https://doi.org/10.1021/acs.jpcc.9b10491.
[73] B. Parruzot, P. Jollivet, D. Rébiscoul, S. Gin, Long-term alteration of basaltic glass: Mechanisms and rates, Geochim. Cosmochim. Acta. 154 (2015) 28–48. https://doi.org/10.1016/j.gca.2014.12.011.
[74] G. Libourel, A. Verney-Carron, A. Morlok, S. Gin, J. Sterpenich, A. Michelin, D. Neff, P. Dillmann, The use of natural and archeological analogues for understanding the long-term behavior of nuclear glasses, Comptes Rendus Geosci. 343 (2011) 237–245. https://doi.org/10.1016/j.crte.2010.12.004.

[75] D. Sprenger, H. Bach, W. Meisel, P. Gütlich, XPS study of leached glass surfaces, J. Non-Cryst. Solids. 126 (1990) 111–129. https://doi.org/10.1016/0022-3093(90)91029-Q.
[76] S. Fearn, D.S. McPhail, V. Oakley, Moisture attack on museum glass measured by SIMS, 46 (2005) 7.
[77] J.B. Clegg, Secondary Ion Mass Spectrometry—a Practical Handbook for Depth Profiling and Bulk Impurity Analyses Wiley, New York, 1989, Surf. Interface Anal. 17 (1991) 221–221. https://doi.org/10.1002/sia.740170411.
[78] J.T. van Elteren, A. Izmer, M. Šala, E.F. Orsega, V.S. Šelih, S. Panighello, F. Vanhaecke, 3D laser ablation-ICP-mass spectrometry mapping for the study of surface layer phenomena – a case study for weathered glass, J. Anal. At. Spectrom. 28 (2013) 994. https://doi.org/10.1039/c3ja30362d.
[79] M. De Bardi, H. Hutter, M. Schreiner, ToF-SIMS analyses for leaching studies of potash–lime–silica glass, Appl. Surf. Sci. 282 (2013) 195–201. https://doi.org/10.1016/j.apsusc.2013.05.101.
[80] L. Robinet, C. Pulham, C. Hall, K. Eremin, S. Fearn, Understanding Glass Deterioration in Museum Collections through Raman Spectroscopy and SIMS analyses, MRS Proceedings 852(2004) 247-254.
[81] Y. Gong, J. Xu, R.C. Buchanan, The aqueous corrosion of nuclear waste glasses revisited: Probing the surface and interfacial phenomena, Corros. Sci. 143 (2018) 65–75. https://doi.org/10.1016/j.corsci.2018.08.028.
[82] V. Oakley, Vessel glass deterioration at the Victoria and Albert museum: Surveying the collection, The Conservator. 14 (1990) 30–36. https://doi.org/10.1080/01410096.1990.9995054.
[83] T. Palomar, N. García-Patrón, P. Pastor, Spanish Royal glasses with crizzling in historical buildings. The importance of environmental monitoring for their conservation, Build. Environ. 202 (2021) 108054. https://doi.org/10.1016/j.buildenv.2021.108054.
[84] B. Cobo del Arco, Survey of the National Museum of Scotland Glass Collection, in: Conserv. Glass Ceram. Res. Pract. Train., N.H. Tennet, (1999) 229–238.
[85] K. Eremin, B. Cobo del Arco, L. Robinet, L. Gibson, Deteriorating Nineteenth and Twentienth - Century British Glass in the National Museums of Scotland, in: 'Deteriorating Ninet. TwentiethCentury Br. Glass Natl. Mus. Scotland,' AIHV, Nottingham, (2005) 380–385.
[86] F. Burghout, M. Slager, Cloudy Patches and Misty Glass: Early Signs of Glass Disease?, in: H. Roemich and K. Van Lookeren Campagne, (2013) 327–329.
[87] S.A. Koob, Conservation and Care of Glass Objects, Archetype Publications / The Corning Museum of Glass, London : Corning, N.Y, (2006).
[88] S. Ulitzka, V. Touchard, Corrosion phenomena of Bohemian and Postdam glasses from 17th and 18th century, in: N.S. Baer, C. Sabbioni, A.I. Sors (Eds.), Sci. Technol. Eur. Cult. Herit., Butterworth-Heinemann, (1991) 872–875. https://doi.org/10.1016/B978-0-7506-0237-2.50158-1.
[89] C.N.& M. Mäder, Endangered glass objects identified by ion beam analyses, in: Cult. Herit. Conserv. Environ. Impact Assess. Non-Destr. Test. Micro-Anal., CRC Press, (2005).
[90] L. Robinet, C. Coupry, K. Eremin, C. Hall, Raman investigation of the structural changes during alteration of historic glasses by organic pollutants, J. Raman Spectrosc. 37 (2006) 1278–1286.

[91] N. Earl, The Investigation of Glass Deterioration as a Result of Storage Systems for Waterlogged Archaeological Glass, in: Conserv. Glass Ceram. Res. Pract. Train., N.H. Tennent, (1999) 96–113.
[92] W. Anaf, Study on the formation of heterogeneous structures in leached layers during the corrosion process of glass, CeROArt. (2010). https://doi.org/10.4000/ceroart.1561.
[93] R.H. Brill, Some Miscallaneous Thoughts on Crizzling, in: Proceedings, Westerville: The American Chemical Society, (1998).
[94] H. Roemich, Laboratory experiments to simulate corrosion on stained glass windows, in: Conserv. Glass Ceram. Res. Pract. Train., London, U. K. : James&James, (1999) 57–65.
[95] R.H. Brill, Crizzling - a problem in glass conservation, Stud. Conserv. 20 (1975) 121–134. https://doi.org/10.1179/sic.1975.s1.021.
[96] O. Schalm, G. Nuyts, K. Janssens, Some critical observations about the degradation of glass: The formation of lamellae explained, J. Non-Cryst. Solids. 569 (2021) 120984. https://doi.org/10.1016/j.jnoncrysol.2021.120984.
[97] L.L. Hench, Characterisation of glass corrosion and durability, J. Non-Cryst. Solids. 19 (1975) 27–39. https://doi.org/10.1016/0022-3093(75)90067-8.
[98] D. Caurant, F. Alloteau, O. Majérus, V. Valbi, L. Patrice, T. Charpentier, I. Biron, A. Seyeux, Alteration mechanisms of ancient glass objects exposed to the atmosphere, (2019).
[99] T. Palomar, M. Garcia, M.-A. Villegas, Model historical glasses under simulated burial conditions, (2012) 5.
[100] D.J. Huisman, S. Pols, I. Joosten, B.J.H. van Os, A. Smit, Degradation processes in colourless Roman glass: cases from the Bocholtz burial, J. Archaeol. Sci. 35 (2008) 398–411. https://doi.org/10.1016/j.jas.2007.04.008.
[101] K.T. Friedrich, P. Degryse, Soil vs. glass: an integrated approach towards the characterisation of soil as a burial environment for the glassware of Cucagna Castle (Friuli, Italy), STAR Sci. Technol. Archaeol. Res. 5 (2019) 138–156. https://doi.org/10.1080/20548923.2019.1688492.
[102] T. Palomar, M. Oujja, M. García-Heras, M.A. Villegas, M. Castillejo, Laser induced breakdown spectroscopy for analyses and characterisation of degradation pathologies of Roman glasses, Spectrochim. Acta Part B At. Spectrosc. 87 (2013) 114–120. https://doi.org/10.1016/j.sab.2013.05.004.
[103] O. Schalm, W. Anaf, Laminated altered layers in historical glass: Density variations of silica nanoparticle random packings as explanation for the observed lamellae, J. Non-Cryst. Solids. 442 (2016) 1–16. https://doi.org/10.1016/j.jnoncrysol.2016.03.019.
[104] R. Arévalo, J. Mosa, M. Aparicio, T. Palomar, The stability of the Ravenscroft's glass. Influence of the composition and the environment, J. Non-Cryst. Solids. 565 (2021) 120854. https://doi.org/10.1016/j.jnoncrysol.2021.120854.
[105] R.G. Newton, S. Davison, Conservation and restoration of glass, Routledge, Abingdon, Oxon, (2011).
[106] G. Verhaar, Glass sickness: Detection and prevention: Investigating unstable glass in museum collections, University of Amsterdam, Amsterdam, (2018).
[107] R. Newton, The Weathering of Medieval Window Glass, J. Glass Stud. 17 (1975) 161–168.

[108] L. Gentaz, T. Lombardo, A. Chabas, C. Loisel, A. Verney-Carron, Impact of neocrystallisations on the SiO2–K2O–CaO glass degradation due to atmospheric dry depositions, Atmos. Environ. 55 (2012) 459–466. https://doi.org/10.1016/j.atmosenv.2012.03.008.
[109] M. De Bardi, H. Hutter, M. Schreiner, R. Bertoncello, Potash-lime-silica glass: protection from weathering, Herit. Sci. 3 (2015) 22. https://doi.org/10.1186/s40494-015-0051-4.
[110] L.B. Brostoff, C.L. Ward-Bamford, S. Zaleski, T. Villafana, A.C. Buechele, I.S. Muller, F. France, M. Loew, Glass at risk: A new approach for the study of 19th century vessel glass, J. Cult. Herit. 54 (2022) 155–166. https://doi.org/10.1016/j.culher.2022.01.013.
[111] G. Frenzel, The Restoration of Medieval Stained Glass, Sci. Am. 252 (1985) 126–135. https://doi.org/10.1038/scientificamerican0585-126.
[112] M. Melcher, M. Schreiner, Statistical evaluation of potash-lime-silica glass weathering, Anal. Bioanal. Chem. 379 (2004) 628-639. https://doi.org/10.1007/s00216-004-2595-0.
[113] T. Lombardo, C. Loisel, L. Gentaz, A. Chabas, M. Verita, I. Pallot-Frossard, Long term assessment of atmospheric decay of stained glass windows, Corros. Eng. Sci. Technol. 45 (2010) 420–424. https://doi.org/10.1179/147842210X12710800383800.
[114] M. Schreiner, Glass of the past: The degradation and deterioration of medieval glass artifacts, Mikrochim. Acta. 104 (1991) 255–264. https://doi.org/10.1007/BF01245513.
[115] G.I. Cooper, G.A. Cox, R.N. Perutz, Infra-red microspectroscopy as a complementary technique to electron-probe microanalyses for the investigation of natural corrosion on potash glasses, J. Microsc. 170 (1993) 111–118. https://doi.org/10.1111/j.1365-2818.1993.tb03329.x.
[116] M.-T. Doménech-Carbó, A. Doménech-Carbó, L. Osete-Cortina, M.-C. Saurí-Peris, A Study on Corrosion Processes of Archaeological Glass from the Valencian Region (Spain) and its Consolidation Treatment, Microchim. Acta. 154 (2006) 123–142. https://doi.org/10.1007/s00604-005-0472-y.
[117] J. Ferrand, S. Rossano, C. Loisel, N. Trcera, E.D. van Hullebusch, F. Bousta, I. Pallot-Frossard, Browning Phenomenon of Medieval Stained Glass Windows, Anal. Chem. 87 (2015) 3662–3669. https://doi.org/10.1021/ac504193z.
[118] C. Kennedy, T. Addyman, K. Murdoch, M. Young, 18th- and 19th- Century Scottish Laboratory Glass: Assessment of Chemical Composition in Relation to Form and Function, J. Glass Stud. 60 (2018) 253–267.
[119] C. Cailleteau, F. Angeli, F. Devreux, S. Gin, J. Jestin, P. Jollivet, O. Spalla, Insight into silicate-glass corrosion mechanisms, Nat. Mater. 7 (2008) 978–983. https://doi.org/10.1038/nmat2301.
[120] A. Lavoisier, Action of water on glass, J. Mem. & Acad. Sci. (Paris). 73 (1770).
[121] H. Zhang, T. Suzuki-Muresan, Y. Morizet, S. Gin, A. Abdelouas, Investigation on boron and iodine behavior during nuclear glass vapor hydration, Npj Mater. Degrad. 5 (2021) 1–9. https://doi.org/10.1038/s41529-021-00157-6.
[122] N.A.R. van Giffen, S.P. Koob, Deterioration of Vitreous Materials, in: S.L. López Varela (Ed.), Encycl. Archaeol. Sci., John Wiley & Sons, Inc., Hoboken, NJ, USA, (2018) 1–4. https://doi.org/10.1002/9781119188230.saseas0179.

[123] T. Palomar, I. Llorente, Decay processes of silicate glasses in river and marine aquatic environments, J. Non-Cryst. Solids. 449 (2016) 20–28. https://doi.org/10.1016/j.jnoncrysol.2016.07.009.
[124] T. Palomar, A. Chabas, D.M. Bastidas, D. de la Fuente, A. Verney-Carron, Effect of marine aerosols on the alteration of silicate glasses, J. Non-Cryst. Solids. 471 (2017) 328–337. https://doi.org/10.1016/j.jnoncrysol.2017.06.013.
[125] A. Rodrigues, S. Fearn, T. Palomar, M. Vilarigues, Early stages of surface alteration of soda-rich-silicate glasses in the museum environment, Corros. Sci. 143 (2018) 362–375. https://doi.org/10.1016/j.corsci.2018.08.012.
[126] T. Palomar, D. de la Fuente, M. Morcillo, M. Alvarez de Buergo, M. Vilarigues, Early stages of glass alteration in the coastal atmosphere, Build. Environ. 147 (2019) 305–313. https://doi.org/10.1016/j.buildenv.2018.10.034.
[127] L.T. Gibson, B.G. Cooksey, D. Littlejohn, N.H. Tennent, Characterisation of an unusual crystalline efflorescence on an Egyptian limestone relief, Anal. Chim. Acta. 337 (1997) 151–164. https://doi.org/10.1016/S0003-2670(96)00428-X.
[128] T. Palomar, M. Silva, M. Vilarigues, I. Pombo Cardoso, D. Giovannacci, Impact of solar radiation and environmental temperature on Art Nouveau glass windows, Herit. Sci. 7 (2019) 82. https://doi.org/10.1186/s40494-019-0325-3.
[129] T. Palomar, Effect of soil pH on the degradation of silicate glasses, Int. J. Appl. Glass Sci. 8 (2017) 177–187. https://doi.org/10.1111/ijag.12226.
[130] H. Roemich, S. Gerlach, P. Mottner, F. Mees, P. Jacobs, D. van Dyck, T. Doménech Carbó, Results from burial experiments with simulated medieval glasses, MRS Proc. 757 (2002) II2.3. https://doi.org/10.1557/PROC-757-II2.3.
[131] R.M. Organ, The safe storage of unstable glass, The Museum Journal. 56 (1957) 265–272.
[132] D. Brewster, XIX.—On the Structure and Optical Phenomena of Ancient Decomposed Glass, Earth Environ. Sci. Trans. R. Soc. Edinb. 23 (1863) 193–204. https://doi.org/10.1017/S0080456800019372.
[133] J.M. Duley, A.C. Fowler, I.R. Moyles, S.B.G. O'Brien, On the Keller–Rubinow model for Liesegang ring formation, Proc. R. Soc. Math. Phys. Eng. Sci. 473 (2017) 20170128. https://doi.org/10.1098/rspa.2017.0128.
[134] J. George, S. Nair, G. Varghese, Role of colloid dynamics in the formation of Liesegang rings in multi-component systems, J. Mater. Sci. 39 (2004) 311–313. https://doi.org/10.1023/B:JMSC.0000007763.81805.a2.
[135] B. Dal Bianco, R. Bertoncello, L. Milanese, S. Barison, Surface study of water influence on chemical corrosion of Roman glass, Surf. Eng. 21 (2005) 393–396. https://doi.org/10.1179/174329305X64376.
[136] F. Barbana, R. Bertoncello, L. Milanese, C. Sada, Alteration and corrosion phenomena in Roman submerged glass fragments, J. Non-Cryst. Solids. 337 (2004) 136–141. https://doi.org/10.1016/j.jnoncrysol.2004.03.118.
[137] M.M. Eltantawy, M.A. Belokon, E.V. Belogub, O.I. Ledovich, E.V. Skorb, S.A. Ulasevich, Self-Assembled Liesegang Rings of Hydroxyapatite for Cell Culturing, Adv. NanoBiomed Res. 1 (2021) 2000048. https://doi.org/10.1002/anbr.202000048.

[138] D.R. Manley, K.H. Stern, Liesegang rings in inhomogeneous media. Powdered glass, J. Colloid Sci. 10 (1955) 409–412. https://doi.org/10.1016/0095-8522(55)90058-1.
[139] J.A. Pask, C.W. Parmelbe, Study of Diffusion in Glass*, J. Am. Ceram. Soc. 26 (1943) 267–277. https://doi.org/10.1111/j.1151-2916.1943.tb15214.x.
[140] B. Dal Bianco, R. Bertoncello, L. Milanese, S. Barison, Glasses on the seabed: surface study of chemical corrosion in sunken Roman glasses, J. Non-Cryst. Solids. 343 (2004) 91–100. https://doi.org/10.1016/j.jnoncrysol.2004.07.002.
[141] A.J. Fisher, N.C. Hyatt, R.J. Hand, C.L. Corkhill, The Formation of Pitted Features on the International Simple Glass during Dynamic Experiments at Alkaline pH, MRS Adv. 4 (2019) 993–999. https://doi.org/10.1557/adv.2019.9.
[142] O. Schalm, K. Proost, K. De Vis, S. Cagno, K. Janssens, F. Mees, P. Jacobs, J. Caen, Manganese staining of archaeological glass: the characterisation of Mn-rich inclusions in leached layers and a hypothesis of its formation., Archaeometry. 53 (2011) 103–122. https://doi.org/10.1111/j.1475-4754.2010.00534.x.
[143] T. Palomar, Chemical composition and alteration processes of glasses from the Cathedral of León (Spain), Bol. Soc. Esp. Cerámica Vidr. 57 (2018) 101–111. https://doi.org/10.1016/j.bsecv.2017.10.001.
[144] S.P. Koob, Crizzling glasses: problems and solutions, Glass Technol. - Eur. J. Glass Sci. Technol. Part A. 53 (2012) 225–227.
[145] J. Kunicki-Goldfinger, J. Kierzek, B. Ma, A.J. Kasprzak, Some observations on crizzled glass (preliminary results of a survey of 18th century central European tableware), 43 (2002) 6.
[146] G.W. Morey, The Corrosion of Glass Surfaces., Ind. Eng. Chem. 17 (1925) 389–392. https://doi.org/10.1021/ie50184a019.
[147] W.E.S. Turner, The Use of Boric Oxide in Glass-Making, J. Am. Ceram. Soc. 7 (1924) 313–317. https://doi.org/10.1111/j.1151-2916.1924.tb18207.x.
[148] K. Cummings, W.A. Lanford, M. Feldmann, Weathering of glass in moist and polluted air, Nucl. Instrum. Methods Phys. Res. Sect. B Beam Interact. Mater. At. 136–138 (1998) 858–862. https://doi.org/10.1016/S0168-583X(97)00758-1.
[149] J.G. Evans, S. Limbrey, The Experimental Earthwork on Morden Bog, Wareham, Dorset, England: 1963 to 1972: Report of the Experimental Earthworks Committee of the British Association for the Advancement of Science, Proc. Prehist. Soc. 40 (1974) 170–202. https://doi.org/10.1017/S0079497X00011385.
[150] M.I. Ojovan, R.J. Hand, N.V. Ojovan, W.E. Lee, Corrosion of alkali–borosilicate waste glass K-26 in non-saturated conditions, J. Nucl. Mater. 340 (2005) 12–24. https://doi.org/10.1016/j.jnucmat.2004.10.095.
[151] M. Fournier, S. Gin, P. Frugier, S. Mercado-Depierre, Contribution of zeolite-seeded experiments to the understanding of resumption of glass alteration, Npj Mater. Degrad. 1 (2017) 1–13. https://doi.org/10.1038/s41529-017-0018-x.
[152] W.W. Fletcher, The Chemical Durability of Glass. a Burial Experiment at Ballidon in Derbyshire, J. Glass Stud. 14 (1972) 149–151.
[153] R.J. Hand, The Ballidon Glass Burial Experiment – 35 years on, Glass Technol. 46 (2005) 237–242.
[154] I. Biron, F. Alloteau, O. Majérus, D. Caurant, P. Lehuédé, eds., Glass Atmospheric Alteration: Cultural Heritage, Industrial and Nuclear Glasses, HERMANN, Paris, (2019).

[155] B. Grambow, Nuclear Waste Glass Dissolution: Mechanism, Model and Application, Swedish Nuclear Fuel and Waste Management Co., Stockholm, (1987).
[156] M. Ojovan, On Alteration Rate Renewal Stage of Nuclear Waste Glass Corrosion, MRS Adv. 5 (2020) 111–120. https://doi.org/10.1557/adv.2020.36.
[157] L.G. Terreni, Le problematiche conservative del vetro antico proveniente da scavi archeologici, Milliarium - Period. Inf. Archeol. (2013) 34–47.
[158] M. Melcher, M. Schreiner, Leaching studies on naturally weathered potash-lime–silica glasses, J. Non-Cryst. Solids. 352 (2006) 368–379. https://doi.org/10.1016/j.jnoncrysol.2006.01.017.
[159] S.P. Koob, N.A.R. van Giffen, Conservation of Vitreous Materials, in: S.L. López Varela (Ed.), Encycl. Archaeol. Sci., John Wiley & Sons, Inc., Hoboken, NJ, USA, (2018) 1–6. https://doi.org/10.1002/9781119188230.saseas0125.
[160] S.P. Koob, Paraloid B-72®: 25 years of use as a consolidant and adhesive for ceramics and glass.
[161] S. Koob, The Use of Paraloid B-72 as an Adhesive: Its Application for Archaeological Ceramics and Other Materials, Stud. Conserv. 31 (1986) 7–14. https://doi.org/10.1179/sic.1986.31.1.7.
[162] S.P. Koob, Manipulating materials: Preparing and using Paraloid B-72 adhesive mixtures, 25 (2018) 9.
[163] S. Chapman, D. Mason, Literature Review: The Use of Paraloid B-72 as a Surface Consolidant for Stained Glass, J. Am. Inst. Conserv. 42 (2003) 381–392. https://doi.org/10.1179/019713603806112813.
[164] I. Coutinho, A. Lima, F. Braz Fernandes, A. Ramos, Studies on degradation of epoxy resins used for conservation of glass, (2008) 127-133. https://doi.org/10.13140/RG.2.1.2799.3124.
[165] L. de Ferri, P.P. Lottici, A. Lorenzi, A. Montenero, G. Vezzalini, Hybrid sol–gel based coatings for the protection of historical window glass, J. Sol-Gel Sci. Technol. 66 (2013) 253–263. https://doi.org/10.1007/s10971-013-3002-0.
[166] A. Al Bawab, R. Al-Omari, R. Abd-Allah, A. Bozeya, R.A. Abu-Zurayk, F. Odeh, The Application of a Modified Sol-Gel Silica Coating for the Protection of Corroded Roman Soda-Lime-Silica Glass: An Experimental and Analytical Study, in: M. Koui, F. Zezza, D. Kouis (Eds.), 10th Int. Symp. Conserv. Monum. Mediterr. Basin Nat. Anthropog. Hazards Sustain. Preserv., Springer International Publishing, Cham, (2018) 189–197. https://doi.org/10.1007/978-3-319-78093-1_19.

CHAPTER 2 – LA-ICP-MS ANALYSES OF ROMAN GLASS TO INVESTIGATE THE SECONDARY GLASS PRODUCTION IN THE ANCIENT AQUILEIA (NORTH OF ITALY) *.

* Part of this chapter is reported in Zanini et al. “Insights into the secondary glass production in Roman Aquileia: a preliminary study” under revision by Journal of Archaeological Science Reports.

Except for a few documented Roman glass workshops – mainly located in Western Europe – archaeological evidence of glass working in the European area during the Roman period is relatively sporadic and often hard to detect. Potential surviving sites require therefore special care to identify, recover, conserve, and interpret glass working evidence. This consideration underlies the work here presented, which focuses on the analyses and interpretation of a selection of specimens from a large glass assemblage identified in 2017 on plough soil surface during an archaeological field-walking survey in the suburbs of Roman Aquileia (north of Italy) [1].These archaeological items included shards from a variety of vessels, working waste (small glass threads, trails, and droplets), and chunks of glass (i.e., blobs of raw or recycled glass – collected, ground up and re-fused – to be re-melted and eventually worked into proper objects), some of which embedding refractory materials. All these items, when found together as part of an 'archaeological assemblage', often indicate the presence of past glassworks.

Archaeological evidence suggests that during the Roman period chunks and lumps of raw glass produced in 'primary' furnaces located near the sources of raw materials (mainly in ancient Palestine and Egypt) were transported to 'secondary' workshops across the Mediterranean for manufacturing vessels and other glass artefacts. A secondary furnace could use raw glass from a single primary source, or it could receive raw glass made in different primary centres. In the latter case, final objects may present several compositional features [2,3]. In addition, the furnace could produce glass items using recycled glass, a common practice in antiquity [4]: glass cullets were widely employed in the production of new artefacts or traded as recyclable production material to supply other workshops during the first centuries of the Roman Empire.

The key role that Aquileia had in antiquity in the consumption, trade, disposal, and possible production of glass artefacts [5,6] is reflected by the large variety of archaeological glass items (whole vessels or fragments) recovered there in the past two centuries of archaeological research and referenced in ancient inscriptions and written sources describing local glass production [7]. A primary involvement of the town also in the trading of recycled material has been conjectured after the recovery of a wood barrel containing 11,000 glass fragments discovered in the wreck of a Roman ship (the so-called '*Julia Felix*') not far from coast south of Aquileia [8].

Despite the numerous clues, however, no glass melting, recycling, or blowing workshops (i.e., secondary furnaces) has been conclusively identified there. So far, only glass waste recoveries [6], a deposit of glass waste intended for re-fusion in the nearby village of Sevegliano [9], and a disputed identification of the remains of a furnace using geophysics prospection [10], have been reported. The identification of a glass workshop site in Aquileia is therefore pivotal to clarify if the role of the city in the broader Mediterranean-level glass trade network was just that of an exchange place or also that of a manufacturing glass centre.

This chapter reports how a selection of the recovered items was analysed using Laser Ablation-Inductively Coupled Plasma-Mass Spectrometry (LA-ICP-MS) to obtain compositional

information that is the key to understand the nature of the site. This analytical technique is the only one that offers the possibility of glass microinvasive quantitative elemental analyses of major, minor and trace elements with virtually no visible damage: it is considered the most efficient technique for compositional characterisation of glass by the conservation science community, as indicated by the growing number of studies reporting its use to tackle specific research questions [11–13]. In addition, data extracted from these preliminary analyses will be used in the future as baseline for designing a more extensive chemical characterisation plan for a larger number of items included in the assemblage, more likely to provide statistically significant answers.

In detail, the overarching aim of this study was to analyse the recovered assemblage of glass fragments to establish if it could be linked to the existence of a still buried glass furnace at the location of discovery, and to determine the nature of the activities ongoing at the site and of the products of such a furnace. To this end, chemical analyses obtained using LA-ICP-MS was used to extrapolate key information that could serve as univocal indicator of the existence of the furnace from a subset of the recovered archaeological items. Three main research objectives were specifically set in order to gain the information needed to evaluate the hypothesis:

i) to find a correlation between glass working waste and (fragments of) artefacts that were part of the same assemblage with the goal of establishing if the composition of their glass was similar and determine if a relationship existed between raw/recycled material and manufactured items;
ii) to ascertain if potential glass working at the site was operated using primary glass imports or glass recycling procedures (or both);
iii) to recognise the provenience of raw sources (sand and flux) for glass making.

2.1. SAMPLES

The subset of the assemblage's items used for analyses consisted of 29 samples, out of the total ca. 500 items artefacts, dating back to the 1st century BC, with later forms up to the 4th century AD.

Visual inspection established that they pertained to three broad types of objects (Figure 2.1), namely chunks (C), artefacts (A) and working waste (W). The chunks, i.e., broken slags of glass that were part of larger blocks or slabs (ingots) of raw glass ready to be melted and worked into specific objects, were mainly in blue-green colour, with some specimens in blue and emerald green. Shards of broken artefacts (rims, bottoms, handles, and walls) were the most numerous finds in the group, in a variety of colours (purple, amber, cobalt blue, and emerald green). Lumps, threads, and trails, which represent the by-product of the glass working process, were less

present. For the elemental analyses via LA-ICP-MS, small pieces (several millimetres) were carefully removed from the glass items and embedded in epoxy resin and polished (Figure 2.2).

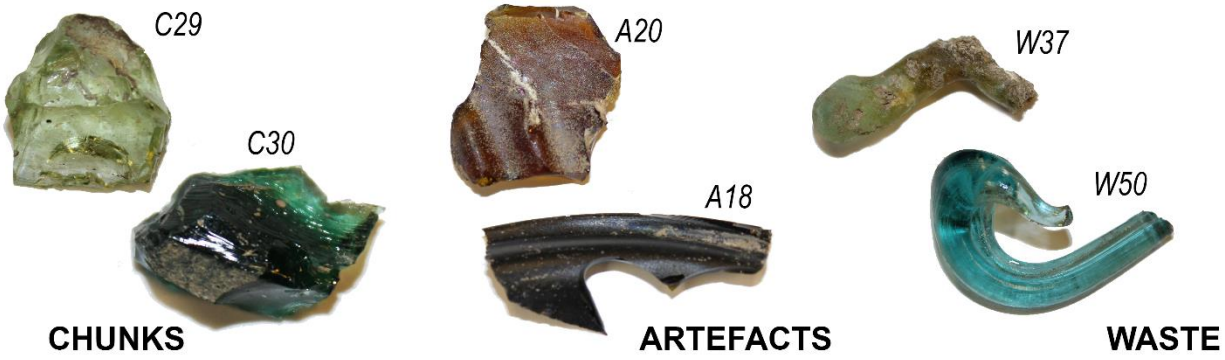

Figure 2.1. Example of the samples collected and their classification in chunks (C), artefacts (A) and waste (W).

Figure 2.2. Small pieces of the glass samples embedded in epoxy resin and polished for LA-ICP-MS analyses.

2.2. ANALYTICAL METHOD

LA-ICP-MS is becoming a well-established analytical method for the characterisation of ancient glass, being able to generate information on the bulk composition and spatial distribution using different measurement and data processing protocols. LA-ICP-MS analyses is based on the direct micro sampling of a solid volume and the subsequent elemental analyses of the generated material via mass spectrometry detector. It is considered a "quasi" non-destructive (or micro-destructive) technique, requiring minimal or no sample preparation, while providing higher sensitivity/lower detection limits (in the ng g^{-1} range) compared to more conventional techniques used for glass characterisation. In addition, it enables full quantitative determination of major, minor, and trace elements within a single analytical run [14]. All these properties make the LA-ICP-MS suited to generate bulk chemical data of ancient glass samples able to provide

information about the provenience of raw materials used for glass manufacturing (sands, fluxes, and chromophores), or about fabrication technologies, which vary widely according to historical period and/or geographical area [15].

The LA-ICP-MS instrument used in this work is equipped with a 193 nm ArF* excimer laser ablation system (Teledyne Photon Machines Analyte G2, Teledyne, Omaha, USA) connected to a quadrupole ICP-MS (7900x ICP-MS, Agilent Technologies, Santa Clara, USA). The system was used in the spot-drilling mode, assuming homogeneous composition of the samples, to measure the bulk elemental oxide composition of the samples. Table 2.1. provides the operational parameters for the spot drilling procedure used. The Analyte G2 is a laser ablation instrument equipped with a dual volume ablation cell (HelEx 2) using helium to transport the ablated material from the ablation cell to the ICP-MS; argon was added as a make-up gas before the torch of the ICP. The mass spectrometer was set up in time-resolved analyses mode, measuring one point per mass and acquiring 55 masses. Measurement of the background gases (He/Ar mixture) served to establish a gas blank signal for all masses. Sampling of the glass artefacts was performed using the spot mode with a laser beam diameter of 80 µm and a repetition rate of 20Hz. The measurements were performed by the Department of Analytical Chemistry of the National Institute of Chemistry in Ljubljana; I have used the data expressed in element's concentration to extrapolate the results reported in the next paragraphs.

Table 2.1: *LA-ICP-MS operating conditions for the LA spot analyses drilling procedure.*

Laser ablation (Cetac Analyte G2)		***ICP-MS (Agilent 7900)***	
Wavelength	193 nm	Rf power	1500 W
Pulse length	<4 ns	Sampling depth	6.5 mm
Spot size	80 µm	Isotopes measured	55 isotopes
Fluence	4.08 J cm^{-2}	Acquisition per isotope time/mass	0.01 – 0.05 s
Repetition rate	20 Hz	Total acquisition time	0.999 s
He flow rate (cup/cell)	0.5/0.3 L min^{-1}	Measurement mode	Time-resolved, TRA(1)
Make-up Ar flow rate	0.8 L min^{-1}	Plasma/auxiliary gas flow rate	15/1 L min^{-1}

A sum normalisation calibration protocol was used for the quantification of elements (as their elemental oxides) in the glass samples [11]. The reference materials selected for LA-ICP-MS

calibration were the following: NIST SRM 610 and 612 (National Institute of Standards and Technology), SGT 2, 3, 4, 5 (Society of Glass Technology), DLH 6, 7, 8 (P&H Developments Ltd.), and standards from the Corning Museum of Glass (CMG B, C, D) [12,16]. The CMG standards mimic the glass composition of ancient glass: in particular, the reference B match the composition of silica-soda-lime (SSL) Egyptian, Mesopotamian, Roman, Byzantine, and Islamic glass, the CMG C is a lead-barium glass similar to those found in East Asia, and the CMG D is a high-Mg, high-Ca potash glass with typical medieval composition [17].

The sum normalisation procedure used in this work is based on summing the concentrations of all matrix-containing elements as their oxides, and normalizing them to 100% [w/w] using external standards [13]. The raw ICP-MS data, obtained from both standards and samples analyses, were corrected using SiO_2 as an internal standard by converting the raw signal I_i (in cps) in each selected point for each element *i*:

$$I_i(corr) = \frac{I_i}{I_{i=Si} \,/\, c_{i=Si}}$$

where $I_{i=Si}$ is the raw signal intensity (in cps) of the internal standard in the sample (Si) and $c_{i=Si}$ is the elemental oxide concentration (in % [w/w]) of the internal standard in the sample (Si). For unknown glass sample the concentration of the SiO_2 as internal standard was assumed to be 50 % [w/w]. For the glass standards a similar protocol is followed but knowing the SiO_2 concentration yielding average elemental sensitivities F_i for each element i. The F_i was determined using a set of reference glass *j* (1 to m) for external calibration with internal standardisation on SiO_2:

$$F_i = \frac{\sum_{j=1}^{m} c_{i,j} I_{i,j(corr)}}{\sum_{j=1}^{m} (c_{i,j})^2}$$

where $c_{i,j}$ is the elemental oxide concentration *i* (in % [w/w]) in reference glass *j* and $I_{i,j(corr)}$ is the corrected signal intensity of elemental oxide *i* in reference glass *j*. This results in a calibration graph for each elemental oxide apart from SiO_2 used as internal standard, with *m* points for each reference glass used. F_i is obtained as a slope of a linear regression line forced thought the origin of the calibration graph.

Then the elemental oxide concentration c_i in the sample (in % [w/w]) can be calculated dividing the corrected signal intensity $I_i(corr)$ to the response factor F_i

$$c_i = \frac{I_{i\,(corr)}}{F_i}$$

and the cumulated elemental oxide concentration c_t in the sample is denoted by

$$c_t = \sum_{i=1}^{n} c_i$$

where *n* is the number of elemental oxides measured including the internal standard SiO_2 (*i*). Since the total elemental oxides concentration c_t calculated is almost certainly not 100%, it is necessary to normalize to 100% [w/w] by converting all individual elemental oxide concentrations c_i to normalised elemental oxide concentrations c_i *(norm)*:

$$c_i(norm) = 100 \times \frac{c_i}{c_t}$$

Finally, during the normalisation the arbitrary elemental oxide concentration initially chosen for the internal standard equal to 50% [w/w] is converted into its actual concentration.

2.3. COMPOSITIONAL CHARACTERISATION OF THE SAMPLES

The chemical composition of the 29 glass samples as determined by LA-ICP-MS is presented in Table 2.2., giving the concentrations of 11 major/minor elements (in wt % of their oxides) and 7 trace elements (in ppm), and including the visually perceived colour of each sample.

The concentrations of some of the major (Ca, Al, Si, Na) and other elements (Ti, Sr, and Zr) determined by LA-ICP-MS were compared via bivariate plots and multivariate analyses to relate chunks, artefacts and working waste to the geographic areas of provenience of the glass (Figs. 2.4.-2.7.). All 29 samples can be characterised as silica-soda-lime glass with natron as flux [18–23], reflecting the typical composition of Roman glass between the 1st century BC and 4th century AD, rich in silica, with soda concentrations in the range of 16-20 wt %, and with levels of Mg, P and K oxides less than 1.5 wt %. Glass with this composition is the most commonly found type in Aquileia [24–27]. However, three samples (C30, A18, and A52) have Mg, K, and P concentrations that are unusually high for natron glass.

They will be discussed separately in Section 2.6.

Concentrations of the major oxides, such as calcium and aluminium oxides, were initially used to gather preliminary information about glassmaking technology and the origin of raw materials. The levels of Ca and Al oxides in the glass are predominantly related to the minerals in the sands used to make frit, and they can be used to identify the primary glass groups, as first suggested by Freestone [28], who identified different typologies of Roman glass through the bivariate plot

(biplot) of CaO vs. Al_2O_3. Figure 2.3 shows such plot for the initial characterisation of the samples. The samples analysed form a clear cluster (C1) in the biplot and show that there is a positive linear correlation between Al and Ca oxides (Figure 2.3, inset), suggesting that the items represented by the values in the cluster must all have been made from primary glass originating from the same geographical area. Calcium and aluminium oxides concentrations of almost all the samples match with those of North-Western European Roman glass dated from the 1st to the 3rd century AD [29], and cluster C1 includes samples with the typical light blue-green colour that characterises the production of vessels from the Roman Imperial period.

Table 2.2.: *Chemical composition of the samples: C=Chunk, A=Artefact, W=Waste (in wt % for the major and minor oxides, in ppm for the trace elements). Colours are based on visual perception. The standard error calculated for wt% is*

Sample	colour	wt %											ppm						
		Na_2O	MgO	Al_2O_3	SiO_2	P_2O_5	K_2O	CaO	TiO_2	MnO	Fe_2O_3	CuO	Co	Sr	Zr	Sn	Sb	Ba	Pb
CHUNKS																			
C03	**Blue**	17.96	0.90	2.52	66.25	0.30	1.19	8.01	0.09	0.63	1.21	0.20	1088	588	61	65	3540	315	896
C10	**Yellow green**	16.70	0.66	2.04	72.01	0.17	1.01	6.19	0.06	0.41	0.50	0.08	18	504	47	76	215	298	79
C29	**Yellow green**	21.09	0.93	1.90	68.79	0.02	0.42	5.45	0.10	0.02	0.59	0.002	2	527	60	1	5206	167	28
C30	**Emerald green**	17.17	1.88	1.99	64.95	0.71	1.82	6.42	0.16	0.74	1.35	1.94	50	588	94	1665	2862	347	2333
C31	**Blue green**	17.95	0.72	2.63	69.14	0.19	0.82	7.14	0.08	0.41	0.61	0.09	19	590	68	86	361	303	134
C33	**Blue green**	18.13	0.71	2.17	69.28	0.21	0.91	7.11	0.07	0.46	0.59	0.11	24	544	59	112	474	294	155
C39	**Blue green**	17.72	0.78	2.42	69.12	0.20	0.83	7.28	0.08	0.48	0.73	0.10	18	590	64	143	522	308	291
C45	**Blue green**	17.87	0.76	2.30	69.31	0.22	0.93	7.26	0.07	0.41	0.55	0.08	20	568	62	194	335	299	119
C46	**Blue green**	17.96	0.71	2.28	69.68	0.19	0.81	6.98	0.08	0.40	0.54	0.10	18	550	65	99	722	277	171
C55	**Blue green**	17.45	0.66	2.03	71.18	0.16	0.73	6.52	0.07	0.39	0.52	0.07	18	510	52	69	493	271	146
C56	**Light blue green**	17.96	0.58	2.01	71.02	0.15	0.68	6.35	0.06	0.42	0.51	0.06	19	512	52	55	308	270	115

C58	**Light blue green**	18.41	0.74	2.20	68.97	0.19	0.97	7.13	0.08	0.43	0.54	0.09	24	559	62	93	539	283	166
ARTEFACTS																			
A14	**Blue**	19.49	0.58	2.38	67.38	0.15	0.67	7.21	0.06	0.50	1.07	0.17	643	576	44	80	682	413	422
A15	**Purple**	21.38	0.64	2.14	65.86	0.11	0.83	6.62	0.05	1.75	0.41	0.008	58	682	42	6	212	362	34
A16	**Light blue**	18.77	0.60	2.35	68.90	0.17	0.77	7.28	0.06	0.36	0.50	0.03	14	562	52	42	299	272	126
A18	**Black (very dark amber)**	20.38	2.26	2.53	63.97	0.67	1.58	5.98	0.23	0.47	1.58	0.07	38	585	130	92	293	286	398
A19	**Colourless**	18.58	0.86	2.39	68.71	0.05	0.54	4.89	0.35	2.13	1.28	0.004	13	504	251	1	1	487	12
A20	**Amber**	20.23	1.06	2.33	65.31	0.08	0.75	9.43	0.06	0.10	0.50	0.002	3	711	47	3	2	241	20
A26	**Blue**	15.73	0.57	2.06	70.83	0.14	0.49	6.48	0.05	0.65	0.88	0.11	588	534	42	4	17535	259	261
A32	**Blue**	17.31	0.53	1.91	70.45	0.17	0.78	6.56	0.04	1.01	0.79	0.16	1375	578	38	8	44	302	16
A52	**Emerald green**	18.20	2.51	2.15	62.11	0.96	2.06	6.73	0.17	0.86	1.49	2.09	59	667	115	2012	1212	326	1384
WASTES																			
W01	**Light green**	17.42	0.52	2.22	70.40	0.13	0.92	7.36	0.06	0.31	0.42	0.02	8	530	44	27	242	273	212
W04	**Light yellow**	17.64	0.43	2.37	70.85	0.09	0.64	7.51	0.05	0.02	0.28	0.001	1	558	44	1	7	236	9
W06	**Blue**	18.64	0.51	2.32	68.75	0.11	0.52	7.11	0.05	0.71	0.95	0.08	441	571	47	10	156	630	33
W07	**Blue green**	18.07	0.76	2.61	68.09	0.17	1.01	8.01	0.07	0.39	0.57	0.03	18	594	57	41	223	310	118
W37	**Yellow green**	16.99	0.56	2.53	69.23	0.12	0.83	8.87	0.05	0.28	0.40	0.001	4	625	43	1	7	258	10
W47	**Blue green**	18.64	0.63	2.47	68.30	0.14	0.72	7.65	0.06	0.44	0.55	0.14	13	569	51	116	374	335	425
W50	**Blue green**	19.35	0.80	1.83	69.93	0.20	0.66	5.48	0.11	0.61	0.70	0.04	14	485	93	65	1006	235	148
W51	**Dark brownish green**	16.82	0.74	2.44	69.22	0.21	0.78	7.12	0.08	0.41	1.80	0.08	21	509	68	577	397	268	577

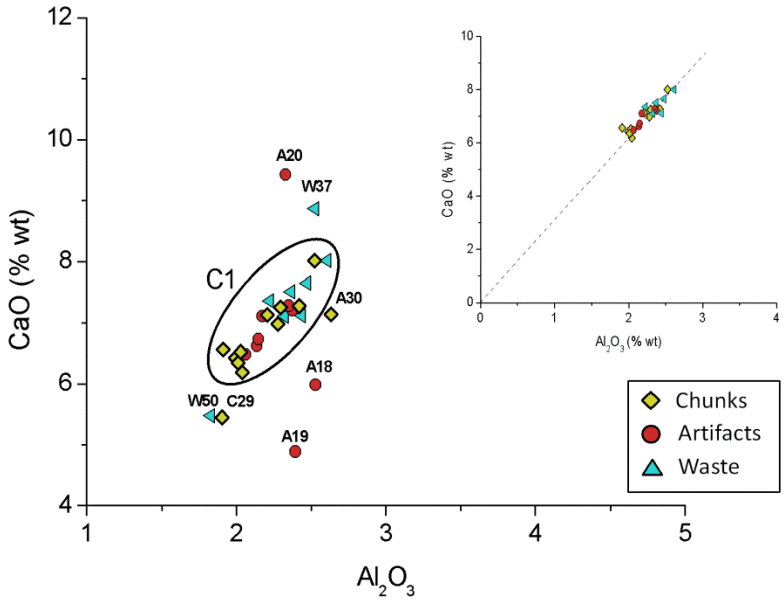

Figure 2.3. Plot of CaO vs. Al_2O_3; the oval encloses cluster C1, a compact group of samples with a strong linear correlation between calcium and aluminum oxides is shown in the inset.

Also, the plot of strontium (Sr) vs. zirconium (Zr) concentrations (Figure 2.4) was aimed to identify the provenience of sands used as raw materials in primary furnaces. In ancient glass, strontium is mainly incorporated (as a trace element) in the lime-bearing material, such as aragonite or calcite, of the sands. Typically, glass produced using coastal sands has low ZrO_2 (<100 ppm) and high SrO (>300 ppm); this latter high value is due to the aragonite of the shells in beach sands. In contrast, glass melted from inland sands, which contains calcium carbonate derived from limestone, shows low SrO (<200 ppm) and high ZrO_2 (>150 ppm) [30–32]. Cluster C1 of Figure 2.3 can also be recognised in cluster C2 in the Zr vs. Sr biplot (Figure 2.4). Cluster C2 is characterised by high Sr and low Zr contents; these values suggest the use of coastal sand as raw material to produce more than two thirds of the analysed samples.

The outlined cluster pattern after principal component analyses (PCA) on a set of 31 oxides (Li, Be, B, Al, Si, Ca, Sc, Ti, Cr, Ga, Sr, Y, Zr, Mo, Ba, Th, U) and 14 REE (from La to Lu, except Pm) for most of the glass samples with similar composition is shown in Figure 2.5. Mentioned elements have been chosen as oxides belonging to sands, excluding all elements that could have originated from minerals added as colorants or opacifiers during the glassmaking phase. The same group is obtained using factor analyses performed on five elements (Ti, Cr, Sr, Zr, Ba and

Cr) (inset of Figure 2.5), considered by Brems & Degryse [33] as the most relevant indicators of the origin of the silica used as raw material.

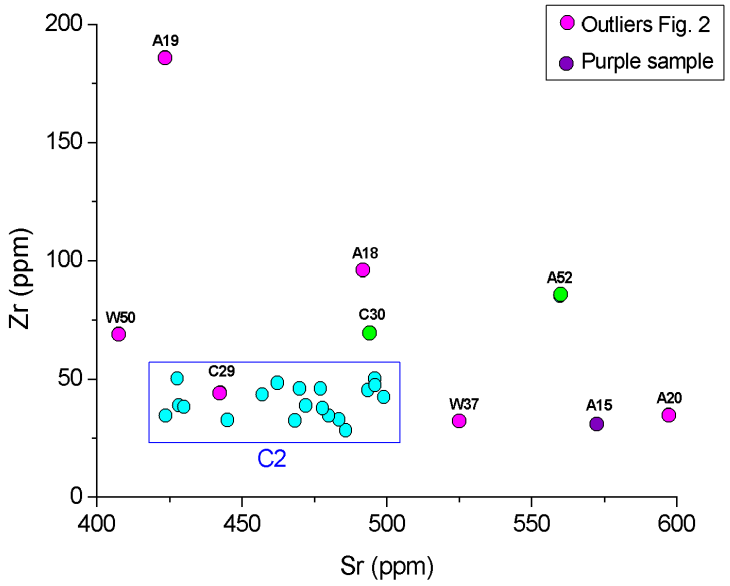

Figure 2.4. Plot of Zr vs. Sr; the rectangle evidences the cluster C2 described in the text. The purple colour of A15 sample is due to the high content of manganese present as Mn^{3+} ion.

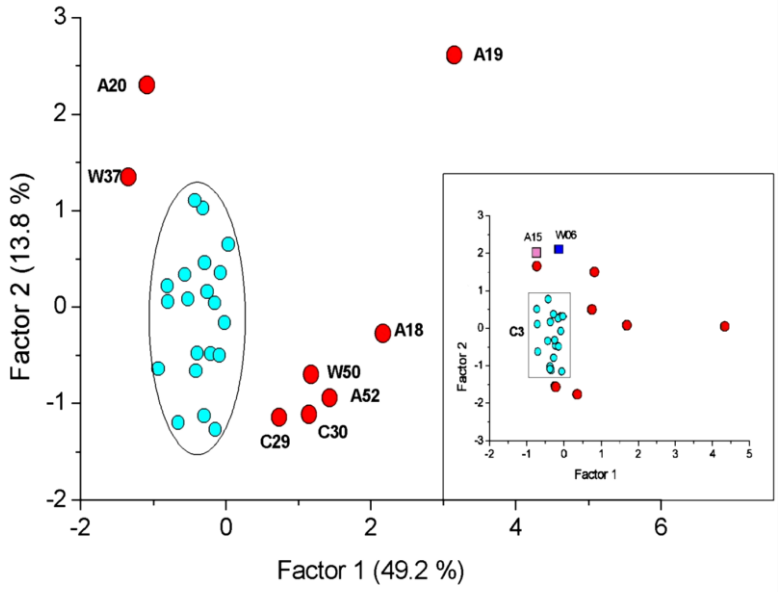

Figure 2.5. Factor analyses on the 31 oxides listed in the text (extraction: principal components; rotation: varimax normalised); in the inset the same type of analyses was performed on Ti, Cr, Sr, Zr and Ba oxides.

The bivariate and multivariate analyses discussed above displayed a cluster of the same 19 samples that share a very similar composition. Moreover, all three plots show values related to "outliers" samples with a composition different from those included in cluster C1 (Figure 2.3). In sample A15 the high level of strontium (~550 ppm) (Figure 2.4) is probably due to the additional content of manganese-strontium bearing minerals, such as Rhodochrosite and Pyrolusite (MnO_2), added to obtain a purple colour. Roman natron glasses decoloured by Mn are usually rich in strontium [30].

The other outliers show a different content of Ca and Al oxides compared to the samples of cluster C1 (Figure 2.3). The amber and brownish samples A20 and W37 have the highest levels of CaO (9.43 and 8.87 wt %, respectively), while samples A19, C29, and W50 have CaO concentrations <6 wt %, which is lower than those of the C1 group, probably due to different sand sources, poor in calcite and feldspars. The latter two samples contain Na oxide values higher than 20 wt % (Table 2.2.). Natron glass manufactured with high purity sand is characterised by low Ca, Al, and Fe, and high Na, and it is typical for glass from the 1st to the 3rd century AD [18]. Compared to the sand source that may be used to produce the samples belonging to cluster C1, the sand used for making the glass of sample A19 seems to have a different geographical provenance as it contains an elevated zirconium concentration (almost 200 ppm) (Figure 2.4).

The plot TiO_2/Al_2O_3 vs. Al_2O_3/SiO_2 (Figure 2.6.) has been used to link the composition of our samples to specific primary production groups. Through this plot Schibille *et al*. [34] classified six different groups, namely Roman manganese-decolourised glass (Rom Mn), Roman antimony-decolourised glass (Rom Sb), Roman mixed antimony and manganese glass (Rom Sb-Mn), Levantine I, Foy-2 and high iron, manganese, and titanium glass (HIMT). These compositional groups have been defined by correlating the chemical composition of the glass to the mineralogical composition of the sands of which they are made, assuming that SiO_2 is an indicator of quartz presence, TiO_2 of heavy minerals, and Al_2O_3 of feldspars; the content in Al_2O_3 and TiO_2 together with the Zr level is the clearest indicator of the origin of the raw sand used in the glass production. The amount of these elements in the composition of glass is used to separate Syro-Palestinian glass from Egyptian glass. In the latter one, the Al_2O_3, TiO_2, and Zr contents are generally higher than 2 wt %, 0.25 wt %, and 190 ppm, respectively. Conversely, glass originating from primary factories in the Levantine zone has an Al_2O_3 content higher than 2 wt %, a TiO_2 content lower than 0.1 wt %, and a Zr content lower than 80 ppm [22].

Among our samples, only sample **W04** shows concentrations of Al_2O_3, TiO_2, and Zr (2.37 wt %, 0.05 wt %, and 44 ppm, respectively) comparable to those that characterise Rom-Mn primary glass produced in coastal areas of ancient Palestine [34].

Sample **C29** (light-yellow) has a high antimony concentration and a very low manganese concentration, and it represents the only sample among those analysed that was decolorised by Sb oxide (Rom Sb). This sample shows a high TiO_2/Al_2O_3 ratio, which is typical of the production

of the primary Rom-Sb glass in Egypt, probably in the area of Alexandria, close to natron sources, as suggested by the high soda content [34]. Other indications of such origin are the low concentrations of Zr (Figure 2.4) and TiO_2, typical for natural quartz sands with a low amount of heavy minerals. Another indicator of Egyptian provenance is the distinctive yellowish colour of the sampled chunk, typical for antimony-decolourised glass, and quite different from the very light blue of Levantine manganese-decolourised glass. The low concentration of CaO and Al_2O_3 (Figure 2.3) suggests that sample C29 can be dated to around the 1st to 2nd century AD, as Sb glass from the late 2nd and early 3rd century AD normally contains high levels of CaO and Al_2O_3 , while in the 4th century there was a rapid decline of antimony colourless glass production [18].
The concentration of the Al, Ti, and Si oxides in samples W04 and C29 are indicative of different geographic areas that supplied the raw materials; if confirmed by additional analyses of a larger samples set of the recovered glass chunks, this would be the first indication that primary glass was sourced by Aquileian glass workshops from both the Syro-Palestinian and Egyptian areas.

Comparing the composition of our samples (Figure 2.6) with the classified primary production groups mentioned above, the samples belonging to cluster C1 (dashed oval in Figure 2.6) match the typical composition of Rom Sb-Mn placed in the graph between the Rom Mn glass and Rom Sb one. The reason to consider the concentration of Mn and Sb in the glass composition is that in Roman glass, antimony and manganese were added to the batch for making colourless glass by oxidizing the iron present as an impurity in the raw materials. However, concentrations of Mn and Sb in the glass higher than their natural background level in sand (0.1 wt % and 30 ppm, respectively), indicate their intentional addition or accidental addition through cullet recycling. Moreover, the concurrent presence of both these decoulorising agents in a glass, as in the C1 cluster, may be an indication of the recycling practice (see Section 2.5).

Another distinct sample in the plot in Figure 2.6. is glass fragment **A19** (blue; outlier), which shows the typical composition of HIMT1 glass that is characterised by high iron, manganese, and titanium concentrations. This compositional group tends to have low lime (Figure 2.3) and high soda contents, in addition to higher concentrations of trace elements, pointing to the use of a less pure silica primary source. Moreover, from a chronological point of view, the latter group is more characteristic for a glass of the early to mid-fourth century as HIMT1 glass was introduced later. Thus, sample A19 can be dated from the mid-4th century onwards [24]. It shows high Sr and Zr concentrations (Figure 2.4), similar to HIMT1 glass from Carthage reported by Schibille [34], which suggests the use of a sand source located elsewhere than the Levantine coast due to the inclusion of marine shells in the batch.

Five samples seem to have extremely different compositions: *i*) **A20** and **W37** (amber yellow glass), *ii)* **A18** (black glass, actually very dark amber yellow), and *iii)* **C30** and **A52** (emerald green glass). They are discussed in Section 2.4.2 and are considered key samples to establish the activities of the Aquileia furnace and the glass manufacturing.

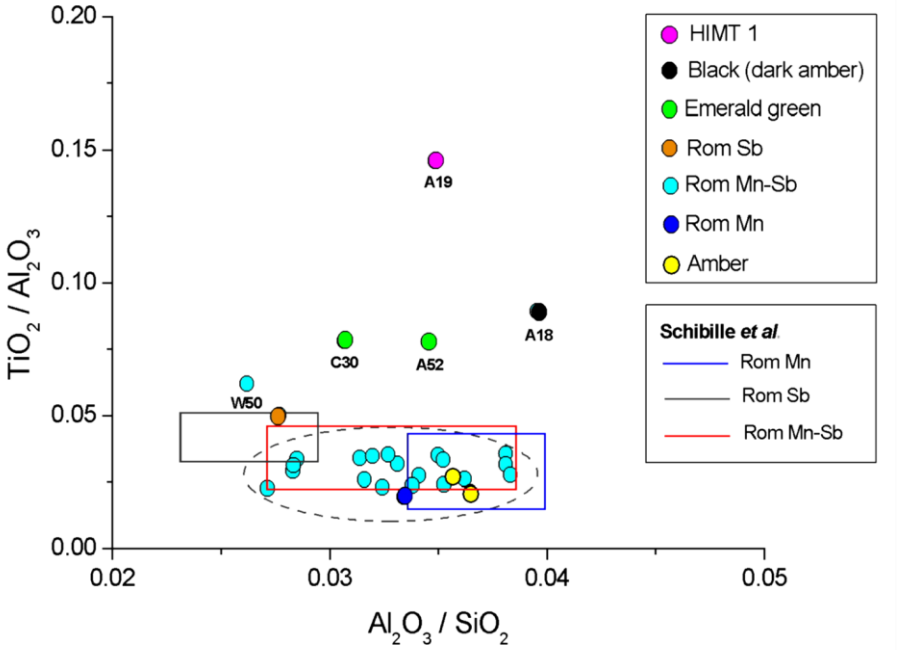

Figure 2.6. Compositional subdivision of primary production groups using the plot of TiO_2/Al_2O_3 vs. Al_2O_3/SiO_2. The dashed oval indicates cluster C1 (Figure 2), whereas the rectangles indicate the various classes of specific primary production groups identified by Schibille et al. [26].

2.3.1. Evidence of recycled glass

Most of the items sampled in this work show evidence of having been manufactured using recycled glass as clearly indicated by:

i. the simultaneous presence in the glass composition of two decolorising agents (manganese and antimony) at concentrations higher than their natural upper limit values (0.1% and 30 ppm respectively), together with the fact that the presence of both decolourising agents has never been found in raw glass from a primary furnace [35];

ii. levels of heavy metals such as Cu, Co, Sb, Sn, Pb over their natural concentration (<100 ppm) are indicative of recycling [33–35] if not intentionally added as colouring (Cu, Co), decolouring (Sb) or opacifying (Sb, Sn, Pb) agents. Most of samples show concentrations of lead and/or tin over 100 ppm, suggesting that their manufacture with recycled glass used also variable amounts of opaque glass.

Almost all samples belonging to the Rom Mn-Sb group show the typical Roman green-blue colour that originates from mixing two primary glass types, manganese- and antimony-decolorised glass (Rom-Mn and Rom-Sb respectively), as part of the recycling process. The bivariate analyses in Figure 2.7 strongly suggests that the ratio between the concentration of the two decolourants in the mixed glass (Rom Sb-Mn) originates from recycling, and it also shows high alumina (Al_2O_3) content in Rom-Mn glass and low alumina in Rom-Sb one. The high fraction of MnO respect to Sb_2O_5 (Figure 2.7) found in the Rom Sb-Mn samples evidences the prevailing use of glass decolourised with manganese (~90%) over that with antimony (~10%) for recycling purpose. It is probable that this mixing rate between the two above mentioned decolourising agents depended on the available glass material. It appears that the two types of the colourless glass from 1st to 4th century AD. were produced in two primary production centres [32]. Some evidence suggests that Rom-Mn glass was produced in Palestina [36], while Rom-Sb one came from Egypt [2,26]. The analyses of a more extended number of samples could give useful information for a more restricted dating.

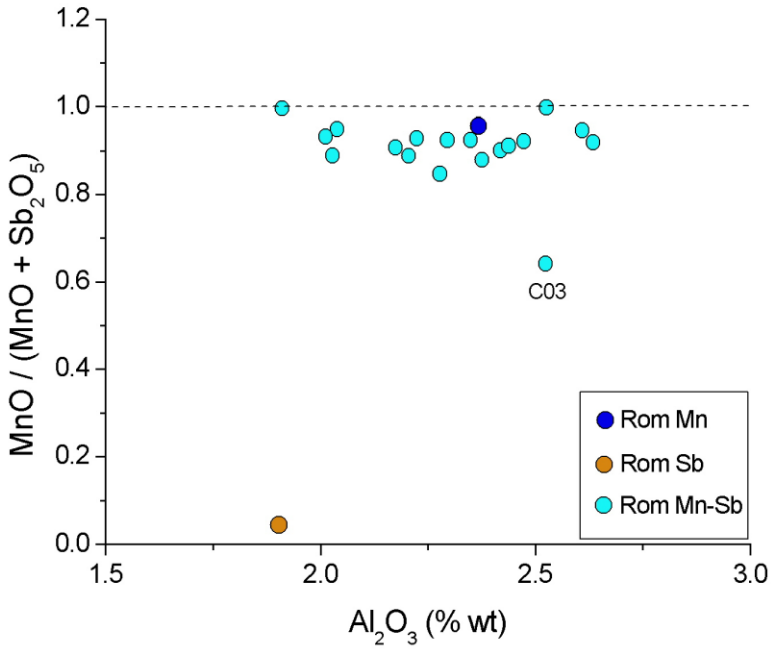

Figure 2.7. Plot of Mn/(Sb+Mn) vs. alumina of the Rom Mn, Rom Sb and Rom Mn-Sb samples. It evidences the general strong prevalence of the Mn-decolourised glass component over the Sb-decolourised one in the Rom Mn-Sb recycled glass.

Only the blue sample C03 shows comparable amounts of Mn and Sb oxides (0.63 and 0.35 wt %) (Figure 2.7), suggesting a production period different from that of the rest of Rom-Mn-Sb samples. Only a few samples seem to be made using not recycled primary glass: amber A20, blue A32, yellow-green W04 and light yellow W37, with amounts of Co, Cu, Sb, Sn, and Pb below 100

ppm. Also, HIMT 1 sample A19 appears to be not a recycled glass: its composition includes high concentrations of iron, manganese, and titanium, typical of this compositional group, but negligible levels of the other heavy metals (Table 2.2.).

The recovery of vessel fragments from recycling could be evidence of glass working at that site. The fact that almost all the chunks, artefact fragments, and waste of the preliminary set of glass here analysed are made from recycled glass could be an indication that there were glass working activities at the site and probably an important recycling centre.

2.3.2. Uncommon glass types

The set of samples analysed includes 5 fragments that stand out as far as their composition is concerned (outside cluster C1, Figure 2.4). They are characterised by less common colours, such as emerald green (**C30** and **A52**), amber (**A20** and **W37**), and black (**A18**). Glass in these three shades, produced starting from the 1st or 2nd century AD, is normally characterised by specific compositions and requires specialised production procedures available in a limited number of furnaces [36,37].

The emerald green samples C30 and A52, and the amber sample A20 contain K, Mg, and P oxides (on average 2.2, 1.9, and 0.83 wt %, respectively) in quantities higher than those normally found in Roman natron glass. Similar high levels of K, Mg, and P are usually related to the use of plant ash flux [38], which is uncommon in the first period of the Roman Empire, but gradually replaced natron from the 9th century AD onwards [39]. From the late 3rd century onwards plant ash fluxes were used only for glass produced in today's Iraq region [40], but they show K, Mg, and P contents much higher than our samples A20, C30, and A52. These levels seem to be related to the addition of plant ash to the natron glass batch in a second step of firing as a reducing agent to obtain the desired emerald green colour [41].

Emerald green samples C30 and A52 have a composition very similar to Roman emerald green glass found in France, England, and Slovenia starting from the 1st century AD [42]. This composition also indicates also the intentional addition of high amounts of CuO (～ 2 wt %) and Fe_2O_3 (～1.5 wt %), together with significant levels of antimony, lead, and tin. The Cu/Sn ratios in the C30 and A52 samples (10.5 and 11.8, respectively) indicate the addition of copper via bronze scraps, while the Pb/Sb ratios around one are very close to the stoichiometry in the yellow opacifier lead antimonate. Based on the concentration of Al_2O_3 and CaO (Figure 2.4), the samples A52 and C30 could be included in cluster C1, but they can be considered outliers because their high levels of Sr, Zr, and Ti (Figures 2.5 and 2.7) that can be associated to the above-mentioned chromophores and/or opacifiers added to the batch.

Sample C30 is representative of the many emerald green chunks recovered at the here studied archaeological site of Aquileia. By considering the exclusive use of emerald green glass to make particular forms of glass objects [41], the recovery of many emerald green chunks suggests the presence of a specialised furnace in this area. It is possible to hypothesize that *i*) raw emerald green glass arrived in Aquileia to fabricate particular forms in a specialised secondary furnace situated in loco, or *ii*) the production of emerald green glass from mineral-soda glass via the addition of green chromophores (Cu, Fe), yellow opacifiers (Sn, Pb, Sb) and plant ash to the batch took place in Aquileia. Besides, one of the main plants used to obtain ashes for glass production is *Salicornia* [43] that grows in saline and swampy environments like those encountered at Aquileia.

Amber sample A20 has a composition like blue-green natron glass, only differing in low Mn and negligible Sb contents. The amber glass production and working were carried out in specialised centres, using selected raw materials, and were coloured during the primary melting of the batch [44]. Like other strong colours, amber glass was produced from the early Imperial period to the early 2nd century AD, becoming relatively rare later [45]. Amber sample A20 has a high content of lime (ca. 9 wt %) and strontium (> 500 μg g^{-1}), suggesting the use of coastal sand particularly rich in marine shells. The low level of iron in the sample (0.5 wt %) is coherent with the presence of natural impurities in the sand source to guarantee the right proportion of Fe^{3+} and S^{2-} ions to achieve the amber hue [46]. To facilitate the development of an amber colour, the addition of a reducing agent such as charcoal was crucial, allowing the control of the redox state of the iron chromophore.

Glassworking sample **W37** (Figure 2.1) is made of primary raw material. Its amber hue suggests that raw glass was re-melted in a secondary furnace at Aquileia to produce amber objects under reducing atmosphere. Moreover, this type of raw glass waste is the most significant for establishing the type of glass made.

Sample **A18** may appear black, but a more accurate visual inspection reveals its very dark amber hue. Unlike the previous amber sample, it shows high concentrations of heavy metals such as copper, antimony, and lead (ca. 700, 300, and 400 ppm, respectively) that are normally associated with recycling. In addition, it shows high contents of Fe (1.6 wt %) and Ti (0.33 wt %) oxides and unusually high levels of K, Mg, and P oxides, similar to the two emerald green samples described above (C30 and A52). This chemical composition may suggest an alternative way to make a glass of that desired colour based on remelting of recycled blue-green glass with the deliberate addition of iron and high quantities of organic reducing agents rich in magnesium to achieve the adequate condition to produce an amber colour mimicking black obsidian.

Black glass from the 1st to the 5th century AD is amply discussed in the literature [41,44,45,47]. Only a few known Roman glass vessels from Northern Europe (3rd century AD) are qualified as dark amber/brown. Their appearance is due to the iron-sulphur chromophore (Fe^{3+}–S^{2-}-3O^{2-}) in combination with the prevailing Fe^{2+} ion (light blue) and the residual Fe^{3+} ion (pale

yellow), obtained under strong reducing conditions [46,48,49]. A black glass fragment from Adria [40] has a composition similar to sample A18, with a comparable content of iron oxide (1.88 wt %), but its black colour was ascribed only to the high iron content.

2.4. DISCUSSION OF THE RESULTS

The elemental analyses of the glass items demonstrated the links existing among the samples, indicating that they represent archaeological evidence for glass working and, thus, implicitly pointing out the potential presence of a secondary furnace in the discovery location. The bivariate and multivariate analyses based on the elements characterising sands and fluxes indicate a similar origin for most of the three types of recovered items. All the samples analysed have in common a colour ranging from blue, blue-green to yellow-green, a good linear correlation between alumina and calcium oxide, and a very similar general composition.

The compositional analyses suggests that some of the raw glass chunks are primary glass from both Syro-Palestinian and Egyptian areas, which might indicate that the glassworkers in Aquileia were able to source raw glass from both Egyptian and Levantine sources, as a direct consequence of the role of the Roman city of Aquileia as a nodal trade connection. This outcome, together with the planned analyses of a larger number of glass fragments from Aquileia, may lead to a revaluation of commercial routes and of the distribution of glass in Europe during the Roman Empire. Besides the production of artefacts directly from raw glass, as suggested by the recovery of waste from primary glass, the presence of many chunks from glass recycling seems to indicate that in Aquileia there was a thriving glass recycling business. All the samples recognised as recycled glass belong to a compact compositional cluster.

Some clues might indicate that Aquileia was also the venue of specialised production both of black glass vessels (dark amber) – obtained by recycling blue-green glass under reducing conditions with the addition of iron and vegetable carbon – and of emerald green glass, evidence of which has been found in the form of a chunk and a shard.

Considering this preliminary analyses, in-depth studies may be performed on hundreds of glass samples recovered all over the suburban areas of Aquileia with the aim of clarifying the role of the city in glassmaking and glass trading. Further information retrieved from chemical analyses of different types of glass from Aquileia (for example crucible fragments, cullet dumps, and glass waste) will then be used to develop and interpret patterns of trade and fabrication that took place at the site.

2.5. REFERENCES

[1] A. Traviglia, L. Mandruzzato, E.F. Orsega, L.M. Moretto, S. Floreani, A. Bernardoni, Picking up the hint: raw glass chunks and glass waste from ploughsoil collection in Aquileia(Italy), Ann. 21e Congrès Int. Pour L39Histoire Verre 3-7 Sept. 2018 Istanb. (2021).

[2] Th. Rehren, I.C. Freestone, Ancient glass: from kaleidoscope to crystal ball, J. Archaeol. Sci. 56 (2015) 233–241. https://doi.org/10.1016/j.jas.2015.02.021.

[3] I.C. Freestone, Y. Gorin-Rosen, M.J. Hughes, Primary glass from Israel and the Production of Glass in Late Antiquity and the early Islamic period, Route Verre M- Nenna Ed Lyon Maison de L'Orient TMO 33 (2000) 65-84.

[4] I. Freestone, The Recycling and Reuse of Roman Glass (Freestone, Journal of Glass Studies 57 (2015) 29-40.

[5] M. Calvi, M. Tornati, Ricerche tecnologiche, in: Vetri Romani Mus. Aquil., (1968) 195–208.

[6] M. Buora, L. Mandruzzato, M. Verità, Vecchie e nuove evidenze di officine vetrarie romane ad Aquileia, Quad. Friulani Archeol. 19 (2009) 51–58.

[7] M. Calvi, Le arti suntuarie, in: Aquil. Venezia Una Mediazione Tra Eur. E Oriente Dal II Secolo AC Al VI Secolo DC, Milano, (1980) 453–490.

[8] A. Silvestri, The coloured glass of Iulia Felix, J. Archaeol. Sci. 35 (2008) 1489–1501. https://doi.org/10.1016/j.jas.2007.10.014.

[9] M. Buora, Vetri antichi del Museo Archeologico di Udine. I vetri di Aquileia della collezione di Toppo e materiali da altre collezioni e da scavi recenti, Ed. Quasar. (2004).

[10] S. Groh, Ricerche sull'urbanistica e le fortificazioni tardoantiche e bizantine di Aquileia, Relazione sulle prospezioni geofisiche condotte nel 2011.

[11] S. Panighello, J.T. Van Elteren, E.F. Orsega, L.M. Moretto, Laser ablation-ICP-MS depth profiling to study ancient glass surface degradation, Anal. Bioanal. Chem. 407 (2015) 3377–3391. https://doi.org/10.1007/s00216-015-8568-7.

[12] B. Wagner, A. Nowak, E. Bulska, K. Hametner, D. Günther, Critical assessment of the elemental composition of Corning archeological reference glasses by LA-ICP-MS, Anal. Bioanal. Chem. 402 (2012) 1667–1677. https://doi.org/10.1007/s00216-011-5597-8.

[13] J.T. van Elteren, N.H. Tennent, V.S. Šelih, Multi-element quantification of ancient/historic glasses by laser ablation inductively coupled plasma mass spectrometry using sum normalisation calibration, Anal. Chim. Acta. 644 (2009) 1–9. https://doi.org/10.1016/j.aca.2009.04.025.

[14] B. Gratuze, Glass Characterisation Using Laser Ablation-Inductively Coupled Plasma-Mass Spectrometry Methods, in: L. Dussubieux, M. Golitko, B. Gratuze (Eds.), Recent Adv. Laser Ablation ICP-MS Archaeol., Springer Berlin Heidelberg, Berlin, Heidelberg, (2016) 179–196. https://doi.org/10.1007/978-3-662-49894-1_12.

[15] K. Janssens, ed., Modern Methods for Analysing Archaeological and Historical Glass, 1st ed., Wiley (2013). https://doi.org/10.1002/9781118314234.

[16] R. Jaćimović, B. Smodiš, T. Bučar, P. Stegnar, k0-NAA quality assessment by analyses of different certified reference materials using the KAYZERO/SOLCOI software, J. Radioanal. Nucl. Chem. 257 (2003) 659–663. https://doi.org/10.1023/A:1026116916580.

[17] M. Bertini, A. Izmer, F. Vanhaecke, E.M. Krupp, Critical evaluation of quantitative methods for the multi-elemental analyses of ancient glasses using laser ablation inductively coupled plasma mass spectrometry, J. Anal. At. Spectrom. 28 (2012) 77–91. https://doi.org/10.1039/C2JA30036B.
[18] C.M. Jackson, S. Paynter, A Great Big Melting Pot: Exploring Patterns of Glass Supply, Consumption and Recycling in Roman Coppergate, York: Glass supply, consumption and recycling in Roman Coppergate, York, Archaeometry. 58 (2016) 68–95. https://doi.org/10.1111/arcm.12158.
[19] I. Freestone, Primary glass sources in the mid-first millennium A.D., Free. C 2003 Prim. Glass Sources -First Millenn. AD Ann. 15e Congr. L'Association Int. Pour L'Histoire Verre (2003) 111-115.
[20] K.H. Wedepohl, A. Baumann, The use of marine molluskan shells for Roman glass and local raw glass production in the Eifel area (western Germany), Naturwissenschaften. 87 (2000) 129–132. https://doi.org/10.1007/s001140050690.
[21] D. Dungworth, Kelp in historic glass: the application of strontium isotope analyses (Dungworth, Degryse and Schneider), Isot. Vitr. Mater. (2009).
[22] P. Degryse, ed., Glass making in the Greco-Roman world: results of the ARCHGLASS project, Leuven University Press, Leuven, Belgium, (2014).
[23] D. Foy, M. Picon, M. Vichy, V. Thirion-Merle, Caractérisation des verres de la fin de l'Antiquité en Méditerranée occidentale : l'émergence de nouveaux courants commerciaux, in Exchanges and trade in glass in the ancient world, international colloquium of AFAV, Aix-en -Provence and Marseille, June (2001) 41-86. [24] H.E. Foster, C.M. Jackson, The composition of 'naturally coloured' late Roman vessel glass from Britain and the implications for models of glass production and supply, J. Archaeol. Sci. 36 (2009) 189–204. https://doi.org/10.1016/j.jas.2008.08.008.
[25] S. Maltoni, A. Silvestri, A. Marcante, G. Molin, The transition from Roman to Late Antique glass: new insights from the Domus of Tito Macro in Aquileia (Italy), J. Archaeol. Sci. 73 (2016) 1–16. https://doi.org/10.1016/j.jas.2016.07.002.
[26] P. Mirti, A. Lepora, L. Saguì, Scientific Analyses of Seventh-Century Glass Fragments from the Crypta Balbi in Rome*, Archaeometry. 42 (2000) 359–374. https://doi.org/10.1111/j.1475-4754.2000.tb00887.x.
[27] A. Toniolo, "...pallentia solphurata fractis permutat vitreis...". Il carico di rottami di vetro del relitto di Grado, in: Vetro NellAlto Adriat. Atti IX Giornate Naz Stud, Imola, (2007) 57–69.
[28] I.C. Freestone, The Provenance of Ancient Glass through Compositional Analyses, MRS Proc. 852 (2004) 188-201 https://doi.org/10.1557/PROC-852-OO8.1.
[29] E. Gliozzo, The composition of colourless glass: a review, Archaeol. Anthropol. Sci. 9 (2017) 455–483. https://doi.org/10.1007/s12520-016-0388-y.
[30] C.M. Jackson, Making colourless glass in the Roman period, Archaeometry. 47 (2005) 763–780. https://doi.org/10.1111/j.1475-4754.2005.00231.x.
[31] P. Degryse, I. Freestone, J. Schneider, S. Jennings, Technology and provenance study of Levantine plant ash glass using Sr-Nd isotope analyses, Glass Byzantium - Prod. Usage Anal. (2010) 83–91.

[32] I.C. Freestone, K.A. Leslie, M. Thirlwall, Y. Gorin-Rosen, Strontium Isotopes in the Investigation of Early Glass Production: Byzantine and Early Islamic Glass from the Near East*, Archaeometry. 45 (2003) 19–32. https://doi.org/10.1111/1475-4754.00094.
[33] D. Brems, P. Degryse, Trace Element Analyses in Provenancing Roman Glass-Making, Archaeometry. 56 (2014) 116–136. https://doi.org/10.1111/arcm.12063.
[34] N. Schibille, A. Sterrett-Krause, I.C. Freestone, Glass groups, glass supply and recycling in late Roman Carthage, Archaeol. Anthropol. Sci. 9 (2017) 1223–1241. https://doi.org/10.1007/s12520-016-0316-1.
[35] I.C.F. Ana Franjic, Glass recycling, in: RECYCLE IDEAS PAST, Zagreb, (2018) 145–161. https://doi.org/10.17234/9789531757232-10.
[36] V. Anvers, du 17e Congrès ANNALES of the 17th Congress, (2006) 39–46. https://doi.org/10.13140/2.1.2923.7121.
[37] T. Rehren, I.C. Freestone, Ancient glass: From kaleidoscope to crystal ball, J. Archaeol. Sci. 56 (2015) 233–241. https://doi.org/10.1016/j.jas.2015.02.021.
[38] R. Arletti, G. Vezzalini, S. Biaggio Simona, F. Maselli Scotti, Archaeometrical studies of roman imperial age glass from canton ticino, Archaeometry. 50 (2008) 606–626. https://doi.org/10.1111/j.1475-4754.2007.00362.x.
[39] F. Gallo, A. Silvestri, G. Molin, Glass from the Archaeological Museum of Adria (North-East Italy): new insights into Early Roman production technologies, J. Archaeol. Sci. 40 (2013) 2589–2605. https://doi.org/10.1016/j.jas.2013.01.017.
[40] P. Mirti, M. Pace, M.M. Negro Ponzi, M. Aceto, ICP–MS analyses of glass fragments of Parthian and Sasanian epoch from Seleucia and Veh Ardašir (central Iraq), Archaeometry. 50 (2008) 429–450. https://doi.org/10.1111/j.1475-4754.2007.00344.x.
[41] V. Van Der Linden, P. Cosyns, O. Schalm, S. Cagno, K. Nys, K. Janssens, A. Nowak, B. Wagner, E. Bulska, Deeply coloured and black glass in the northern provinces of the Roman empire: Differences and similarities in chemical composition before and after AD 150, Archaeometry. 51 (2009) 822–844. https://doi.org/10.1111/j.1475-4754.2008.00434.x.
[42] C.M. Jackson, S. Cottam, “A green thought in a green shade”; Compositional and typological observations concerning the production of emerald green glass vessels in the 1st century A.D., J. Archaeol. Sci. 61 (2015) 139–148. https://doi.org/10.1016/j.jas.2015.05.004.
[43] J. Henderson, the Raw Materials of Early Glass Production, Oxf. J. Archaeol. 4 (1985) 267–291. https://doi.org/10.1111/j.1468-0092.1985.tb00248.x.
[44] S. Cagno, P. Cosyns, V. Van der Linden, O. Schalm, A. Izmer, I. Deconinck, F. Vanhaecke, A. Nowak, B. Wagner, E. Bulska, K. Nys, K. Janssens, Composition data of a large collection of black-appearing Roman glass, Open J. Archaeom. 1 (2013) 22. https://doi.org/10.4081/arc.2013.e22.
[45] A. Ceglia, G. Nuyts, S. Cagno, W. Meulebroeck, K. Baert, P. Cosyns, K. Nys, H. Thienpont, K. Janssens, H. Terryn, A XANES study of chromophores: The case of black glass, Anal. Methods. 6 (2014) 2662–2671. https://doi.org/10.1039/c3ay42029a.
[46] J.W.H. Schreurs, R.H. Brill, Iron and sulfur related colors in ancient glasses, Archaeometry. 26 (1984) 199–209. https://doi.org/10.1111/j.1475-4754.1984.tb00334.x.

[47] K. Baert, W. Meulebroeck, H. Wouters, P. Cosyns, K. Nys, H. Thienpont, H. Terryn, Using Raman spectroscopy as a tool for the detection of iron in glass, J. Raman Spectrosc. 42 (2011) 1789–1795. https://doi.org/10.1002/jrs.2935.
[48] J.B. Sanderson, D.C.W., Hutchings, The origins and measurement of colour in archaeological glasses, Glass Technol. 28 (1987) 99–105.
[49] C.M. Jackson, S. Paynter, M.D. Nenna, P. Degryse, Glassmaking using natron from el-Barnugi (Egypt); Pliny and the Roman glass industry, Archaeol. Anthropol. Sci. 10 (2018) 1179–1191. https://doi.org/10.1007/s12520-016-0447-4.

CHAPTER 3 –
STUDYING THE ROLE OF THE INTERACTION BETWEEN SOIL AND ARCHAEOLOGICAL GLASS DURING ITS ALTERATION IN BURIAL ENVIRONMENT.

As mentioned in the first Chapter of this dissertation, the mechanism of glass corrosion is a process that involve the interaction between the surface of glass and different environmental factors that affect the decomposition of glass: temperature, time, pH of the attacking liquid, the ratio of the surface area and the volume of the attacking liquid, micro-organisms, vibrations and previous inadequate conservation treatments. The influence of these factors on the result and on the kinetic of the corrosion process is an interesting topic of research in the field of ancient glass conservation that are capturing the attention of the scientific glass community.

Considering the environment of alteration, we can generally classify ancient glass in two main categories: the archaeological glass that aged and degraded in burial conditions, and the historical glass that are stored for centuries in old and noble houses or in museums [1]. From the macroscopic point of view, the glass objects that are part of the first category present discoloration or the formation of pitting or iridescent patina on the surface as alteration phenomena; instead, the historical glass object are mainly affected by weeping or crizzling. Thus, it is reasonable to suppose that the different external factors that interact with a glass object in burial (liquid water, pH of the soil, soluble salts of the soil) or in museum (relative humidity, temperature, pollutants) environment led to a formation of specific alteration features as result of a specific mechanism of glass dissolution.

The burial corrosion is the result of several factors linked to the chemical composition of glass and to the physico-chemical properties of the soil. Among these, hydrological factors have the greatest impact on buried glass artefacts, as water is the principal deteriorating agent, able to trigger the alkali leaching process, change the local pH and cause spontaneous crack propagation [2–4]. The types and the concentration of the solutes, as well as the organic matter dissolved in soil, determine secondary reactions and the precipitation of corrosion products on the glass surface. Moreover, the alkaline or acidic condition of the burial context is another factor influencing the glass items preservation [4] since most of the corrosion reactions involve H^+ and OH^- species, thus affecting the preferential leaching of some cations or the dissolution of the silica network [5].

As mentioned in the first chapter of this dissertation, following the chemical implications of the Random Network Theory [6], it can be deduced that an acid aqueous environment accelerates the leaching of cations from the glass network. On the other hand, alkaline conditions have a much more destructive effect, since the OH^- species are strong enough to break the oxygen bonds of the silica tetrahedra, leading to the breakdown of the glass structure [7]. These assumptions were confirmed by many experimental studies, showing that the stability of archaeological alkali-silicate glass is clearly influenced by its chemical composition and the proton activity [2,8–11].

Considerable research developed in order to understand the role and the effects of external factors during the glass alteration mechanisms, but almost all the investigations were

conducted on glass mock-ups by the artificial acceleration of the corrosion process [12–17]. Differently, this PhD thesis reports the attribution of specific types of alteration from the direct correlation between the interactions of ancient glass objects with soils where they were buried. In particular, by a non-invasive analyses of archaeological Roman glass samples found in Aquileia and the chemical characterisation of the soils too, we can try to associate the different forms of surface alteration with specific chemical-physical properties of soils, such as low or high pH values and different cation exchange capacities.

One of the peculiarities of this approach is the opportunity to sample and analyse the soils that preserved but also degraded glass fragments, allowing to verify, confirm and/or add information to relevant literature about the mechanism of glass alteration.

3.1. SOIL PROPERTIES

The burial environment is a complex system where the chemical and physical properties of the soil play a role in the process of ancient material alteration. It can be defined a three-phases system as it includes solid particles (soil) in addition to water and air occupying spaces between them. The soil matrix includes both the inorganic and organic particles that can differ in chemical composition and shape. The geometric form of the soil structure define the voids and the pores where water (liquid phase) and air (gaseous phase) are retained [18,19].

The composition of the three-phases system gives to the soil some specific physical and chemical properties. For example, the texture or the porosity, that determines the movement of water and air into the burial system, or the colour of the soil particles that depends on the mineral and organic matter content.

One relevant property of the soil is the electrical conductivity, which proportionally depends on the amount of soluble salts contained in the soil matrix [20]. The soluble salts are either cations (Ca^{2+}, Mg^{2+}, K^{+}, Na^{+}) or anions (Cl^{-}, HCO_3^{-}, CO_2^{-}, SO_4^{2-}) present in crystallised form or dissolved in soil solution. Moreover, the variable having a central role in controlling soil reactions is pH [21]. An excess of H cations over OH anions determines the acidic character of soil [22]. Actually, the acidic nature of the soil is also determined by the presence of Al^{3+}, which indirectly contributes to soil acidity through the hydrolysis reactions shown in Equation 3.1.[21,22].

$$Al^{3+} + H_2O \rightleftarrows Al(OH)^{2+} + H^+ \quad \textit{(Eq. 3.1.a)}$$

$$Al(OH)^{2+} + H_2O \rightleftarrows Al(OH)_2^+ + H^+ \quad \textit{(Eq. 3.1.b)}$$

$$Al(OH)_2^+ + H_2O \rightleftarrows Al(OH)_3(s) \downarrow + H^+ \quad \textit{(Eq. 3.1.c)}$$

Being soil solution a dynamic system, the pH level detected in soil is not localised, but it may change due to external factors as plant roots respiration, mineralisation of organic matter and rainfalls, which contribute to continuous addiction of H^+ ions in soil [18].

Another crucial variable to take in consideration for the soil-glass interaction is the cation exchange capacity (CEC), defined as the sum of positive charges of all cations that the soil can adsorb at a specific pH level per unit weight and it is expressed in milliequivalents per 100 g of soil (meq·100 g^{-1}) or in centimoles of positive charges per kilogram (cmol(+)·kg^{-1}) [18].

To better understand the ion exchange process, we must remember the structure of the clay particles, which include various cations that are not part of the lattice structure, being adsorbed to its surface because of the clay negative charge. Actually, the tetrahedral and octahedral structures of the clay particles may be subjected to isomorphous replacements where some principal elements of the lattice are substituted with other ions with similar radius. Therefore, the clay particles gain a negative charge that is balanced by adsorption of positive ions, such as Na^+, K^+, or Ca^{2+}. Since those cations are not part of the internal structure, clay can exchange them in what is called *cation exchange process* (Equation 3.2.) [19,22].

$$Na_2[clay] + Ca^{2+} \rightleftarrows Ca[clay] + 2Na^+ \quad \text{(Eq. 3.2)}$$

A similar mechanism occurs with anions adsorbed from soil particles where the surface is positively charged. Cationic and anionic exchange contribute together to the ion exchange capacity [18,23]. The soli capacity to adsorb cations vary according to the ion concentration in soil solutions and to the soil adsorption energy: the higher these two parameters are, the more the absorption capacity increases. The adsorption energy, which may be defined as how strongly the ion is attracted by the surface, depends on the ion valence and on the degree of hydration. For example, between calcium and sodium ions, the first one is adsorbed more strongly than the second one, because of Ca^{2+} (divalent ion) has twice the adsorption energy than Na^+ (monovalent ion). Thus, the sequence of relative adsorption energy is $Al^{3+} > Ca^{2+} > Mg^{2+} > K^+ > Na^+$ [18,23].

CEC depending on numerous factors. In particular, the process is pH-dependent since the pH of the soil produces a temporary source of charge upon the surface of some colloidal particles. When the pH decreases, the concentration of H^+ in soil solution is high and it tends to bond with

negative charges exposed on the surfaces of the soil particles. Otherwise, when the pH increases and the OH^- concentration is higher than H^+, the exposed charges remain negative [23].

3.2. SOIL CHARACTERISATION

Soil samples were sampled in July 2021 from three different agricultural fields around Aquileia (Figure 3.1.). The sampling was decided considering both the permits obtained by landowners and in which fields the glass fragments that present the greatest state of degradation were found. Each of them was sampled three times with soil cores (Ø 10 cm) at different depths, namely at 30 cm, 60 cm and 90 cm, from the starting point at 10 cm below the footstep level.

Figure 3.1.Maps of the sampled lands near Aquileia.

The AQ50 land is located near the Grado Lagoon. The soil samples collected there appeared to be made of clay and were highly moistened. Observing the soil sample coming from AQ50 we note that they become darker in colour going in depth. The AQ115 and AQ117 are, instead, sited inland closer to the current city of Aquileia. The AQ117 was sampled in a spot where the land was characterised by a light mark highly visible from satellite images and where crops grew less in height than in most of the location. These peculiar cropmarks are proxies for the existence of archaeological structures underneath the soil.

The soil samples were prepared for the analyses following the standard approach used for soil characterisation in geological contest [24]:

(a) the samples were roughly fractionated into small parts;

(b) the soils have been dried in an oven at 40° C for at least 48 hours. Dry soils are shown in Figure 3.2;

(c) soils were fractionated and transformed into fine sand in a mortar and passed through a 2 mm sieve;

(d) every soil sample was divided into eight portions with a Rotating Sample Divider (Retsch);

(e) two portions for each sample were successively treated with Planetary Mill Pulverisette (Fritsch) to obtain talc-like fine dust. The latter sample preparation is specific for MP-AES analyses.

Figure 3.2 Dried soils.

In the following sections the results obtained from the analyses of each level of sampling (I, II, and II) and their average (a) are reported.

3.3.1. pH measurements

One of the main factors affecting glass preservation in burial environment is the pH [2,4,13,21]. The level of pH was measured on saturated solutions of the soil samples used the recommended method to assess reactivity for cultivated soils that involve the use of calcium chloride ($CaCl_2$) solution since it is not affected by the concentration of soluble salts, and, moreover, it results unaltered even after long air conservation of the sample.

The pH level was determined by potentiometric device. The analytical method requires 10 g of each soil to be added with 25 mL of $CaCl_2$ 0.01 M solution. The saline solution was prepared previously starting from $CaCl_2 \cdot 2H_2O$ solid salt dissolved in pure water and stored at room temperature. Soil and solutions were mixed in 50 mL beakers and shaken for 2 hours at 120 rpm. Samples were left to decant for some minutes and pH values were then recorded. A benchtop meter HI5522 by Hanna Instruments was used with a digital pH glass electrode HI10530 specific for soils. Calibration was performed with standard solutions before the measurements. Table 3.1 reports the pH value for each soil samples. The AQ115 and AQ117 soils have similar pH values, just above 8, indicating a moderately alkaline property of these field, while AQ50 has a more neutral pH. In addition, the data show the heterogeneities of results: the pH values of the AQ115 and AQ117 samples range between 7.9 and 8.2, confirming the alkaline nature of the soils at the three levels of sampling. Differently, the results obtained from AQ50 analyses show a peculiar trend: the first 30 cm of depth has 7.5 pH value, which identifies it as slightly alkaline, but the pH level decreases to 7.1 for the 60 cm until the strongly acidic value of 5.4 for the deepest sample (Table 3.1).

Table 3.1. pH value of the soil samples. The uncertainty of the measures is 0.1.

Sample	pH value
AQ50I	7.5
AQ50II	7.1
AQ50III	5.4
AQ50a	**6.7**
AQ115I	7.9
AQ115II	8.2
AQ115III	8.2
AQ115a	**8.1**
AQ117I	8.0
AQ117II	8.1
AQ117III	8.1
AQ117a	**8.1**

3.3.2. Electrical conductivity measurements

The total amount of soluble salts in soil was assessed indirectly with electrical conductivity (EC) measurement. EC measurements are performed on saturated paste prepared with 10 g of soil and 20 mL of pure water; samples were shaken for 2 hours at 120 rpm and decanted overnight. Then, samples were filtered through Whatman filter paper grade 42 at least twice. Such water extracts were used for the analyses. The extract soil-water in 1:2 ratio is used generally for soil in humid regions and intensively fertilised, as the case of the Aquileia fields. Electrical conductivity was determined with a conductivity electrode HI76312 coupled with Hanna benchtop meter HI5522. Calibration was performed with standard solutions before the measurements.

The results obtained from the measurement of the water extract are presented in Figure 3.3. AQ50 has an EC value extremely high than the values obtained from AQ115 and AQ117 analyses. Data related to the three levels of sampling in AQ50 reveal the increment of EC value considering the depth of the sampling. Differently, both AQ115 and AQ117 have homogeneous EC values at the different depths.

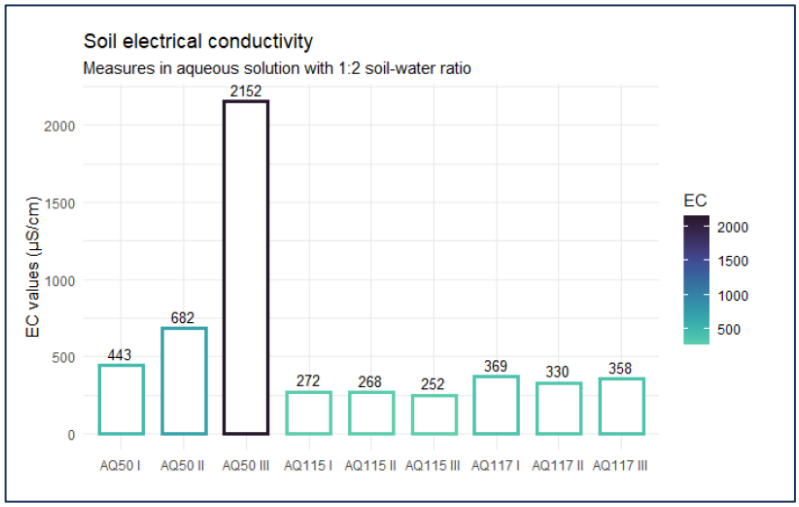

Figure 3.3. Graphical representation of the EC results of the soil samples. The values are expressed in µS·cm^{-1}. Colour is function of the EC value.

3.3.3. Cation exchange capacity measurements

Cation exchange capacity (CEC) was assessed with the aim to determine the ion mobility in the soil samples. CEC indicates the sum of the cations adsorbed by soil particles that are exchanged with the soil solution, playing a determinant role in defining soil reactivity [18,19,22,23].

The sample preparation for the titration method adopted for the analyses involve the use of 2 g of soil that were added to 25 mL of $BaCl_2$ solution at pH=8.2 inside a 50 mL centrifuge flask. The saline solution was previously prepared with $BaCl_2 \cdot 2H_2O$ salt dissolved in pure water and triethanolamine. The pH level of 8.2 was reached through the addition of HCl 1M solution. The samples were shaken for 1 hour at 150 rpm and then centrifuged for 10 minutes at 6000 rpm. Then, the supernatant was removed. These phases of rinsing the samples with BaCl2 solution were repeated three times totally.

Soil residues were added to 25 ml of $MgSO_4$ 5 $cmol \cdot L^{-1}$ solution. The solution was previously prepared using $MgSO_4 \cdot 7H_2O$ dissolved in pure water and stored at room temperature. Samples were shaken for 5 minutes at 150 rpm and then centrifuged for 10 minutes at 6000 rpm. For the tritation analyses the supernatant was used as the sample.

The complexometric titration was carried out using ethylenediaminetetraacetic acid (EDTA) 2.5 $cmol \cdot L^{-1}$ as chelating agent. It was previously prepared from the disodium EDTA salt dissolved in pure water and stored at room temperature. A buffer solution at pH=10 was prepared with NH_4Cl and NH_4OH dissolved in pure water. The solution to be titrated was prepared with 10 ml of $MgSO_4$ soil solution, 100 mL of deionised water, 10 mL of buffer solution at pH=10 and the indicator made of sodium chloride and eriochrome black T. Blank solution was prepared in the same way but adding 10 mL of fresh $MgSO_4$ solution. The final volume was recorded when the solution turned blue. The CEC value of soils is derived from the EDTA amount added for titration.

The principle which the titration method relies on is the saturation of soil sample with barium and the addition of known solution of $MgSO_4$. The exchange reaction between Ba^{2+} and Mg^{2+} brings the formation of insoluble $BaSO_4$. The total content of barium added to saturate the sample is exchanged with magnesium: this means that the excess of Mg^{2+} in solution, which is determined by complexometric titration with EDTA, defines the content of barium exchanged. Lower is the concentration of Mg^{2+} in solution, higher is the CEC of the soil because it has exchanged a great part of Ba^{2+} content with Mg^{2+}.

Table 3.2 reports the CEC values expressed in $cmol(+) \cdot kg^{-1}$ of soil mass. The results show that, although the capacity of cation exchange is elevated in all the soil samples, the sample AQ50 is characterised by the highest values. As reported in Table 3.2. CEC values obtained from AQ50 and AQ115 analyses of the three sampling in depth are homogeneous, whereas data from AQ117 have a different trend. For this latter sample, it is possible to note that the exchange capacity decreases with depth as clearly demonstrate by the value associated to the second level of sampling –60 cm below the footstep level – that strongly varies from the value revealed in AQ117I.

Table 3.2.CEC values of the soil samples. Data are in cmol(+)·kg^{-1} and the uncertainty of the measures is reported.

Sample	CEC values
AQ50I	45±5
AQ50II	43±2
AQ50III	40±10
AQ50a	**43±7**
AQ115I	23.6±0.2
AQ115II	24±5
AQ115III	26±2
AQ115a	**24±3**
AQ117I	37±1
AQ117II	26±3
AQ117III	24±9
AQ117a	**29±17**

3.3.4. Elemental analyses

The elemental characterisation of soil samples was performed using Agilent 4210 Microwave Plasma Atomic Emission Spectroscopy (MP-AES). The elemental quantification is obtained by the collection of the electromagnetic emission originated from the return to their fundamental state of atoms previously excited. The wavelengths chosen for the analyses of each element were selected to minimise the spectral interferences. Calibration curves were accepted with correlation coefficient greater than 0.999 and less than 10% calibration fit error was set for each standard element. The standard solutions were prepared from element reference solutions in 2% HNO_3. In order to accurately detect the Ca content, the soil water extracts were diluted 1:10 or 1:50.

To analyse the elemental composition, the soil samples were prepared in a medium suitable for the instrument and equally able to digest totally the organic and inorganic matter. Total digestion of soil samples was carried out using Milestone Ethos Up microwave digestion system. The procedure required 0.1 g of soil added in 3 mL of aqua regia, 1.5 mL of concentrated HF and 3 mL of pure water. Blank sample was prepared using the same procedure without any initial soil mass. To control the digestion grade, a sample of standard reference material 2711a Montana II soil was digested in the same conditions. The microwave run the digestion for 1 hour reaching 200° C of temperature. After 30 minutes of cooling, digested samples were added in 3 mL of H_3BO_3 oversaturated solution. Digested soil samples were left to rest for 15 minutes and

then brought up to 50 mL volume of pure water. Then the samples were stored at low temperatures.

Table 3.3 reports the concentration of the elements of interest detected from the MP-AES analyses expressed in g·kg^{-1} of soil mass. To better visualize these data, their graphical representation is shown in Figure 3.4.

Table 3.3. MP-AES data of the soil samples. Data are in g·kg-1 and the uncertainty of the measures is reported.

Sample	Element content in g·kg^{-1}							
	Al	***Ca***	***Cu***	***Fe***	***K***	***Mg***	***Na***	***Pb***
AQ50I	34±1	12±1	<1	21±2	8±1	14±3	2.9±0.3	-
AQ50II	34±1	13±1	<1	20±1	7.7±0.2	16±6	2.8±0.1	<1
AQ50III	35±2	4.5±0.5	<1	20±1	8.0±0.2	15±1	2.9±0.1	-
AQ50a	**35±1**	**10±12**	<1	**20±1**	**7.9±0.4**	**15±2**	**2.9±0.2**	**-**
AQ115I	3±2	100±40	<1	<1	9±1	13±1	3.3±0.2	<1
AQ115II	2±1	110±30	<1	<1	8±2	14±2	3.3±0.1	<1
AQ115III	2.43±0.01	110±20	<1	23±1	9.5±0.2	13±2	3.5±0.2	<1
AQ115a	**2.5±0.5**	**110±10**	<1	<1	**9±2**	**14±2**	**3.3±0.5**	<1
AQ117I	2.9±0.4	105±6	5±3	47±3	12.9±0.3	2.3±0.2	4.8±0.1	2.1±0.1
AQ117II	3±1	110±10	2.4±0.1	47±1	13.4±0.3	2.3±0.4	5±1	2±3
AQ117III	2±1	109±5	<1	41±1	13±1	0.8±0.3	6.3±0.4	<1
AQ117a	**3±1**	**108±6**	**3±5**	**45±5**	**13±1**	**2±2**	**5±2**	**2±2**

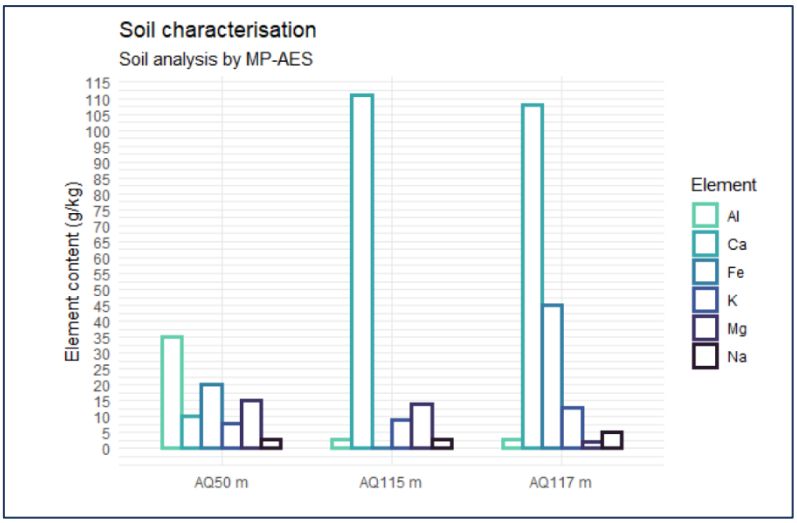

Figure 3.4. Graphical representation of the average concentration of the most representative elements of the soil samples. Data are in g·kg^{-1}. Colours identify different elements.

Al, Ca, Fe, K, Mg and Na are the elements detected in higher concentration in the soil samples. Comparing the results obtained from the soils analyses we observe a great variability in Al, Ca, Fe, Mg and Pb concentration among the different samples. The levels of Al and Ca detected in the AQ50 soil are remarkably different from the values reported for AQ115 and AQ117 (Figure 3.4). This difference has an important impact in the soil characterisation since Al and Ca, generally present in soil in the form of silicates and carbonates, allow to distinguish a clayey soil – in this case, the AQ50 soil - from a calcareous one – as the case of AQ115 and AQ117 soils.

In addition, as mentioned above, the presence of aluminum in a soil promotes the lowering of pH toward more acidic values, as confirmed by pH analyses that revealed the acidic nature of soil AQ5O, being characterised by a high aluminum content (Table 3.3).

3.3. GLASS CHARACTERISATION

Archaeological glass samples coming from a series of survey campaigns in the site of Aquileia (north of Italy) were analysed with optical and electron microscopy to observe the morphology and to identify the nature of the alteration features that are present on the surface. The studied glass fragments are different in shape, dimension, colour, and degradation pattern. In particular, two main alteration phenomena can be distinguished observing the glass samples: pitting and the formation of iridescent patina (Figure 3.5. and 3.6.).

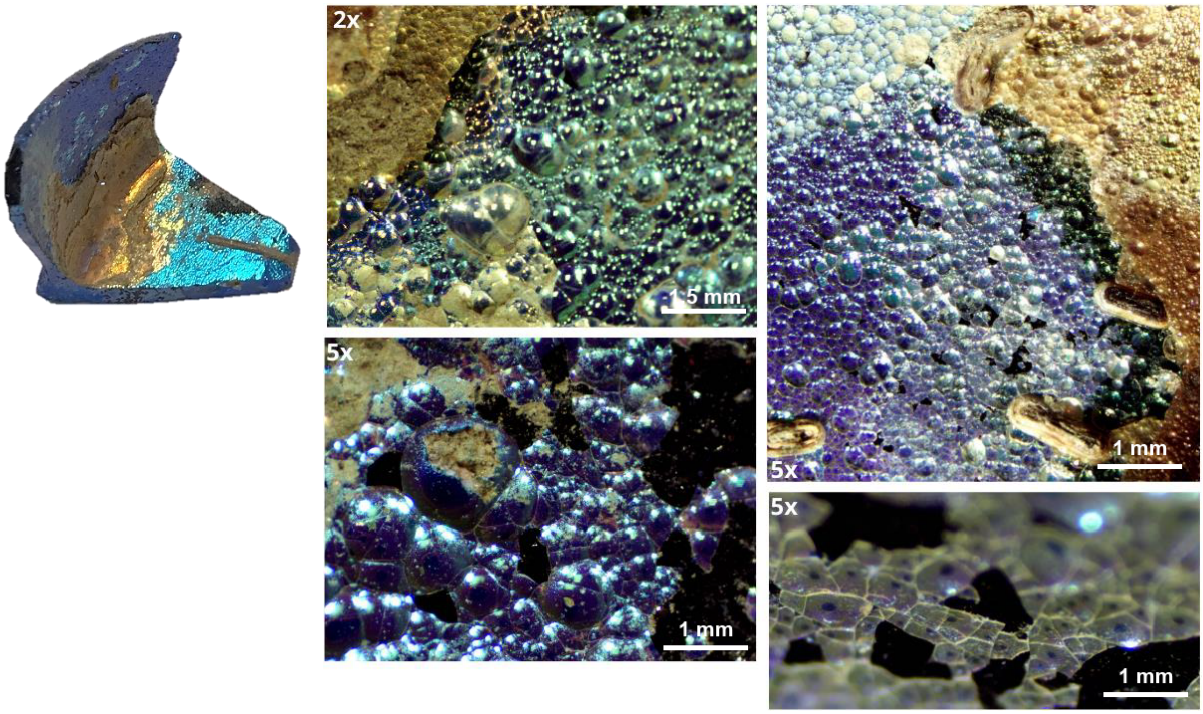

Figure 3.5. On the left AQ50-1 sample. On the right, Bright Field Optical Microscopy images of the iridescent multilayer patina on a AQ50-1 sample, collected with Olympus BX43F optical microscope, magnification is reported in the images.

The sample AQ50-1 in Figure 3.5 is shown as representative of the category of archaeological samples that show the formation of an iridescent patina on the surface as a consequence of the alteration mechanism in the burial environment. This sample is affected by distinct degradation features with both the external and the internal surface entirely covered by blue and ochre iridescent multilayer patina. The iridescent layer is intense blue in great part of the surface and changes in shade between whitish, ochre, and light blue in different areas. In some areas the multilayered structure of the patina is clearly visible. Plenty of small flakes of patina are lost leaving the pristine glass accessible and showing its original colour as a dark shade of blue, close to black.

The sample AQ117, instead, is marked by a diffuse pitting on its surface (Figure 3.6.). From the optical images it is possible to appreciate the round shaped of the pits and the interconnections among them. Moreover, the profilometer image shows that pits develop in the depth of the glass sample, and they seem to be filled by soil probably coming from the burial environment.

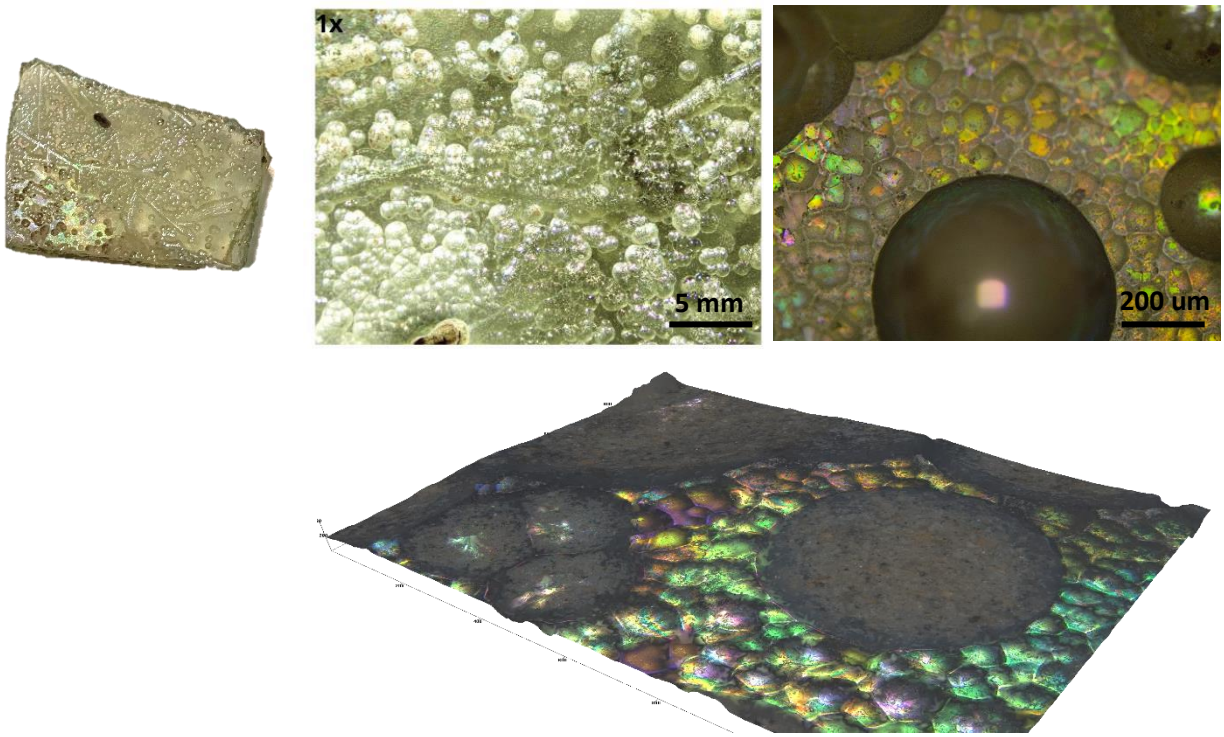

Figure 3.6. On the left, AQ117 sample. On the right Bright Field Optical Microscopy images of pitting marks present on AQ117 sample, collected with Olympus BX43F optical microscope, magnification is reported in the images (above); profilometer image collected with KLA Zeta™-20 Optical Profiler (below).

The secondary electron images (SEI) obtained from the SEM analyses of the AQ50-1 sample, show the thick patina developed on the surface characterised by a heterogeneous and highly fractured structure (Figure 3.7). In some spots the patina flaked away revealing the presence of other layers underneath. In the cross-section, the layered nature of the patina is clearly visible. The thickness of the surface layer is around 15 µm. The chemical analyses of a flake of the iridescent patina, obtained using an EDS probe (Figure 3.7), evidenced the presence of layer enriched in Si and depleted in alkali and alkaline-earth ions (Na, K, Mg, and Ca).

SEM images of the sample AQ117 are collected in Figure 3.8. The alteration surface of the sample is marked by numerous little pits, with diameter equal to 500 µm or smaller. In some

areas of the sample the degradation is so advanced that pits are fused together covering the entire surface.

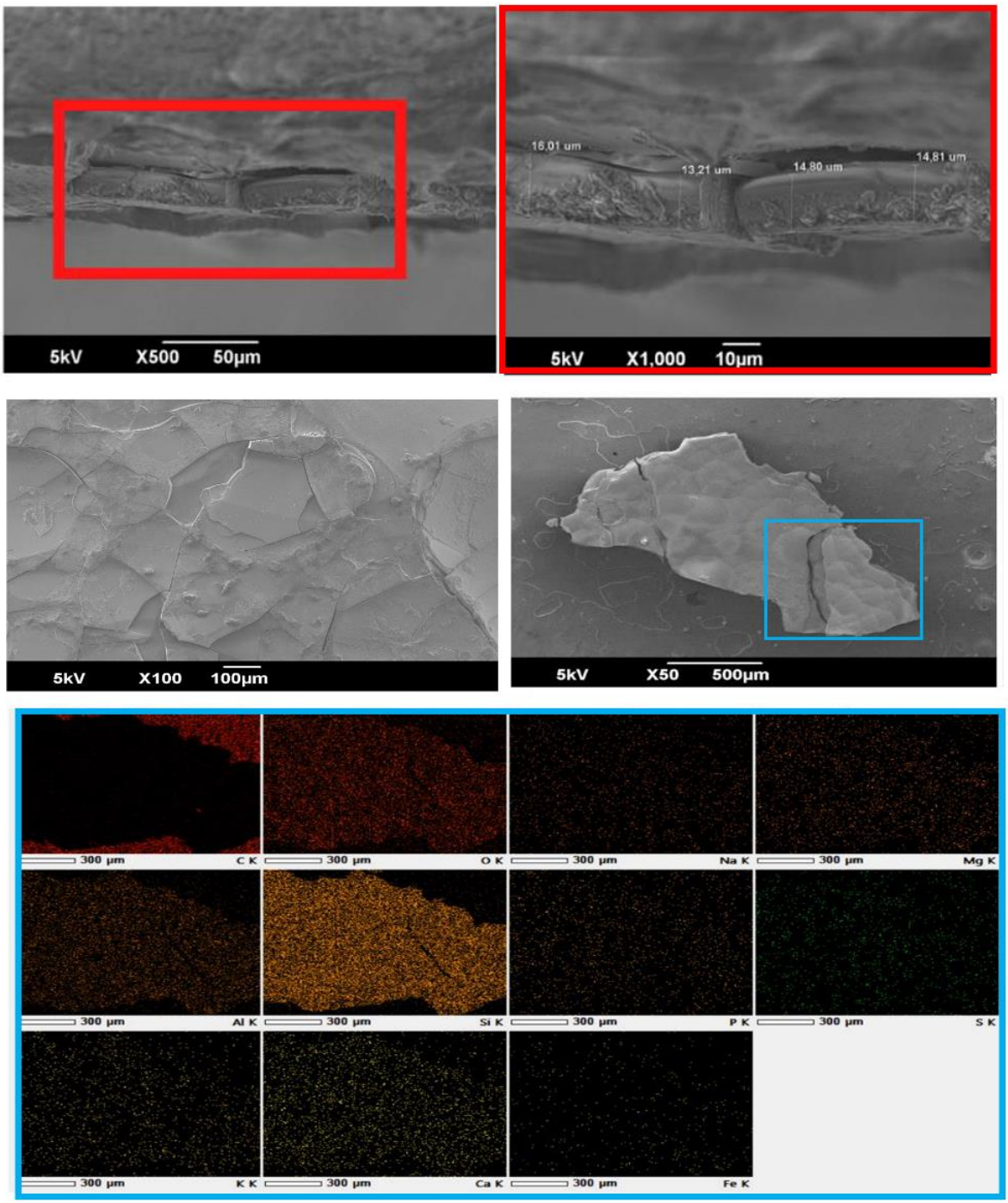

Figure 3.7. SEM secondary electrons images of the sample AQ50-1 (top); SEM-EDS analyses of a flake from the surface patina of the sample AQ50-1 (bottom).

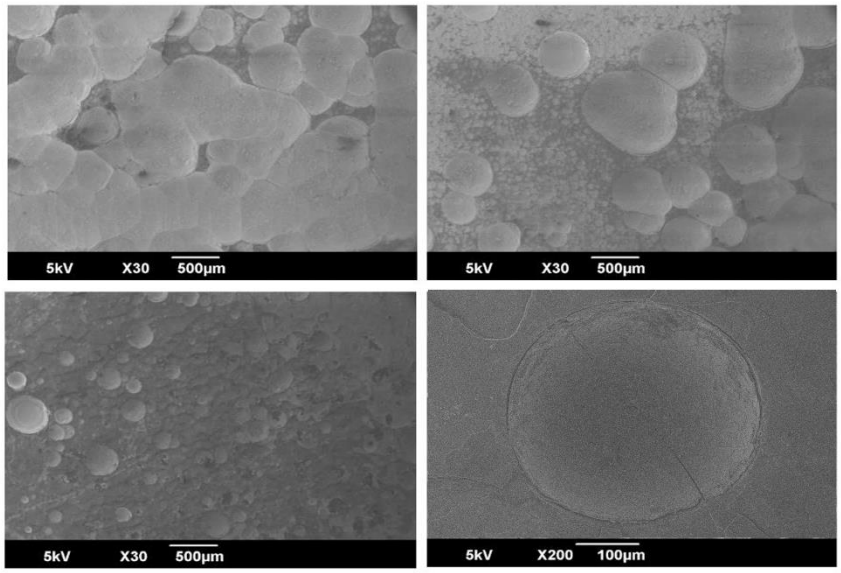

Figure 3.8. SEM secondary electrons images of the sample AQ117.

3.4. DIRECT CORRELATION BETWEEN THE ALTERATION FEATURES AND THE PROPERTIES OF SOIL

The archaeological glass considered in this work has the silica-soda-lime (SSL) composition typical of Roman glass. This type of glass composition is known to be the most chemically stable among ancient glass, yet the fragments considered in this case study have highly corroded surfaces, thus suggesting that some specific characteristics of the soil environment could be responsible to the formation of these visible signs of alteration.

Several published research have investigated the effect of environmental parameters on the kinetics of the glass corrosion process, considering pH as one of the crucial extrinsic factors in the context of alteration in burial environments. For example, a study conducted by Palomar [13] reports that, following accelerated ageing tests, isolated and/or interconnected cracks develop on the surface of Roman type glass under acidic pH conditions. However, the cracks do not turn into pits due to the presence of silylene groups (-Si-OH), which are formed through the bond between the Si ions on the glass surface and the hydroxyl ions remaining in the solution after the leaching process. The silanol groups are resistant to degradation and protect the surface from further damage. On the contrary, in basic and neutral soils, the initial cracks turn into pits due to the continuous loss of matter from the matrix caused by the presence of many OH^- ions

close to the glass, which break the siloxane bonds and thus accelerate the growth rate of the pits. These results confirm that the growth rate of pitting on the glass surface depends on the pH of the surrounding environment. Indeed, in acidic soils, pits formed on the glass surface due to the stresses generated during the degradation process, but these pits did not grow due to the [Si-OH] groups formed during dealkalisation. The dissolution of the glass matrix is thus associated with external conditions with pH>9 [3,25] and the degradation that occurred in the tested glasses shows that the pH increases locally at the glass/solution interface.

Experimental results from published studies support that the final appearance of the surface after the corrosion process is related to the chemical and physical properties of the burial soils in which the glass has aged for centuries. In the work presented here, the data obtained from the characterisation of soil samples allow us to consider two classes of soil in order to make a correlation between the properties of the soil and the result of visible corrosion on the glass samples. From this consideration, the samples AQ115 and AQ117 can therefore be grouped together as they exhibit similar chemical-physical characteristics.

Looking at the glass fragments found on the fields of Aquileia, iridescence appears to be the most evident surface degradation present on the surface of archaeological sample AQ50-1, and this correlation is reflected in several other samples found in this area (in and near field AQ50). Samples from other soils - AQ115 and AQ117 - show pitting as the primary form of corrosion. This distinction based on the type of surface alteration formed on the considered glass samples correlates with the properties of the soils in which they are aged. Indeed, the AQ50 soil is characterised by a slightly acidic pH between 7.5 and 5.4 and decreasing with depth. This value is far removed from the values obtained from the analyses of soils AQ115 and AQ117, which are more alkaline (pH≥8). As discussed above, the pH level is closely related to the corrosion that is triggered between the glass surface and the environment. Assuming that the pH of the soil in the past has not changed much compared to the measured value - which is reasonable considering that the pH depends largely on the soil matrix and that the buffering capacity of soils is known - the hypothesis (as follows in an alkaline context) is that OH^- species attack the -Si-O-Si- bonds of the glassy matrix, leading to the local formation of pits and craters and the final formation of pitting. On the contrary, in acidic conditions, H^+ ions favour the leaching of alkaline cations and contribute to the formation of the silica gel layer on the surface [13,26]. This mechanism would explain the presence of a thick iridescent patina on the surfaces of the glasses from AQ50 and the prevalence of pitting in the other fragments. The surface of the samples AQ117 is marked by a diffused pitting.

Recent research published by Palomar and Llorente [17] describes the formation of pits as a natural consequence of cracks. Upon contact with an alkaline solution, the surface of the glass develops cracks, then basic species concentrate within the cracks and the attack of water causes the cracks to widen into growing pits. The growth of the pits slows down when the

concentration of basic species decreases as water enters (Figure 3.9). This interpretation explains the random distribution of the pits on the surface.

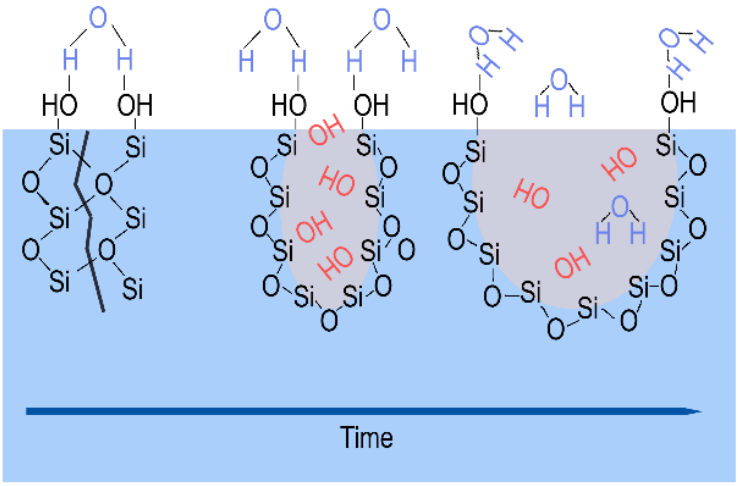

Figure 3.9. Graphical representation of the pit formation process.

In contrast, sample AQ50-1 shows a multilayer iridescent patina on the surface. Iridescence - as described by Emami et al. [27] - is an optical effect resulting from the refraction of light at different angles from the glass surface due to the presence of different constituents and their structure. This patina (variously called hydrated gel, hydrated silica, silica gel, etc.) is formed by the continuous leaching and subsequent deposition of ions (both modifiers and formers) within the corroded layers through the evaporation of water, thus developing the foliated structure. The altered patina observed in the glass fragments, particularly the one covering sample 50, is composed of many overlapping layers that chemically manifest the loss of alkali ions, as evidenced by EDS analyses, and structurally its fragility as the crust tends to flake off in some areas. The characteristic fragility of the patina was observed by Dal Bianco et al. [28] when studying the archaeological glass from the wreck of Iulia Felix. The altered layers tend to peel off as a consequence of dehydration: as the foils alternate with areas rich in water and silanol groups, the layers tend to peel off as the water evaporates. Considering the presence of water in the burial context, it is possible that after excavation the fragments underwent a similar mechanism. Furthermore, the results obtained from SEM-EDS analyses are consistent with the presence of a silica-rich gel layer on the surface of the glass as a consequence of an ion exchange process and the reorganisation of depleted glass network [29,30].

Characterisation of the soil samples revealed certain physico-chemical characteristics that may have contributed to the corrosion of the glass fragments. The prevalence of specific minerals allows the soils to be defined as calcareous - such as soils AQ115 and AQ117 - or clayey - soil

AQ50. This note reflects the distinction of soils according to pH level and the corresponding degradation that occurs in the buried glass. In addition to this and the pH level, which is the most suitable parameter to describe the soil's ability to corrode archaeological glass, other extrinsic factors must be considered. One of these is the cation exchange capacity of the soil, which defines the availability of ions in the environmental context, able to influence the pH [19,22,23]. The three soils under study have a high exchange capacity, but the highest value is possessed by soil AQ50. It is the only soil sample with an acidic pH and its electrical conductivity reaches very high values in the deepest sampling level. Together, these parameters contribute to the corrosion of buried glass, but the degree of their impact is still difficult to assess. What can be seen is that the soil with the most extreme conditions - the AQ50 soil - is the one whose buried glass shows the most advanced corrosion.

3.5. MAIN CONSIDERATIONS

In this work, a multi-analytical approach was designed for the investigation of the interactions between ancient glasses and the soil during the alteration process occurred for centuries in a burial contest. The typology and the extent of the deterioration in archaeological glasses was evaluated considering the physicochemical properties of a specific burial environment.

This case study analyses a limited number of severely corroded glass artefacts from the archaeological site related to the ancient Roman city of Aquileia. The degradation that has developed on the archaeological glass is the result of its interaction with the properties of the soil. The multilayer iridescent patina developed in the archaeological glass from the AQ50 soil, where the high concentration of H^+ ions produced a strong ionic depletion. In contrast, the alkaline environment present in soils AQ115 and AQ117 resulted in advanced pitting. Soil AQ50, which presents the most extreme conditions, is the only one consisting of clay, which means that the mineralogical composition probably has an impact on the preservation of ancient glass.

Glass degradation is a complex combination of mechanisms, and the direct study of ancient Roman glass has made it possible to validate shared and published models of the mechanisms of glass alteration described through artificial ageing test. This case study reveals that it is possible to establish a reasonable relationship between the pH of the soil and the final alteration state of the glass. When buried in acidic soil, SSL glass degrade to form patinas of alteration resulting from the ion-exchange process. Buried in neutral or basic soil, SSL glass degraded forming pits.

3.7. REFERENCES

[1] N.A.R. van Giffen, S.P. Koob, Deterioration of Vitreous Materials, in: S.L. López Varela (Ed.), Encycl. Archaeol. Sci., John Wiley & Sons, Inc., Hoboken, NJ, USA, (2018) 1–4. https://doi.org/10.1002/9781119188230.saseas0179.

[2] C.M. Jackson, D. Greenfield, L.A. Howie, An Assessment of Compositional and Morphological Changes in Model Archaeological Glasses in an Acid Burial Matrix, Archaeometry. 54 (2012) 489–507. https://doi.org/10.1111/j.1475-4754.2011.00632.x.

[3] K. Janssens, ed., Modern Methods for Analysing Archaeological and Historical Glass, 1st ed., Wiley (2013). https://doi.org/10.1002/9781118314234.

[4] M. Kibblewhite, G. Tóth, T. Hermann, Predicting the preservation of cultural artefacts and buried materials in soil, Sci. Total Environ. 529 (2015) 249–263. https://doi.org/10.1016/j.scitotenv.2015.04.036.

[5] Y. Gong, J. Xu, R.C. Buchanan, The aqueous corrosion of nuclear waste glasses revisited: Probing the surface and interfacial phenomena, Corros. Sci. 143 (2018) 65–75. https://doi.org/10.1016/j.corsci.2018.08.028.

[6] W.H. Zachariasen, The atomic arrangement in glass, J. Am. Chem. Soc. 54 (1932) 3841–3851. https://doi.org/10.1021/ja01349a006.

[7] V.S. Molchanov, N.E. Prikhidko, Corrosion of silicate glasses by alkaline solutions, Bull. Acad. Sci. USSR Div. Chem. Sci. 6 (1957) 1179–1184. https://doi.org/10.1007/BF01167384.

[8] M. De Bardi, R. Wiesinger, M. Schreiner, Leaching studies of potash–lime–silica glass with medieval composition by IRRAS, J. Non-Cryst. Solids. 360 (2013) 57–63. https://doi.org/10.1016/j.jnoncrysol.2012.06.035.

[9] L. de Ferri, D. Bersani, Ph. Colomban, P.P. Lottici, G. Simon, G. Vezzalini, Raman study of model glass with medieval compositions: artificial weathering and comparison with ancient samples, J. Raman Spectrosc. 43 (2012) 1817–1823. https://doi.org/10.1002/jrs.4103.

[10] M. Melcher, M. Schreiner, Evaluation procedure for leaching studies on naturally weathered potash-lime-silica glasses with medieval composition by scanning electron microscopy, J. Non-Cryst. Solids. 351 (2005) 1210.

[11] W.W. Fletcher, The Chemical Durability of Glass. a Burial Experiment at Ballidon in Derbyshire, J. Glass Stud. 14 (1972) 149–151.

[12] T. Palomar, M. Garcia, M.-A. Villegas, Model historical glasses under simulated burial conditions, Coalition 23 (2012) 2-6.

[13] T. Palomar, Effect of soil pH on the degradation of silicate glasses, Int. J. Appl. Glass Sci. 8 (2017) 177–187. https://doi.org/10.1111/ijag.12226.

[14] P.P. Poluektov, O.V. Schmidt, V.A. Kascheev, M.I. Ojovan, Modelling aqueous corrosion of nuclear waste phosphate glass, J. Nucl. Mater. 484 (2017) 357–366. https://doi.org/10.1016/j.jnucmat.2016.10.033.

[15] N. Stone-Weiss, R.E. Youngman, R. Thorpe, N.J. Smith, E.M. Pierce, A. Goel, An insight into the corrosion of alkali aluminoborosilicate glasses in acidic environments, Phys. Chem. Chem. Phys. 22 (2020) 1881–1896. https://doi.org/10.1039/C9CP06064B.

[16] R. Arévalo, J. Mosa, M. Aparicio, T. Palomar, The stability of the Ravenscroft's glass. Influence of the composition and the environment, J. Non-Cryst. Solids. 565 (2021) 120854. https://doi.org/10.1016/j.jnoncrysol.2021.120854.
[17] T. Palomar, I. Llorente, Decay processes of silicate glasses in river and marine aquatic environments, J. Non-Cryst. Solids. 449 (2016) 20–28. https://doi.org/10.1016/j.jnoncrysol.2016.07.009.
[18] H.D. Foth, Fundamentals of Soil Science, 8th Edition, Wiley, (1991).
[19] D. Hillel, Evironmental Soil Physics, 1st ed., Elsevier, (1998).
[20] M. Pansu, J. Gautheyrou, Handbook of Soil Analyses, Springer, (2006).
[21] M.B. McBride, Environmental chemistry of soils, Oxford University Press, New York, (1994).
[22] C.B. Nyle, The nature and properties of soils, Macmillan Publishing Company, 1984.
[23] T.T. Meetei, Y.B. Devi, T.T. Chanu, Ion Exchange: The Most Important Chemical Reaction on Earth after Photosynthesis, Int. Res. J. Pure Appl. Chem. (2020) 31–42. https://doi.org/10.9734/irjpac/2020/v21i630174.
[24] Ministero delle Politiche Agricole e Forestali, International Union of Soil Sciences, Società Italiana della Scienza del Suolo, Metodi di Analisi Chimica del Suolo, Roma, Italy: Franco Angeli, (2000).
[25] R.G. Newton, S. Davison, Conservation and restoration of glass, Routledge, Abingdon, Oxon, (2011).
[26] T. Palomar, Characterisation of the alteration processes of historical glasses on the seabed, Mater. Chem. Phys. 214 (2018) 391–401. https://doi.org/10.1016/j.matchemphys.2018.04.107.
[27] M. Emami, S. Nekouei, H. Ahmadi, C. Pritzel, R. Trettin, Iridescence in Ancient Glass: A Morphological and Chemical Investigation, Int. J. Appl. Glass Sci. 7 (2016) 59–68. https://doi.org/10.1111/ijag.12182.
[28] B. Dal Bianco, R. Bertoncello, L. Milanese, S. Barison, Surface study of water influence on chemical corrosion of Roman glass, Surf. Eng. 21 (2005) 393–396. https://doi.org/10.1179/174329305X64376.
[29] J. Hopf, J.R. Eskelsen, M. Chiu, A.V. Ievlev, O.S. Ovchinnikova, D. Leonard, E.M. Pierce, Toward an understanding of surface layer formation, growth, and transformation at the glass–fluid interface, Geochim. Cosmochim. Acta. 229 (2018) 65–84. https://doi.org/10.1016/j.gca.2018.01.035.
[30] S. Gin, A.H. Mir, A. Jan, J.M. Delaye, E. Chauvet, Y. De Puydt, A. Gourgiotis, S. Kerisit, A General Mechanism for Gel Layer Formation on Borosilicate Glass under Aqueous Corrosion, J. Phys. Chem. C. 124 (2020) 5132–5144. https://doi.org/10.1021/acs.jpcc.9b10491.

CHAPTER 4 - SYNCROTHRON AND LAB X-RAY COMPUTED MICROTOMOGRAPHY OF CORRODED ROMAN SAMPLES

The X-ray radiography and computed tomography (CT) are non-invasive and non-destructive diagnostic techniques used to obtain information about the structure and internal composition of an object. Among the best-known fields of application, the medical one is definitely the most involved, but, especially in recent decades, the use of these techniques is increasing in both the industrial and cultural heritage fields. In recent years, in fact, there has been a considerable increase in the number of scientific diagnostic investigations that employ CT scans to obtain information about the construction technique, the structure and state of conservation of an artefact, and thus to plan a correct strategy of restoration[1–4].

Unlike a radiography, a CT analyses allows to produce the 3D reconstruction of an artefact by acquiring several X-ray projections from different angles of sample rotation [5]. The main components of a tomographic system are essentially two: the X-ray source (usually an X-ray tube) and a digital detector that records the radiation that has not been absorbed by the object. The X-ray source can also be the synchrotron radiation, produced when the path of relativistic electrons is curved by magnetic fields. By using a monochromators, it is possible to produce a very narrow energy bands, resulting in a collection of high-resolution images. In addition, a tomographic system used for cultural heritage applications differs to clinical CT scans in the handling system for the object[3]. It is composed by a rotating sample holder that allows the acquisition of images at different angles of the sample, while the source-detector system remains fixed.

While it is well known that the general mechanism of glass corrosion is induced by intrinsic (i.e., material composition) and extrinsic (i.e., environmental) factors simultaneously attacking the material integrity the full comprehension of the processes occurring when the glass degrades in natural environment is still a topic of debate. The different macroscopic alteration marks of archaeological corroded glass are indicative of specific alteration mechanisms [6,7]. As already explained, weathering is the type of glass corrosion related to the interaction of the glass surface with water, which leads to the leaching of alkaline and alkaline earth ions (Na^+ and Ca^{2+}) from the glass network. These cations react with the compounds present in the surrounding environment forming the alteration products that precipitate on the glass surface. The consequence of these processes is the progressive glass weakening and dissolution.

Glass corrosion is commonly studied using traditional techniques like Raman spectroscopy [8], SEM EDX and other surface /volume technique [9] that have limited spectral and spatial resolution if compared with the 2D and 3D heterogeneous features of altered glass samples. In addition, these techniques require the sample to be prepared, e.g., by making embedded cross-sections, and are therefore limited to sacrificial samples for which sampling is possible.

In the light of the above, the aim is to validate a non-invasive analytical procedure to achieve a better understanding of the degradation mechanisms of ancient glass, as well as the role played by its interaction with the surrounding environment within archaeological strata. In

particular, we propose to explore, in a non-destructive manner, the 3D material density of ancient glass thanks to both X-ray micro-computed tomography and the phase contrast synchrotron X-ray computed microtomography. Different types of degraded glass will be analysed: glass with diffused 3D cracking, glass with the formation of pitting, and iridescent glass with multi layered patina on the surface.

As a final outcome, we want to demonstrate as CT technique, never used before to investigate the microstructure of archaeological altered glass samples, represents an outstanding opportunity to understand how the interaction with the external environment can drive the process of alteration.

4.1. MATERIALS AND METHODS

The environment in which archaeological glass has been buried produces both morphological and chemical modifications on it, affecting the material from its surface to the bulk. The samples analysed were selected in order to investigate the main alteration phenomena concerning archaeological glass: the formation of cracks, pits and the presence of an iridescent patina on its surface (Figure 4.1).

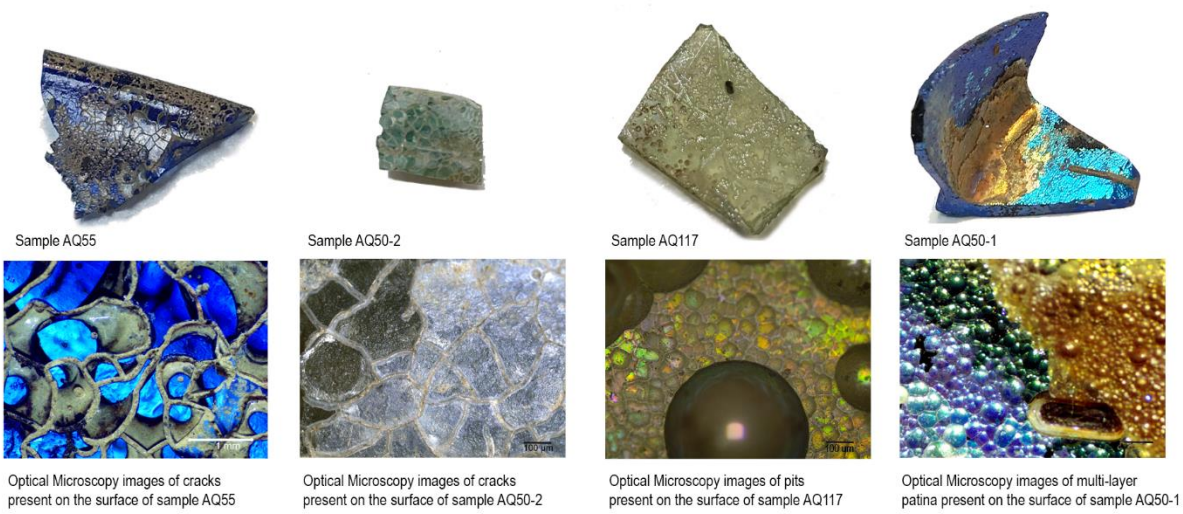

Figure 4.1. Picture of the samples analysed using X-ray computed microtomography (top); optical microscope images of the alteration features that affect the archaeological glass samples (bottom).

The samples reported in Figure 4.1. were characterised combing medium resolution scans obtained with a laboratory CT instrument (OpenAIAr grant) and high-resolution synchrotron radiation microtomography (SX mCT) (Proposal n. 20222195). The objective is to fully characterize four archaeological glass samples showing signs of alteration like those shown in Fig. 4.1. Overview scans (one for each sample) with effective pixel size of 7 µm were performed at the University of Torino. After the overview scan, selected areas of interest were identified for each sample and scanned at higher spatial resolution using a synchrotron radiation (effective pixel size ~ 2 µm corresponding to a detector field of view of approximately 4 mm × 4 mm).

The instrument installed at the University of Torino, Dipartimento di Fisica, have been designed for “ad hoc” analyses necessary in the study of works of art with different size, shape and constitutive material. The X-ray source used in the laboratory to irradiate archaeological glass is Microfocus L8121-03 manufactured by Hamamatsu. The beryllium emission window is 200 µm thick and it is oriented towards the sample. The irradiation cone has an angle of 43° approximately, and the minimum source-object distance is 17 mm, this being the intended distance between focal spot and beryllium window. The detector used is a Teledyne Dalsa model (Shad-o-Box 6K HS), a flat panel consisting of a 2304×2940 pixel matrix corresponding to an active area of 11.4 × 14.6 cm^2. Image reading and transfer takes place in an extremely fast time with a reading speed of up to 9 frames/sec. Each pixel has an area of 49.5 × 49.5 μm^2 and consists of a caesium direct contact scintillator, a photodiode and a CMOS transistor. Newport's URS50BPP turntable is placed on a triangular support that allows it to be moved and to adjust its inclination. The complete set-up used for the analyses is shown in Figure 4.2.

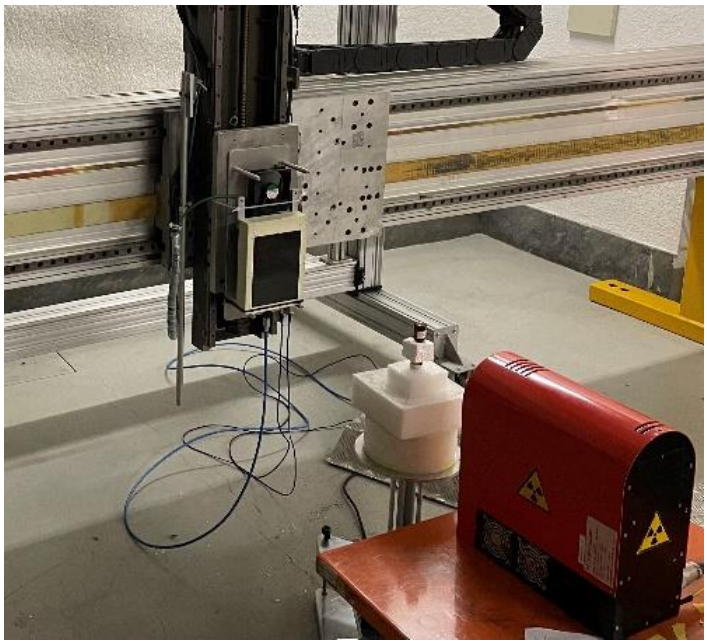

Figure 4.2. Set-up used for the X-ray micro-computed tomography of the glass samples, available at the University of Torino Dipartimento di Fisica.

The key element of tomographic analyses is the acquisition of radiographs of the specimen, also known as projections. To obtain good quality projections, it is necessary to carefully choose the various parameters to be used, such as current, voltage, focal spot size of the source, the acquisition time, and the angular step, which determines the final number of projections. In this work the parameters used are the following:

- ✓ focal spot size of ≈7 µm in order to achieve a better spatial resolution;
- ✓ X-ray tube voltage of 90 kV, which allows a sufficient output signal considering the size of the analysed samples;
- ✓ X-ray tube current of ≈ 110 µA to reduce the acquisition time as much as possible;
- ✓ considering the geometry used and the voltage and current values chosen, the integration time, which enables to fully utilise the approximately 16,000 grey levels of the detector, is 3 seconds;
- ✓ angular step of rotation of 0.15°, resulting in a total number of projections equal to 2400.

The source-object-detector distances chosen for sample analyses are reported in Table 4.1.

During the acquisition phase, the sample, placed inside a polystyrene support, a material chosen because it is few attenuating for the energies used, is rotated 360° around its vertical axis whit small angular increments (0.15°), and an X-ray image is acquired for each of these positions. The projections obtained are then processed and corrected with various software (*Matlab, Parec*) to obtain the reconstructions of the vertical (XZ), horizontal (XY) and lateral (YZ) slices. Finally, the reconstructions obtained were analysed with 3D rendering software (*Dragonfly*) to extract the necessary information for each sample.

Table 4.1. Geometry used for the microtomography analyses

	AQ55	**AQ50-2**	**AQ117**	**AQ50-1**
Source-detector (mm)	650	650	650	650
Source-object (mm)	100	100	150	100
Object-detector (mm)	550	550	500	550
Magnification	6.50	6.50	4.33	6.50
Resulting semi-shade (µm)	38.5	38.5	23.3	38.5
Voxel (µm)	7.62	7.62	11.43	7.62

The higher resolution images were acquired performing X-ray phase-contrast microtomography at SYRMEP (Synchrotron Radiation MEdical Physics) beamline of Elettra Sincrotrone Trieste S.C.p.A., in Italy [10]. The experiment was carried out in parallel beam geometry using polychromatic X-ray beam (white / pink beam) filtered with 1.5 mm of Si and 3.5 mm of Al. Thus, a peaked mean energy of 26.9 keV was achieved. Phase-contrast was obtained with free space propagation setting the sample-to-detector distance equal to 150 mm. The CT scan was accomplished collecting 1800 projections (i.e., sample radiographies) over 180 degrees.

In addition, 20 flat fields (i.e., background images) and 20 dark-fields (i.e., dark images) were collected before and after the microCT scan. The images were acquired with 2 s exposure time using ORCA Flash 4.0 Hamamatsu sCMOS detector (2048 x 2048 pixels, physical pixel size 6.5 µm) with a 17 µm thick GGG scintillator screen. The detector, equipped of a zoom system, enabled to collect images with an effective pixel size of 2X2 µm or 1X1 µm for some higher resolution details. The acquisition comprised multiple vertical microCT scans with an overlap of. Tomographic reconstructions were obtained using the open-source software SYRMEP Tomo-Project [11].

4.2. RESULTS AND DISCUSSION

4.2.1. Cracked samples

The two archaeological samples with cracked surfaces (AQ55 and AQ50-2) were scanned in their totality using computed tomography with the set-up optimised in the laboratory of University of Turin. In both samples, the cracks formed because of the corrosion process have a rounded end. The mechanical action of soil may have played an important role in the formation of the fractures: during glass erosion, the soil, may have formed this rounded point that characterises the fractures, clearly visible within the samples by tomographic analyses.

Figure 4.3 shows several images obtained from the reconstruction of the slices acquired from the analyses of the sample AQ50-2, a blue-green Roman glass bead. The images highlight the dense network of fractures that covers the surface of the sample and affect its entire volume, occupying more than 10% of the glass volume (Figure 4.3.b). The slices reported in Figure 4.3 c and d show how the cracks are interconnected and propagate very deep into the sample until they reach the central hole, which appears to be filled with material coming from the soil in which the glass fragments have been buried for centuries. Some fractures appear to start from the central hole and propagate towards the surface until they join those arising from it.

The slices in Figures 4.3 enable to observe the cracks in section and to appreciate their internal structure and size. They are approximately 0.1-0.3 mm wide. It is also possible to recognize an area at the interface between the crack's void and the glass volume that appears visually of a different grey level, suggesting the presence of a material with different density than the glassy matrix. A material with the same texture also seems to cover the entire glass fragment as suggested by the grey outline visible in the Figure 4.3 c, d and e. One possible explanation for the nature of this material may be its attribution to the formation of a layer of hydrated silica as a consequence of the glass alteration process. As explained in the first chapter of this thesis, a recent description of the transformation process of glass surface is based on an ion exchange process where protons from the solution surrounding the glass diffuse into the silicate network leaching out the mobile alkaline and alkaline-earth cations, followed by an interface coupled dissolution-reprecipitation (ICDP) front that transforms the leached silicate skeleton into

amorphous silica [12]. This coupled process of leaching and re-precipitation with the formation of the hydrated silica layer may have occurred both on the surface of the glass sample but also within the cracks. As these latter are very wide and deep, their walls have become another available surface where these dissolution processes can take place.

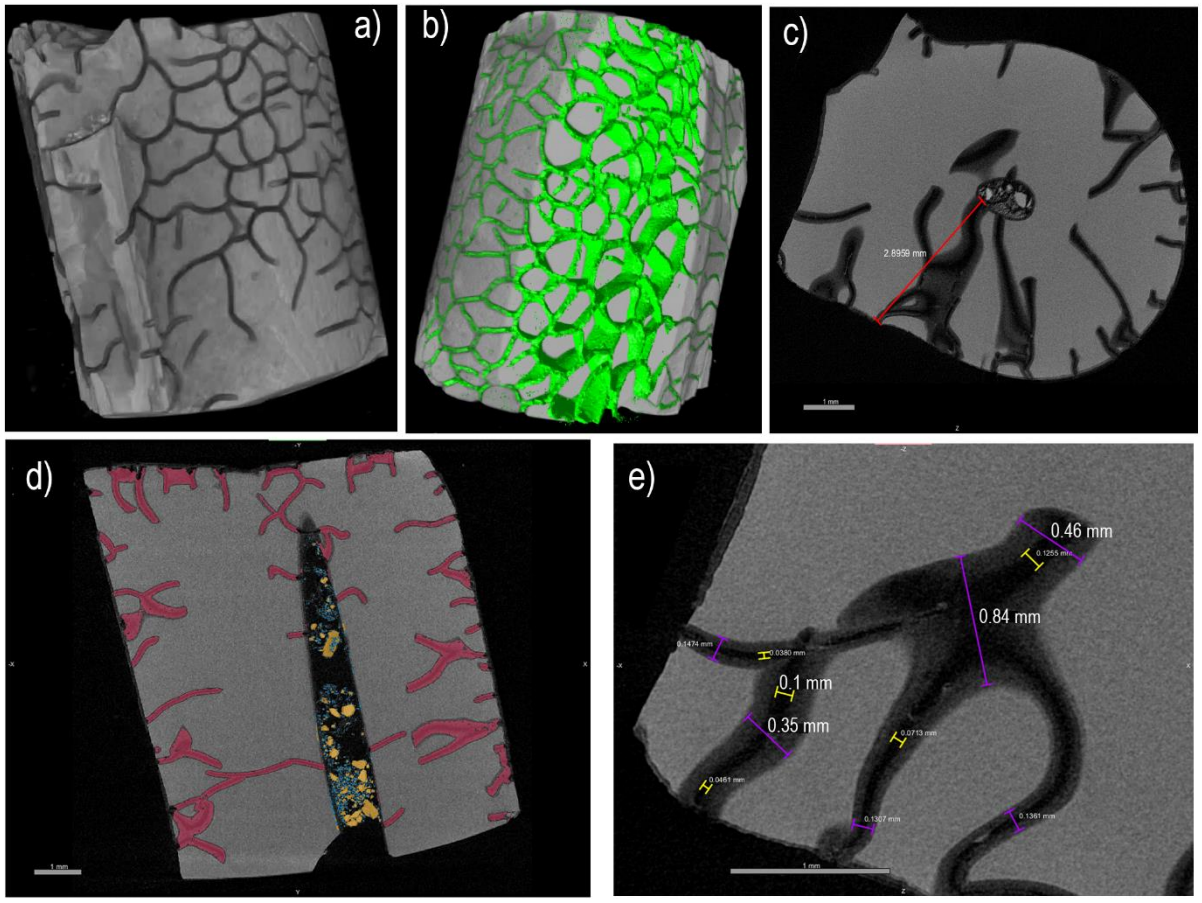

Figure 4.3. Laboratory XmCT scan of the sample AQ50-2. a) 3D rendering; b) volume overlap with mask of the cracks; c) tomographic slice; d) cross section with overlap of different masks: pink mask for cracks, yellow mask for bigger gains of soil and blue mask for smaller grains of soil; e) detail of the crack size measurement result.

The geometry of the cracking propagation observed on the surface of the sample AQ55 by optical microscopy appeared atypical with cracks totally filled with mineralised material, possibly coming from the soil in which the object was buried for centuries. XmCT images collected with the laboratory station confirmed the presence of a dense filling material and enables additionally to reconstruct the 3D geometry of the crack network (Figure 4.4). In this case, the cracks appear to be less wide than those present on the sample AQ50-2, occupying a smaller volume of the glass (about 7.3%). Most cracks are partially or entirely filled with adventitious

material (presumably from the soil). Due to the low contrast between glass and filling material, the crack shows irregular edges that affect the quality of the segmentation.

Several filled cracks extend into the bulk below the glass surface as visible in the slices reported in Figure 4.4. In particular, in the slice reported in Figure 4.4.a it is possible to show larger areas where mineralised material is present and appear with a leopard-like texture. Looking at the surface of the AQ55 sample (Figure 4.1), it is possible to note that these areas correspond to whitish areas visible on the surface of the glass fragment. The images obtained from the tomographic analyses therefore suggest that the material within the cracks, which run under a first superficial layer of the glass, make the colour of the glass itself whitish instead of blue (its original colour). Actually, the colour visible on the sample surface, which coincide with the leopard-spot areas, is that of the 'soil' present in the cracks.

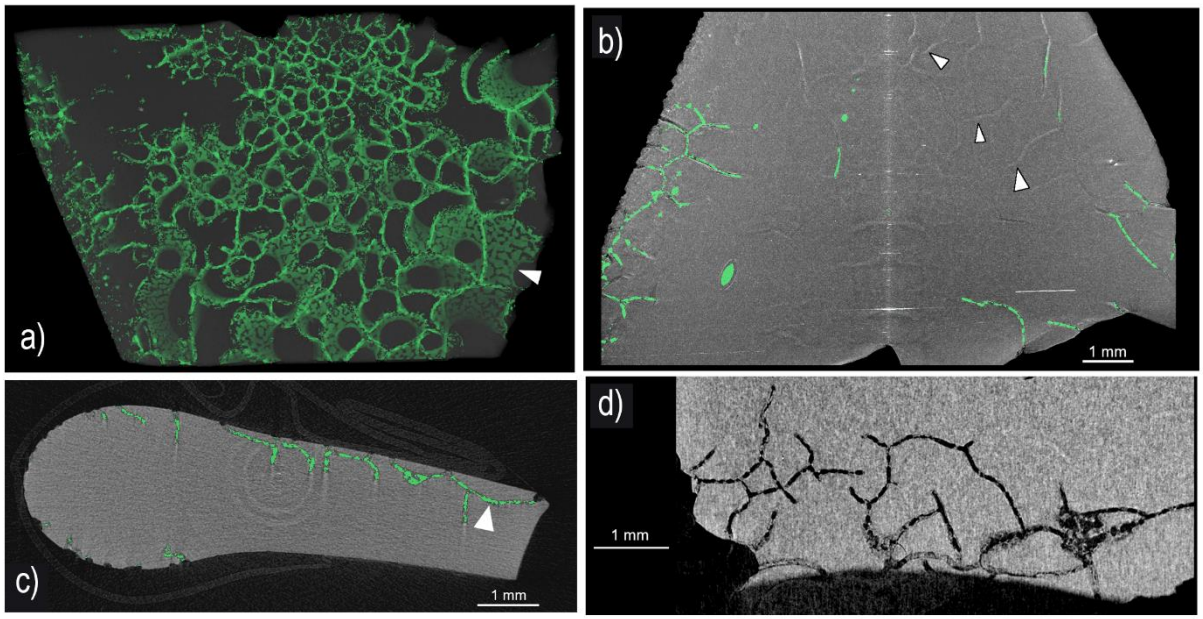

Figure 4.4. Laboratory XmCT scan of the sample AQ55 a) Cracks network (green label) connected to the glass surface. b) Pattern of internal voids running parallel to the sample surface. c) Detail of glass alteration. d) Maximum projection image of a 0.75-mm-deep glass slab parallel to the sample surface.

Sample AQ55 was also analysed using phase contrast synchrotron X-ray computed micro tomography in order to obtain higher resolution images of a portion of the glass fragment. A 3D volume reconstruction obtained from the data acquired is reported in Figure 4.5. The slices obtained from the synchrotron analyses highlight the higher resolution available using this source, which allowed the material filling the fractures to be observed in greater detail (Figure 4.5). The grains of the soil are clearly distinguishable as well as the areas into the cracks where air is present. Moreover, it is also better visible, compared to scans obtained with laboratory instrumentation, how the fractures connect under the surface of the glass, creating small fragments that seem to be welded by soil acting as cement. This information is very valuable in

the case of a restoration action of a glass object with the same altered condition, because it entails that a too deep cleaning of the sample could result in the removal of soil in the cracks and the consequent loss of cohesion between the small 'islands' of glass that have formed on the surface.

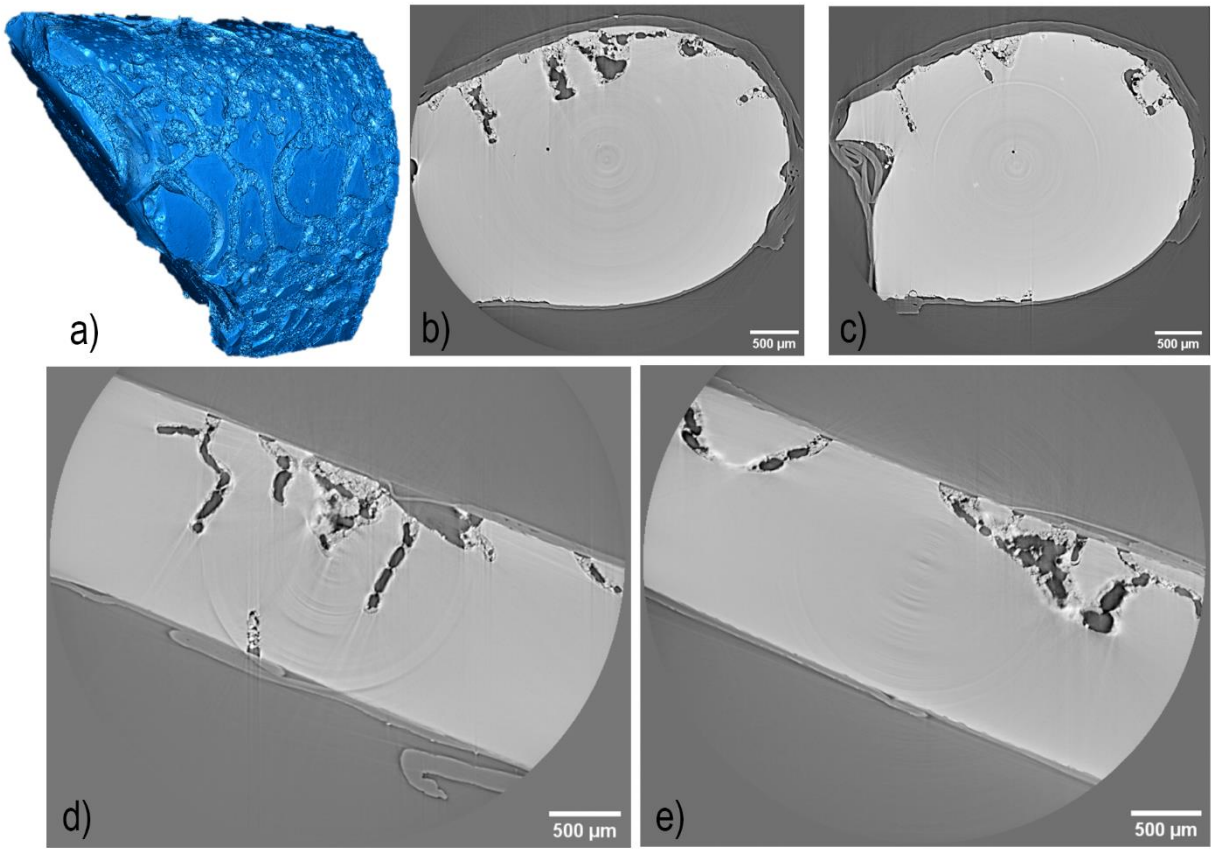

Figure 4.5.a) 3D volume rendering of a corner of the cracked sample AQ55 obtained from SXmCT analyses; others) tomographic slices obtained from SXmCT analyses.

4.3.2. Pitting

Differently form the other samples analysed and considering the dimension of the glass fragment, the voxel size (i.e., the size of the single element volume into which the 3D object representation id divided) obtained for the analyses of the AQ117 sample is 11.43 µm.

Sample AQ117 shows the formation of pits as a corrosion phenomenon with no evidence of patina formation on the surface. As reported in Chapter 3, the sample was presumably in contact with a more alkaline soil where the presence of higher concentration of OH^- favoured the dissolution of the Si-O-Si network instead of the leaching of the modifier ions present in the glass matrix.

The surface of the sample appears almost completely covered with interconnecting pits of different sizes. From slices c in Figure 4.6 one can appreciate the perfectly concave profile of these alteration marks. Some of them have dissolved the siliceous matrix to a depth of about 0.3 mm. The total volume of glass dissolved by the formation of pits is about 12%.

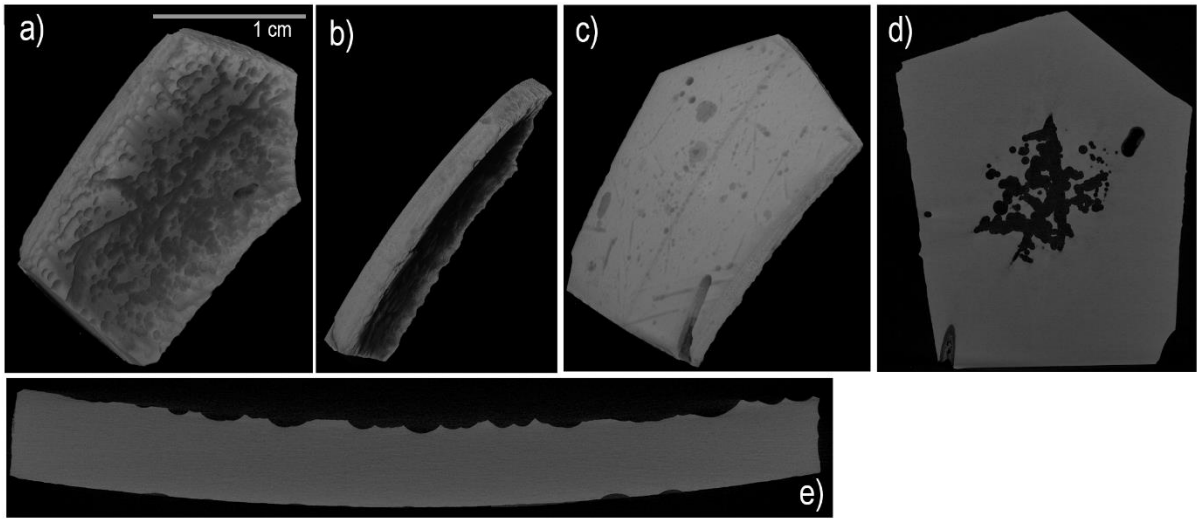

Figure 4.6.3D rendering of the sample AQ117: a) front, b) side, and c) back; d) and e) tomographic slices from two different orthogonal places obtained from laboratory XmCT analyses.

4.2.3. Iridescent patina

XmCT allowed the characterisation of the thickness, shape, and separation of each layer composing the surface iridescent patina of the sample AQ50-1. The slices in Figure 4.7 show the multilayer structure of the overall 1.95 mm thick surface patina. It can be seen how the various layers that constitute the patina are organised in packets of different thicknesses separated by zone of air (darker areas in the images). Each packet is composed of a different number of micro layers, as reported in literature[13,14].

From tomographic reconstructions, it is also possible to appreciate the glass-patina interface and the interface between the various packets. Observing the images reported in Figure 4.7, it is clear how the profile of the patina follows that of the glass, just as it had detached itself from the bulk of the glass. Actually, this structure is the result of the glass alteration governed by the dissolution and re-precipitation process. This process involves as initial stage of the water-glass interaction the congruent dissolution of the glass until (super)saturation of amorphous silica is reached in a solution boundary layer at the glass surface. The glass dissolution reactions are coupled in space and time to the precipitation of amorphous silica so that a dissolution-precipitation interface moves into the glass leaving behind a surface alteration layer composed of amorphous silica, which mimic the initial glass surface [12].

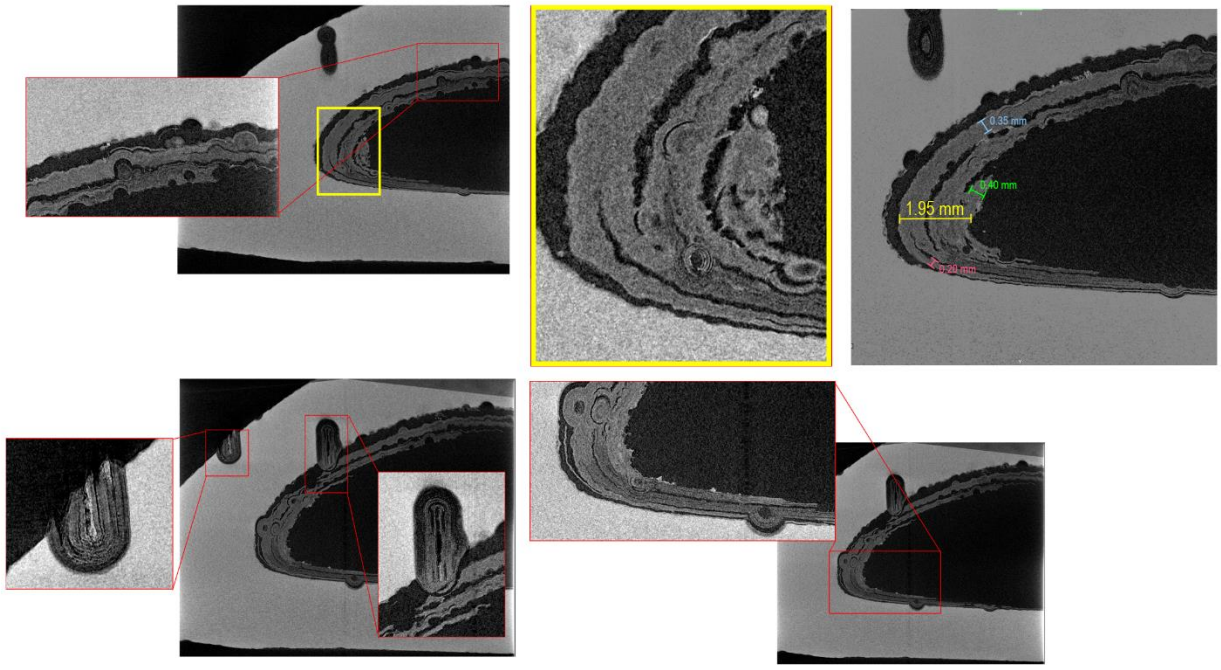

Figure 4.7. Tomographic slices of the sample AQ50-1 obtained from laboratory XmCT analyses.

The images also show the presence of two pits on the vertical side of the sample, one of which runs completely through the wall of the glass fragment. These pits also have an ordered structure of concentric layers. Recent work [15] reports the possible formation of various corrosion marks on tektite glass, such as pitting, V-grooves and U-grooves; formations that can be generally extended for all glass. The pits formed on the analysed sample AQ50-1 can be classified as U-groove. Their formation is linked with a process that involve a no crack propagation or a mechanism of corrosion that proceeds faster than crack propagation [15]. This explanation is somewhat simplistic as it does not consider the many factors that act in the corrosion process of an archaeological glass, such as the composition of the glass itself and environmental parameters, as for example soil pH, temperature, the amount of water available, and the mechanical action of the soil. For this reason, more investigations are necessary to understand the kinetic of the formation mechanism of these marks of glass corrosion.

From this perspective, SXmCT measurements of the sample AQ50-1 has been performed at SYRMEP beamline exploiting the advantages of synchrotron radiation.

Using synchrotron light as source of the analyses, the tip of the horizontal side of the sample was scanned where the biggest pit is present, obtaining a high-resolution (1 µm) 3D reconstruction (Figure 4.8b). Data show the internal structure of the pit formed by ordered, concentric layers. The spatial resolution achieved enables a very detailed image of the pit

structure to be obtained, where it is possible to distinguish almost every single layer forming within the pit and the alternating air zones (darker layers). This high-resolution image also highlights the presence of micro cracks perpendicular to the layer structure, which are mainly present in the innermost area of the pit.

Moreover, the slice shown in Figure 4.8c allows also to observe the presence of heterogeneous distribution of microcrystals within the pit. The crystals result in white colour in the tomographic images suggesting that they are composed by a denser material than the glass and pit layers. A fast statistical analysis revealed that there is a correlation between the depth at which these crystalline particles are placed and their sphericity and size. In particular, the graphs in Figure 4.8d, e and f show that the largest and least spherical particles are positioned in the innermost and deepest part of the pit, while on the contrary, the smallest and seemingly rhomboid-shaped ones are placed in the most superficial areas of the pit and close to the original glass surface. This can be correlated with the mechanism of pit formation itself suggesting that the innermost part of the pit is the one that formed first, and that pit growth occurs not from the centre but from the outermost areas of the pit.

The three distinct parts that form the pit are well represented in the 3D reconstruction of the pit shown in the Figure 4.8g and h: the layers represented in green, the voids in blue and the crystals in colours ranging from yellow to red depending on their size. This representation shows that the crystals are positioned in the pit voids. This evidence can also help to understand the kinetics of pit formation. Always considering the coupled dissolution and re-precipitation model to describe the glass corrosion process, we can define the layers as packets of dissolved and re-precipitated hydrated silica in form of nanoparticles, and the crystals as precipitation of secondary phases with higher density than silica (carbonates or feldspars). This cyclically repeated process led to the dissolution of the glass network and the formation of this concentric structure that tomographic analyses allowed to see.

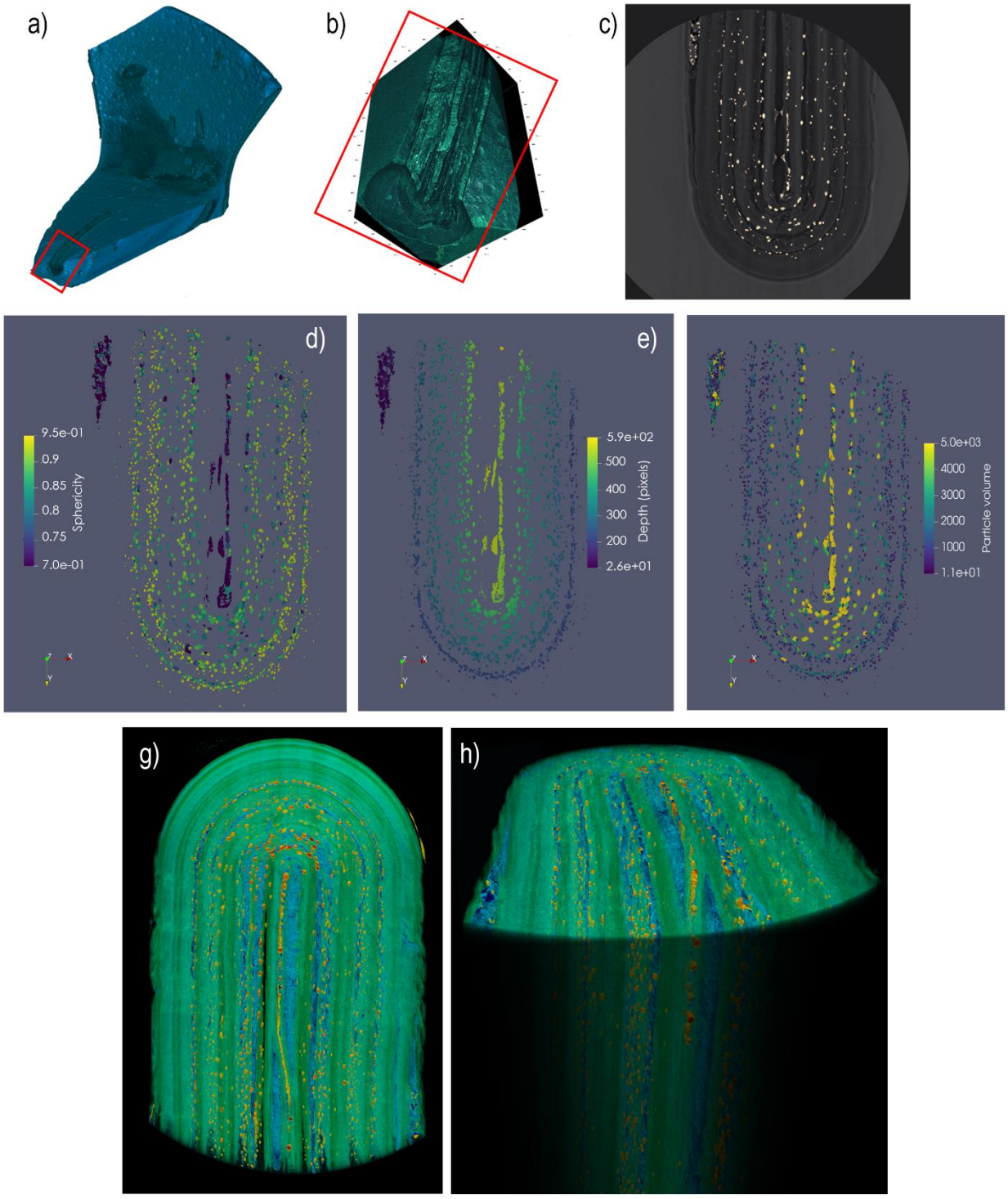

Figure 4.8.a) 3D rendering of the sample AQ50-1 obtained from laboratory XmCT analyses; b) 3D rendering of the pit obtained from SXmCT analyses; c) tomographic slice of the pit obtained from SXmCT analyses; d), e), and f) masks of the crystals present in the pit; g) and h) 3D rendering of the pit highlighting the layers of the pit (green), the voids of the pit (blue) and the crystals (red to yellow).

4.4. MAIN CONSIDERATIONS

The CT analyses of an iridescent sample allowed the characterisation of the thickness shape, and separation of each layer composing the surface iridescent patina in 3D. The CT analyses of samples affected by cracking provided, instead, 3D information on the size, morphology, and distribution of crack in the samples bulk, thus helping to understand the mechanisms of cracks formation, and to appreciate the effect of the interaction between glass and burial environment during the alteration processes. This information will enable us to understand whether the cracking process is still ongoing, through the propagation of active microcracks that are not visible with 2D imaging techniques. There is not clear evidence of these fractures on archaeological glass in literature but studying them and understanding how they formed can be of considerable importance in nuclear glass research. Indeed, there is a great deal of attention in the scientific community to evaluate and improve the chemical and mechanical resistance of this type of glass in the burial context. In this sense, the characterisation and study of the long-term alteration of Roman glass (such as that analysed in this work) can help to understand the long-term behaviour of a particular type of glass in a specific alteration context.

There are currently very few published works that used this approach in the context of the study and conservation of glass materials. However, considering the results obtained, this approach can be considered of great relevance in defining a complementary and exhaustive method for a completely non-invasive characterisation of glass objects of historical and archaeological interest in order to obtain information related to their state of conservation, but also to shed light technical information about the decorative technique used by ancient Roman craftsmen to produce decorated glass objects.

In summary, we showed the advantages of using this non-invasive technique to study and provide new information about the result of the corrosion process that has transformed the surface of an archaeological glass; moreover, we demonstrated that there is no risk of visible transformation of material, considering the possibility to evaluate the beam damage for analyses performed with synchrotron light.

4.5. REFERENCES

[1] F. Albertin, M. Bettuzzi, R. Brancaccio, M.P. Morigi, F. Casali, X-Ray Computed Tomography In Situ: An Opportunity for Museums and Restoration Laboratories, Heritage. 2 (2019) 2028–2038. https://doi.org/10.3390/heritage2030122.

[2] V.A.J. Jaques, M. Zemek, J. Šalplachta, T. Zikmund, D. Ožvoldík, J. Kaiser, X-ray high resolution computed tomography for cultural heritage material micro-inspection, in: Opt. Arts Archit. Archaeol. VIII, SPIE, (2021) 111–118. https://doi.org/10.1117/12.2592310.

[3] M.P. Morigi, F. Casali, M. Bettuzzi, R. Brancaccio, V. D'Errico, Application of X-ray Computed Tomography to Cultural Heritage diagnostics, Appl. Phys. A. 100 (2010) 653–661. https://doi.org/10.1007/s00339-010-5648-6.

[4] L. Vigorelli, A. Re, L. Guidorzi, R. Brancaccio, C. Bortolin, N. Grassi, G. Mila, N. Pastrone, R. Sacchi, S. Grassini, G. Mangiapane, R. Boano, A.L. Giudice, The study of ancient archaeological finds through X-ray tomography: the case of the "Tintinnabulum" from the Museum of Anthropology and Ethnography of Torino, J. Phys. Conf. Ser. 2204 (2022) 012034. https://doi.org/10.1088/1742-6596/2204/1/012034.

[5] P.J. Withers, C. Bouman, S. Carmignato, V. Cnudde, D. Grimaldi, C.K. Hagen, E. Maire, M. Manley, A. Du Plessis, S.R. Stock, X-ray computed tomography, Nat. Rev. Methods Primer. 1 (2021) 1–21. https://doi.org/10.1038/s43586-021-00015-4.

[6] F. Alloteau, O. Majérus, V. Valbi, I. Biron, P. Lehuédé, D. Caurant, T. Charpentier, A. Seyeux, Evidence for different behaviors of atmospheric glass alteration as a function of glass composition, Npj Mater. Degrad. 4 (2020) 36. https://doi.org/10.1038/s41529-020-00138-1.

[7] R.G. Newton, S. Davison, Conservation and restoration of glass, Routledge, Abingdon, Oxon, (2011).

[8] B. Hruška, A. Nowicka, M. Chromčíková, E. Greiner-Wrona, J. Smolík, V. Soltézs, M. Liška, Raman spectroscopic study of corroded historical glass, Int. J. Appl. Glass Sci. 12 (2021) 613–620. https://doi.org/10.1111/ijag.16010.

[9] A. Tournie, P. Ricciardi, P. Colomban, Glass corrosion mechanisms: A multiscale analyses, Solid State Ion. 179 (2008) 2142–2154. https://doi.org/10.1016/j.ssi.2008.07.019.

[10] C. Dullin, F. di Lillo, A. Svetlove, J. Albers, W. Wagner, A. Markus, N. Sodini, D. Dreossi, F. Alves, G. Tromba, Multiscale biomedical imaging at the SYRMEP beamline of Elettra - Closing the gap between preclinical research and patient applications, Phys. Open. 6 (2021) 100050. https://doi.org/10.1016/j.physo.2020.100050.

[11] F. Brun, L. Massimi, M. Fratini, D. Dreossi, F. Billé, A. Accardo, R. Pugliese, A. Cedola, SYRMEP Tomo Project: a graphical user interface for customizing CT reconstruction workflows, Adv. Struct. Chem. Imaging. 3 (2017) 4. https://doi.org/10.1186/s40679-016-0036-8.

[12] C. Lenting, O. Plümper, M. Kilburn, P. Guagliardo, M. Klinkenberg, T. Geisler, Towards a unifying mechanistic model for silicate glass corrosion, Npj Mater. Degrad. 2 (2018) 28. https://doi.org/10.1038/s41529-018-0048-z.

[13] O. Schalm, W. Anaf, Laminated altered layers in historical glass: Density variations of silica nanoparticle random packings as explanation for the observed lamellae, J. Non-Cryst. Solids. 442 (2016) 1–16. https://doi.org/10.1016/j.jnoncrysol.2016.03.019.
[14] T. Lombardo, L. Gentaz, A. Verney-Carron, A. Chabas, C. Loisel, D. Neff, E. Leroy, Characterisation of complex alteration layers in medieval glasses, Corros. Sci. 72 (2013) 10–19. https://doi.org/10.1016/j.corsci.2013.02.004.
[15] A. Krauss, A. Whymark, The influence of crack propagation on tektite glass corrosion sculpture, in: 52nd Lunar and Planetary Science Conference 15-19 March 2021 (2021) 2548.

CHAPTER 5 - LA-ICP-MS ELEMENTAL MAPS OF CORRODED ROMAN SAMPLES*

* Part of this chapter is reported in Zanini et al. “High-speed and high-resolution 2D and 3D elemental imaging of corroded ancient glass by Laser Ablation-ICPMS” accepted to be published in Journal of Analytical Atomic Spectrometry.

Archaeological glass is often found in a poor state of conservation due to the burial conditions in which the archaeological items have been ageing for centuries. The degree of surface alteration can range from unperceivable to so heavily degraded that the original aspect of the glass is no longer perceptible because of its complete transformation into corrosion products. The partial or total physico-chemical transformation of archaeological glass can induce a variety of alteration marks that are optically observable on its surface, such as iridescence, discoloration, pitting, and cracking (see Chapter 1 Section 4.9.). Often, one or more of these visible manifestations of deterioration can simultaneously develop across the surface of a glass artefact.

In most of the cases, the investigation of the chemical composition of the ancient glass surface and its morphology, of the degradation pathologies that affect it, and of the corrosion products deposited on it is carried out by conventional techniques such as X-ray fluorescence (XRF) spectroscopy [1], optical or scanning electron microscopy (SEM) [2], and Raman spectroscopy [3]. Portable XRF spectrometers are typically used for in-situ characterisation of glass museum collection, but the failure of this technique to monitor Na concentration limits its application for studying corrosion, being Na – as explained in the previous chapters - one of the main elements involved in the leaching process during glass alteration [4]. SEM coupled to energy dispersive X-ray (EDX) spectroscopy allows to obtain the chemical characterisation of ancient glass, but data collection is limited to the first microns of depth. In addition, both SEM and XRF techniques provide only semi-quantitative data [5]. Raman spectroscopy, instead, is a suitable non-destructive technique to obtain qualitative information about glass samples. The small laser spot size (>1 μm) [6] available using μ-Raman technique enables a very punctual analyses, but this represent a limit when analysing degraded glass that shows a heterogeneous aspect at the scale of hundreds of microns. Overall, all these analytical approaches have several limitations when examining corroded glass since the alteration phenomena, which often interest a considerable thickness of the glass surface and led to a heavy transformation of glass surface, requires high but adjustable in-depth and lateral resolution investigation. LA-ICP-MS, instead, can overcome some of these shortcomings.

The main objective of the research reported in this chapter was to produce high-resolution multi-elemental imaging of corroded archaeological glass for studying glass weathering mechanisms using laser ablation inductively coupled plasma mass spectrometry (LA-ICP-MS). This powerful analytical technique has been successfully used here to investigate the mechanisms of natural and long-term glass corrosion as developed on ancient glass items in burial conditions. From a methodological point of view, this study reports the set-up of analytical approach applied in a pilot research activity aimed at optimising the operational conditions to achieve high-speed and high-resolution imaging of corroded Roman glass.

Here an optimisation of a published protocol [7] is reported expanding it to the 3rd dimension (depth) and applied to real samples of historical interest, thus obtaining high-quality

images and the opportunity to perform an innovative and comprehensive characterisation of the corrosion layers of archaeological glass. Actually, LA-ICP-MS enabled to obtain 2D and 3D elemental imaging of heavily degraded archaeological glass by retrieving information on the lateral and in-depth distribution of elements that is crucial for a more complete investigation of the corrosion mechanism of ancient glass. The obtained results demonstrate how LA-ICP-MS can be successfully used to investigate the deterioration features that formed on archaeological glass: this represents a great opportunity to study and better understand the processes involved in glass corrosion on the long term.

5.1. MATERIALS AND METHODS

5.1.1. Laser Ablation ICP-MS

LA-ICP-MS can be considered a well-established analytical technique for the characterisation of ancient glass [8–10], as explain in the chapter 2. Nevertheless, its use remains mostly limited for obtaining the bulk chemical composition of the (unaltered) substrate, whereas published works in which this technique is used to specifically study the surface degradation are really scarce [11–13].

The LA-ICP-MS analyses of a solid sample can be performed using the single spot mode or using the line scanning mode where the sample is moved at a constant speed while shooting (Figure 5.1). Both modes can potentially be applied in a raster framework to generate 2D elemental maps, and in multiple per-point ablations to generate 3D maps.

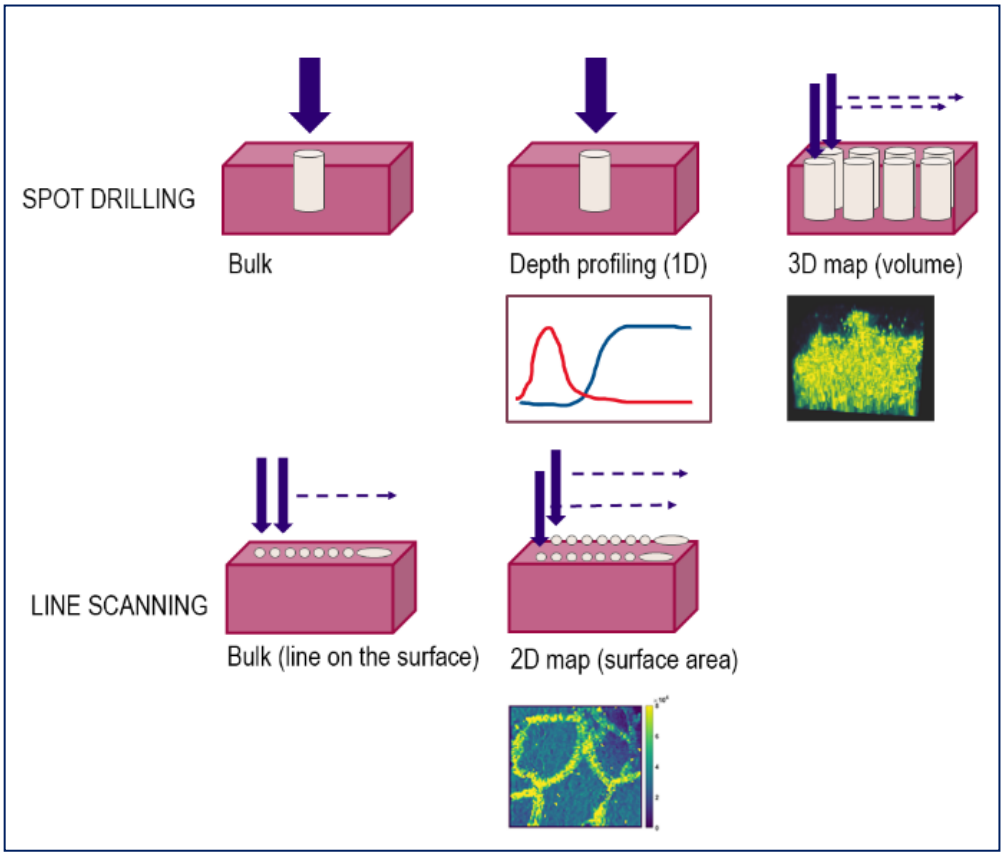

Figure 5.1. Laser ablation modes of operation.

The LA-ICP-MS instrument used in this research consists of an Analyte Excite ArF excimer 193 nm laser (Teledyne CETAC Photon Machines) coupled to an iCAP-RQ quadrupole ICP-MS (Thermo Scientific). The laser ablation device is equipped with a HelEx II two-volume ablation cell mounted on a high-precision xy stage. The samples were placed on a standard LA holder and fixed in-place with double-sided tape. A rapid aerosol transfer line (ARIS, Teledyne CETAC Technologies) and helium as carrier gas were used to transport the ablated materials from the surface of the sample to the ICP-MS. The addition of ARIS enables achieving a faster washout time (WOT), typically in the range of 20 ms, specifically designed for high-speed imaging. Being applied to weathered glass analyses, the WOT was calculated on NIST 612 as reference, since the glass samples are characterised by a heterogeneous and unknown surface composition, resulting into larger but unsystematic WOT (see section 5.2.2.). The maps were obtained using a monodirectional area scan mode with a 20X20 μm^2 square spot size, a laser fluence of 4 Jcm^{-2}, and fixed dosage of 7. Three-dimensional elemental maps were obtained by repeated ablation of the same region of interest (ROI) in the same operating conditions. Each map for 3D imaging was acquired and saved individually as a .csv file, to be then stacked in the processing phase. This

enabled to monitor consistently both the elemental composition of a single ablated layer or the 3D volume distribution of elements.

The LA-ICP-MS operating parameters were adapted according to the approach by Van Elteren et al.[20], which is the ideal setup for high-speed imaging without artefacts. Once calculated the WOT and preselected the dosage and the spot size, the laser repetition rate (Hz) was fixed to 1000*dosage/washout time, while the resulting scan speed equalled [(spot size)/(washout time/1000)]. A repetition rate of 280 Hz corresponding to 800 µm s^{-1} of scanning speed, considerably faster than the set up used in the previous study of LA-ICPMS glass imaging [19], was adopted. In addition, the selection of a higher dosage enabled the generation of each pixel based on the multiple – partially overlapping – laser pulses that improve the signal-to-noise ratio and the image quality, especially when a smaller spot size is used and multi elements are required. Such a fast laser frequency required fast aerosol transport (achieved using the ARIS), but also accurate synchronisation with the ICPMS acquisition method. The use of a quadrupole (sequential) detector forced to select a small group of analytes/isotopes to be monitored within a total sweep time equivalent to the WOT. The elements of interest were selected based on preliminary line scanning of the surface nearby the ROI. Based on the same preliminary data, the individual dwell time of selected elements were adjusted to be inversely proportional to their expected signal intensity (concentration). Six elements/masses were routinely recorded per image, depending on the specific glass sample composition, choosing among ^{23}Na, ^{27}Al, ^{29}Si, ^{39}K, ^{43}Ca, ^{55}Mn, ^{57}Fe, and ^{59}Co. Detailed laser ablation ICP-MS operating parameters are reported in Table 5.1.

Table 5.1: Operating parameters of the LA-ICP-MS 2D and 3D imaging of weathered ancient glasses.

Laser	
Laser type	ArF excimer 193 nm
He gas flow cell	0.25 L min^{-1}
He gas flow cup	0.25 L min^{-1}
Transfer line	ARIS
Fluence	4.0 J cm^{-2}
Spot size	20 µm square
Washout time	20 ms
Ablation mode	Fixed dosage (7)
Repetition rate	280 Hz
Scanning mode	Monodiretional raster
ICP-MS	
RF power	1550 W
Cooling gas flow	14 L min^{-1}
Auxiliary gas flow	0.8 L min^{-1}
Ar makeup gas flow	0.8 L min^{-1}
Monitored masses	^{23}Na, ^{27}Al, ^{29}Si, ^{39}K, ^{43}Ca,
Total sweep time	20 ms (60 %)

This setup considered high dosage, high-repetition lasing mode and fast WOT as the optimal operational conditions to obtain fast mapping and avoid aliasing and other image artefacts. The data elaboration steps (including background subtraction, drift correction, image reconstruction and quantitative calibration) were performed using the software HDIP (Teledyne Photon Machines, Bozeman, MT, USA). The raw images produced by HDIP were calibrated using a reference set of certificated standards and the elemental concentration obtained was transformed in corresponding oxide concentration. The maps were then normalised to 100% using a correction factor calculated from the 98^{th} percentile of the sum of all the monitored elements for each ablated layer. Eight reference materials were used for LA-ICP-MS calibration:

(i) Corning Museum of Glass synthetic glass standard material A, B, C, and D, replicating the composition of ancient glass; (ii) Society of Glass Technology glass standards 7, 10, and 11; and (iii) NIST SRM glass 612. The latter was used also for signal drift correction throughout the elaboration. Linear scans on each reference glass were carried out before (and after in the case of NIST SRM 612) the acquisition of each map. 3D elemental maps were obtained using the same operational conditions used for acquiring the 2D maps, through the layer-by-layer ablation of the same ROI; each ablation was then individually saved and elaborated using HDIP and MatLab.

The purpose of the normalisation was to obtain maps comparable to each other in order to visualise and compare the data. Standard calibration and normalisation parameters have been adopted considering the components of glass samples as oxides and thus obtaining a consistent scale for all the ablated layers. However, since corroded glass is not only composed of oxides, this method should not be understood as a definitive chemical (and mineralogical) interpretation of the components that are ususally present on archaeological glass.

This optimised LA-ICP-MS imaging methods have been used to analyse Roman glass shards that have been recovered from topsoil during field walking surveys in Aquileia (NE Italy), having surfaced from their buried stratigraphic context after centuries due to ploughing [21]. The samples are dated between the 1st and the 4th century BC and they have a silica-soda-lime composition typical of the glass production during those years. These shards show different types of degradation including pits, cracks, dark deposition, and iridescent patina. The glass fragments to be used were selected based on both size and sufficiently regular and flat surface to be analysed without the need for resin mounting or sub-sampling. No organic solvent was used to clean the samples, nor they were polished. Pre-ablation was not performed prior to the analyses to preserve all the valuable information about the glass surface composition, which maintains traces of all the effects determined by the environment triggering natural glass alteration. Data on possible contamination of the surface due to the interaction between the glass surface and the burial environment would be also retained as they can provide further relevant information. The analytical choice to avoid pre-ablation and the connected advantages and limitations are specifically discussed in the following sections of this chapter.

5.1.2. Optimised LA-ICP-MS method to obtain 2D and 3D high-resolution imaging.

According to one of the pioneer works about 2D LA-ICP-MS elemental imaging [22], a correct selection of optimal acquisition conditions (such as beam size, scanning speed, repetition rate, and washout/dwell time) is pivotal to obtain fast high-resolution analyses with minimal image degradation in terms of blur, aliasing, smear, and noise. In particular, maintaining a consistent synchronisation between LA and ICP-MS parameters is essential to avoid the occurrence of aliasing and interference patterns.

In previous applications of LA-ICP-MS for studying glass corrosion phenomena, 3D elemental maps of weathered glass were obtained by employing a drilling procedure based on 50 laser pulses per grid point at a pulse rate of 1 Hz [12]. This tested procedure limits element fractionation and re-ablation of earlier deposited material on the ablation crater walls or surface. These are the commonly encountered problems that occur in deep craters due to the reduction of ablated mass per pulse and/or ineffective transport of aerosolised particles at increasing depth, both resulting in decay of signal intensities with time, and possibly elemental fractionation [23].

The optimized LA-ICP-MS imaging approach here presented points out the advantages in the laser systems optimisation, in particular as far as the scanning mode analyses is concerned. The choice of using a square laser spot and a mono-directional, continuous scanning mode – instead of using a drilling mode procedure with a circular laser spot – gives a more complete regional coverage (Figure 5.2) providing a more representative chemical characterisation of the whole ROI. The heterogeneous aspect of corroded samples at the micro-scale (see for example the alteration pits in Figure 5.5), smaller than the spot size used in the previous work (diameter of 80 µm) [12], shows that it is crucial to cover completely the area of analyses and to reap a quantitative data that is representative of the whole surface. In addition, the spatially continue ablation of all the ROI minimises the probability to fall into elemental fractionation issues due to the proximity of the crater walls, as in the case of Figure 5.2(a).

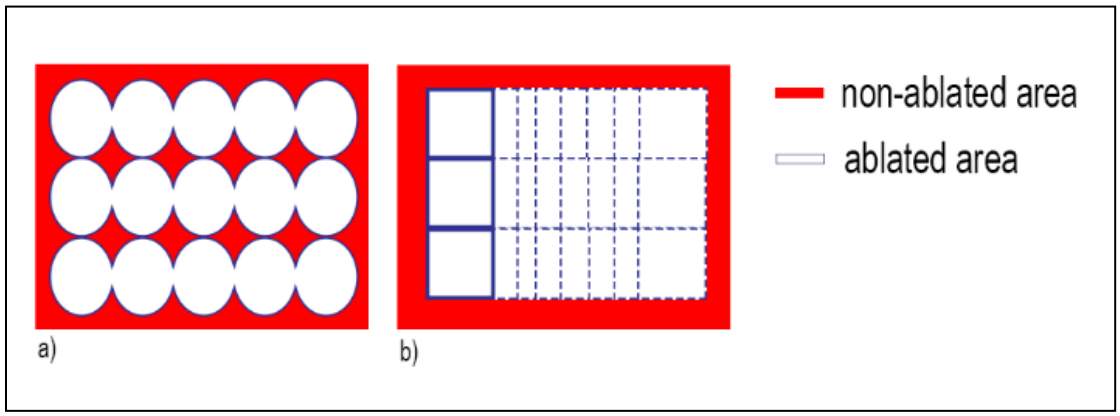

Figure 5.2. (a) Drilling mode with circular spot size procedure used by Panighello et al.]; (b) continuous scanning mode with square spot size procedure used in the present work.

The use of a smaller laser beam spot size (20 µm) proved to be important for clearly defining some morphological details of glass alteration present on the surface – or below it – improving the image resolution. By operating in a rastering mode, it is also possible to continuously ablate material up to greater depths into the sample (a few microns) without encountering edge effects and signal decrease.

In addition, it has been demonstrated that overlapping laser pulses (dosage > 1) are preferable to obtain high quality images in multi elemental imaging [24]. Recent developments in the optimisation of LA-ICP-MS imaging setup have established that high repetition rate laser system and fast washout time are key conditions to achieve "fast mapping with excellent image quality" [7,24]. The LA-system equipped with the ARIS enables achieving very low WOT. In this study, the WOT is calculated daily based on the ablation of the certified reference material NIST 612, instead of the archaeological sample object of the study. This choice is determined by the heterogeneous aspect of the altered archaeological glass, as its surface morphology makes the robust WOT evaluation virtually impossible, given that it requires a stable and repeatable signal, which is impossible to obtain by ablating a contiguous area on the real corroded sample. A feasible solution may be to quantify the WOT on different sample's area, but the estimate would not be sufficiently robust, in any case, considering that the scan would interest heterogeneous areas of the sample. In addition, the latter strategy results in multiple region-specific WOTs that implicate a challenging assessment of which is the best to use. For these reasons –and for time efficiency– WOT was evaluated ablating the NIST 612, as robust and standardised approach.

The resulting value is more representative of the instrumental configuration/status than of the specific sample to be analysed, but this approach can be trusted to obtain high quality images without artefacts from real samples (as visible in the following Figures 5.4, 5.5, 5.6, and 5.7). To better explain the motivations on the basis of this choice, Figure 5.3 represents a synthesis of WOT measurements based on monitoring ^{43}Ca on NIST 612 and on an archaeological glass sample using a 20 µm square spot size. Comparing the repeatability of peak width, the necessity of using NIST 612 to achieve a systematically reliable estimate of the WOT is evident.

Once the WOT was evaluated, the dwell time (ms) was optimised for each element individually and for each sample specifically, to be inversely proportional to the expected spatial average of signal intensity (i.e., elemental concentration, based on a preliminary quick measurement) and constrained to a total dwell time equal to the WOT (20 ms).

It should be noted that fast scanning speed and washout time in the ms range limit the number of elements that can be acquired by using sequential detectors such as the quadrupole MS [7]. For this reason, six elements were monitored within a single run. The published 3D LA-ICP-MS mapping for studying the weathering phenomena using a drilling procedure reports that 19 masses (including major, minor, and trace elements) were acquired. Still, only Si, Mg, and Mn were discussed as representative for three corresponding types of leaching mechanism, showing that fewer but carefully selected elements could still provide all significant information.

Investing in map quality (absence of artefacts, resolution, size and spatial representation of the ROI) appears to be a richer strategy for the study of the alteration mechanisms of archaeological glass using 2D and 3D elemental imaging.

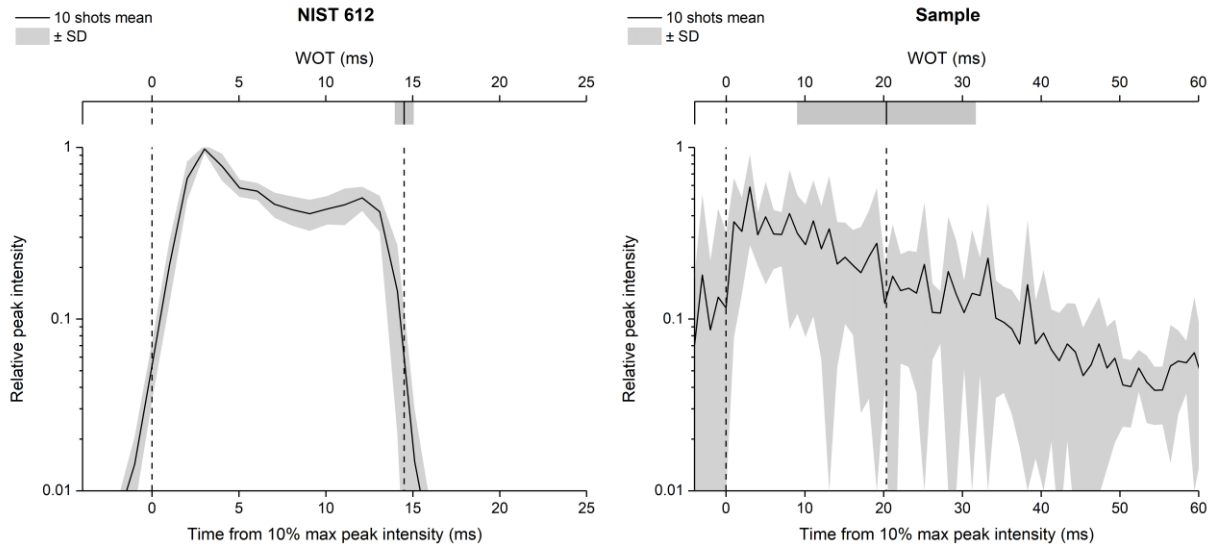

Figure 5.3. Example of single shot peak profiles for WOT calculation based on NIST 612 and real sample: mean of 10 consecutive shots ± standard deviation (SD). The results in WOTs are 14.5±0.5 ms for NIST and 20±11 ms for sample.

5.2. PROCEDURE APPLICATION ON ARCHAEOLOGICAL ALTERED GLASS

As already mentioned, the analytical method described in the previous section has been applied for the characterisation of Roman glass samples that exhibited different types of alteration: cracking, pitting, and the formation of iridescent patina. The concentration gradient of different elements was captured (in its variations from the surface to the bulk of pristine glass) by multiple ablations on degraded regions of interest to observe the dissolution of the glass network due to the hydration and leaching processes that occur during its alteration. The results brought to light the specific alteration process responsible for the formation of the different alteration phenomena investigated: ion-exchange process leads to the formation of iridescent patina (see Section 5.3.3.), instead network dissolution leads to the formation of pits on the surface of glass thought the breaking of Si-O bonds (see Section 5.3.2.).

5.2.1. Cracked sample

Figure 5.4 shows the elemental distribution of a cracked glass sample. This unique type of glass alteration is quite rare and there is little evidence in literature of similar grooves formation on archaeological glass [25]. A recently published article [26] has proposed a theoretical explanation of the U/V-grooves' formation and propagation on tektite glass, which is, like all glass, subjected to weathering. Its authors stated in the paper that formation and propagation of cracks are controlled by internal tensile stresses and by the corrosion rate.

The used beam spot size of 20 µm allows to pinpoint sharp boundaries between the composition of the glass matrix and that of the cracks, as clearly shown by the comparison of Na and Al distribution (Figure 5.4.d). The cracks, which extend throughout the entire sample, seem to be filled by mineralised material acting as a cement. The presence of Si, Ca, and high levels of Al and K into the cracks (Figure 5.4.c) suggests that this filler might be related to the soil in which the sample aged for centuries (buried conditions).

Calcium appears to accumulate mainly along the edges of glass fragments and its concentration on the glassy parts of the map is unexpectedly low considering that the archaeological sample is expected to have a significant level of CaO as stabiliser, being a soda-silica-lime Roman glass [27]. The formation of cracks could be the consequence of a low Ca concentration in the glass matrix, being such element a stabilizer into the glass network and the main factor that determines the chemical stability of glass itself [28]. The low level of Ca in the glass network causes the leaching of Na and the formation of a surface altered layer that is continuously exposed to drying and wetting cycles due to the action of seasonality and soil condition (pH, salt concentration, and permeability). During such cycles, the glass shrinks and expands, inducing mechanical stress at the interface between the pristine glass and the altered layer, and resulting finally in the formation of cracks.

The blue colour of this glass fragment is determined by the chromophore Co^{2+}, which is exclusively present in the glassy parts of the sample (Figure 5.4.c), resembling the distribution of Na. The concentration of Co is uniform over the entire surface of the sample even though it is possible to observe whitish zones in the ablated area (indicated in Figure 5.4.b with a red dot). After analysing this sample using Micro-CT (see Chapter 4 section 4.3.1.), it can be said that the appearance of white colour of these areas is due to the presence of the soil inside the fractures that are developed under the surface of the glass. Being very thin the portion of glass surface remaining over the filling soil, it appears as transparent glass at naked eye even if it contains cobalt as chromophore (whitish areas).

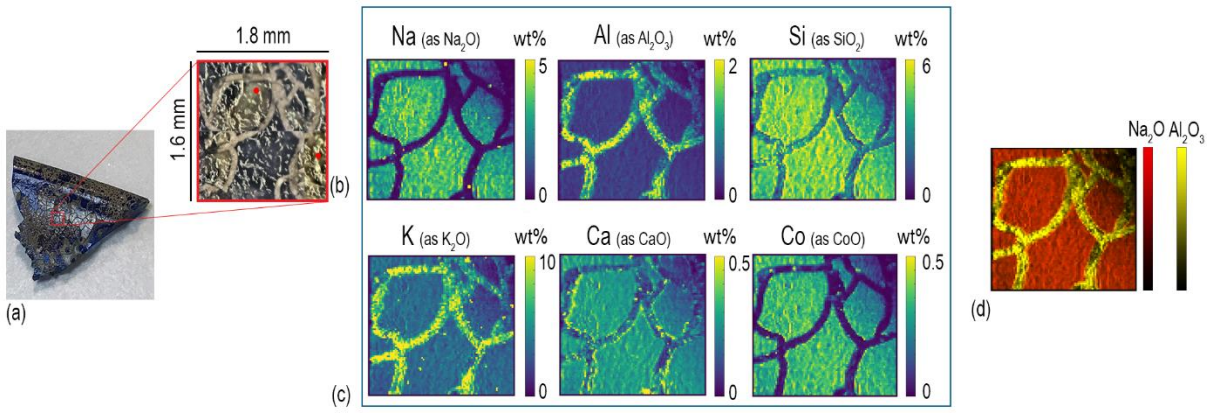

Figure 5.4. (a) Roman archaeological glass fragment found in Aquileia area (NE Italy); (b) a mosaic of LA optical images of the ablated area; (c) elemental maps of Na, Al, Si, K, Ca, and Co concentrations, conventionally expressed as normalised level of their respective oxides in % by weight; (d) overlay distribution of Na and Al in the same area of analyses. The 2D elemental maps of the cracked sample show a decrease of the intensity at the top right for all the monitored elements due to the focus loss in this area. Concentrations are conventionally reported as oxides normalised to 100 for consistent visualisation purposes between layers but should not be assumed as the actual mineralogical/chemical composition of the sample.

5.2.2. Pitting formation

Figure 5.5 shows the in-depth elemental distribution of an archaeological Roman glass sample where the corrosion phenomenon appears mainly by the presence of scattered pits. The ablation was performed ten times on the same area of this sample, resulting in ten maps corresponding to different layers and showing the overall distribution of the monitored elements from the surface to the bulk of the sample.

As for the previously described glass analyses (Figure 5.4), also in this case the sharp concentration gradients between the glassy surface and the pits composition were seen using a small spot size (20 µm), as shown in Figure 5.5. The maps show that Ca, Mn, and Al are accumulated into the pits, a phenomenon likely due to deposition of soil minerals. Conversely, Si is mostly concentrated in the glassy areas of the sample. Starting from the second layer ablated from the surface, the Si maps point out several cracks that are not visible to the naked eye due to the deposition of soil material on the glass surface. This evidence is congruent with a deterioration of vitreous material in burial conditions as reported by a study of Palomar et al.[29], which investigated glass corrosion using a model extracted from historical glass under simulated burial conditions. This latter study described the appearance of cracks on the surface of the glass as one of the first steps of the alteration that affects typical Roman glass. Such cracks grow later in pits that became interconnected during advanced corrosion stages.

The concentration of elements in the top layer of the glass appears completely different from those of bulk. In particular, the amount of Al on the surface is eight times higher compared to what is found from the second ablated layer onward, and, on the contrary, the concentration of Si at the surface is considerably lower than that monitored in the glass bulk (Figure 5.5). These superficial concentrations suggest that soil and moist material directly in contact with the surface

of the sample for centuries have strongly contaminated it. Generally, when LA-ICP- MS is used to measure the bulk composition of ancient glass, pre-ablation is performed to remove potential surface contaminations prior to the analyses [30–32]. Here, instead, the objective was to obtain a specific characterisation of glass alteration at the surface level. Thus, pre-ablation of the specimen was avoided to preserve the chemical information coming from the top layer, which can be considered as the interface between the glassy material and the surrounding environment [15]. Inevitably, this implies the need of special care in the interpretation of the top layer and the potential contamination derived from burial conditions be carefully taken into account (Figure 5.5). With similar concerns in mind, preliminary cleaning of the specimen should be done in a very cautious way, in order to avoid artefact on the surface analyses, moreover, manual polishing should be avoided. As a matter of fact, these operations could result in uneven topographical features to which laser irradiation conditions (e.g., focus) can be very limitedly adapted within a single ablation run (layer map). For this reason, an accurate selection of ROIs is therefore key to a successful analysis.

The maps from the second to the tenth layers clearly show, instead, the concentration of the elements on the glassy material and its structural diversity. The 3D elemental distribution map indicates an increase of Si, Al, and Na concentration in the first few nanometres under the surface area. This distribution could be the result of a process of cations' leaching during the initial stage of glass corrosion started when the glass object was buried on soil [33].

The lower concentration of Si inside the pits is, instead, linked to the process of their formation, suggesting that the dissolution of silica network is the main alteration phenomena that occurred during the corrosion process. In detail, during the alteration process in alkaline conditions, the dissolution of the glass network is the predominant deterioration mechanism, when isolated fissures appear on the surface of the glass (like those visible on the Si maps in Figure 5.5) due to the dissolving of Si-O-Si bonds. Subsequently, the prolonged exposure of the glass surface to the soil causes an increase of the attacking solution pH, involving the formation of basic species (OH^-) that progressively break the Si-O-Si bonds. This causes the widening of the fissures and, ultimately, the formation of pits as the result of the local dissolution of glass network [34]. The graphical representation of the pit formation process is reported in Figure 3.9 in Chapter 3 Section 3.5.

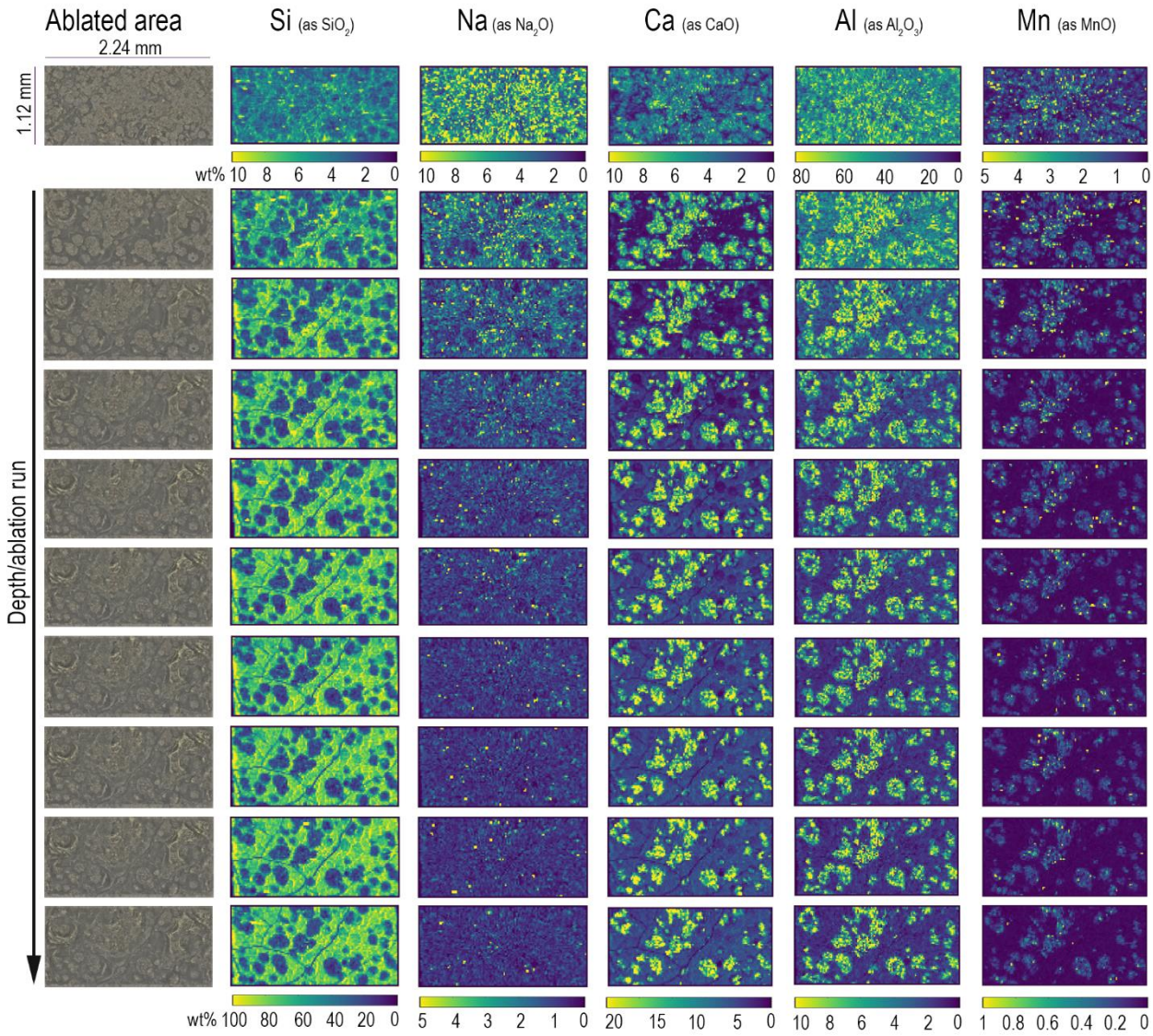

Figure 5.5. Exploded 3D maps of Si, Na, Ca, Al, and Mn distributions, conventionally expressed as normalised level of their respective oxides in % by weight, in an archaeological glass sample showing pitting corrosion.

5.2.3. Iridescent patina

Another visible effect of degradation, which is most found on glass recovered from archaeological excavation sites (where it has been aging under soil) is iridescence [35]. This is caused by changes in the composition of the surface of weathered glass due to the interaction of the object with soil elements in direct contact, often resulting in the disintegration and flaking of the glass surface. Generally, archaeological glass is characterised by a metallic aspect resulting from the formation of a multi-layer patina (with empty spaces between one layer and the other filled with air) which determines a rainbow-like effect due to the reflection of light. This type of glass alteration has been investigated in this work through the 3D multi-elemental maps of a remarkably iridescent Roman glass sample. The area selected for the analyses of this sample was ablated ten times monitoring six elements: Si, Na, Ca, Al, Mn, and Co.

Figure 5.6 shows the changes in element concentration profiles, starting from the surface towards the bulk of the glassy matrix. Three main types of leaching mechanisms can be identified observing the depth profiles related to SiO_2 (network former), to Na_2O (network modifier) and to Co^{2+} (heavy metal present in the glass composition as chromophore). Starting from the surface, the first to be identified is a layer mainly composed of Si (Figure 5.6). Silica, as network former, appears to be relatively concentrated on the surface of the glass sample due to the solubilisation and depletion of alkali and alkaline-earth ions, while hydrated silica gel forms and accumulates on the surface of altered glass, often composed by multi-layer structure. As already reported, a recent study has analytically demonstrated that this laminated alteration, with a thicknesses ranging between 0.1 and 10 µm, consists of a random packing of amorphous silica nanoparticles and it can be considered as one of the by-products of the leaching process that occurs in alkaline environment [36].

The depth distributions of Na and Ca demonstrate a completely different leaching behaviour. The map of Na (one of the most mobile ions in soda-silica-lime glass) shows that the concentration of alkaline ions increases moving from the surface to the bulk. The top layer shows the presence of Na in the most iridescent area of the altered surface. Conversely, deeper ablation layers show an increase in Na concentration in the bulk of the sample, which appears more and more homogeneous in the deepest layer. This depth distribution reflects the depletion of sodium in the altered surface layers due to the leaching process, which is more likely to occur for smaller ions such as Na^+. Similarly, the distribution of Co shows the reduction of its concentration on the top layers, but the depth of depletion of these ions is less than that of Na. This difference in the modifier distribution could be explained considering the classic theory of glass corrosion [37], which suggests that the preferential dissolution of more soluble cations happens during the initial part of the leaching process. Since each modifier cation has different diffusion coefficients, their diffusion through the glass network changes, depending on their size and charge, and on the

composition of glass itself [38]. To make these leaching mechanisms visually clearer, Figure 5.7 summarizes them graphically.

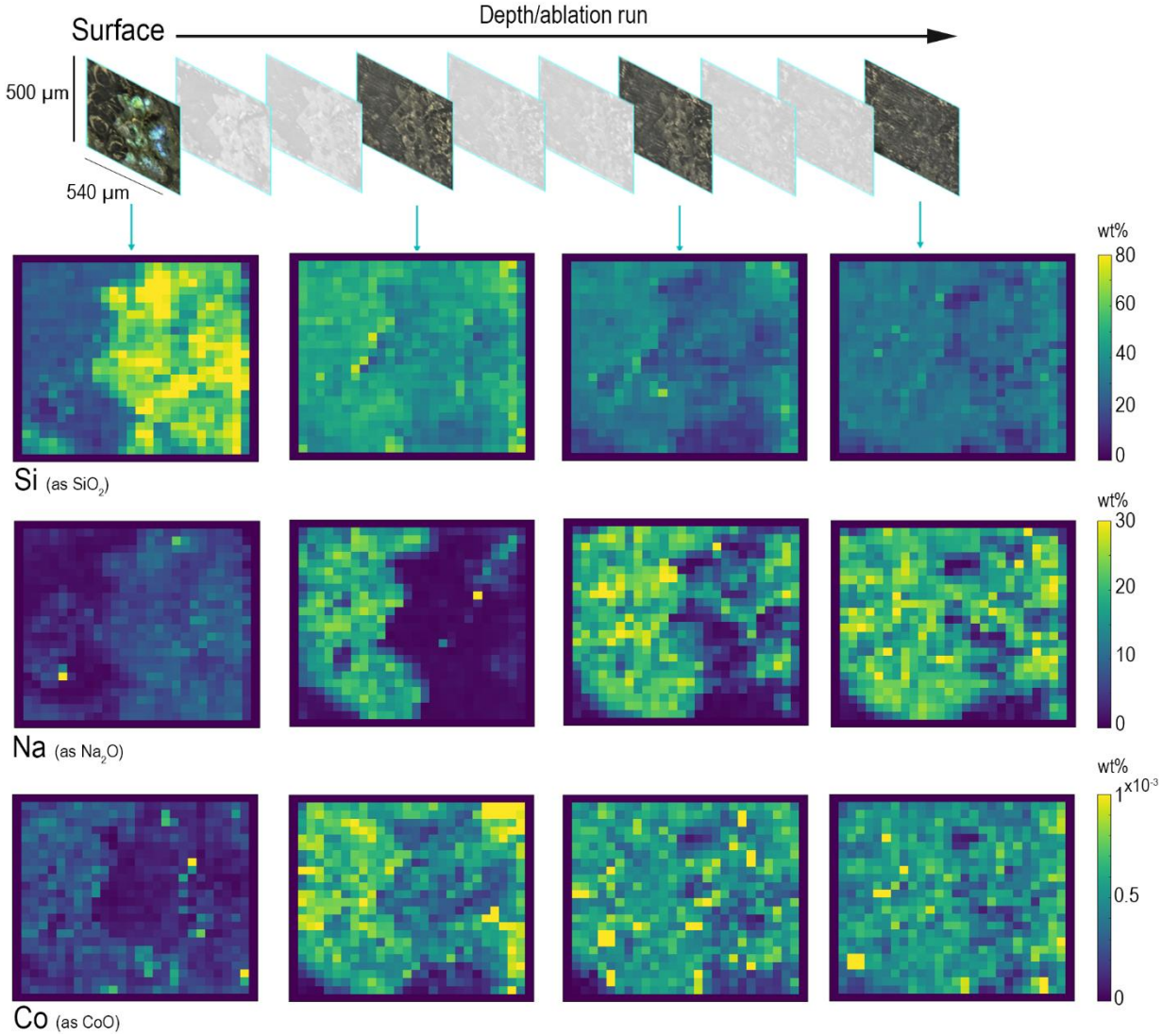

Figure 5.6. Exploded 3D maps of Si, Na, and Co distributions, conventionally expressed as normalised level of their respective oxides in % by weight, in an archaeological glass sample that presents iridescent patina on the surface.

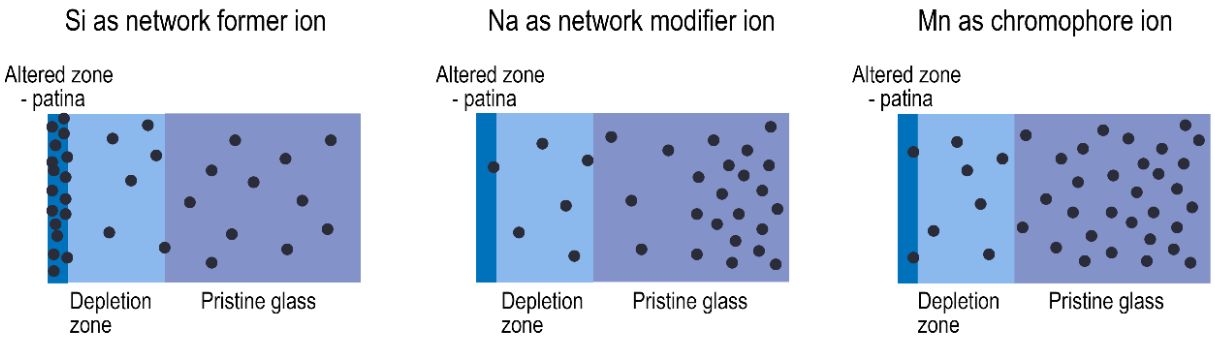

Figure 5.7. Graphic representation of the leaching behaviour of S, Na, and Mn.

In addition, the elemental maps obtained from the analyses of iridescent Roman sample also show that the altered layers formed on the surface seems to act as a diffusion barrier to the further extraction of alkaline ions as sodium (Figure 5.8) [39]. The images of the 3D elemental distribution clearly evidence that the silica layer blocks the ions migration outside the glass network: actually, Na and the other metals ions present in the sample (Fe, Co, and Mn), are present at the surface only in the triangular area where a flaked of the iridescent patina is detached (see image of the ablated area before the ablation run in Figure 5.8). In this confined area, these network modifiers can meet the hydrogen ions (H^+) of the atmosphere and ion exchange process can occurs [38,40].

Observing the elemental distribution from the surface to the bulk of the sample (Figure 5.8), it is possible to appreciate the different depths of leaching of the different elements monitored (as in the case seen above in Figure 5.6).

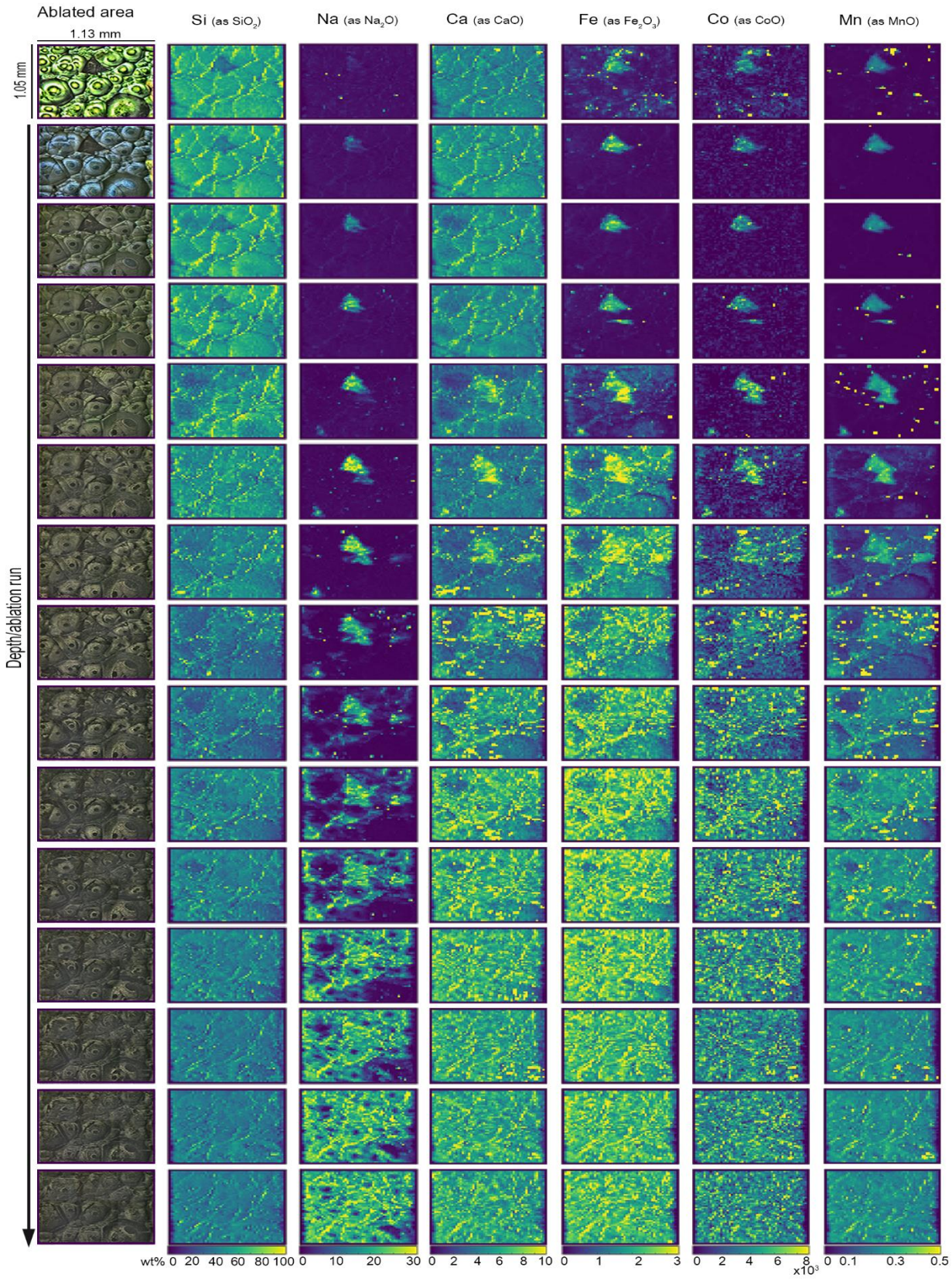

Figure 5.8. Exploded 3D maps of Si, Na, Ca, Fe, Co, and Mn distributions, conventionally expressed as normalised level of their respective oxides in % by weight, in an archaeological glass sample that presents iridescent patina on the surface.

These results represent another evidence of the glass alteration mechanism, supporting the preferential leaching theory [41] during the ion-exchange process and highlighting, once again, the great mobility of sodium into the glass matrix if compared to the others ions (in this case Fe^{2+}, Mn^{2+}, and Co^{2+}).

Figure 5.9 reports the 3D volume distribution of Si and Na, showing both distribution channel of Na towards the surface where the patina is not present, and the absence of Na in the other areas where its mobility is blocked by the formation of iridescent patina. Figure 5.9 also shows the higher accumulation of Si in the first few layers of the sample surface. Analysing the elemental maps and the 3D reconstruction in Figure 5.9 and following the recent theory of glass corrosion (see Chapter 1 section 1.4.4.), the formation of patina should be the result of the congruent depletion of both formers and modifiers elements and the consequent precipitation of hydrated nano-silica on the glass surface [42]. As reported in literature [42], the effect of iridescence is probably due to the packing of nano-silica in well-structured layers that reflects light at different angles.

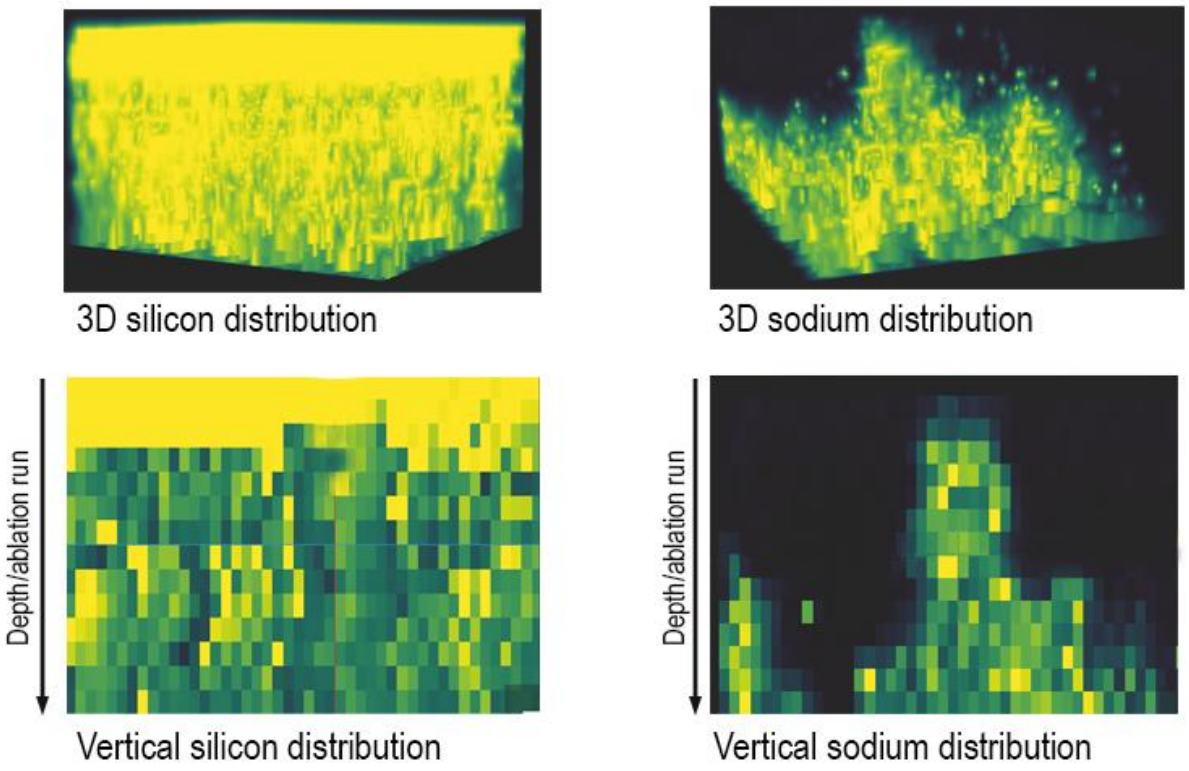

Figure 5.9.3D volume reconstruction of the Na and Si distribution obtain from the multiple ablations of the Roman iridescent glass sample.

The maps of the Figure 5.6 and Figure 5.8 demonstrate that the process of glass alteration much probably occurred because of ions depletion, both alkaline ions (Na^{+}) and heavy metal ions (Mn^{2+}, Fe^{2+}, and Co^{2+}). These results evidence that the dealkalinisation process acted on the element distribution at the surface level while the glass was buried in soil, showing how the composition changes from the bulk to the surface of the samples and providing information about the corrosion mechanism responsible for the formation of iridescent patina too [37].

5.3. DISCUSSION

By investigation of Roman glass that has been lying underground for over 2000 years, the outcomes of the research offer insights to trace back the transformation of the vitreous structure of ancient glass specimens and to correlate it to the natural mechanism of glass deterioration. This approach also provides evidence of the intrinsic effectiveness of multi-elemental LA-ICP-MS analyses to investigate the process of glass corrosion. The possibility to look closely at the layer-by-layer elemental distribution – in its variations going from the bulk to the surface of the samples – gives the chance to observe how the composition of glass changes, exposing novel information about the progression of the corrosion phenomenon. In particular, the results suggest that the formation of an iridescent patina derives from a combined effect of the local presence of water and of the composition of glass that determines the diffusion of ionic species from the external layers, with a consequent re-precipitation of hydrated silica and other alkali-derived compounds. Instead, the formation of pits is mainly caused by the local dissolution of glass network thought the breaking of Si-O-Si bonds, an alteration mechanism that predominantly occurs in alkaline environment.

This analytical approach offers significant improvements compared to the current state-of-the-art in terms of lateral and depth resolution and of image quality. The obtained results thus provide promising foundation for further investigation of different phenomena of alteration affecting archaeological and historical glass, confirming that the surface corrosion is related to the chemical and physical properties of the burial soils as evidenced in Chapter 3 through the chemical study of buried soils.

Additional studies can be performed with the aim of decreasing the spot size of the laser beam to reach higher lateral resolution with the goal of investigating other related phenomena of glass alteration that are still not completely known or understood (i.e., the formation of rings or crizzling), usually occurring in ancient glass with a bulk composition different from the Roman's one or in different environmental conditions from the buried one. In turn, the obtained information will be used as background knowledge for the development of novel consolidation and preservation strategies for ancient glass, a very challenging area of research.

5.4. REFERENCES

[1] G. Nuyts, S. Cagno, K. Hellemans, G. Veronesi, M. Cotte, K. Janssens, Study of the Early Stages of Mn Intrusion in Corroded Glass by Means of Combined SR FTIR/μXRF Imaging and XANES Spectroscopy, Procedia Chem. 8 (2013) 239–247. https://doi.org/10.1016/j.proche.2013.03.030.

[2] P. Bellendorf, S. Gerlach, P. Mottner, E. López, K. Wittstadt, Archaeological Glass: The Surface and Beyond.

[3] B. Hruška, A. Nowicka, M. Chromčíková, E. Greiner-Wrona, J. Smolík, V. Soltézs, M. Liška, Raman spectroscopic study of corroded historical glass, Int. J. Appl. Glass Sci. 12 (2021) 613–620. https://doi.org/10.1111/ijag.16010.

[4] I. Liritzis, N. Zacharias, Portable XRF of Archaeological Artifacts: Current Research, Potentials and Limitations, in: M.S. Shackley (Ed.), X-Ray Fluoresc. Spectrom. XRF Geoarchaeology, Springer, New York, NY, (2011) 109–142. https://doi.org/10.1007/978-1-4419-6886-9_6.

[5] K. Janssens, ed., Modern Methods for Analysing Archaeological and Historical Glass, 1st ed., Wiley (2013). https://doi.org/10.1002/9781118314234.

[6] I. a. Balakhnina, N. n. Brandt, A. y. Chikishev, A. a. Mankova, E. a. Morozova, I. g. Shpachenko, V. a. Yuryev, T. v. Yuryeva, Raman microspectroscopy of blue-green historical beads: Comparative study of undamaged and strongly degraded samples, J. Raman Spectrosc. 49 (2018) 506–512. https://doi.org/10.1002/jrs.5305.

[7] J.T. van Elteren, D. Metarapi, M. Šala, V.S. Šelih, C.C. Stremtan, Fine-tuning of LA-ICP-QMS conditions for elemental mapping, J. Anal. At. Spectrom. 35 (2020) 2494–2497. https://doi.org/10.1039/D0JA00322K.

[8] P. Robertshaw, M. Wood, A. Haour, K. Karklins, H. Neff, Chemical analyses, chronology, and context of a European glass bead assemblage from Garumele, Niger, J. Archaeol. Sci. 41 (2014) 591–604. https://doi.org/10.1016/j.jas.2013.08.023.

[9] J. Varberg, B. Gratuze, F. Kaul, Between Egypt, Mesopotamia and Scandinavia: Late Bronze Age glass beads found in Denmark, J. Archaeol. Sci. Rep. 54 (2015) 168–181. https://doi.org/10.1016/j.jas.2014.11.036.

[10] H. Walder, Stylistic and Chemical Investigation of Turquoise-Blue Glass Artifacts from the Contact Era of Wisconsin, Midcont. J. Archaeol. 38 (2013) 119–142. https://doi.org/10.1179/mca.2013.003.

[11] S. Panighello, J.T. Van Elteren, E.F. Orsega, L.M. Moretto, Laser ablation-ICP-MS depth profiling to study ancient glass surface degradation, Anal. Bioanal. Chem. 407 (2015) 3377–3391. https://doi.org/10.1007/s00216-015-8568-7.

[12] J.T. van Elteren, A. Izmer, M. Šala, E.F. Orsega, V.S. Šelih, S. Panighello, F. Vanhaecke, 3D laser ablation-ICP-mass spectrometry mapping for the study of surface layer phenomena – a case study for weathered glass, J. Anal. At. Spectrom. 28 (2013) 994. https://doi.org/10.1039/c3ja30362d.

[13] L. Dussubieux, P. Robertshaw, M.D. Glascock, LA-ICP-MS analyses of African glass beads: Laboratory inter-comparison with an emphasis on the impact of corrosion on data

interpretation, Int. J. Mass Spectrom. 284 (2009) 152–161. https://doi.org/10.1016/j.ijms.2008.11.003.
[14] M. Guillong, D. Günther, Effect of particle size distribution on ICP-induced elemental fractionation in laser ablation-inductively coupled plasma-mass spectrometry, J Anal Spectrom. 17 (2002) 831–837. https://doi.org/10.1039/B202988J.
[15] J.T. van Elteren, S. Panighello, V.S. Šelih, E.F. Orsega, Optimisation of 2D LA-ICP-MS Mapping of Glass with Decorative Colored Features: Application to Analyses of a Polychrome Vessel Fragment from the Iron Age, in: L. Dussubieux, M. Golitko, B. Gratuze (Eds.), Recent Adv. Laser Ablation ICP-MS Archaeol., Springer, Berlin, Heidelberg, (2016) 53–71. https://doi.org/10.1007/978-3-662-49894-1_4.
[16] B. Wagner, A. Nowak, E. Bulska, J. Kunicki-Goldfinger, O. Schalm, K. Janssens, Complementary analyses of historical glass by scanning electron microscopy with energy dispersive X-ray spectroscopy and laser ablation inductively coupled plasma mass spectrometry, Microchim. Acta. 162 (2008) 415–424. https://doi.org/10.1007/s00604-007-0835-7.
[17] M.D. Glascock, R.J. Speakman, R.L. Burger, Sources of Archaeological Obsidian in Peru: Descriptions and Geochemistry, in: Archaeol. Chem., American Chemical Society, 2007: pp. 522–552. https://doi.org/10.1021/bk-2007-0968.ch028.
[18] S. Cagno, L. Favaretto, M. Mendera, A. Izmer, F. Vanhaecke, K. Janssens, Evidence of early medieval soda ash glass in the archaeological site of San Genesio (Tuscany), J. Archaeol. Sci. 39 (2012) 1540–1552. https://doi.org/10.1016/j.jas.2011.12.031.
[19] S. Panighello, V.S. Šelih, J.T. van Elteren, G. Sommariva, E.F. Orsega, Elemental mapping of polychrome ancient glasses by laser ablation ICP-MS and EPMA-WDS: a new approach to the study of elemental distribution and correlation., Proceedings Volume 8422, Integrated Approaches to the Study of Historical Glass; 842202 (2012) https://doi.org/10.1117/12.975698.
[20] J.T. van Elteren, M. Šala, V.S. Šelih, Perceptual Image Quality Metrics Concept in Continuous Scanning 2D Laser Ablation-Inductively Coupled Plasma Mass Spectrometry Bioimaging, Anal. Chem. 90 (2018) 5916–5922. https://doi.org/10.1021/acs.analchem.8b00751.
[21] A. Traviglia, L. Mandruzzato, E.F. Orsega, L.M. Moretto, S. Floreani, A. Bernardoni, Picking up the hint: raw glass chuncks and glass wastes from ploughsoil collection in Aquileia (Italy), Ann. 21e Congrès Int. Pour L39Histoire Verre 3-7 Sept. 2018 Istanb. (2021).
[22] J.T. van Elteren, V.S. Šelih, M. Šala, Insights into the selection of 2D LA-ICP-MS (multi)elemental mapping conditions, J. Anal. At. Spectrom. 34 (2019) 1919–1931. https://doi.org/10.1039/C9JA00166B.
[23] A.J.G. Mank, P.R.D. Mason, A critical assessment of laser ablation ICP-MS as an analytical tool for depth analyses in silica-based glass samples, J. Anal. At. Spectrom. 14 (1999) 1143–1153. https://doi.org/10.1039/A903304A.
[24] M. Šala, V.S. Šelih, C.C. Stremtan, J.T. van Elteren, Analytical performance of a high-repetition rate laser head (500 Hz) for HR LA-ICP-QMS imaging, J. Anal. At. Spectrom. 35 (2020) 1827–1831. https://doi.org/10.1039/C9JA00421A.

[25] H. Roemich, S. Gerlach, P. Mottner, F. Mees, P. Jacobs, D. van Dyck, T. Doménech Carbó, Results from burial experiments with simulated medieval glasses, MRS Proc. 757 (2002) II2.3. https://doi.org/10.1557/PROC-757-II2.3.
[26] A.Krauss, A. Whymark, The influence of crack propagation on tektite glass corrosion sculpture, 52nd Lunar and Planetary Science Conference15-19 March 2021 Contribution No. 2548 (2021).
[27] J. Henderson, Ancient Glass: An Interdisciplinary Exploration, Reprint edition, Cambridge University Press, Cambridge, United Kingdom New York, NY, USA Port Melbourne, VIC, Australia, (2016).
[28] D.J. Huisman, S. Pols, I. Joosten, B.J.H. van Os, A. Smit, Degradation processes in colourless Roman glass: cases from the Bocholtz burial, J. Archaeol. Sci. 35 (2008) 398–411. https://doi.org/10.1016/j.jas.2007.04.008.
[29] T. Palomar, M. Garcia, M.-A. Villegas, Model historical glasses under simulated burial conditions, Coalition (2012) 2-6.
[30] N. Schibille, P. Degryse, M. Corremans, C.G. Specht, Chemical characterisation of glass mosaic tesserae from sixth-century Sagalassos (south-west Turkey): chronology and production techniques, J. Archaeol. Sci. 39 (2012) 1480–1492. https://doi.org/10.1016/j.jas.2012.01.020.
[31] M. Truffa Giachet, B. Gratuze, S. Ozainne, A. Mayor, E. Huysecom, A Phoenician glass eye bead from 7th–5th c. cal BCE Nin-Bèrè 3, Mali: Compositional characterisation by LA–ICP–MS, J. Archaeol. Sci. Rep. 24 (2019) 748–758. https://doi.org/10.1016/j.jasrep.2019.02.032.
[32] B. Giussani, D. Monticelli, L. Rampazzi, Role of laser ablation–inductively coupled plasma–mass spectrometry in cultural heritage research: A review, Anal. Chim. Acta. 635 (2009) 6–21. https://doi.org/10.1016/j.aca.2008.12.040.
[33] T. Palomar, Effect of soil pH on the degradation of silicate glasses, Int. J. Appl. Glass Sci. 8 (2017) 177–187. https://doi.org/10.1111/ijag.12226.
[34] T. Palomar, I. Llorente, Decay processes of silicate glasses in river and marine aquatic environments, J. Non-Cryst. Solids. 449 (2016) 20–28. https://doi.org/10.1016/j.jnoncrysol.2016.07.009.
[35] N.A.R. van Giffen, S.P. Koob, Deterioration of Vitreous Materials, in: S.L. López Varela (Ed.), Encycl. Archaeol. Sci., John Wiley & Sons, Inc., Hoboken, NJ, USA, (2018) 1–4. https://doi.org/10.1002/9781119188230.saseas0179.
[36] O. Schalm, W. Anaf, Laminated altered layers in historical glass: Density variations of silica nanoparticle random packings as explanation for the observed lamellae, J. Non-Cryst. Solids. 442 (2016) 1–16. https://doi.org/10.1016/j.jnoncrysol.2016.03.019.
[37] C. Lenting, O. Plümper, M. Kilburn, P. Guagliardo, M. Klinkenberg, T. Geisler, Towards a unifying mechanistic model for silicate glass corrosion, Npj Mater. Degrad. 2 (2018) 28. https://doi.org/10.1038/s41529-018-0048-z.
[38] R.H. Doremus, Interdiffusion of hydrogen and alkali ions in a glass surface, J. Non-Cryst. Solids. 19 (1975) 137–144. https://doi.org/10.1016/0022-3093(75)90079-4.

[39] D. Rebiscoul, P. Frugier, S. Gin, A. Ayral, Protective properties and dissolution ability of the gel formed during nuclear glass alteration, J. Nucl. Mater. 342 (2005) 26–34. https://doi.org/10.1016/j.jnucmat.2005.03.018.
[40] B. Dal Bianco, R. Bertoncello, L. Milanese, S. Barison, Surface study of water influence on chemical corrosion of Roman glass, Surf. Eng. 21 (2005) 393–396. https://doi.org/10.1179/174329305X64376.
[41] B. White, Theory of Corrosion of Glass and Ceramics, in: Corros. Glass Ceram. Ceram. Supercond., Noyes Publications, Park Ridge, (1992).
[42] S. Gin, A.H. Mir, A. Jan, J.M. Delaye, E. Chauvet, Y. De Puydt, A. Gourgiotis, S. Kerisit, A General Mechanism for Gel Layer Formation on Borosilicate Glass under Aqueous Corrosion, J. Phys. Chem. C. 124 (2020) 5132–5144. https://doi.org/10.1021/acs.jpcc.9b10491.

CHAPTER 6 – SURFACE CHARACTERISATION USING XPS-SIMS TO MONITOR THE CHANGES IN GLASS COMPOSITION DURING THE ALTERATION PROCESS

The interaction of glass with the surrounding atmosphere starts form its surface, the boundary interface between the solid and its environment. During this interaction, gas and liquid molecules penetrate the glass network through its excess volume and may react with the glass. Great attention must be paid to consider and carefully characterize the glass surface, because it is the interfacial zone between glass and environment, i.e., the region where the first processes of glass alteration take place.

The surface of the glass possesses hydrophilic properties, and it is over time subjected to a corrosion process by moisture and an aqueous solution of the environment. The chemisorption of water molecules starts from the first layers of the glass surface, which is more subjected to physical and chemical transformation. As soon as the silica network of a freshly made glass encounters moisture from the environment, the chemisorption of water molecules starts from the first layers of the surface. Thus, moving from the bulk to the surface of glass, the amount of water into the glass network increases. The annealing treatment at 100 °C allows the desorption of water molecules from the glass network, but a higher temperature is necessary to reform the siloxane groups on surface [1].

Not only water but also organic compounds may be adsorbed by the surface of the glass. In addition, during annealing treatments, sodium or other volatile alkaline ions can vaporize from the superficial regions of glass and condense in deeper ones making the composition of the glass surface very heterogeneous. For this reason, an extensive study of glass surface composition is essential to reach a comprehensive description of the glass leaching and corrosion process [2].

To experimentally study the aging effects on historical glasses, it is a good practice to prepare glass samples of similar composition and - during the various artificial aging steps - investigate them with techniques able of giving compositional and chemical information relating to the glass surface. High-resolution surface techniques, such as X-ray Photoemission Spectroscopy (XPS) and ToF and/or dynamic Secondary Ion-emission Mass Spectrometry (SIMS), allow to investigate the chemical composition of the first nanometres of the glass surface and to monitor its modification during the alteration process [3,4]. In particular, SIMS is one of the most appropriate techniques to study corroded glass, thanks to its capability to detect hydrogen.

The extensive study of glass surface composition, using these advanced analytical techniques, is still seldom considered for investigating the corrosion mechanism of glass using an artificial aging approach in laboratory. Often, only SIMS data obtained after glass aging are reported in literature taking for granted the pristine surface composition of the glass sample. It is essential to highlight that each surface technique has its own peculiar applications and limitations, for instance the sampling depth, but a combination of different techniques allows a complementary and more comprehensive characterisation of corroded glass surface.

The combined use of SIMS and XPS allowed to investigate both the first few nm of the glass surface and its inner part, thus giving evidence of possible in-depth accumulation and/or depletion of some elements, as well as variation of their chemical state. The use of these

investigation techniques is then relevant in the field of materials science, archaeometry, and conservation science but, considering their properties and limitations, it is essential to combine their use.

6.1. MATERIAL AND METHODS

The structure of glass composition was investigated using silica-soda-lime (SSL) glass replica that were prepared in the workshops of the *Stazione Sperimentale del Vetro (SSV) – The glass research centre*, a specialised laboratory based in Murano (Venice, Italy) providing "technical and scientific support to the entire supply chain of glass". Replica samples were created imitating the typical composition of Roman SSL glass type, with a high content of SiO_2, CaO, and Na_2O, and low concentration of MgO and K_2O. The presence of impure raw materials (to replicate the inclusion of various minerals contained in sand) was obtained by adding in the glass mock-ups heavy metals, such as Fe and Cu. Mn and Sb oxides were added as bleaching agents [5]. Table 6.1 reports the chemical composition of the glass replica.

The raw materials were heated at 1400°C in a platinum crucible to reach the melting point and the resulting molten glass was slowly cooled until complete solidification. The raw glass was annealed at 550°C for 1 hour and then slowly cooled down to room temperature for 1 day to prevent the formation of mechanical stress, due to gradients of temperature between surface and bulk of the glass object. The raw glass was then thinly sliced (10×10×2 mm3) to create the testing samples. The surface of the glass was not polished to maintain the original chemical information of the top layers. All the samples were simply washed following an internal protocol using soapy water, deionised water, acetone, trichloroethylene, and absolute ethanol with 5 minutes of sonication for each immersion in mentioned solvents.

Table 6.1. Chemical nominal composition of SSL glass mock-up (in wt% oxide).

Oxide (% wt)	SSV_01
SiO2	67.6
Al2O3	1.97
Na2O	18.6
K2O	0.40
MgO	0.68
CaO	8.05
SO3	0.24
Sb2O3	0.10
P2O5	0.14
Fe2O3	0.68
MnO	0.59
CuO	0.10
CoO	<0.01
Cl	0.9
TiO2	0.02

The SIMS depth profiles were obtained with a dynamic SIMS SC-ultra, with Cs^+ primary ion sputtering beam at 3 keV of impact energy and 64° incidence angle. The acquired secondary species are positive MCs^+ molecular ions, where M indicates each one of the elements of interest. All SIMS data have been normalised point by point to the Cs^+ secondary ion signal acquired at the same depth. This normalisation method can correct possible drifts on the secondary ion intensities, for instance induced by charging effects, when the ion sputtering erodes dielectric samples as glass. A thin gold capping layer has been deposited on all sample surfaces: this conductive layer and the aid of electron flood gun are necessary to remove the excess of positive electric charge induced by the Cs^+ ion sputtering. All depth profiles have been normalised to the average silicon intensity in the glass bulk. The relative intensities - in counts per second - among the different secondary ion species do not represent their real relative concentrations, depending on their different ion yields. The depth scale has been calibrated with the measurement of the final sputtered craters, by using a Tencor P6 mechanical profilometer.

X-ray Photoelectron Spectroscopy (XPS) analyses were carried out with a Kratos Axis UltraDLD spectrometer using a monochromatic Al Kα source (20 mA, 15 kV). Survey scan analyses were carried out with an analyses area of 300 x 700 microns and a pass energy of 160 eV. High resolution analyses were carried out with the same analyses area and a pass energy of 20 eV. The Kratos charge neutraliser system was used on all specimens. For the pristine glass analyses (T0 and T0 bulk) the charge compensation and calibration of the binding energy (BE) scale were done setting the BE of Si2p band at 103.4 eV [6–8]. For the rest of the sampling, instead, several

attempts were made to correct the BEs as best as possible. In the end, the correction made considering the C1s peak of the carbonates turned out to be the most convincing one, placing the BE of this peak at 289.6 eV (as reported in literature [9]). In this way, the Ca peak results centred to BE values that correspond to carbonate compounds, as reported in the literature [10].

The use an internal reference was preferred to the usual C1s position for the adventitious (hydro)carbon contamination layer because in literature the C-C/C-H signal is coreported to fall in a very large BE range (284.0–285.6 eV), thus making extremely difficult a reliable energy scale calibration [11,12]. Deconvolution of the different components in the XPS signals were performed with XPSPEAK41 software [13]. The final uncertainty on the determined BE is around 0.2 eV.

During the ageing test, the samples were subjected to high level of temperature, which was kept constant throughout the experiment at 80 °C, and cyclical variation of humidity as reported in the Figure 6.1. The glass samples were placed in oven inside two glass desiccators. During the wet phases to lead the humidity to high levels a glass petri dish filled with water was added on the bottom of the desiccator (as visible in Figure 6.2). Only pure water (MilliQ) was used during the artificial ageing to prevent any undesired effect of interaction between the samples and the external agents (e.g., salts present in tap water).

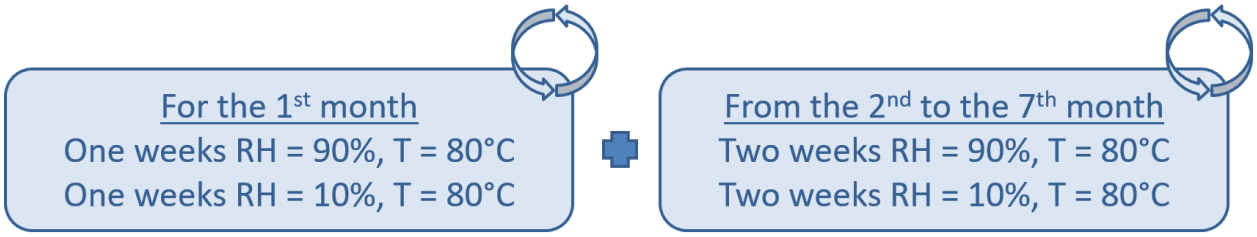

Figure 6.1. Protocol used for the cyclical artificial ageing of SSL glass samples.

Figure 6.2. Set- up for the experimental ageing of glass mock-ups.

The artificial ageing lasted in total seven months and the XPS and SIMS analyses were performed before the ageing (as pristine glass), and after each cycle of ageing. In addition, SIMS analyses of the glass samples was also performed after an annealing treatment at 600 °C for 6 hours in air (on a piece of the pristine glass), and the XPS analyses of the pristine samples was performed immediately after the cleaning treatment both on the sample surface (pristine glass, T0) and on the inner region (T0 bulk) after fracturing the sample.

XPS quantitative results are reported before and after the correction for hydrocarbon contamination layer[14]; its presence causes the attenuation of photoelectron signals coming from elements present just below the contamination layer, thus masking the true atomic concentrations.

6.2. RESULTS

6.2.1. XPS and SIMS data of the pristine glass samples and after two weeks of ageing

The results of the SIMS analyses on the pristine sample SSV_01 are reported in Figure 6.3, which shows the concentration profile of the monitored elements from the first layer of the surface up to 1-2 microns in the glass. The in-depth analyses were performed until the plateau of the element's concentration in the glass bulk was reached. The different concentration of alkaline ions (Na) between the surface and the deeper region of the samples is evident. The elemental profiles showed a sharp increase of Na concentration at about 350-400 nm from the surface, after which it stabilises on a bulk value. Silicon and aluminium (representing the glass formers ions) and calcium (alkaline-earth stabiliser) were arranged in a homogeneous concentration from the surface to the bulk of the sample. The unexpected Na depletion in the first 350-400 nm under the surface could be explained as the loss of volatile Na^+ from the surface of melt glass during its preparation process. Evaporation of glass melt components commonly leads to the depletion of volatile glass compounds at the surface layer of a melt [15], a phenomenon remediated by annealing the solidified glass at proper temperatures. However, the time and temperature adopted for the annealing treatments during the production of mock-ups (see Section 6.2) may be sometimes insufficient to assure or complete homogenisation in the composition.

The compositional analyses of the pristine glass revealed the presence of hydrogen ions in the first 200 nm of the glass surface (Fig. 6.3). This could be due the diffusion of water molecules that happens just when the freshly made glass encounters surrounding air (during glass cooling) resulting in the formation of a water film on the surface of glass [1]. The possibility that hydrogen presence could be originated by molecular hydrogen diffusion should also be considered.

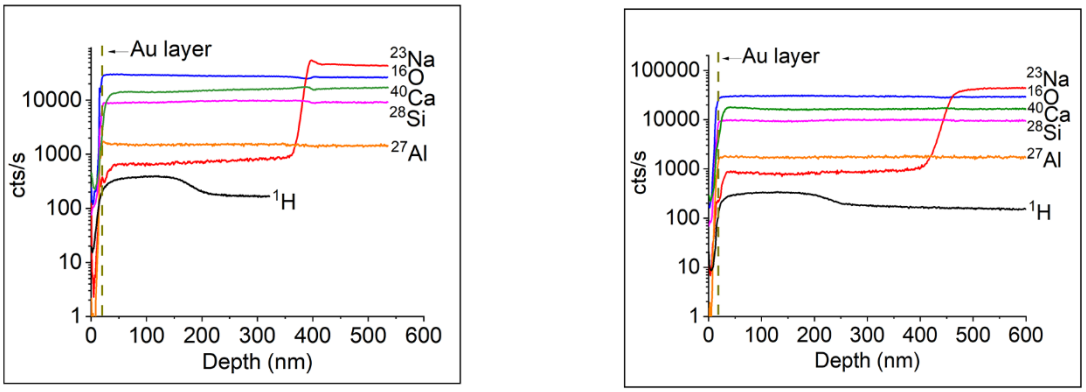

Figure 6.3. The element depth profile of pristine silica-soda-lime in two different point of SSV_01 mock-up.

XPS results provided information complementing those acquired by SIMS analyses thanks to its extremely superficial sampling depth (the first 5-10 nm) that enables investigation of the top layers of the glass surface. Table 6.2 (first column) reports the average values of surface composition of the sample before (T0 pristine and T0 bulk) and after (T1) the two weeks of artificial ageing, in which a large amount of carbon contamination is present (C1s signal centred around 285 eV of BE). From the analytical point of view, it is incorrect to perform a simple quantitative data renormalisation excluding the carbon contribution (Table 6.2, second column): the presence of the hydrocarbon contamination layer induces the attenuation of the photoelectron signals coming from the other elements in the sample, but this intensity reduction is different for different elements because it depends on the photoelectron kinetic energy. We consider as covering contamination layer only the amount of carbon forming hydrocarbon contamination and detected as the low BE component of C1s band (around 80% of the whole C1s intensity, after deconvolution procedure), thus assuming that the other carbon atoms are involved in chemical bonds with the glass matrix surface.

Based on the work of G.C. Smith [14] the estimation of the contamination layer thickness (0.6 nm for T0; 0.6 nm for T0 bulk; 4.9 nm for T1) allowed to estimate the consequent correction of the composition (Table 6.2, third column). The determination of the contamination layer thickness (thus, of the final composition) assumes that all the detected (hydro)carbon contamination originates from a homogeneous and constant-in-thickness contamination layer, covering the whole sample surface. Considering more realistically that some region of the sample surface could be differently covered (or maybe uncovered) by carbon contamination, then the true values of the relative atomic composition of the investigated surface should reasonably lie in the range determined by the values reported in 2nd and 3rd column of Table 6.2.

Table 6.2. Average composition data obtained by XPS analyses of the sample as pristine glass on the surface (T0), on the bulk of sample (T0 bulk), and on the surface after two weeks of artificial ageing (T1). All the reported data are expressed in atomic percentage (see text for explanation). We consider as covering contamination layer only the amount of carbon related to hydrocarbon contamination, i.e., not including other carbon atoms. The last column shows the detected intensity ratio of Na1s and Na2s bands.

	BEFORE CARBON CORRECTION			**BEFORE CARBON CORRECTION (without hydrocarbon)**			**AFTER CARBON CORRECTION**			**Na1s/Na2s**		
	T0	*T0 bulk*	*T1*	*T0*	*T0 bulk*	*T1*	*T0*	*T0 bulk*	*T1*	*T0*	*T0 bulk*	*T1*
Al 2p	2.3	0.5	-	2.7	0.6	-	2.6	0.5	-			
C 1s (contam)	16.6	15.4	75.3	-	-	-	-	-	-			
C 1s (other)	2.6	2.7	5.7	3.4	3.2	23.1	2.8	2.9	6.7			
Ca 2p	2.4	2.3	0.6	2.9	2.7	2.4	2.8	2.6	1.2			
Cu 2p	0.2	-	0.1	0.2	-	0.4	0.3	-	0.8			
Mg 2p	0.1	0.3	0.1	0.1	0.3	0.4	0.1	0.3	0.1			
Na 1s	1.0	8.8	3.4	1.2	10.4	13.8	1.5	12.8	54.3	5.2	8.3	8.3
O 1s	52.0	47.4	12.6	62.3	56.1	51.0	63.8	55.9	33.4			
Si 2p	22.7	22.6	2.2	27.1	26.7	8.9	26.0	25.0	3.5			
Zn 2p	0.1	-	-	0.1	-	-	0.1	-	-			

The concentration of sodium in the pristine glass at time T0 is much lower on the surface than in the bulk of the sample (T0 bulk), and the Na1s band is centred around 1072.7 eV and 1073.0 eV of BE, respectively (Figure 6.4). On the other hand, after two weeks of artificial ageing, sodium concentration on the superficial layers of the sample increases abruptly (Table 6.2). This increment is clear evidence of chemical driving forces inducing diffusion and accumulation of sodium atoms on the first few surface layers because of the environmental conditions. This superficial accumulation determines the presence of a zone of aggregation and disorder in which the compositional and structural properties are different from those determining the macroscopic physico-chemical behaviour of glass, as testified by the different BE detected for the Na1s band (1071.7 eV) (Figure 6.4). In summary, the Na1s peak of the analyses at T0 has a similar BE both for surface and bulk analyses, but at time T1 the BE of Na1s shifts at lower value (Figure 6.4). This change of BE may be indicative of a different nature of sodium: in the pristine glass,

sodium is in the glass network acting as modifier ion; conversely, after an artificial alteration (sample at T1) the sodium detected by XPS is present in different compounds, most likely sodium carbonates[6,16] formed on the glass surface. The chemical stress induced on glass mock-up by artificial ageing – characterised by high level of temperature and humidity - caused the leaching of sodium and its accumulation on the surface, where it can react with the surrounding environment.

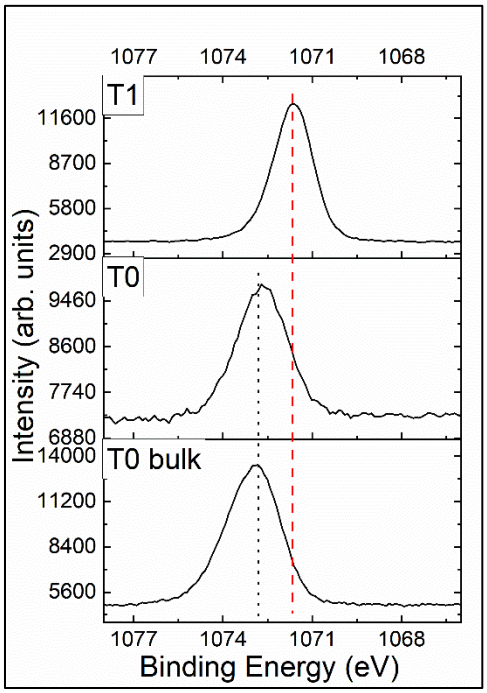

Figure 6.4. Na1s band recorded on the three samples. Intensities are normalised for clarity.

The formation of sodium carbonates on T1 sample was suggested also by the analyses of the O1s band (Fig. 6.5). The signal centred around 536-537 eV is not related to oxygen, being part of the NaKLL band: its different relative intensity in the three samples is directly related to the different Na amount, as reported in Table 6.2. About the true O1s signal, in the T0 bulk sample the band clearly showed the presence of two components, falling around 532.9 eV and 531.2 eV and related to BOs (Bridging Oxygens) and to NBOs (Non-Bridging Oxygens): these signals are characteristics of soda-lime silicate glasses [17].

On the surface of the pristine glass (T0 sample), the lower amount of Na induces a decrease of the NBOs band intensity. In the T1 sample, the different composition of the surface – rich in sodium and strongly contaminated by carbon – affects the structure of O1s band. Indeed, the BOs band is reduced in intensity, and a new much intense component appears, centred on 531.9 eV of BE. This band was attributed to the presence of Na carbonates at the sample

surface[6], formed during the ageing process. Analyses of C1s signal recorded on T1 sample confirmed this attribution (Fig. 6.6) because, in addition to the main component related to adventitious carbon contamination (usually falling around 285-286 eV of BE), a less intense band centred at 288.9 eV is detected. This last band can be attributed to sodium carbonates[6], and/or to sodium hydrocarbonates.

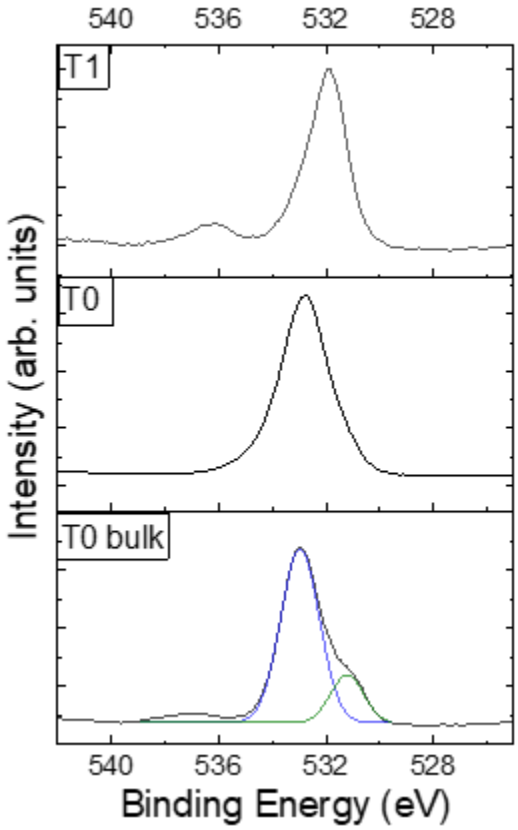

Figure 6.5. O1s band recorded on the three samples. Intensities are normalised for clarity.

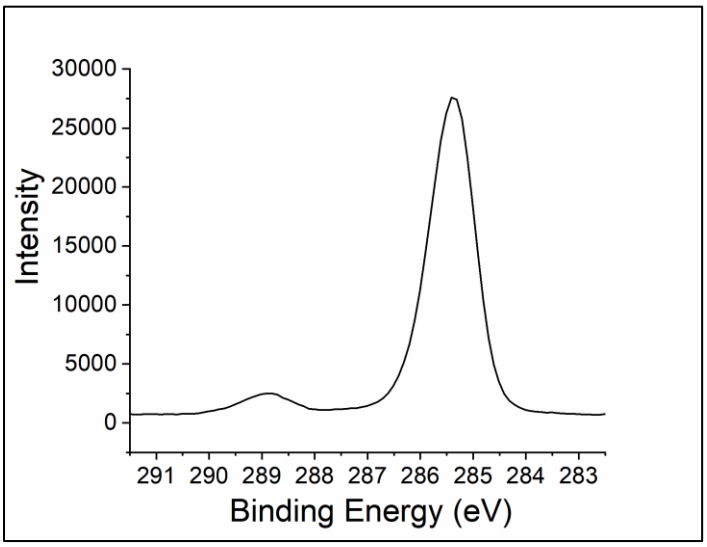

Figure 6.6. C1s band recorded on the T1 sample.

The presence of the Na2s band is easily visible in the low BE region of the XPS survey (not reported). This signal is originated by photoelectrons having high kinetic energy, thus coming also from Na atoms that are present in deeper regions of the sample surface. With the instrument used, the expected ratio of the RSF (Relative Sensitivity Factor) for Na1s and Na2s bands is around 10 for a homogeneous sample. The different intensity ratio experimentally detected on the three samples for these two Na signals, Na1s/Na2s (Table 6.2), showed a very low value for the T0 sample, suggesting that an important sodium concentration gradient is present in the first 5-10 nm of the surface, with a marked depletion in the first few layers (possibly 1-2 nm) of the region investigated by the XPS technique.

6.2.2. XPS and SIMS data of the other cycles of ageing test.

By observing the samples during the artificial ageing test (Figure 6.7), it is possible to appreciate how the surface of the glass mock-ups alters to form an increasingly thick whitish patina.

The optical microscope images reported in Figure 6.7 show the formation of micro cracks on the surface of the samples as early as the second sampling, which grow into real fractures (T5). During the ageing, the fractures are joined by the formation of a patina that gradually becomes more and more indented and at the end of the test appears as a multilayer structure (T7).

The SIMS element depth profile of SSV_01 mock-up in two different point for each step of analyses are shown in Figure 6.8. Starting from the first sampling (T1), the gradual redistribution towards the surface of the alkali elements (Na and K) can be seen, until reaching an increasingly homogeneous distribution towards the third sampling (T3). The Ca profile, on the other hand, shows a superficial accumulation already from the first sampling, which for Na we can only observe from the fourth sampling (T4). This probably happens because, in the pristine glass, the Ca was homogeneously distributed in the sample and thus already in high concentration near the surface where the first chemical reactions with the compounds in the environment take place (CO_2, H_2O). Na, instead, which in the pristine glass is present in lower concentrations at the surface, tends to homogenise its distribution before accumulating on the surface and reacting with the external elements.

SIMS profiles show that the distribution in the glass samples of Si (present in the samples as network formers) remains constant during the alteration process. Al also shows a similar trend except for the first sample (T1) where it seems to decrease at the surface perhaps at the expense of the growth of alkaline and alkaline-earth elements, the concentration of which, instead, increase in the same area. These results suggest that the concentration of Si and Al is nearly constant throughout the altered layer that is formed on the surface of glass.

Looking at the distribution profile of H, its migration towards deeper areas of the sample can be noted comparing the time T1 to the pristine sample, in which the presence of hydrogen only affected the first few hundreds nm of the surface. This trend is in line with the reactions involved in the glass corrosion mechanisms, related to the ion exchange process between the H^+ ions of the aqueous medium (in this case high humidity) and the alkaline and alkaline-earth ions (Na^+, K^+, Ca^{2+}) present in the glass network [18,19].

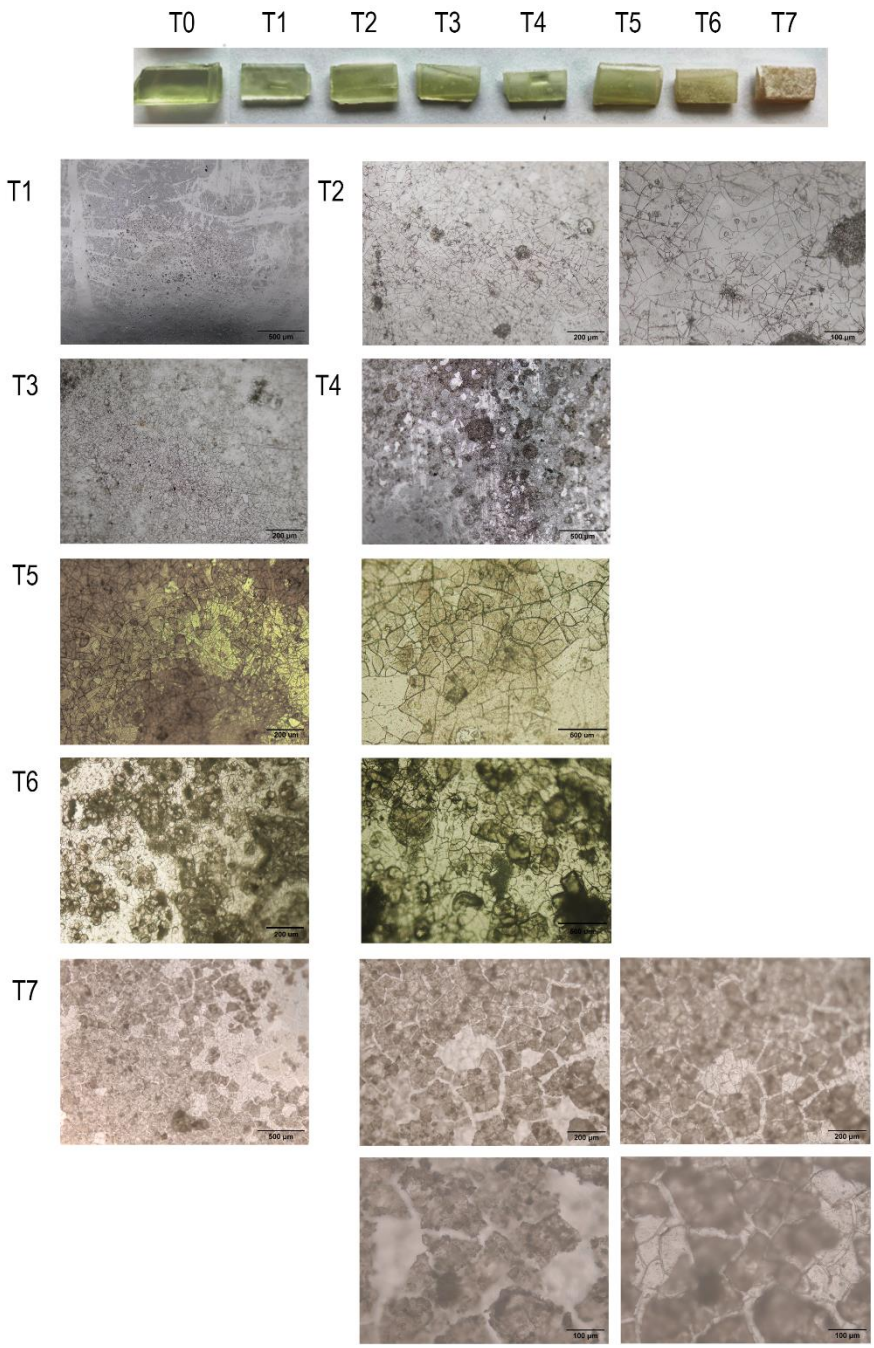

Figure 6.7. Optical microscope images of the SSV_O1 samples during the different sampling of the ageing test.

SIMS results obtained from the fifth sampling onwards are very noisy and difficult to interpret. As can be seen from the images of the samples surface in Figure 6.7, from the T5 point of the artificial ageing, a thick patina begins to form, which is visible even to the naked eye, making the surface of the samples highly degraded and irregular. This causes different analytical problems such as the fact that grains of material detach from the samples, despite the gold

coating, as well as making electrical charge compensation complicated. In certain areas, the surface of the underlying bulk remains exposed. Not being able to optically distinguish, during the ion beam alignment, the original areas of aged surface from those where layers of the patina have detached, some SIMS measurements could actually give the composition of the bulk glass. In addition, the sample's area analysed using the SIMS technique is approximately 100x100 µm and therefore not wholly representative, considering the great heterogeneity of the altered surface of the samples. Thus, the interpretation of the results cannot therefore be extended to the entire sample surface. Actually, in the case of strongly altered surface, the SIMS technique cannot give reliable information if the analyses is limited to only few point of the surface, moreover, the intrinsic difficult to control the charging effects on a very irregular surface can induce artefacts during the analyses, preventing the reliability of the experimental depth profiles.

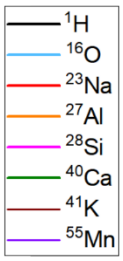
^{1}H
^{16}O
^{23}Na
^{27}Al
^{28}Si
^{40}Ca
^{41}K
^{55}Mn

T1

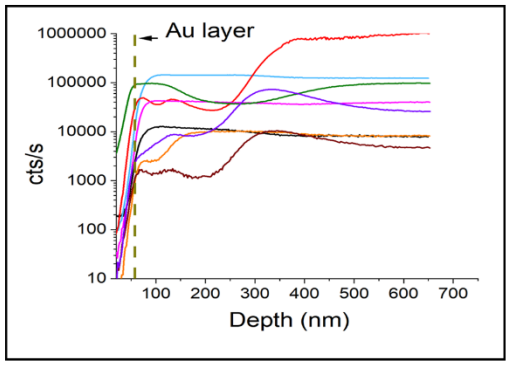
Au layer
cts/s
Depth (nm)

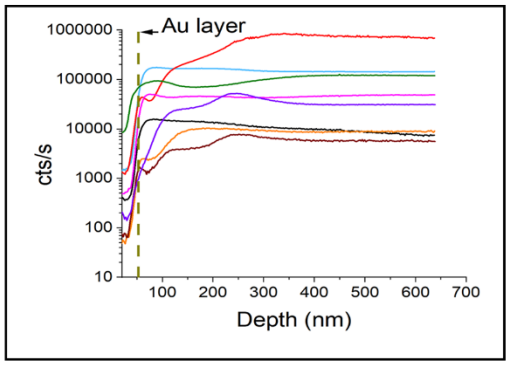
Au layer
cts/s
Depth (nm)

T2

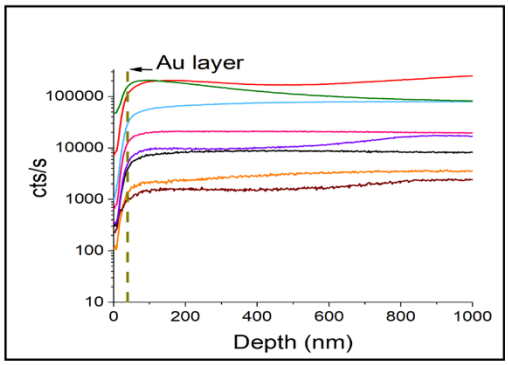
Au layer
cts/s
Depth (nm)

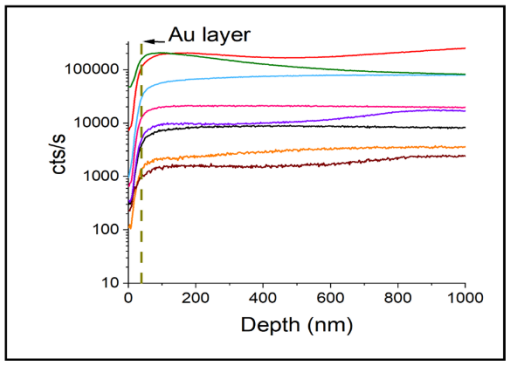
Au layer
cts/s
Depth (nm)

T3

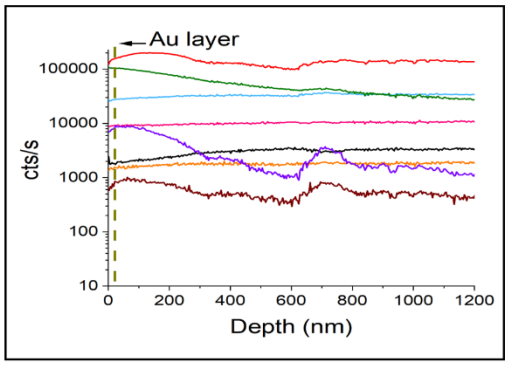
Au layer
cts/s
Depth (nm)

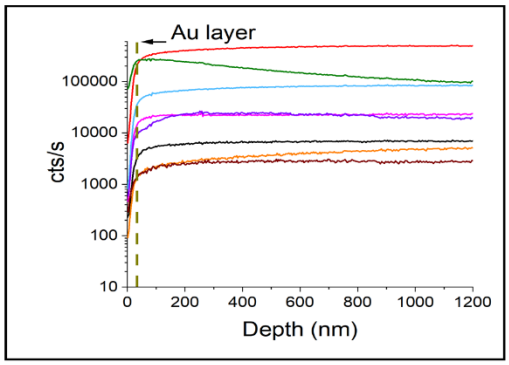
Au layer
cts/s
Depth (nm)

T4

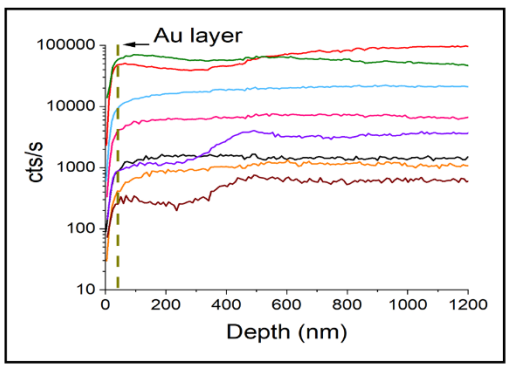
Au layer
cts/s
Depth (nm)

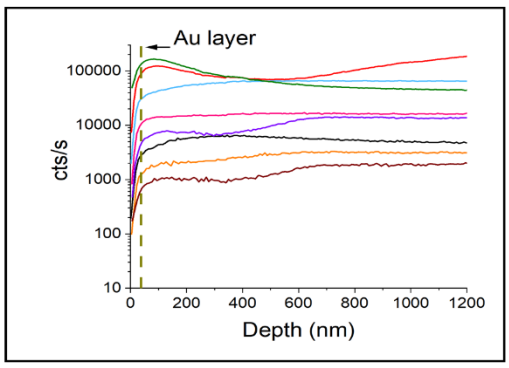
Au layer
cts/s
Depth (nm)

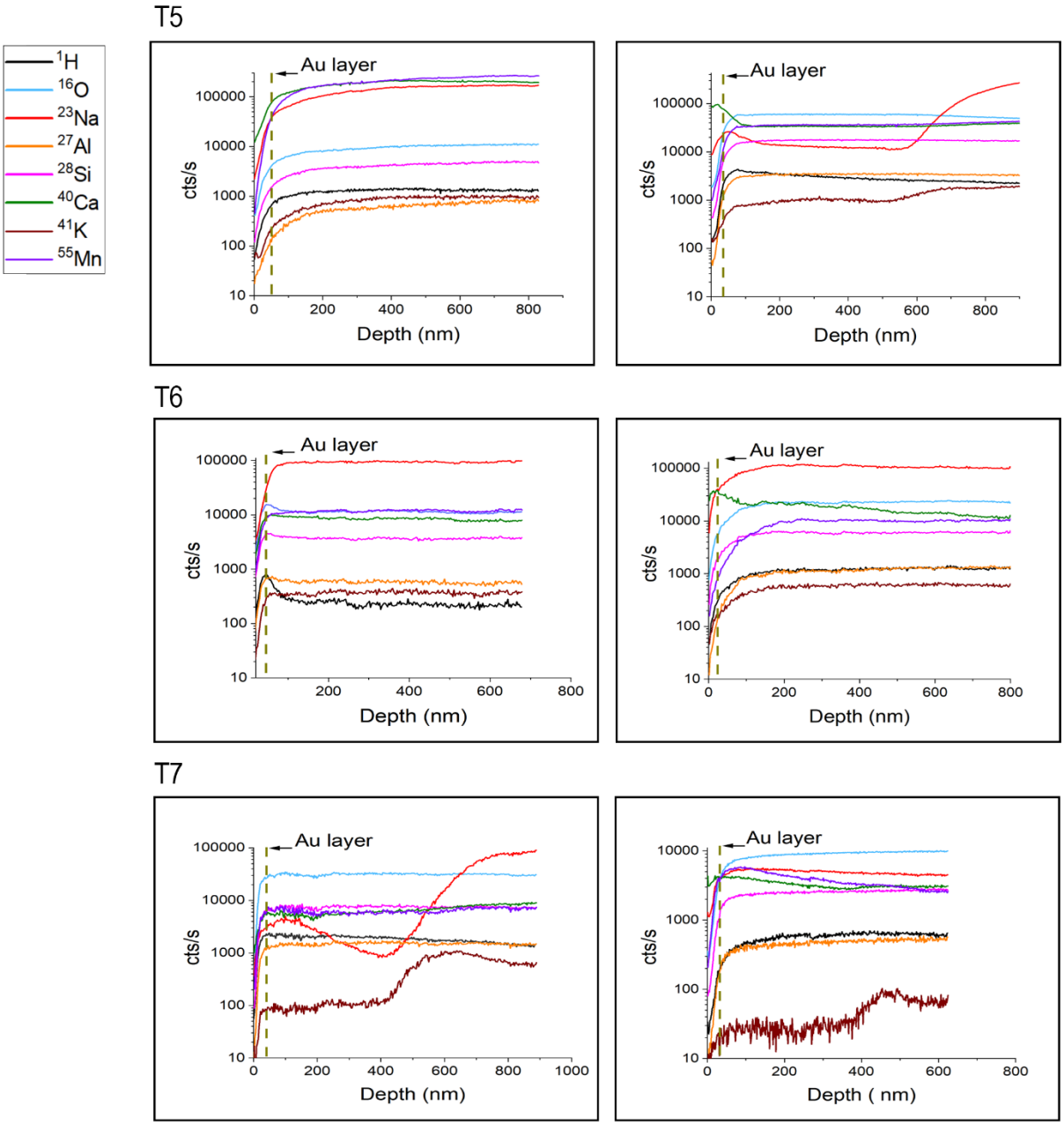

Figure 6.8. The element depth profile of SSV_01 mock-up in two different point for each step of analyses.

XPS analyses, on the other hand, covers a larger sampling area, around 500x500 µm, which can provide a more representative information of the elemental composition of the samples, bearing in mind that this technique investigates the first few nm of the sample surface (5-10 nm), thus a different depth compared to that investigated by SIMS [20].

Table 6.3 shows the quantitative data obtained from the XPS analyses on the samples during the ageing test, from T1 to T7. The concentration of the elements has been corrected by subtracting the contamination carbon (as done for the data discussed in the paragraph above)

but considering in the calculation of the contamination layer thickness only the area of the C1s peak related to the contamination carbon.

Table 6.3. Average composition data obtained by XPS analyses of the sample during the ageing test (from T1 to T7). All the reported data are expressed in atomic percentage and are corrected considering the carbon contamination (see text for explanation).

	T1	T2	T3	T4	T5	T6	T7
C 1s (carb.)	32.47	27.78	28.07	24.73	14.41	9.32	24.46
Ca 2p	6.64	7.15	14.84	10.61	0.51	3.61	2.95
Na 1s	28.43	30.78	17.90	23.41	18.30	9.77	29.58
O 1s	79.92	82.63	72.77	70.20	67.86	69.01	72.26
Si 2p	10.56	4.79	5.71	8.22	14.98	23.17	9.21

The reported data show an increase in Na and Ca concentration at the surface already from the first sampling, demonstrating that the process of leaching of modifier ions is the first process that is triggered when the glass is subjected to stress from the external environment (high temperature and humidity). However, it is interesting to note that from the sampling T4 onwards, the concentration of Na and especially that of Ca seems to decrease, while silicon on the surface increases. Given that the concentration of carbon (which refers to carbon in its carbonate form) also follows the trend of Ca and Na, it can be asserted that sodium and calcium carbonates are forming on the surface of the samples. In fact, looking at the quantitative data obtained in the various samples and reasoning on a molecular level, it is possible to suppose that all the Ca and Na accumulated on the surface is in the form of carbonates and that the oxygen amount not involved in carbonate species results to be approximately the right one for the Si-O-Si bond. To allow this estimation, we considered the number of atoms involves in the formation of the carbonate species $CaCo_3$ and Na_2CO_3.

From the chemical point of view, the formation of calcium or sodium carbonate involve the reaction of Ca and Na ions leached out from the glass network with water and CO_2 present in the ageing environment [21], as reported in the equation 6.1:

[6.1] $$H_2O + CO_2 \rightarrow HCO_3 \rightarrow CO_3^{2-} + Ca^{2+}/Na^{+} \rightarrow CaCO_3/Na_2CO_3$$

H^+ H^+

The trend of the C1s carbonate peak shown in Figure 6.9 also supports the formation and growth of carbonate species on the surface of the glass mock-ups during the ageing process. As can be seen, the carbonate peak at higher BE (around 290 eV), which is not present in pristine glass, increases in intensity from T1 to T5.

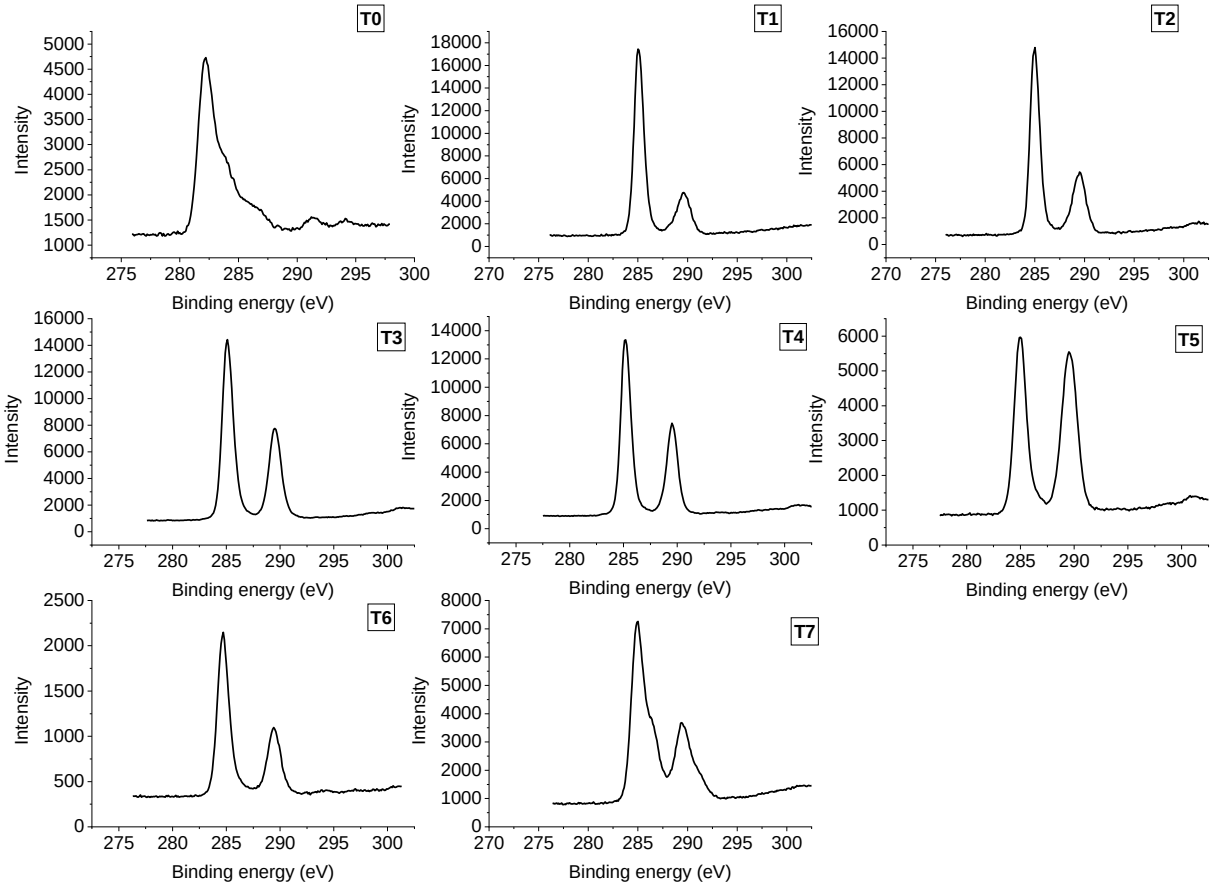

Figure 6.9. C1s band recorded on the samples from T0 to T7.

In addition, the trend of C, Ca, Na and Si reported on Figure 6.10 help to visualize the changes of the chemical composition of the glass surface. As mentioned above, the growing amount of modifier ions on the surface is accompanied by a decrease in silicon in the early stages of the test, while conversely, when silicon begins to increase on the surface from T4, the level of Ca, Na and C decreases. This trend depicts a first leaching step in which the modifier ions, diffusing towards the surface for exchanging with hydrogen coming from the atmosphere, react to form carbonates at the surface, and a second step in which possibly the altered surface detaches from the glass exposing a silica-rich surface layer.

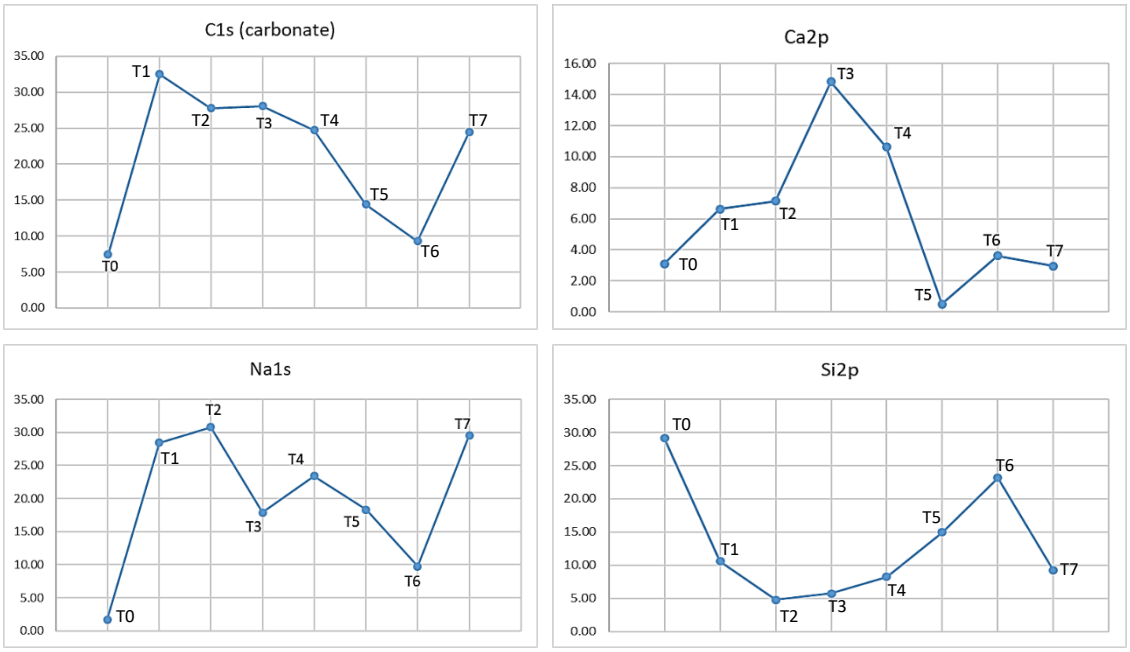

Figure 6.10. Trend in C, Ca, Na and Si concentration from sampling T0 to T7.

6.2.3. SIMS analyses after annealing treatment of pristine glass

The SIMS profiles obtained analysing the pristine glass (T0) clearly indicated the presence of a region under the glass surface marked by very low sodium concentration. This last, starts to rise around a depth of 0.5 µm. A similar trend has been observed in different points of the samples. We performed the same SIMS measurements after an annealing treatment at 600°C to check the Na behaviour and mobility into the glass network, and to verify if it would be redistributed into the depleted region. Data collected on different points of the sample surface (Fig. 6.11) indicated an extreme variability of the heat treatment effect, showing in some cases a redistribution of Na that seems to reoccupy the superficial layer initially depleted of Na (Fig. 6.11 point 2 and 3), while in other cases (point 1) SIMS analyses suggested a progression of the alkaline emptying zone, interesting more than one micron into the glass bulk.

Considering more closely the shape of the signal related to sodium, in point 2 and 3 of Fig. 6.11 the changing slope in the region around 500 nm is consistent with a back-diffusion (i.e., toward the surface) of sodium induced by the thermal treatment (the sodium atoms concentration was high only at depths larger than 400 nm before the thermal treatment). At point 1 of Fig. 6.11, instead, the sodium depth profile does not show a similar behaviour: even if this profile could suggest an increase of the depletion zone induced by the thermal treatment,

we cannot exclude that in this point of the sample the starting depletion was much larger than 400 nm. This lacking compositional homogeneity in the first 1-2 microns below the glass surface is not only detected by varying the depth but also laterally at the same depth: Fig. 6.12 shows the Na distribution map (in direct image) at the start and at the end of the in-depth profile, showing a marked non-uniform lateral presence of Na in the whole analysed glass region, suggesting that the chemical composition (and consequently) of a glass surface could be in general far from being homogeneous and isotropic.

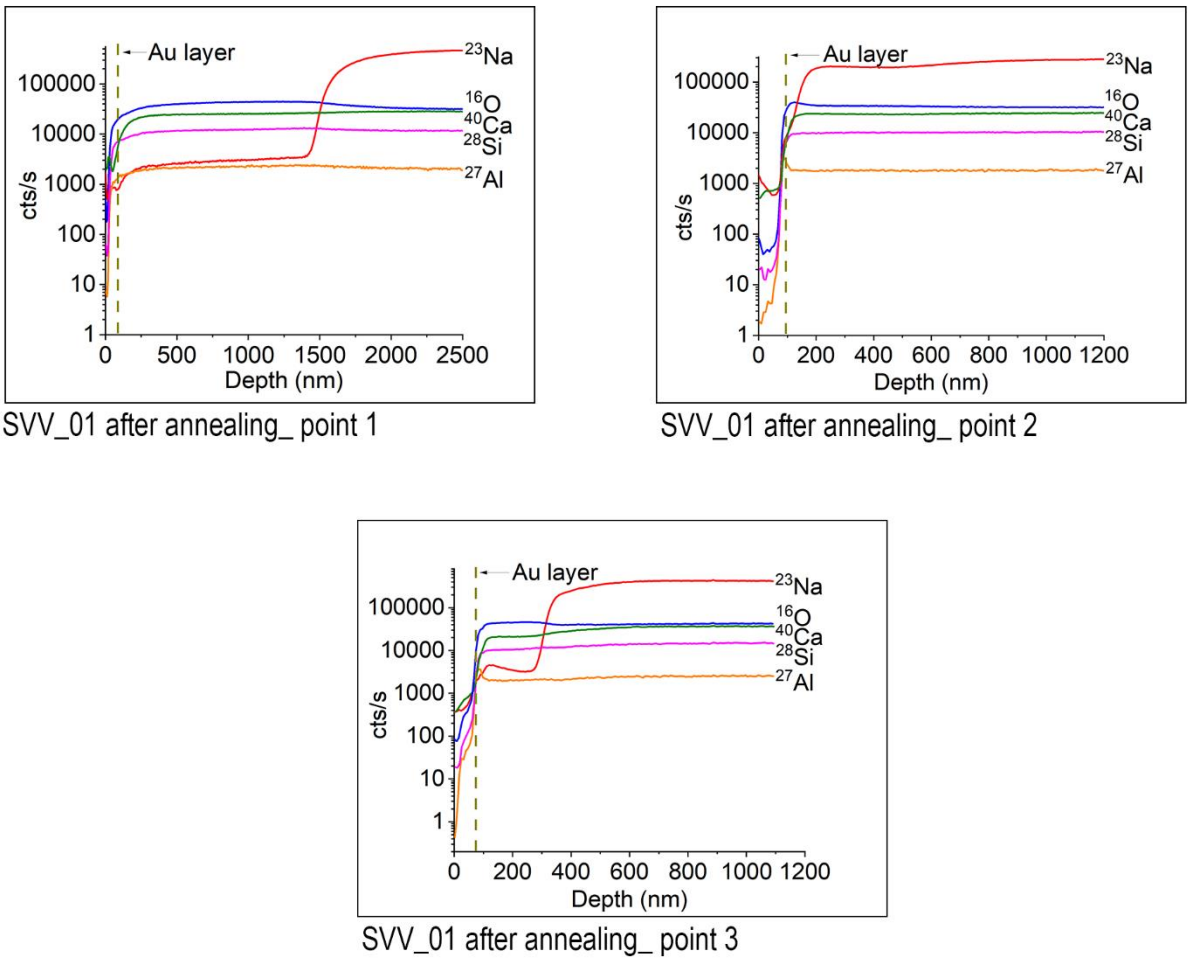

Figure 6.11 The element depth profile on three different point of silica-soda-lime mock-up after annealing treatment at 600°C for 6 hours

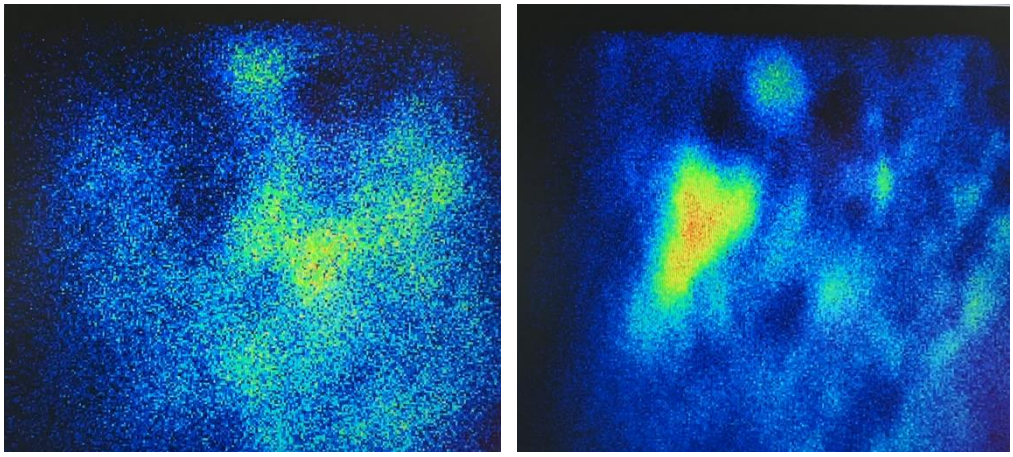

Figure 6.12. SIMS maps with the planar distribution of the intensity of 23Na ion signal at the start and at the end of the SIMS analyses of the SSV-01 sample after annealing. The analysed area dimension is 300×300μm^2. Yellow signal means high values of counts/s.

6.3. RESULTS INTERPRETATION

The results obtained by XPS and SIMS analyses confirmed the different elemental composition of the glass network between the glass bulk and the first 1-2 microns of the surface. In particular, the in-depth elemental profiles showed the different mobility of glass formers and glass modifiers (in particular, Na) during both the melting and cooling processes of the glass preparation, as well as the interaction of the surface of the final glass with the surrounding environment. It is likely that sodium atom concentration at the glass surface differs from the bulk material because of sodium volatility during the glass melt [22].

Descriptions of the detected behaviour and a similar in-depth concentration difference of alkaline elements could not be found in literature. Papers describing investigation of glass corrosion by SIMS technique reported approaches that did not deliver the same experimental findings here described, probably because dynamic SIMS was not performed beyond 100-200 nm of depth from the surface. Authors reported SIMS analyses of aged glasses assuming they had the same composition along the entire sample (i.e., from the surface to the bulk), or after polishing the glass samples before the artificial alteration thus losing crucial information about the pristine glass [23–26]. Our investigation of the glass surface, instead, enabled to identify a transition area between the glass and the environment instead of an abrupt hiatus. When studying glass from bulk to the surface, we can observe that the hydrogen content of the glass is rising, because glass is attracting water from the atmosphere and the alkaline ions content decreases. When final glass cools down after its preparation, its surface can react with water

molecules forming silanol group. The phenomenon of glass surface hydration keeps then progressing due to the interaction between water molecules and silanol groups (through hydrogen bonding). In this way, the glass surface gets covered by several monolayers of water depending on the water partial pressure in the atmosphere. An annealing treatment at 100°C leads to the desorption of water from the glass surface matrix, but it is necessary to expose glass to higher temperature to form again siloxane groups on its surface[1].

Considering the processes involved in the corrosion mechanism of glass and the results obtained from the SIMS and XPS analyses of the aged samples, it can be assumed that the micro-fractures formed at the surface of glass mock-ups (Figure 6.7) are the result of the leaching of modifier ions present in the glass that allowed water in the form of hydrogen ions to enter in the glass matrix (during the wet ageing cycle). During the period of ageing with very low humidity (around 10%), the water 'penetrated' into the glass evaporates, inducing the fracture formation. The ions, on the other hand, that reach the glass surface react with compounds present in the atmosphere to form salts or carbonates[27]. Subsequently, these compounds are washed out during periods of high humidity, leaving a patina of hydrated silica on the glass surface. These results seem consistent with the dissolution and re-precipitation model proposed in the literature and described in the introductory chapter of this thesis. Indeed, the chemical composition of the altered glass surface obtained as a final result of this artificial alteration experiment reflects the proposed structure of the model that it is based on an interface-coupled glass dissolution-silica precipitation reaction as the main surface alteration layer forming process. However, it is essential to consider the boundary conditions used in the ageing test that contributed to obtaining this final structure[28]. In particular, having carried out high and low humidity cycles, this is certainly a parameter that may have influenced the final result. For this reason, it is necessary to consider the hypotheses formulated in this work as closely related to the particular characteristics of the performed experiment both in terms of the external parameters set (temperature, humidity, alteration time and cyclic variation) and in terms of the chemical composition of the samples.

Experimental findings coming from SIMS and XPS analyses showed that the surface composition of the glass under analyses (before and after the additional thermal treatment) is unexpectedly far from being homogeneous, up to depths in the micron range. Moreover, the evidence of an extended surface region with a sodium depletion - surprisingly present on the pristine glass - should force us to think different about the glass degradation mechanisms usually considered, being them strongly dependent on the starting composition of the glass surface [29].

This study provides strong analytical evidence of the heterogeneity in the chemical composition of glass surface and its modification – before and after the artificial ageing – related to the interaction with external factors (temperature and humidity). It is possible to assume that a zone of abrupt change exists between solid glass (which is defined by its chemical composition) and the surrounding air. The analyses' results clearly indicate the presence of changes in the glass

surface composition because of external environmental conditions, showing a considerable increase of sodium content on the glass surface and the possible change of its chemical configuration. In particular, the sodium content near the surface appears lower than in the bulk material, possibly as a consequence of its vaporisation in some regions of the glass surface, due to its volatile nature under glass heating conditions.

Thus, these experimental findings can be placed in the position of proposing a more detailed and comprehensive model to describe the surface structure of pristine glass, that can be useful both for the improvement of manufacturing technologies for industrial glass, and for underpinning the understand of ancient glass corrosion mechanisms, for developing new solution for its conservation.

However, we also report the limitations of using SIMS as a surface technique for monitoring the distribution of elements from the surface to the bulk of a strongly altered glass, due to the marked heterogeneity of structure formed on the sample both laterally and in depth. Therefore, considering these results and those obtained from the characterisation of altered archaeological samples with LA-ICP-MS, it is clear how the potential of the latter technique can also be exploited for the characterisation of artificially altered glass samples. In fact, its high spatial and lateral resolution makes it possible to observe how the distribution of the different elements changes during the sequence of the alteration phases, following the kinetics of the process, overcoming the problems of surface [30,31]. This type of analyses is ongoing to validate this expectation.

6.4. REFERENCES

[1] F. Trier, U. Ranke, The Glass Surface and Ways of Its Modification, Https://Www.Ksr.Tul.Cz/. (n.d.). https://www.ksr.tul.cz/ (accessed November 4, 2022).

[2] J. Hopf, J.R. Eskelsen, M. Chiu, A.V. Ievlev, O.S. Ovchinnikova, D. Leonard, E.M. Pierce, Toward an understanding of surface layer formation, growth, and transformation at the glass–fluid interface, Geochim. Cosmochim. Acta. 229 (2018) 65–84. https://doi.org/10.1016/j.gca.2018.01.035.

[3] Y. Yamamoto, Precise XPS depth analyses of soda-lime-silica glass surface after various treatments: Precise XPS depth analyses of soda-lime-silica glass surface, Surf. Interface Anal. 44 (2012) 931–933. https://doi.org/10.1002/sia.4836.

[4] D. Sprenger, H. Bach, W. Meisel, P. Gütlich, XPS study of leached glass surfaces, J. Non-Cryst. Solids. 126 (1990) 111–129. https://doi.org/10.1016/0022-3093(90)91029-Q.

[5] J. Henderson, Ancient Glass: An Interdisciplinary Exploration, Reprint edition, Cambridge University Press, Cambridge, United Kingdom New York, NY, USA Port Melbourne, VIC, Australia, 2016.

[6] C.D. Wagner, The NIST X-ray photoelectron spectroscopy (XPS) database, (n.d.) 76.

[7] A. Vanleenhove, F.C. Mascarenhas, I. Hoflijk, I. Vaesen, C. Zborowski, T. Conard, HAXPES on SiO2 with Ga Kα photons, Surf. Sci. Spectra. 29 (2022) 014012. https://doi.org/10.1116/6.0001523.

[8] S.M. CASTANHO, R. MORENO, J.L.G. FIERRO, Influence of process conditions on the surface oxidation of silicon nitride green compacts, J. Mater. Sci. 32 (1997) 157–162. https://doi.org/10.1023/A:1018543703475.

[9] C 1s - Carbonates, (n.d.). http://www.xpsfitting.com/2011/03/c-1s-carbonates.html (accessed November 22, 2022).

[10] M. Ni, B. Ratner, Differentiation of Calcium Carbonate Polymorphs by Surface Analyses Techniques - An XPS and TOF-SIMS study, Surf. Interface Anal. 40 (2008). https://doi.org/10.1002/sia.2904.

[11] G. Greczynski, L. Hultman, X-ray photoelectron spectroscopy: Towards reliable binding energy referencing, Prog. Mater. Sci. 107 (2020) 100591. https://doi.org/10.1016/j.pmatsci.2019.100591.

[12] G. Greczynski, L. Hultman, The same chemical state of carbon gives rise to two peaks in X-ray photoelectron spectroscopy, Sci. Rep. 11 (2021) 11195. https://doi.org/10.1038/s41598-021-90780-9.

[13] XPSPEAK 4.1 Download (Free) - XPSPEAK41.exe, (n.d.). https://xpspeak.software.informer.com/4.1/.

[14] G.C. Smith, Evaluation of a simple correction for the hydrocarbon contamination layer in quantitative surface analyses by XPS, J. Electron Spectrosc. Relat. Phenom. 1 (2005) 21–28. https://doi.org/10.1016/j.elspec.2005.02.004.

[15] H. Van Limpt, R. Beerkens, O. Verheijen, Models and Experiments for Sodium Evaporation From Sodium-Containing Silicate Melts, J. Am. Ceram. Soc. 89 (2006) 3446–3455. https://doi.org/10.1111/j.1551-2916.2006.01233.x.

[16] R. Würz, M. Rusu, Th. Schedel-Niedrig, M.Ch. Lux-Steiner, H. Bluhm, M. Hävecker, E. Kleimenov, A. Knop-Gericke, R. Schlögl, In situ X-ray photoelectron spectroscopy study of the oxidation of CuGaSe2, Surf. Sci. 580 (2005) 80–94. https://doi.org/10.1016/j.susc.2005.01.054.
[17] G. Pintori, E. Cattaruzza, XPS/ESCA on glass surfaces: A useful tool for ancient and modern materials, Opt. Mater. X. 13 (2022) 100108. https://doi.org/10.1016/j.omx.2021.100108.
[18] D.J. Backhouse, A.J. Fisher, J.J. Neeway, C.L. Corkhill, N.C. Hyatt, R.J. Hand, Corrosion of the International Simple Glass under acidic to hyperalkaline conditions, Npj Mater. Degrad. 2 (2018) 1–10. https://doi.org/10.1038/s41529-018-0050-5.
[19] M. Melcher, M. Schreiner, Leaching studies on naturally weathered potash-lime–silica glasses, J. Non-Cryst. Solids. 352 (2006) 368–379. https://doi.org/10.1016/j.jnoncrysol.2006.01.017.
[20] K. Janssens, ed., Modern Methods for Analysing Archaeological and Historical Glass, 1st ed., Wiley, 2013. https://doi.org/10.1002/9781118314234.
[21] O. Velts, M. Uibu, J. Kallas, R. Kuusik, CO2 mineral trapping: Modeling of calcium carbonate precipitation in a semi-batch reactor, Energy Procedia. 4 (2011) 771–778. https://doi.org/10.1016/j.egypro.2011.01.118.
[22] E. Le Bourhis, Glass: Mechanics and Technology, 1st ed., Wiley, 2007. https://doi.org/10.1002/9783527617029.
[23] S. Fearn, D.S. McPhail, V. Oakley, Moisture attack on museum glass measured by SIMS, 46 (2005) 7.
[24] R. Hellmann, S. Cotte, E. Cadel, S. Malladi, L.S. Karlsson, S. Lozano-Perez, M. Cabié, A. Seyeux, Nanometre-scale evidence for interfacial dissolution–reprecipitation control of silicate glass corrosion, Nat. Mater. 14 (2015) 307–311. https://doi.org/10.1038/nmat4172.
[25] K. Cummings, W.A. Lanford, M. Feldmann, Weathering of glass in moist and polluted air, Nucl. Instrum. Methods Phys. Res. Sect. B Beam Interact. Mater. At. 136–138 (1998) 858–862. https://doi.org/10.1016/S0168-583X(97)00758-1.
[26] A. Tournie, P. Ricciardi, P. Colomban, Glass corrosion mechanisms: A multiscale analyses, Solid State Ion. 179 (2008) 2142–2154. https://doi.org/10.1016/j.ssi.2008.07.019.
[27] S. Gin, J.-M. Delaye, F. Angeli, S. Schuller, Aqueous alteration of silicate glass: state of knowledge and perspectives, Npj Mater. Degrad. 5 (2021) 42. https://doi.org/10.1038/s41529-021-00190-5.
[28] I. Biron, F. Alloteau, O. Majérus, D. Caurant, P. Lehuédé, eds., Glass Atmospheric Alteration: Cultural Heritage, Industrial and Nuclear Glasses, HERMANN, Paris, 2019.
[29] L.L. Hench, Characterisation of glass corrosion and durability, J. Non-Cryst. Solids. 19 (1975) 27–39. https://doi.org/10.1016/0022-3093(75)90067-8.
[30] M. Šala, V.S. Šelih, C.C. Stremtan, J.T. van Elteren, Analytical performance of a high-repetition rate laser head (500 Hz) for HR LA-ICP-QMS imaging, J. Anal. At. Spectrom. 35 (2020) 1827–1831. https://doi.org/10.1039/C9JA00421A.
[31] J.T. van Elteren, M. Šala, V.S. Šelih, Perceptual Image Quality Metrics Concept in Continuous Scanning 2D Laser Ablation-Inductively Coupled Plasma Mass Spectrometry

Bioimaging, Anal. Chem. 90 (2018) 5916–5922.
https://doi.org/10.1021/acs.analchem.8b00751.

CONCLUSION AND FUTURE PERSPECTIVE IN THE FIELD OF ANCIENT GLASS CONSERVATION

Glass has unique properties. The combination of transparency and hardness at room temperature, together with good mechanic properties and excellent corrosion resistance in the main conventional environments, makes glass ideal for many applications, from the artistic (e.g., stained glass) to the industrial and technological ones (e.g., windows on a spacecraft). However, evidence of the transformation of the vitreous structure due to the action of aggressive agents, such as humidity, water, strong acidic/alkaline solution, is easily observed on ancient glasses, proving its "fragility" over time.

Research on the chemical corrosion of glass assumes obviously considerable importance not only in the field of conservation of historical and archaeological glass objects, but also for the preservation and protection of modern glass, often subjected to similar stresses although for much shorter periods of time.

The comprehensive study of ancient glass that this PhD project proposed represents an opportunity to validate or contradict the various glass corrosion models. The obtained information will drive hopefully to a better understating of the complex phenomena of glass alteration and to the development of new products, or protocols, for the restoration and conservation of vitreous items (for instance, in museums). Among the different experimental findings of this thesis work, the characterisation of altered archaeological samples using LA-ICP-MS proved that the silica gel formed on the surface as an altered layer acts as a protective barrier by limiting the ion exchange between the glass components and hydrogen in the environment. Again, SIMS data obtained from the analyses of pristine glass mock-ups showed the presence of a surface layer rich in formers and stabilisers (Si, Al and Ca) and depleted of modifiers (Na and K): this chemical structure is probably more chemically stable than the glass bulk because, being a more polymerised area of the glass network, it limit the interaction between the modifier ions of the glass and the hydrogen ions of the air and their subsequent ion-exchange.

All this information can serve as guidelines for developing new and targeted strategies for the conservation of ancient glass, an issue still opens in the cultural heritage sector. In this field, indeed, chemical research on the composition of ancient glass and their relative causes of deterioration are achieving important results, but a practical outcome in the field of restoration products is still inadequate. Following the Carta Italiana del Restauro 1972, every material

employed for restoration work on Cultural Heritage must meet the prerequisite of reversibility, long-term stability, respect for the characteristics of the artefact (mechanical, chemical, and optical), and nontoxic for the environment and for the operators. In practice, it is usually necessary to reach a compromise between these properties.

Nowadays, technological advancement and the provision of sophisticated implements of research open new doors also in the field of conservation of cultural heritage. In particular, with the advent of nanotechnologies, materials with new properties (not present in their natural forms) have made their appearance, which have opened new scenarios in the fields of chemistry, medicine, construction and construction, electronics, and others, which can be scaled in the field of conservation of cultural heritage.

By means of nanotechnologies, today, it is also possible to treat all surfaces with the aim at preserving and protecting them from any damage and wear and tear over time, opening the field to renovations and restoration. The goal is to increase the performance characteristics of the cultural material, including water repellency, anti-graffiti, antifreeze (against the disruptive action of frost), pro or anti UV rays and anti-slip.

However, the application of nanotechnologies as conservation products raises some issue related to the prerequisites cited in the above reported Carta Italiana del Restauro 1972, in particular with the reversibility requirement. Among the scientific community there is an open debate related to the ethics of conservation, on reversibility of the treatment. It is generally agreed that all conservation/restoration practices should be fully reversible, which means that it should be possible to take the artefact back to its state before the treatment, even after several years. In practice, reversibility should be considered on a less rigorous basis: for example, in the case of flaking layers, the consolidation process implies the penetration between the glass and the layers and the hardening to hold the structure together. In this situation, the removal of the consolidant will harm the artefact, no matter which material is used.

In conclusion, based on the results obtained from the research activities described in this work (often obtained by the application of new investigation approaches) I want to support the conservation solution related to the innovative idea of the **Reversibility of Chemical Degradation**. This idea is based on the realisation of an in-depth chemical investigation of the altered layers present on the glass artefacts, in order to reach the blockage and stabilisation of the alteration itself by consolidation interventions and try to restore the chemical balance of the glass matrix composition: in some way, almost a return to the initial state. The basic idea is to address the research towards the development of a product that could be 100% compatible with the glassy material to be consolidated. In this way, both chemical and physical imbalance problems, which can develop over time considering that each material reacts in a different way depending on the action of external agents could be avoided. Using a glass-based product to consolidate a glass object prevents chemical instability developing between the consolidating material and the original surface over time; on the contrary, the two "materials" will age

together. In addition, the problem to remove the consolidating product, which is necessary today due to the degradation of polymer-based products used for the consolidation of glassy objects, will not arise. In this perspective, we will no longer talk about reversibility but about the prospect to re-treating as a requirement that a product must have if used in the field of conservation of cultural heritage. In this way the reason to remove a material that is exactly the same as the material to be consolidated and that degrades with it, without developing visible effects that limit the usability of the work of art, disappears.

Another important aspect in the field of conservation of cultural heritage objects, especially in this historical context, is the necessity of thinking green practices to provide conservators with solutions characterised by lower energy consumption, less toxic materials, and fewer plastics. Many current preservation materials and methods are harmful and outdated in terms of environmental sustainability, and conservation professionals are unaware of the general impact of their actions on the environment.

In this perspective, new green materials for stabilisation will chemically stabilise the progression of corrosion on glass. Innovative treatments will be based on materials from renewable resources, comparing their performance with existing stabilisation systems based mostly on organic coatings. Taking inspiration from the innate capacity for self-regeneration of tissues in living organisms, silica-based precursors can be proposed as a novel consolidation treatment for glass, allowing the chemical stabilisation of altered structural parts on the nano-metric scale. Thus, the formulation for glass stabilisation will focus on the selection of optimal precursors to obtain the most sustainable final composition of silica-gel nanostructure. From a green formulation perspective, the possible synthesis of silica-gel nanostructures must be optimised to take place at room temperature and in water, while minimizing the amount of alcohol used as solvent, the use of precursors, the reaction time and the water intake (i.e., with green gel delivery systems). Moreover, the chemical precursors for the synthesis should be substituted with agroindustry by-products with high Si content (i.e., eggshells, rice husks, sugarcane pulp or maize stalk) that have recently gained interests in the field of materials science as eco-friendly compounds from renewable sources. In addition to the objective of stabilising the altered glass structure, other desired physicochemical properties (hydrophobicity, porosity, antimicrobial, etc.) should be achieved, for instance introducing specific functional groups or molecular geometries, by chemical grafting. The final nanosilica gels prepared in water should allow to form a continuous network of Si-O-Si bonds that will be able to consolidate the damaged objects and reconsolidate the altered historical glass at room temperature.

In conclusion, the chapters of this thesis describe an advanced strategy to address the problem of ancient glass conservation. This starts with the study of real glass objects altered over the centuries and is complemented by the observation of the chemical and structural modification of the glass surface during an artificial ageing process, demonstrating how the

results obtained from this combined analytical approach brought to light concrete evidence on the transformation of the glass structure that can be used as a starting point to develop cutting edge and specific conservation strategies in order to overcome the current obsolete and inefficient conservation and restoration methods used today of glass objects with historical and artistic value.

ACKNOWLEDGEMENTS

I would like to thank all the people who collaborated in the various research activities of this thesis project. In particular, Professor Marco Roman of the Ca'Foscari University of Venice for his support in the methodological development phase with LA-ICP-MS, Mario Barozzi and Roberto Canteri of the Bruno Kessler Foundation of Trento for the SIMS characterisations, and Mirko Prato, coordinator of the materials characterisation facility at the Italian Institute of Technology, for carrying out the XPS analyses. Thanks also to Professor Alessandro Re and his research group at the University of Turin for supervising the project on the characterisation of archaeological glass using X-ray tomography.

I would also like to sincerely thank Professor Ligia Maria Moretto for her kind support of my early activities during the initial period of my doctoral program.